DECENTRALIZED POWER AND HEAT DERIVED FROM AN ECO-INNOVATIVE INTEGRATED GASIFICATION FUEL CELL COMBINED CYCLE FUELLED BY WASTE

A thesis submitted in partial fulfilment of the requirements for the degree of

Engineering Doctorate in Environmental Technology

by

Tygue Stuart Doyle

February 2015

Brunel University

School of Engineering and Design

in Partnership with and Sponsored by:

DECLARATION

This thesis is a presentation of my original research work. Wherever contributions of others are involved, every effort is made to indicate this clearly, with due reference to the literature, and acknowledgement of collaborative research and discussions.

Signature:

Date:

ABSTRACT

DECENTRALIZED POWER AND HEAT DERIVED FROM AN ECO-INNOVATIVE INTEGRATED GASIFICATION FUEL CELL COMBINED CYCLE FUELLED BY WASTE.

By Tygue S. Doyle

This research investigates the energy, financial and environmental performance of an innovative integrated gasification fuel cell combined cycle fuelled by municipal solid waste that includes hydrogen storage and electrolysis. The suitability for fuel cells to run on synthesis gas coming from the gasification of waste is determined by the sensitivity of the fuel cell to run on contaminated fuel. Out of the available fuel cell technologies solid oxide fuel cells (SOFCs), because of their ceramic construction and high operating temperatures, are best suited for syngas operation. Their high operating temperature (>650°C) and the presence of nickel at the anode means that it is possible to reform hydrocarbons to provide further hydrogen.

A major contaminant to be considered in gasification systems is tar which can foul pipework and cause substantial performance losses to the plant. Experimental research on the effects of tar on a SOFC at varying concentrations and operating conditions show; that some carbon deposition serves to improve the performance of the fuel cell by reducing the ohmic resistance, and there is a tendency for the tar to reform which improves overall performance. These improvements are seen at moderate tar concentrations but at higher concentrations carbon deposition causes substantial performance degradation.

Numerical simulations representing all aspects of the proposed system have been developed to understand the energy performance of the system as a whole as well as the financial and environmental benefits. Taking into account variations in the waste composition, and the wholesale electricity price the proposed system, scaled to process 100,000 tonnes of waste per year (40,000 removed for recycling), has a simple payback period of 7.2 years whilst providing CO_2 savings of 13%. Over the year the proposed system will provide enough electricity to supply more than 23,000 homes and enough heat for more than 5,800 homes (supplying 25% of the electrically supplied homes).

ACKNOWLEDGEMENTS

This journey was unexpected and if not for the encouragement of my supervisor Zahir I would not have thought it possible. So my thanks go out to Dr. Zahir Dehouche and my industrial sponsors BDSP Partnership for making this opportunity possible and for supporting me throughout these years. Specifically at BDSP I'd like to thank Dr. Alan Harries for supervising and helping me through the early times and for picking up the reins during the writing of an excellent FP7 proposal, to Dr. Neil Campbell and Ivan Jovanovic for the advice and thought provoking discussions, to Ioannis Rizos for introducing me to the world of thermal modelling and for the help along the way, and lastly to Sinisa Stankovic for supporting the EngD programme and for having faith in my ability.

At Brunel University I'd like to thank Janet Wheeler in the Research Office, Dr. Yulia Matskevich in the Research and Development Office, and Meg Griffiths in Computing for working behind the scenes keeping myself and the other students on track. Prof. Luiz Wrobel for always finding the time to listen and help, and Prof. Ibrahim Esat for the social visits and your help in setting up the engineering society.

I have been fortunate enough to work with Dr. P.V. Aravind, who is a leader in the field of solid oxide fuel cells and their many applications, my special thanks go to him for not only playing an instrumental role in the FP7 proposal but for inviting me to TU Delft to carry out my own tar-laden syngas experiments that led to an excellent journal publication. Thanks to Dr. Ming Liu at TU Delft for assisting and supervising the experiments and to Ab Streppel for showing me how to use the equipment.

To my fellow EngD colleagues James and Mitch, the modules would not have been the same without you.

To my mother and father, thank you for always supporting and believing in my potential, for pushing me to not only finish what I started but to do it properly.

To my wife Irma, whom I met on an EngD module in Surrey, if there is anything I am grateful for over the past four years meeting you supersedes all others. Thank you for being there to talk me through the tough times – especially towards the end when I didn't always give you the time and attention you deserve – thank you for your patience.

Finally, my gratitude goes to the EPSRC for co-funding the EngD programme, and to the BRISK Transnational Access programme that funded my experimental research at TU Delft.

LIST OF PUBLICATIONS

JOURNAL PAPERS

Doyle T. S., Dehouche Z., Stankovic S., 2015. *Decentralized Power and Heat Derived from an eco-Innovative Integrated Gasification Fuel Cell Combined Cycle Fuelled by Waste*. International Journal of Hydrogen Energy 40, 9013-9025.

Doyle T. S., Dehouche Z., Aravind P., Liu M., Stankovic S., 2014. *Investigating the impact and reaction pathway of toluene on a SOFC running on syngas*. International Journal of Hydrogen Energy 39, 12083-12091.

Doyle T. S., Dehouche Z., Harries A., Rizos I., 2013. *Financial, Environmental and Energy Analysis of Various Micro-CHP Systems within the UK Domestic Market*. Journal of Clean Energy Technologies 1 (2), 96-100.

CONFERENCE PRESENTATIONS

Doyle T. S., Dehouche Z., Harries A., Rizos I., 2013. *Financial, Environmental and Energy Analysis of Various Micro-CHP Systems within the UK Domestic Market*. International Conference on Future Environment and Energy-ICFEE 2013, Rome, Italy.

Doyle T. S., Dehouche Z., Stankovic S., 2014. *The pivotal role of solid state hydrogen storage in advanced waste-to-energy*. International Discussion on Hydrogen Energy and Application (IDHEA) 2014, Nantes, France.

TABLE OF CONTENTS

LIST OF TABLES

LIST OF FIGURES

NOMENCLATURE

A	Area (m^2)
a	Coefficient for overvoltage on the electrolyser electrodes (V)
b	Coefficient for overvoltage on the electrolyser electrodes (m^2/A)
CCE	Carbon Conversion Efficiency (%)
c^*	Concentration at reaction surface (mol/cm^2)
c	Concentration (mol/m^3)
c_p	Specific Heat Capacity (kJ/kmol.K)
D	Diffusivity (m^2/s)
Dh	Hydraulic diameter (m)
E	Electrical Potential Difference (V)
E_a	Activation Energy (J/mol)
ECE	Energy Conversion Efficiency (%)
F	Faraday's constant (C/mol)
f	Reaction rate constant (1/s)
f_1	Parameter related to Faraday efficiency (mA^2/cm^4)
f_2	Parameter related to Faraday efficiency (-)
G, g	Gibbs free energy (kJ, kJ/mol)
H	Enthalpy (kJ)
h	Planck's constant (J.s), enthalpy (J/mol)
i	Current (A)
J	Surface molar reaction rate (mol/cm^2s)
j	Current density (A/m^2)
K	Equilibrium constant (-)
k	Boltzmann's constant (J/K), thermal conductivity (W/m.K), proportionality constant (-)
L	Thickness (m)
M	Molar mass (g/mol)
m	Mass (kg)
n	Number of moles (mol)

$\dot{n}$	*Molar flow rate (mol/s)*
n_e	*Number of electrons*
N	*Diffusion flux (mol/cm^2.s)*
Nu	*Nusselt number (-)*
P	*Total Pressure (kPa)*
p	*Partial Pressure (kPa)*
q	*Energy (J)*
r	*Reaction rate (mol/L.s)*
R	*Universal Gas Constant (J/molK)*
r	*Parameter related to ohmic resistance of the electrolyser electrolyte (Ω.m^2)*
r_e	*Effective radius (m)*
SB	*Steam to Biomass ratio (-)*
SB^*	*Modified Steam-to-Biomass ratio (-)*
s	*Entropy (J/molK)*
T	*Temperature (K)*
W	*Work (J)*
V	*Voltage (V)*
x	*Molar fraction (mol/mol)*
z	*Valence number (-)*
α	*Charge transfer coefficient (-)*
ξ	*Porosity (-)*
ε	Lennard-Jones Energy (-)
Ω	*Collision integral; ohm resistance (ohm)*
γ	*Pre-exponential factor (A/m^2)*
η	*Voltage (V)*
σ	*Characteristic length (A$^\circ$); electrical and ionic conductivity ($1/\Omega.cm \equiv S/cm$)*
τ	*Tortuosity (-)*
λ	Stoichiometric oxygen ratio (-)

Subscripts/Superscript

0	*Reference point*
a, c	*Anode, cathode*
act	*Activation*
C	*Cold*
ch	*Channel*
chem	*Chemical*
conc	*Concentration*
conv	*Convection*
e	*Equilibrium*
eff	*Effective*
elec	*Electrical*
F	*Faraday*
f	*Forward*
gen	*Generation*
H	*Hot*
i, j	*Component species i, j*
k	*Knudsen*
L	*Limit*
M	*Molecular*
P	*Product; pressure*
R	*Reactant*
r	*Reverse*
rad	*Radiation*
ref	*Reference*
rev	*Reversible*
rxn	*Reaction*
T	*Temperature dependant*

ABBREVIATIONS

AFC	*Alkaline Fuel Cell*
APP	*Advanced Plasma Power*
ASR	*Area Specific Resistance*
ASU	*Air Separation Unit*
BCC	*Body Centred Cubic*
BGCC	*Biomass Gasification Combined Cycle*
BGFC	*Biomass Gasification Fuel Cell*
CCGT	*Combined Cycle Gas Turbine*
CGE	*Cold Gas Efficiency*
CHP	*Combined Heat and Power*
CO_2e	*Carbon dioxide equivalent*
CVD	*Chemical Vapour Deposition*
DEA	*Diethanolamine*
DECC	*Department of Energy & Climate Change*
DEPG	Dimethyl Ether of Polyethylene Glycol
EC	*European Commission*
ECN	*Energy Research Centre for the Netherlands*
EDS	*Energy Dispersive Spectroscopy*
EIS	*Electrochemical Impedance Spectroscopy*
EPJ	*EquiPlasmaJet*
FIT	*Feed-in-tariff*
GHG	*Greenhouse Gas*
GT	*Gas Turbine*
hhs	*Households*
HHV	*Higher Heating Value*
HS-GC/MS	*Headspace Gas Chromatography/Mass Spectrometry*
H-SOFC	*Proton conduction SOFC*

HTFC *High Temperature Fuel Cell*

IGCC *Integrated Gasification Combined Cycle*

IGFCC *Integrated Gasification Fuel Cell Combined Cycle*

LHV *Lower Heating Value*

LSCF *Lanthanum Strontium Cobalt Ferrite*

LSM *Lanthanum Strontium Manganite*

MCFC *Molten Carbonate Fuel Cell*

MDEA Methyldiethanolamine

MEA *Monoethanolamine*

MIEC Mixed Ionic and Electronic Conductor

MRF *Material Recovery Facility*

MSW *Municipal Solid Waste*

OCV *Open Circuit Voltage*

PAFC *Phosphoric Acid Fuel Cell*

PEM *Proton Exchange Membrane*

PEN *Positive electrode, Electrolyte, Negative Electrode*

PSA *Pressure Swing Absorber*

RDF *Refuse Derived Fuel*

RHI *Renewable Heat Incentive*

ROC *Renewable Obligation Certificate*

SB *Steam to Biomass ratio*

SDC *Samaria-doped Ceria*

SFEE *Steady Flow Energy Equation*

SOFC *Solid Oxide Fuel Cell*

SYTO Y-doped $SrTiO_3$

TPB *Triple Phase Boundary*

VOC *Volatile Organic Compound*

WGS *Water Gas Shift*

WtE *Waste-to-Energy*

YSZ *Yttria-Stabilised Zirconia*

EXECUTIVE SUMMARY

Escalating energy demands, energy security issues and the current political drive to reduce carbon emissions have created an overwhelming need for innovative and future-proof decentralised energy production and management solutions to tackle the area of sustainable energy production. Over the past century there has been an exponential growth in energy consumption of which 80% is derived from fossil fuels (*WEC, 2013*). Current estimations see coal as the only fossil fuel to be available after 2042 and will only be available up to 2112 (*Shafiee, 2009*). At the same time there is growing concern surrounding the emission of greenhouse gases which contribute to global warming disrupting the current climate rhythm, *Figure (ES) 1*.

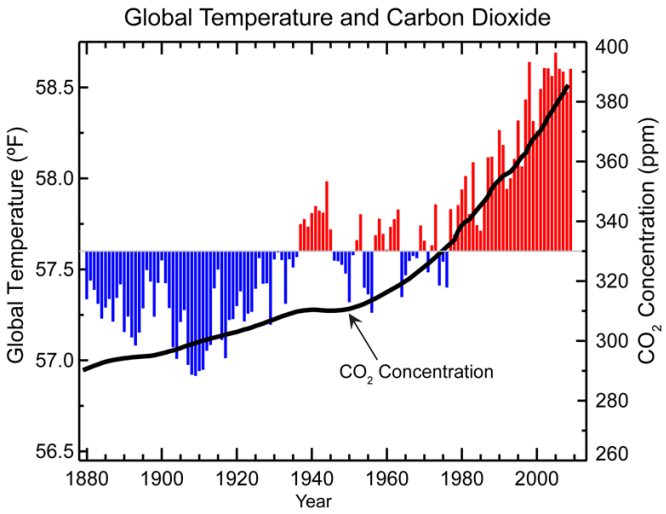

Figure (ES) 1: Average annual global temperature showing annual values above and below the 1901-2000 average temperature. The black line shows the change in atmospheric carbon dioxide concentration (*NCDC, 2014*).

This has led to substantial interest and deployment of solar powered renewable technologies such as wind turbines, photovoltaics (PV), and biomass. As an energy resource the potential for wind energy in the UK is very strong and is considered to the best wind resource in Europe (*Sinden, 2005*). Whilst wind turbines and PVs are fundamentally sustainable with relatively short energy payback periods they are inherently intermittent which means the electricity grid will struggle to support their deployment at large scale. Therefore, further technologies dealing with the dynamic relationship between demand and supply will be required to support the large-scale penetration of any intermittent energy sources.

There is also a need for effective and sustainable waste management at a time when households are producing ever more waste. In some cases this waste is sent to large centralised waste incinerators that are unable to make full use of the waste heat (which is >65% (*Khartchenko et al., 2013*) of the total energy content) and therefore unable to fully re-capture the embodied energy. They also have disadvantages in terms of emissions and solid by-products which are often classified as hazardous.

In order to maximise efficiency and to bring these WtE systems closer to the end users - where waste heat can be utilised in intelligent building-to-building thermal energy networks - new technologies must be introduced.

There are several different WtE processes that can be split into:

Thermo-chemical conversion processes

- Incineration
- Co-combustion
- Thermal gasification
- Pyrolysis

Bio-chemical conversion processes

- Anaerobic digestion (producing biogas)
- Fermentation (producing bio-ethanol)
- Dark fermentation and photo-fermentation (producing hydrogen)
- Biogas from landfill

Apart from incineration, pyrolysis and gasification can be used for WtE but instead of directly releasing heat via combustion pyrolysis and gasification processes are used to produce secondary products, such as syngas, which can be used to generate energy. The syngas produced from the gasification of carbonaceous material is rich in hydrogen, carbon monoxide and methane that can fuel SOFCs.

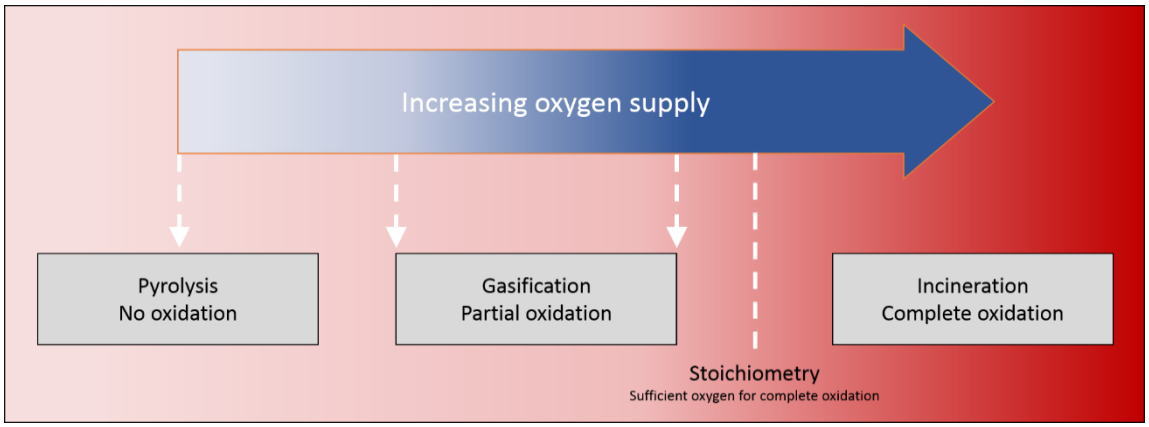

Figure (ES) 2: The difference between pyrolysis, gasification and incineration is identified by amount of oxygen present during the thermal treatment.

Pyrolysis and gasification differ from incineration by the amount of oxygen that is supplied to the process, *Figure (ES) 2*.

By limiting the amount of oxygen during pyrolysis and gasification the feedstock is decomposed in a reducing environment which enables the production of hydrogen that can be used to drive a fuel cell.

Currently only 6% of the municipal waste produced in Europe (EU 28) is sent to incineration plants (*Eurostat, 2012*), and of the waste generated in the UK it is estimated that 40% is considered to be bio-waste (*Dohogne, 2014; Europa, 2010*). Therefore there is a large potential to provide carbon emission savings by diverting waste away from landfill to WtE plants that can efficiently recover the

embodied energy within the waste to produce energy. The biofraction of the waste stream is considered as a renewable source of energy thereby providing carbon savings.

The renewability and sustainability credentials given to biomass stem from the fact that carbon dioxide is consumed and stored in plants through photosynthesis and released during biomass conversion (Siedlecki et al., 2011).

This indicates a clear need for mutually complementary innovative solutions to four key areas:

1. **Waste disposal**

Transforming the problem of waste disposal, especially Municipal Solid Waste (MSW), into a commercially viable business that recovers and uses the embodied energy content. Exploiting MSW as a principal source of energy can also mitigate the environmental impacts associated with landfill disposal and incineration.

2. **Local electricity production**

Providing a means of local electricity generation and storage introduces precious flexibility into the grid in order to provide a SMART means of dealing with peak production/demands as well as maximising the potential for renewable electricity grid penetration.

3. **Clean hydrogen production**

Initiating the successful growth of a commercially viable distributed hydrogen infrastructure for clean (non-polluting) vehicles which do not rely on fossil fuel energy sources.

4. **Heat networks**

Incentivising the adoption of intelligent building-to-building thermal energy supply networks to take advantage of waste energy exchange between buildings as well as to distribute energy from MSW and renewable or low carbon sources such as solar thermal, ground source heat pumps and traditional CHP schemes.

RESEARCH AIMS AND OBJECTIVES

Although there is and has been much said about the potential advantages and possibilities of using gasification technologies (using coal or waste), building them requires substantial levels of investment. It is the aim of this research to quantify the environmental and economic performance of an Integrated Gasification Fuel Cell Combined Cycle (IGFCC) fuelled by MSW through numerical modelling techniques and based on First Law energy conservation. Beyond this and as an ambitious contribution to knowledge this research will look to expand the original process design taking into account the real world application of these plants as well as future aspects that are already affecting the global energy market.

AIMS

- The overall aim of this project will be to develop a numerical model(s) with the aim to understand the flow of energy throughout the proposed IGFCC system whilst operating under varying inputs and against realistic market dynamics.
- To quantify the economic return of investment using different market economics.
- In terms of scaling an important result to come from modelling will be to size the energy storage facility. This will be affected by a number of factors such as; fuel cell size, upper and lower fuel cell H_2 limits, waste composition fluctuations, maintenance downtime and also the price of wholesale electricity.
- As a numerical model primarily based on first principles the model must have the flexibility to utilise any values obtained through experimental work done in the laboratory.
- A fundamental aim will be to quantify the environmental impact and CO_2 savings of the facility compared to existing energy sources.
- The feasibility of the added process of hydrogen production and storage will be measured as it could prove to be a solution to some of the issues facing these IGFCC systems.
- To understand the dynamic behaviour of the various energy systems and how their integration performs against expected performance.

OBJECTIVES

This thesis aims to demonstrate, through numerical modelling, the operation of an IGFCC at district scale (MW) whilst implementing various strategies that deal with current external influences impacting operational and financial performance of the plant. Some of the questions to be answered include:

- With the integration of current gasification technologies with fuel cell and GT systems, along with the ancillary equipment needed for them to operate, can the plant exceed 25% electrical efficiency?
- How will variations in the waste composition affect the performance of the plant?
- Understanding the thermal sensitivity of SOFCs how will the thermal performance of the fuel cell deal with the low hydrogen concentrations, and will the exothermic reaction be able to maintain the required operating temperature?
- In terms of plant performance how important will the implementation of large scale hydrogen storage be and can the plant feasibly produce enough hydrogen to maintain the hydrogen storage strategy?
- Using the available laboratory facilities test the fuel cell's tolerance to tar coming from the gasifier, and what can be done to prevent cell degradation?
- Taking into account the fluctuations of the wholesale electricity market is it feasible to build such systems?
- Can such WtE systems provide meaningful reductions in CO_2 emissions thereby helping the UK meet the 2050 carbon dioxide reduction targets?
- Can it be economically viable to use electricity (produced onsite) to generate hydrogen as opposed to selling it to the grid during periods of low market demand?
- Can these systems be implemented in an urban and/or industrial contexts allowing heat from the plant to be exploited as a combined heat and power supplier?
- Can combined heat and power units provide substantial CO_2 savings whilst being financially attractive?
- How much heat and power will be available for a plant scaled to treat 100,000 tonnes of MSW per year (based on existing commercial plant size[APP, 2012]), and how many houses will this supply?
- Can WtE systems support the EU's waste hierarchy?

THE WASTE, HYDROGEN, HEAT AND ELECTRICITY (WHHE) CONCEPT

This concept and research relies on the successful integration of proven cutting-edge fuel processing, energy production and energy storage technology in a new and innovative manner to achieve a highly efficient and flexible decentralized energy system for the building industry. These technologies include: thermal plasma gasification, gas filtering, hybrid fuel cell/heat engine combined cycle, hydrogen production (electrolysis), hydrogen storage (nanostructured high capacity metal hydrides), enhanced heat exchange and effective thermal management systems, *Figure (ES) 3*. This system represents an ambitious step in the direction of energy decarbonisation and security by providing decentralised clean and efficient energy centres for the long term, comprehensive management of heat, electricity, hydrogen and waste.

WHHE Energy Centres support four key areas:

1. Ultra clean waste disposal and high efficiency energy recovery.
2. High efficiency hydrogen production to supply infrastructure for local clean vehicles.
3. Waste heat energy supply to boost the uptake of intelligent thermal energy networks which efficiently exchange heat between local buildings.
4. Local high efficiency electricity production and management to maximise local decentralised renewable energy penetration and enable a low-carbon, flexible, smart electrical grid.

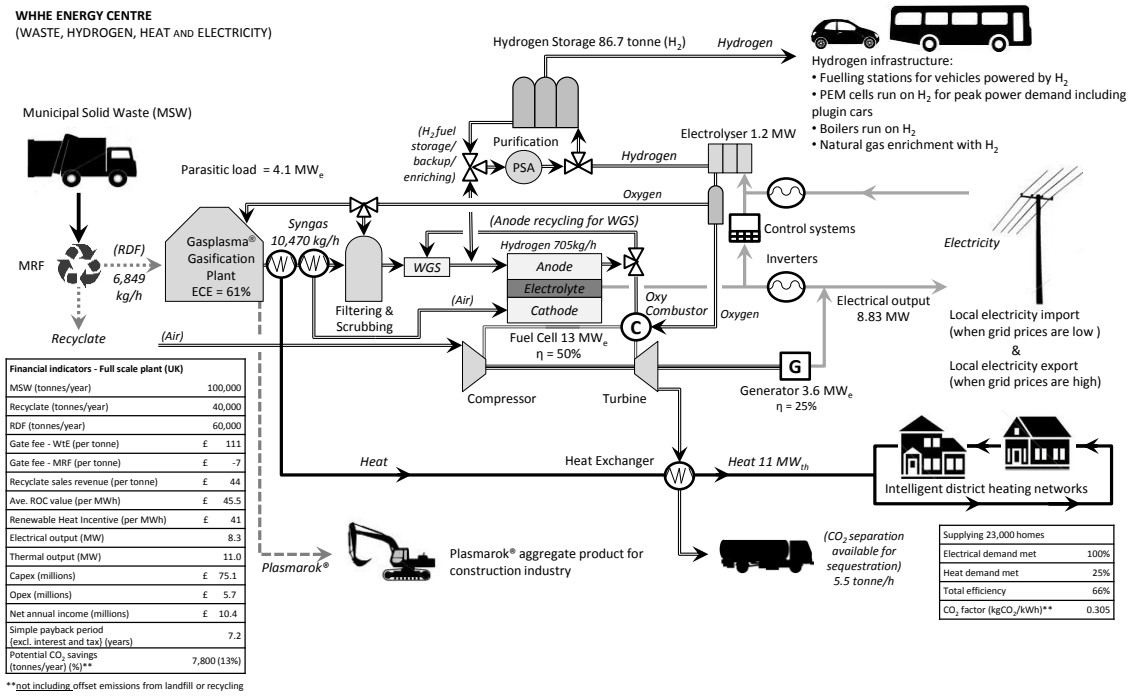

Figure (ES) 3: Schematic of a Dual fluidised bed/plasma gasification, hydrogen storage, SOFC/GT hybrid system.

Benefits of the system include:

- To produce energy from waste more efficiently, and with the inclusion of hydrogen storage more profitably.
- Waste-to-energy sites can be cleaner, smaller and located more centrally, offering district heating opportunities.
- Hydrogen infrastructure can be introduced into the built environment.
- District heating infrastructure can be introduced into the built environment.
- High efficiency electricity production and flexibility can be introduced into the grid.
- Increased grid penetration of renewables facilitated by hydrogen storage.
- MSW could be enriched by locally sourced biomass.
- Land reclamation as landfill sites can be mined and cleaned-up.
- Promote recycling through the recovery of material prior to gasification.
- Commerciality driven by income from gate fees, renewable obligation certificates and other incentives such as the UK's renewable heat incentive.

Challenges include:

- Filtration and purification of gases can be costly and energy intensive and if not designed to account for the whole life cycle will merely transfer the environmental threat to another medium.
- WtE plants are not well understood and accepted by the general public and the challenge will be to make these systems unobtrusive whilst overcoming public perception.
- In terms of energy storage the challenge will be to design a solution that flexible to the dynamics of the power grid whilst being technically, economically and financially feasible.
- There is much uncertaintity surrounding the future of a hydrogen economy and many of components being investigated will rely technical maturity of hydrogen systems as well as the ecomony of scale that follows. As a source of renewable hydrogen a hydrogen economy would also maximise the potential of the WtE being investigated.
- The success and overall benefit of this system will rely on supplying heat in standard CHP heat networks which will require more interest and implementation in local communities.

METHODOLOGY

As an overview, this research and proposed system advances the state-of-the-art of energy management centres by:

1. Modelling a state-of-the-art 2-stage plasma gasification process to meet the required gas purity via the introduction of a bespoke filtering gas processing design to deal with contaminants and to increase the hydrogen yield.
2. Including a state-of-the-art solid-oxide fuel cell (SOFC) operating on syngas.
3. Introducing a combined cycle heat engine to boost electrical efficiencies to >25%.
4. Introducing an electrolyser to allow the SOFC to run at continuous optimum conditions and the system to operate in multiple modes, e.g. to import/export electricity in order to take advantage of the frequent/large grid price fluctuations and introduce precious flexibility into the grid.
5. Utilising state-of-the-art high efficiency solid state hydrogen storage materials and system for use with the PSA and electrolyser. Gravimetric energy density is less of a concern for stationary applications as volume is much more at a premium than weight. Furthermore, low pressure storage is preferred due to reasons of system safety and lower costs for compression.
6. Create state-of-the-art mathematical models, such as dynamic simulations, in order to optimise the system at end-user scales - which include intelligent district heating networks.

This research is timely and a similar system is already being trialled in Korea. In October 2011, Ballard & GS Platech's South Korean Waste-to-Energy Fuel Cell Plant was commissioned to demonstrate a plasma gasification waste-to-energy plant which uses a 50kW PEM fuel cell system to supply power to the local Cheongsong grid. Although this system is similar, its gas clean-up is much more costly and space consuming than that of a WHHE Energy Centre which uses a more robust (and more efficient) SOFC combined cycle. In addition, it would be less flexible than the WHHE Energy Centre which is able to dynamically interact with the grid (via the hydrogen storage system) in order to benefit commercially from the variations in wholesale electricity prices.

MODEL DEVELOPMENT

In this research Simulink®, which is an interactive graphical block programming tool that integrates with MatLab®, is used to carry out selective modelling of several of the energy processes. The algorithms used to describe the various processes are based on static and dynamic equations that are either derived from experimental results or obtained through literature.

For those processes where Simulink modelling is not best suited ChemCad has been used. ChemCad is ideally suited to modelling of the chemical processes such as gasification, gas filtration and separation, and heat management.

SYSTEM BOUNDARIES

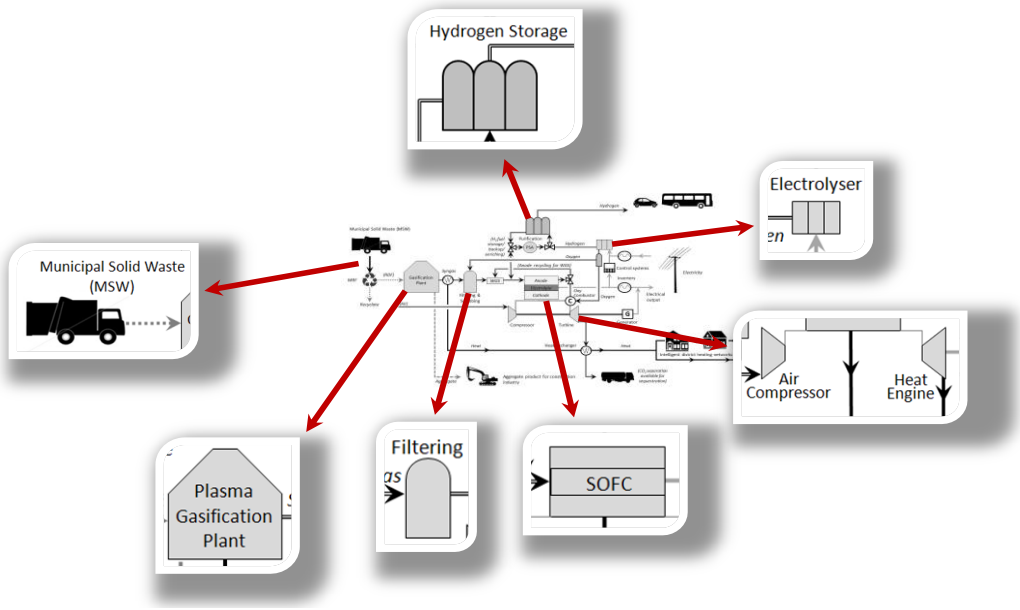

Figure (ES) 4: Highlighting of system boundaries identified for modelling.

MATHEMATICAL DESCRIPTORS

SIMULINK MODELLING

- **SOFC**

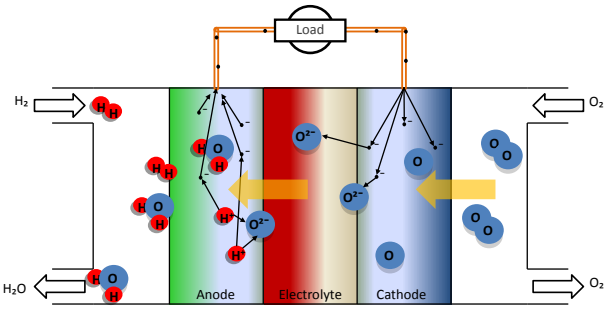

Figure (ES) 5: Transport process within a SOFC.

The simulation of the SOFC offers the greatest challenge as their operation in such systems is relatively unknown and uncertain. Therefore modelling of the SOFC goes into much more details than the remaining systems and the complexity of the approach is well suited to the functionality and capabilities of Simulink's modelling environment.

The performance of the SOFC is defined by the Nernst equations which describes the reversible voltage as a function of the partial pressure of product (H_2O) and the reactants (H_2, O_2):

$$E = E^o + \frac{RT}{nF} ln\left[\left(\frac{p_{H_2}}{p_{H_2O}}\right)\left(\frac{p_{O_2}}{p_0}\right)^{1/2}\right]$$

Therefore, in order to accurately simulate the interaction of the various gases, introduced via the syngas composition, mass transport calculations are carried out for Knudsen, ordinary and effective diffusion coefficients which are applied to the Maxwell-Stefan diffusion model for binary mixtures. The Maxwell-Stefan model is then manipulated to calculate the partial pressures to be used in the Nernst equation (*Nehrir et al., 2009*):

$$p^*_{H_2} = p_{ch,H_2} - \frac{jRTt_a}{2FD_{H_2,H_2O}};$$

$$p^*_{H_2O} = p_{ch,H_2O} + \frac{jRTt_a}{2FD_{H_2,H_2O}};$$

$$p^*_{O_2} = P_{ch,c} - \left(P_{ch,c} - p_{ch,O_2}\right)\exp\left(\frac{jRTt_c}{4FP_{ch,c}D_{O_2,N_2}}\right)$$

Losses at the fuel cell come from; activation losses (activation energy required to overcome the charge double layer), concentration losses (restricted transportation of reactants and products to/from the reaction site), and ohmic losses (losses due to resistance – imperfect conduction).

Activation losses are calculated using the cell's current density and exchange current density:

$$\eta_{act} = \frac{RT}{\alpha nF} log\left(\frac{j}{j_0}\right)$$

Where the exchange current density is calculated according to the Arrhenius law - which is again a function of the partial pressures of the product and reactants at the anode and cathode:

$$j_{0,an} = \gamma_{an}\left(\frac{p_{H_2}}{P_{ref}}\right)\left(\frac{p_{H_2O}}{P_{ref}}\right)\exp\left(-\frac{E_{act,an}}{RT}\right)$$

$$j_{0,cat} = \gamma_{cat}\left(\frac{p_{O_2}}{P_{ref}}\right)^{0.25}\exp\left(-\frac{E_{act,cat}}{RT}\right)$$

Concentration losses are most noticeable at high current densities where the cell is starved from insufficient reactants reaching the reaction site, and where the product is struggling to move away from the reaction site. Therefore, by manipulating the Nernst equation the concentration losses can be defined by a limiting current density:

$$\eta_{conc} = \frac{RT}{nF}\ln\frac{j_L}{j_L - j}$$

where

$$j_L = nFD_{ij,eff}\frac{c_R^0}{t}$$

Lastly, ohmic losses are dependent on geometry which is why the fuel cell's resistance is often normalised by area and known as the area-specific resistance (ASR). Combined ASR values for cell components should not exceed 0.5 $\Omega\, cm^2$ and ideally would be ca.0.1 Ωcm^2 (*Steele et al., 2001*):

$$\eta_{ohmic} = j(ASR_{ohmic})$$

where

$$ASR = \frac{L}{\sigma}$$

and

$$\sigma_0 = A_{SOFC}e^{-\Delta G_{act}/RT}$$

where A_{SOFC} is derived from the Nernst-Einstein equation for conducitivity (*refer to Section 5.6.5 for further explanation*) and is dependant on the electrolyte material:

$$A_{SOFC} = \frac{c(zF)^2 D_0}{RT}$$

- **HEAT TRANSFER**

Heat transfer within the fuel cell is carried out by means of; convection, radiation and mass flow. Based on the conservation of energy the heat is generated from the electrochemical reaction and the total heat balance can be defined as:

$$\dot{q}_{in} = \dot{q}_{gen} = \dot{q}_{chem} - \dot{q}_{elec}$$
$$\dot{q}_{out} = \dot{q}_{rad} + \dot{q}_{conv} + \dot{q}_{flow}$$
$$\therefore \dot{q}_{net} = \dot{q}_{in} - \dot{q}_{out} = m_{cell} c_{cell} \frac{\mathrm{d}T_{cell}}{\mathrm{d}t}$$

where

$$\dot{q}_{chem} = \dot{n}_{H_2,consumed} . \Delta H$$
$$\dot{q}_{elec} = V_{out} . i$$
$$\dot{q}_{rad} = \varepsilon \sigma A (T_{hot}^4 - T_{cold}^4)$$
$$\dot{q}_{conv} = hA(T_{hot} - T_{cold})$$
$$\dot{q}_{flow} = \sum_i n_i \, C_{p,i} \left(\frac{dT}{dt}\right)$$

- **GAS TURBINE**

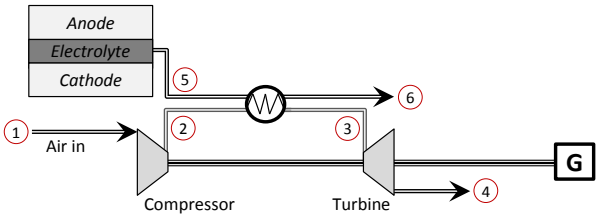

Figure (ES) 6: Unpressurised SOFC-GT hybrid configuration.

Gas turbine (GT) theory and modelling is very mature so derivation into Simulink is straight forward. *Figure (ES) 6* illustrates how the GT is implemented making use of heat from the fuel cell to charge the compressed air coming from the compressor via a heat exchanger.

The thermodynamic expression for the change in temperature for a given pressure ratio and isentropic efficiency is given by:

$$T_{02} - T_{01} = \frac{T_{01}}{\eta_c} \left[\left(\frac{p_{02}}{p_{01}} \right)^{(\gamma-1)/\gamma} - 1 \right]$$

Where γ is the ratio of specific heats for the fluid – in this case air.

Similarly for the turbine:

$$T_{03} - T_{04} = \eta_t T_{03} \left[1 - \left(\frac{1}{p_{03}/p_{04}} \right)^{(\gamma-1)/\gamma} \right]$$

The power generated after the energy required to drive the compressor is deducted using:

$$\therefore \dot{W}_{net} = \dot{W}_{tur} - \dot{W}_{com}$$
$$\Longrightarrow \dot{W} = \dot{m} c_p \Delta T$$

- **ELECTROLYSER**

Electrolysis is the function of a fuel cell working in reverse. By passing a current between two electrodes separated by an electrolyte we are able to decompose water into its elementary components H_2 and O_2.

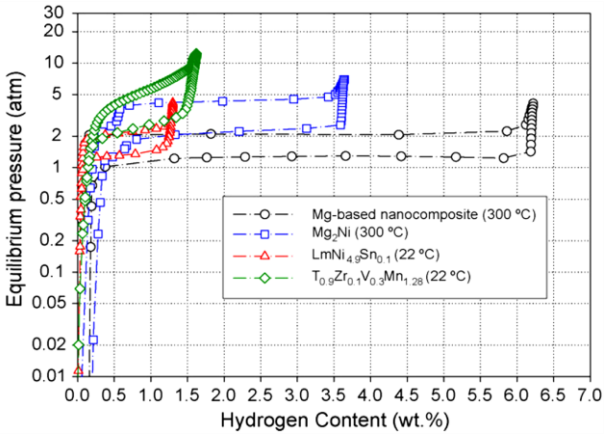

Figure (ES) 7: Pressure-composition isotherms of different types of metal hydrides showing Mg-based nanocomposites offer higher energy densities at lower pressures (*Dehouche et al., 2008*).

According to Faraday's law the production of hydrogen is directly proportional to the amount of current provided (*Uzunoglu et al., 2009; Ural et al., 2013*):

$$\dot{n}_{H_2} = \eta_F \frac{i_e}{2F}$$

Where η_F is the Faraday efficiency which is the ratio between the theoretical and actual maximum amount of hydrogen produced by the electrolyser, and i_e is the electrolyser current (A). The Faraday efficiency (η_F) can be derived as (*Uzunoglu et al., 2009; Ural et al., 2013*):

$$\eta_F = \frac{j^2}{f_1 + j^2} f_2$$

Where j is the current density (A/m^2), and f_1 and f_2 are coefficients derived from experimental results and vary linearly with temperature (*Ulleberg, 2003*).

Table (ES) 1: Faraday efficiency coefficients (Ulleberg, 2003).

T (C°)	40	60	80
f_1	150	200	250
f_2	0.990	0.985	0.980

- **HYDROGEN STORAGE**

The potential to store hydrogen in solid state hydrogen storage containers commonly uses hydride materials consisting of binary, ternary, or quaternary hydride compounds. The reaction of hydrogen with these metallic compounds involves changes in enthalpy with absorption being exothermic and desorption endothermic. The change in free energy in a gas compressed isothermally can be expressed as:

$$\Delta G = RT \ln \frac{p}{p_0}$$

When considering the various materials available the materials used in current commercial applications are magnesium based (MgH_2). MgH_2 presents advantages of high storage capacity by weight (7.6% H-wt% [*de Rango et al., 2007*]), and materials are abundant and cheap. However,

disadvantages are that magnesium based materials have slow sorption kinetics and high thermodynamic stability ranges therefore requiring higher temperatures for desorption. The high temperatures required for desorption is not a major factor for this research as there is an abundant supply of high grade heat (>350°C) supplied by both the GT and fuel cell. Therefore, the application of magnesium based hydrogen storage is well suited. The storage capacity will be limited by the amount of heat available above the operating temperature for desorption, but must be large enough to cover scheduled maintenance of the gasifier. Absorption can be carried out at ambient conditions but because of the exothermic nature of the reaction energy for cooling will be required to maintain the absorption kinetics. Therefore, in order to identify the amount of heat required to be removed and provided during absorption and desorption the enthalpy of formation is required. Typical values of the reaction enthalpy for MgH_2 is 37.5kJ/(mol H_2) (*Dornheim, 2011; Zhong et al., 2011*). Therefore, for simulation purposes a value of 37.5 MJ/(kg H_2) has been used to calculate the required heat transfer. Absorption takes place at 2bar and 30°C and desorption will take place at atmospheric pressure and 320°C. *Figure (ES) 7* illustrates the absorption and desorption characteristics of Mg-based nanocomposite materials operating at 300°C and near atmospheric pressure. *Figure (ES) 7* also shows that magnesium based metal hydrides show favourable energy densities when compared to other metal hydrides (*Dehouche et al., 2008*).

From this information the heat transfer to and from the hydrogen unit can be calculated via:

$$Q = mC_p\Delta T$$

Isolating the required mass flow results in:

For cooling $$\dot{m}_{air} = \frac{\dot{m}_{H_2}37.5\times10^3}{C_{p_{air}}(303-T_{amb})}$$

For heating $$\dot{m}_{hot} = \frac{\dot{m}_{H_2}37.5\times10^3}{C_{p_{hot}}(T_{hot}-593)}$$

- **OXY COMBUSTOR**

The exhaust gas leaving the fuel cell will still contain unutilised fuel in the form of H_2 and CO. So, in order to capture this remaining energy a combustion chamber is used to oxidise the remaining fuel; thereby increasing the turbine inlet temperature.

It must be assumed that the combustion is complete, therefore having a complete conversion of H_2 to H_2O, and CO to CO_2, enabling us to calculate the molar quantities after combustion. The simplest method of calculating the adiabatic flame temperature is to use a constant average C_p (*McAllister et al., 2011*):

$$T_P \approx T_R + \frac{-Q^0_{rxn,p}}{\sum_i n_{i,P}C_{pi}}$$

where

$$-Q^0_{rxn,p} = \sum_i n_{i,R}\Delta\hat{h}^0_{i,R} - \sum_i n_{i,P}\Delta\hat{h}^0_{i,P}$$

CHEMCAD MODELLING

- **GASIFICATION**

Using ChemCAD to model gasification equilibrium reactions are calculated by Gibbs free energy minimisation using a GIBs UnitOp. The equation calculating the change in Gibbs free energy where the equilibrium constant is used is known as the van't Hoff isotherm:

$$\Delta G = -RT \ln K_e$$

ΔG is used to measure how far a given reaction is away from equilibrium. If ΔG is large and negative the reaction is spontaneous, and far from equilibrium. Therefore only when $\Delta G = 0$ will a position of equilibrium be found.

Calculations for gasification are based on thermodynamics, mass and energy flow, operating conditions (temperature and pressure), and the addition or subtraction of indirect heat. Therefore in order simulate the gasification of MSW the ultimate analysis of the feedstock is required. For MSW the following information has been found in literature [*Table (ES) 2*]:

Table (ES) 2: Ultimate analysis of various sources of MSW within the UK.

	MSW (*CIWM, 2003*)	**MSW** (*Ricketts et al., 2002*)	**RDF** (*Ricketts et al., 2002*)	**MSW** (*Optimat Ltd., 2001*)	**MSW** (*Ray et al., 2012*)	**RDF** (*Davidson R., 1999*)
Ultimate analysis, wt%						
C	24.0%	22.2%	54.5%	22.1%	43.0%	28.3%
H	3.2%	3.2%	7.6%	3.2%	5.6%	4.2%
O	15.9%	14.2%	20.5%	14.2%	26.6%	24.3%
N	0.7%	0.6%	0.7%	0.6%	0.6%	0.6%
S	0.1%	0.1%	0.2%	0.1%	0.3%	0.3%
Cl	0.7%	0.6%	0.8%	0.6%	0.3%	0.0%
Si (Ash)	24.2%	27.8%	11.7%	27.8%	12.1%	11.6%
Moisture	31.2%	31.4%	4.1%	31.4%	11.5%	30.7%
HHV/**LHV** (MJ/kg)	**10.6**	9.4	23.5	9.39	21.0 **(dry)**	11.17

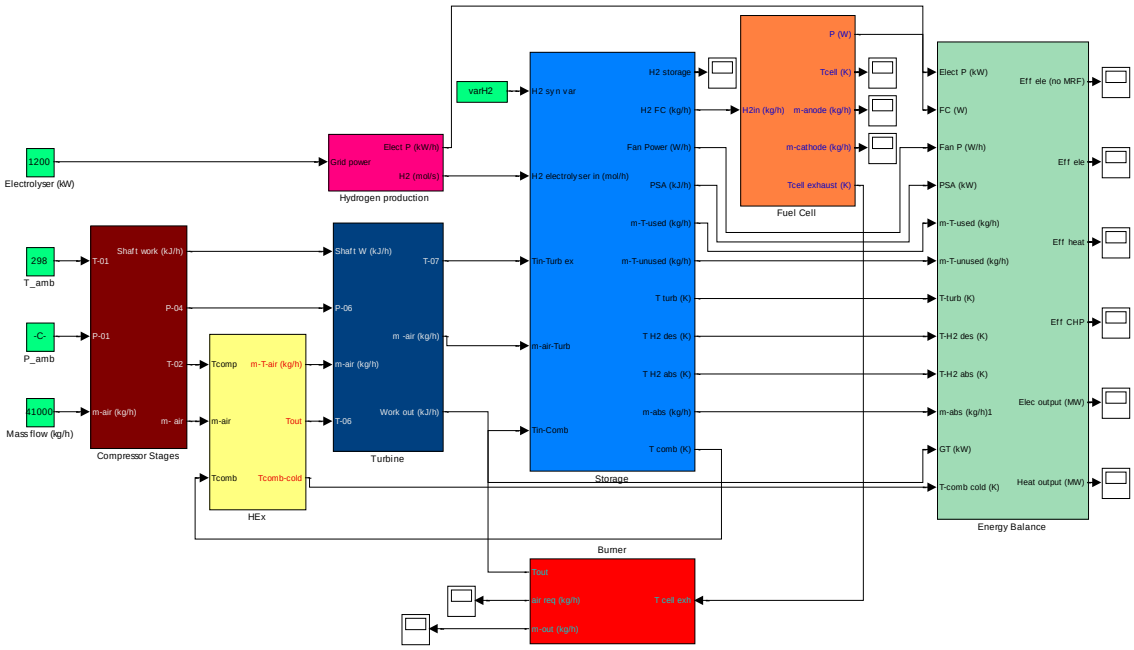

Figure (ES) 8: Complete Simulink model showing GT, SOFC, hydrogen storage, electrolyser, oxy combustor and energy balance subsystems.

- **GASIFICATION OPERATION**

As mentioned previously, the gasifier has a number of variables to consider during operation all of which have an effect on the performance of the gasifier and the quality of the syngas produced. The most important aspects to look at are:

STOICHIOMETRIC OXYGEN RATIO (λ):

$$\lambda = \frac{external\ O_2\ supply/fuel\ supply}{stoichiometric\ O_2\ requirement/unit\ of\ fuel\ input}$$

STEAM-TO-BIOMASS RATIO (SB):

$$SB = \frac{steam\ mass\ flow}{fuel\ feed\ flow}$$

MODIFIED STEAM-TO-BIOMASS RATIO (SB*):

$$SB^* = \frac{steam\ mass\ flow + fuel\ moisture\ mass\ flow}{dry, ash - free\ fuel\ feed\ flow}$$

ENERGY CONVERSION EFFICIENCY (ECE):

$$ECE = \frac{net\ energy\ content\ of\ the\ syngas\ [MW]}{net\ energy\ content\ of\ the\ input\ fuel\ [MW]}$$

CARBON CONVERSION EFFICIENCY (CCE):

$$CCE = \left(1 - \frac{carbon\ content\ of\ residue\ [kmol/h]}{carbon\ content\ of\ input\ fuel\ [kmol/h]}\right)$$

The stoichiometric oxygen ratio (also called equivalence ratio) is used to identify different oxidation approaches as λ=1 refers to combustion, λ=0 refers to pyrolysis, and $0 < \lambda < 1$ represents gasification. Exothermic oxidation is also used to control the operating temperature of the reactor so whilst very low λ values will generate high yields of hydrogen and carbon monoxide greater levels of oxygen are required to maintain the required operating temperature to sustain the gasification process. Typical λ values used in fluidised bed gasification vary between 0.2 and 0.4 (*Siedlecki et al., 2011; Chapman et al., 2010*).

Although the most common fluidisation/moderator and oxidation medium used for gasification is air high levels of nitrogen within the product gas will significantly lower the heating value of the gas. Therefore it is more beneficial to use a combination of oxygen and steam as steam can contribute to the quality of the syngas.

This leads to the significance of knowing the moisture content and to expand to the modified steam-to-biomass ratio (SB*) as controlling the potential steam content will influence the carbon conversion efficiency, energy conversion efficiency, and heating value of the syngas (values for SB between 0.3 and 1.0 have shown to have a positive effect on these factors)(*Siedlecki et al., 2011*).

The plasma converter is modelled by assuming a fixed operating temperature which is required to breakdown the tar contaminants. The electrical power required to maintain the thermal plasma reactor temperature is derived from literature (*Materazzi et al., 2013b*).

- **GAS FILTERING AND PROCESSING**

The modelling of the gas filtering and processing encompasses the ASU, ceramic hot gas filtering using sodium bicarbonate, high temperature and low temperature shift reactions, and desulphurisation using Selexol™.

- **AIR SEPARATION UNIT**

Although the plant will benefit from a supply of pure oxygen from the electrolyser the ASU will have to be scaled to meet peak demand in order to cover periods where the electrolyser will not be operating. Because the proposed system is not technically sensitive to the inclusion of nitrogen, and because the size of the plant is relatively small, oxygen purification has been modelled using PSA theory.

- **HOT GAS FILTERING**

To simulate the influence of sodium bicarbonate in the ceramic gas filtering process an equilibrium reactor is used to simulate the following reactions:

$$NaHCO_3 + HCl \longrightarrow NaCl + H_2O + CO_2$$

$$2NaHCO_3 + SO_2 + \frac{1}{2}O_2 \longrightarrow Na_2SO_4 + 2CO_2 + H_2O$$

The syngas from the gasifier must be cooled before entering the hot gas filtration unit so a heat exchanger is used to control the inlet temperature using air, this air will be used at the inlet to the fuel cell cathode. To simulate the removal of the solid build-up on the filters a solid separation unit is used to remove the salts formed.

- **HIGH AND LOW TEMPERATURE SHIFT REACTIONS**

Simulation of the high and low temperature shift reactions is carried out using predefined shift equilibrium reactors where reactions are allowed to be carried out adiabatically. The purpose of using two reactors at high and low temperatures is to maximise the hydrogen yield by using various catalysts which are sensitive to temperature (*Byun at al., 2011*). The cooling fluid used to recover and control the temperatures before and after the various reactors is water. Water is inlet to both shift reactors but in the case of the high temperature reactor a heat exchanger is used as a steam generator for the incoming water which serves to control the reactor temperature. Conversely water is directly fed into the low temperature reactor in order to keep the reactor temperature down.

- **DESULPHURISATION**

Simulation of Selexol™ adsorption is carried out using a standard distillation column operating at elevated pressures and near ambient temperatures. The syngas is compressed and cooled before entering the bottom of the adsorption tower. The filtered syngas then exits from the top of the column where the gas is flashed back to ambient temperature. The Selexol™, rich in H_2S, CO_2 and some COS, is pumped from the adsorption column to a secondary column for regeneration where contaminants desorb from the Selexol™. Regeneration is carried out at a lower pressure and higher temperature than adsorption. The lean Selexol™ is then recycled back to the adsorption column to continue the cycle.

The recovered H_2S, CO_2 and COS can then be sent to a Claus reactor to produce elemental sulphur from the contaminants.

Figure (ES) 9 shows the complete ChemCad design showing the various process boundaries and fluid flows.

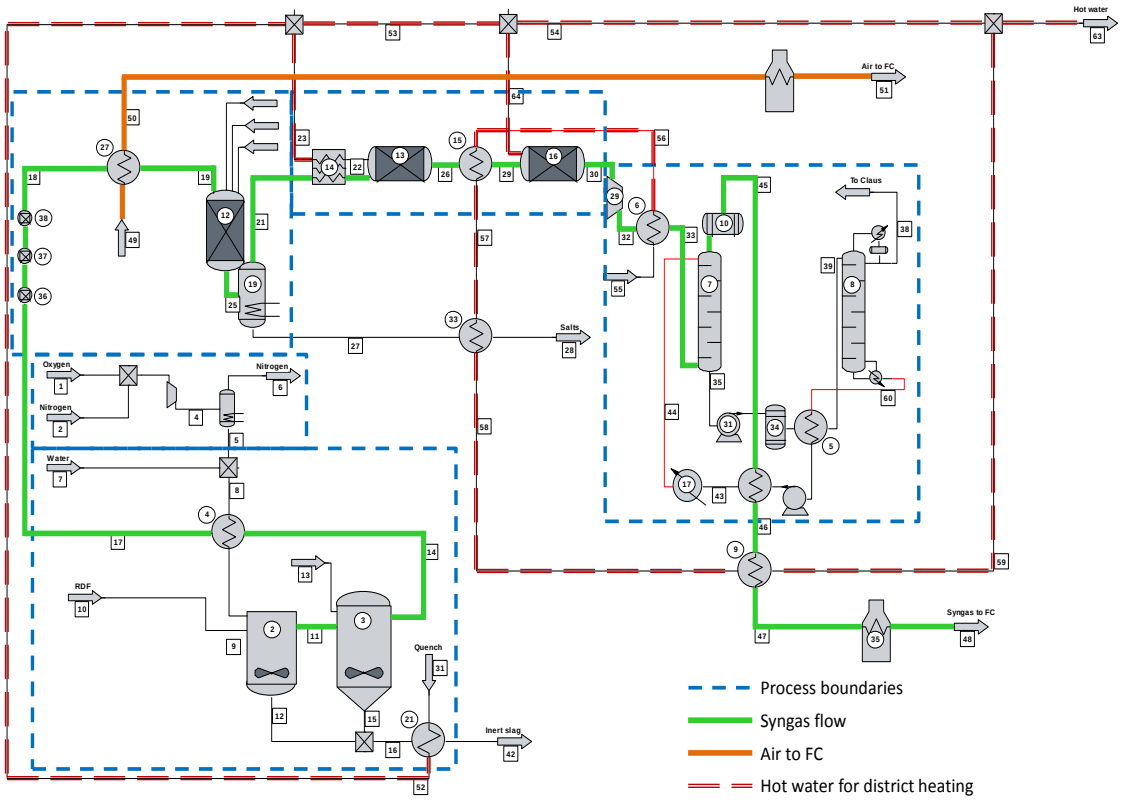

Figure (ES) 9: Illustration of the Chemcad user interface showing the various UnitOps. Various processes have been highlighted using boundary lines and the flows of syngas, hot air and hot water have been highlighted.

- **FUEL DYNAMICS**

The composition of waste is never fixed and understanding these variations can be very important for waste management planning. There is a number of factors that contribute to these variations and they include; seasonal variations, different regional areas, cultural and ethnic diversity, socio-economic profile, urban context and many other factors that influence consumer trends (*EB Nationwide, 2004; NWRWMG, 2010; Jones et al., 2008*).

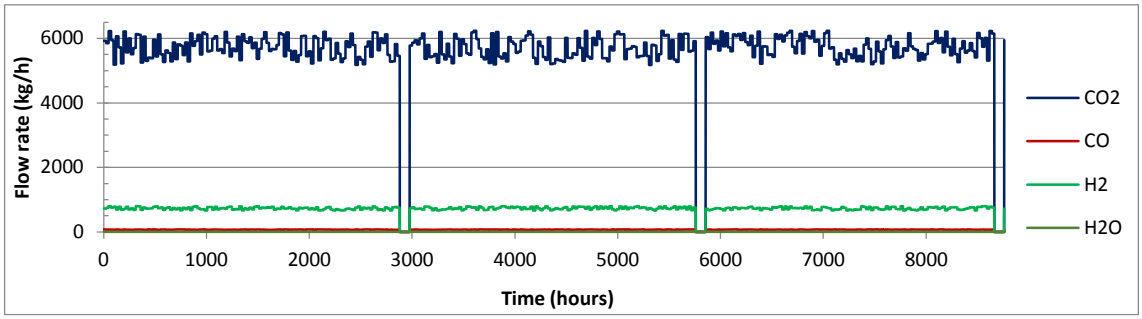

Figure (ES) 10: Variations in syngas composition including three 4 day maintenance periods.

To take this into account the variation of the waste composition (and subsequent syngas) variations have been added to the results obtained from ChemCad. For simplification variations are made every 24 hours and as seen in *Figure (ES) 10* the scheduled maintenance periods over the year have been simulated using three 4 day breaks of no fuel.

The operating strategy also calls for a reliable supply of hydrogen to the fuel cell meaning an upper and lower limit (shown in *Figure (ES) 11*) must be set for the amount of hydrogen sent to the fuel cell. The excess hydrogen above the upper threshold must then be sent for storage whilst deficiencies must be buoyed by hydrogen coming from storage. This includes maintenance periods where the hydrogen storage must provide the minimum required amount of hydrogen to keep the fuel cell operational (i.e. to prevent the fuel cell from cooling).

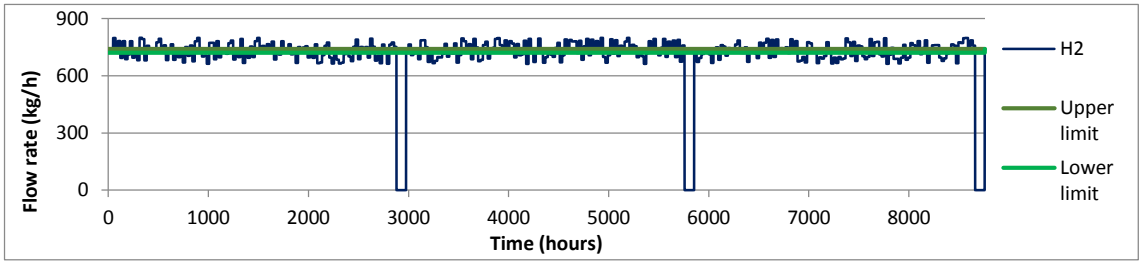

Figure (ES) 11: Upper and lower limit showing excesses and deficiencies coming from the variations in the syngas.

RESULTS

The WHHE Energy Centre is sized to handle 100,000 tonnes/year of MSW, of which 40% will be recycled with the remaining 60% converted to RDF. Outputs from the centre will be; electricity, hydrogen, inert slag (aggregate), NaCl (kitchen salt), Na_2SO_4 (sodium salt used as detergent filler), H_2S and COS (and finally elemental sulphur), CO_2 (available for sequestration), hot air (for the fuel cell), and hot water (<100°C) to be used in district heating.

- **GASIFICATION AND FILTRATION**

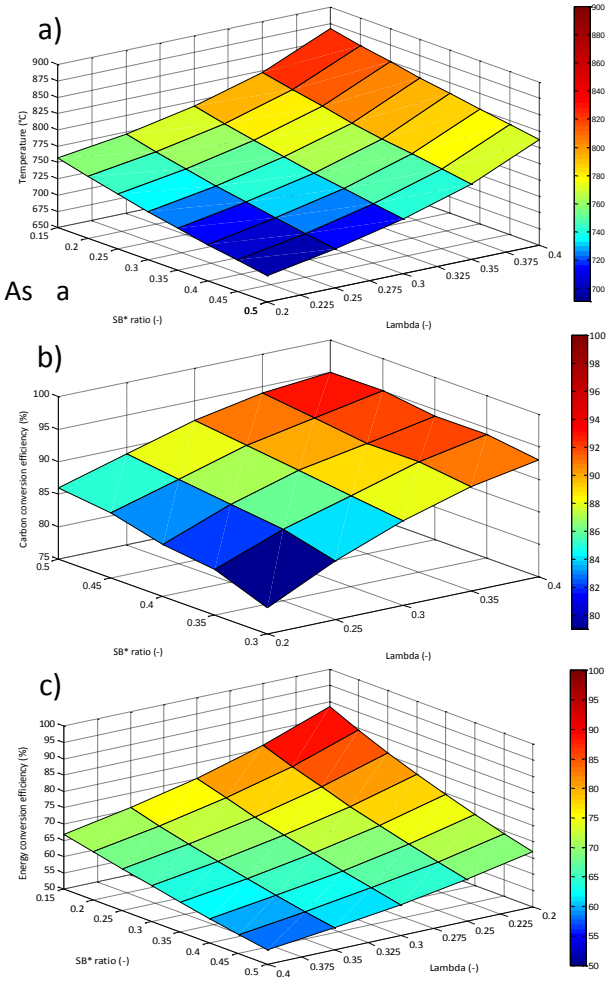

Figure (ES) 12: 3D surface plot showing a) temperature according to λ and SB*, b) the CCE according to λ and SB* when operating at 850°C, and c) ECE according to λ and SB*.

By plotting temperature, carbon conversion efficiency and energy conversion efficiency as a function of SB* and λ using 3-D surface plots it is possible to select a moisture level and oxygen flow rate that can provide syngas at the required quality and efficiency.

As a result the selected values for λ and SB* are 0.35 and 0.2 respectively producing the following syngas composition at 816°C [*Table (ES) 3*]:

Table (ES) 3: Molar % of syngas coming from the gasifier at 816°C.

Heating values (60 F)	
Gross kJ/kg	1.098E+004
Net kJ/kg	9644.
Component mole %	
Hydrogen	38.833204
Methane	0.037993
Carbon Monoxide	31.395420
Carbon Dioxide	12.924461
Water	16.076790
Oxygen	0.000000
Nitrogen	0.325323
Benzene	0.000000
Toluene	0.000000
Hydrogen Chlorid	0.146969
Sulfur Dioxide	0.000000
Nitrogen Dioxide	0.000000
Hydrogen Sulfide	0.117369

The inert slag being produced at a rate of 929kg/h is quenched in water where heat is captured through a heat exchanger and serves to supply the water demands of the high and low temperature shift reactors before being exported via the district heating network.

Before the syngas can be filtered through the ceramic hot gas filtration unit it must be cooled to ca. 450°C, and because of the high grade heat (>1100°C) available this is an excellent opportunity to preheat the air required by the fuel cell. At the ceramic filter the gas is injected with sodium

bicarbonate which converts the HCl and SO_2 to valuable NaCl (table salt) and Na_2SO_4 (detergent filler material). The solid materials are removed from the gas where the salts can be extracted and sold.

Results from the high and low temperature shift reactions show a 30% increase in H_2 as a result of the high temperature shift reactor, and a 55% increase from the low temperature shift giving a total increase of 103%.

From the low temperature shift the gas is then compressed and cooled in preparation for desulphurisation. The Selexol™ adsorbent then extracts H_2S, COS, CO_2, N_2 and a small amount of H_2 at high pressure (40bar) and near ambient temperature in a 20 stage distillation column. The rich Selexol™ is then pumped to a secondary 6 stage distillation column that includes a condenser and reboiler. Before entering the secondary column the pressure of the Selexol™ is dropped to 6.9bar and heated to 125°C. The column itself operates at ambient pressure and the distillate temperature for condensing is 100°C and the reboiler recycles the now lean Selexol™ from the bottom of the column at 150°C. Before being recycled back to the first column the Selexol™ must be cooled to -6°C. Much of this is done by heating the purified syngas as it leaves the first column as the gas experiences a drop in temperature when expanding from 40bar to ambient pressure. The remaining cooling is carried out through a refrigeration cycle which will add to the parasitic load.

Table (ES) 4 provides a complete breakdown of contaminants and the level of purification achieved.

Table (ES) 4: Composition of the syngas entering and exiting the desulphurisation cycle showing the reduction in contaminants.

Compound	Syngas in kg/h	Syngas out kg/h	Reduction (%)
H_2	737.216	731.379	0.8%
CH_4	0.0036	0.0033	8.3%
CO	73.142	71.509	2.2%
CO_2	10143.836	5708.770	43.7%
H_2O	1215.622	2.906	99.8%
O_2	0.0088	0.0084	4.5%
N_2	699.184	683.568	2.2%
HCl	0.0819	0.0354	56.8%
H_2S	20.826	0.901	95.7%
COS	1.761	0.0271	98.5%
NH_3	0.026	0.000	100.0%

Table (ES) 5: Review of ChemCad simulation results.

MSW feed-rate	6,849	kg/h
MSW LHV	15.7	MJ/kg
Lambda	0.35	(-)
SB*	0.2	(-)
Gasifier temperature	814	°C
ECE	61.4	%
CCE	76.9	%
Plasma temperature	1,200	°C
Hot gas filtering temperature	345	°C
Sodium bicarbonate flow rate	71.44	kg/h
Sodium chloride out flow rate	45.052	kg/h
Sodium sulfate out flow rate	0.155	kg/h
High temperature shift temperature	482	°C
Low temperature shift temperature	140	°C
Desulphurisation pressure	40	Bar
Desulphurisation temperature	14.7	°C
Regeneration pressure	1	Bar
Regeneration temperature	150	°C
CO_2 out	4,435.09	kg/h
H_2S out	19.92	kg/h
COS out	1.73	kg/h
H_2O out	1,212.72	kg/h
Heat recovery		
Water flow rate (@86°C)	7,320	kg/h
Air flow rate	24,000	kg/h
Purified Syngas Composition		
Total flow rate	6,976	kg/h
Gas composition	wt %	
H_2	10.16%	
CH_4	0.00%	
CO	0.99%	
CO_2	79.30%	
H_2O	0.04%	
O_2	0.00%	
N_2	9.50%	
C_6H_6	0.00%	
HCl	0.00%	
SO_2	0.00%	
NO_2	0.00%	
H_2S	0.01%	
NH_3	0.00%	

The syngas and air destined for the fuel cell may require heating as the exothermic reaction in the fuel cell may not be sufficient to maintain the required operating temperature. To do this auxiliary heaters have been used in ChemCad and results from the Matlab simulation will be used to determine the inlet temperatures required.

- **SOFC**

Using the mathematical descriptors j-V and efficiency curves have been generated to describe the overall performance of the fuel cell according to the annual fluctuations in the fuel supply and a hydrogen flow rate - between 702 - 707kg/h (shown in *Chapter 6*).

The variation in electrical efficiency fluctuates according the flow of hydrogen to the fuel cell and benefits when the fuel cell is supplied with pure hydrogen over the maintenance periods showing spikes above 55%. The efficiency curves follow the same pattern shown in the output cell voltage presented in *Figure (ES) 13*.

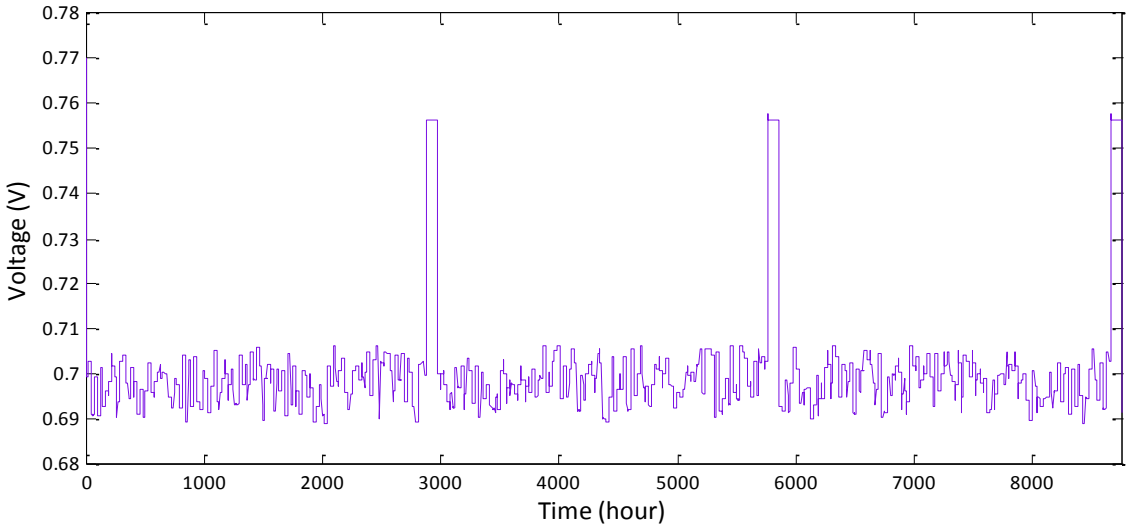

Figure (ES) 13: Variation in voltage according to variations in fuel supply. Increased voltage is seen during the maintenance periods as the supply of hydrogen is undiluted thereby providing higher partial pressures.

Figure (ES) 14 shows that by applying an inlet temperature of 760°C and by using the annual variation of the syngas composition the fuel cell will continue to operate close to its designated 850°C. *Figure (ES) 14* also shows sharp drops in temperature as the fuel composition changes during the scheduled maintenance periods. Further investigation shows these drops are mainly caused by the overall thermal conductivity (*k*) that increases over these periods causing greater heat transfer and hence greater heat removal.

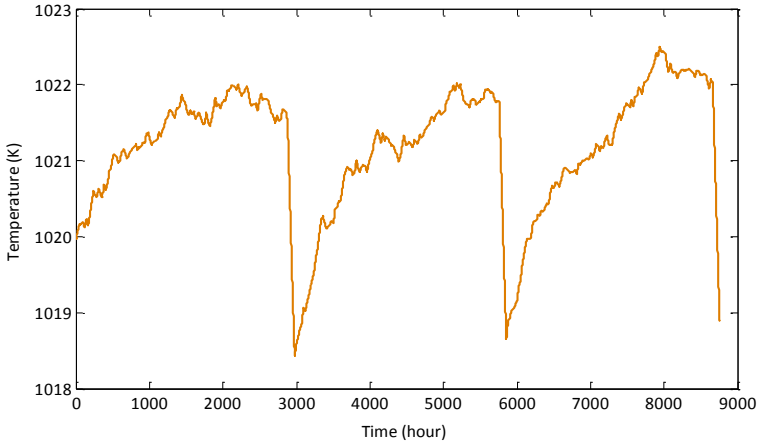

Figure (ES) 14: Cell temperature as a function of the annual syngas fluctuations whilst using an inlet temperature of 760°C.

- **HYDROGEN PRODUCTION AND STORAGE**

There are important aspects to consider when implementing hydrogen storage especially when scaled to cover the maintenance period of such a large system. Hydrogen is collected from excess coming from fluctuations in the syngas and from an electrolyser whose operation is controlled by the feasibility of the wholesale electricity price. This means the accumulation of hydrogen is determined by; the upper and lower hydrogen tolerance limits, feasibility threshold, and size of electrolyser. *Figure (ES) 15* shows the accumulation of hydrogen when relying purely on hydrogen from the syngas. *Figure (ES) 15* shows the hourly flow rate of hydrogen coming from the electrolyser sized at 1.2MW. In this scenario it is important to keep the feasibility ratio as low as possible as the hydrogen produced by the electrolyser includes losses from the fuel cell, electrolyser and eventually the hydrogen storage unit when considering the initial hydrogen coming from the syngas. This will become less of an issue as more renewable energy comes on line and the spot price of electricity comes down during periods where grid flexibility is required. This could be made easier by directly connecting these renewables to WHHE Energy Centres.

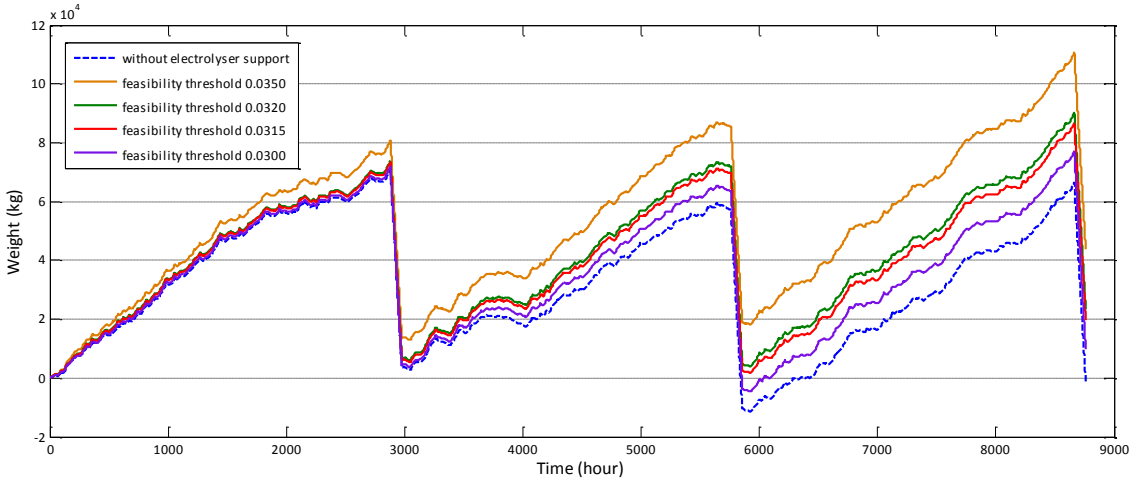

Figure (ES) 15: Meeting annual hydrogen demand by changes to feasibility threshold showing for the given upper and lower hydrogen limits a feasibility threshold of 0.0315 £/kWh.

- **HEAT ENGINE**

The gas turbine operates with a pressure of 10 bar with heat coming from the fuel cell and oxy combustor. The compressor and expander have simulated with isentropic efficiencies of 85% and 86% respectively. During the scheduled maintenance periods the priority is to ensure the fuel cell remains operational meaning the heat required by the hydrogen storage becomes of greater importance. This means during these periods heat from the burner could be diverted to the hydrogen storage before entering the GT heat exchanger thereby affecting performance as shown in *Figure (ES) 16*.

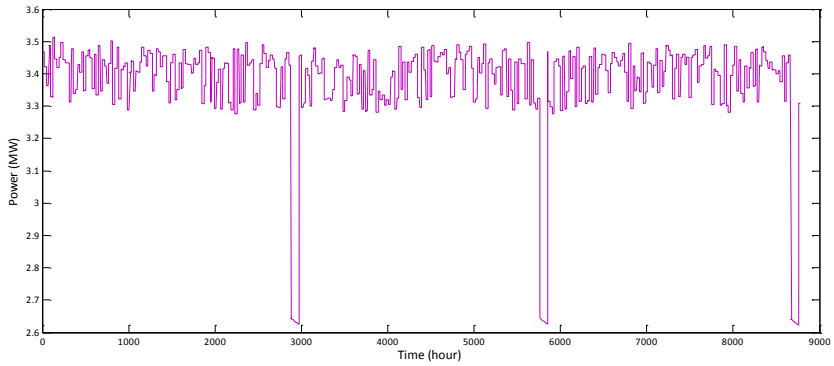

Figure (ES) 16: Power fluctuations according to changes in fuel composition to the burner and heat used to drive the hydrogen storage during scheduled maintenance.

- **OVERALL PERFORMANCE**

The parasitic load for the WHHE Energy Centre include; material recovery facility, air separation unit, plasma torch, the desulphurisation circuit (compressor, pumps, refrigeration), hot water pumps, hydrogen storage cooling fans, and the electrolyser. The material recovery facility is assumed to consume 20kWh/tonne (*DECCW NSW, 2010; RMCT, 2003*).

The average annual output and demand of the various components are shown in *Figure (ES) 17* and *Table (ES) 7.*

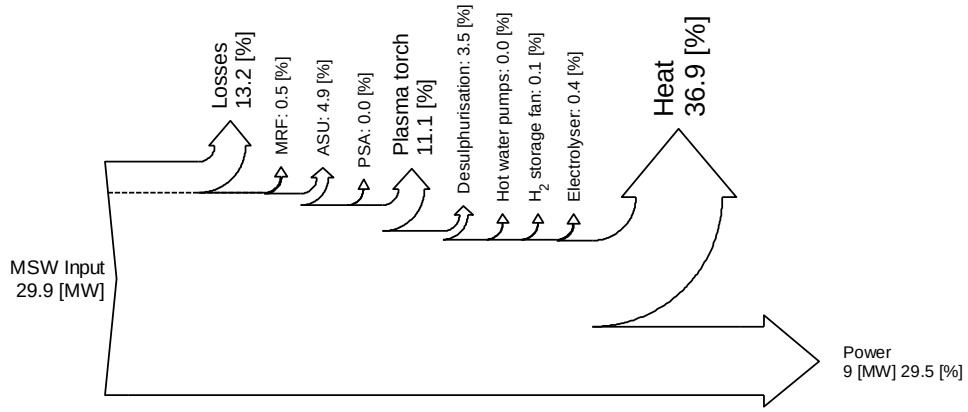

Figure (ES) 17: Sankey diagram showing losses and outputs.

Table (ES) 6: Overall average outputs.

Parasitic load	**MW**
MRF	0.137
ASU	1.47
PSA	0.0025
Plasma torch	3.311
Desulphurisation cycle	1.055
Hot water pumps	0.00022
H_2 storage fan	0.024
Electrolyser	0.106
Outputs	
Heat output (thermal)	11.02
Electrical output (FC)	11.56
Electrical output (GT)	3.38
Net electrical output	**8.83**
Overall efficiencies	
Electrical efficiency	29.5%
Heat efficiency	36.9%
CHP efficiency	66.4%

The annual performance of the plant shows good electrical efficiencies hovering below 30% (including the material recovery facility) which is above the industry target of 25%. During the scheduled maintenance period the parasitic losses associated with the operation of the gasifier fall away and explains the improved values shown in *Figure (ES) 18*.Due to the high demand for heat from the hydrogen storage unit and because of the lack of heat coming from the gasifier over the maintenance periods the heat and CHP efficiencies see drops in values (*Figure (ES) 18*).

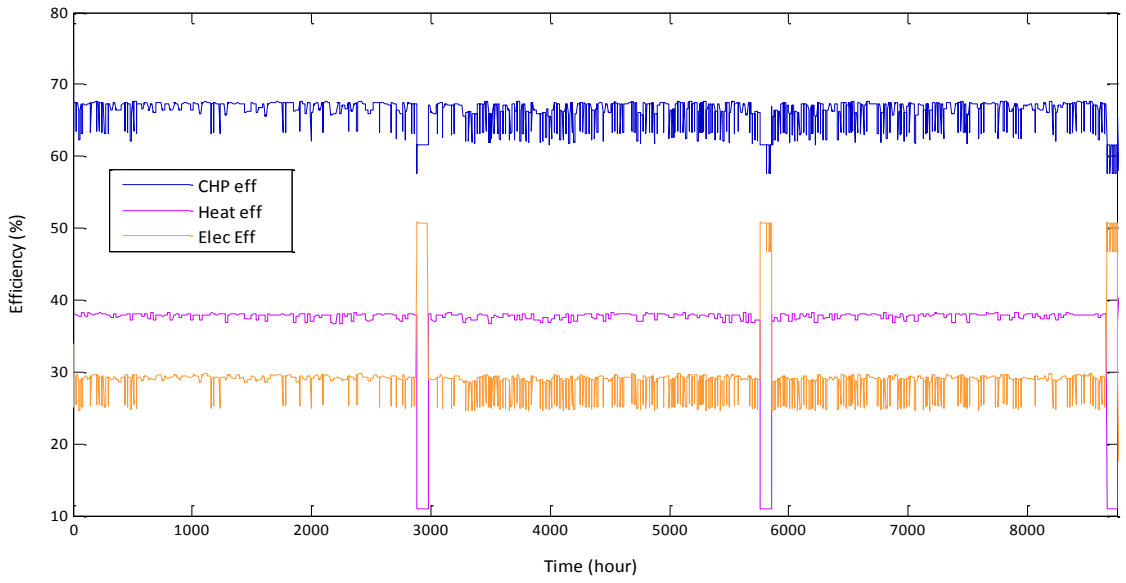

Figure (ES) 18: Annual electrical, heat and CHP efficiencies.

Readers Guide

- Overview
- 1. Introduction
  - Gasification of MSW
  - Challenges
  - Aims and Objectives
- 2. Literature Digest
- 3. SOFCs
- 4. The WHHE Concept
- 5. Modelling
- 6. Modelling Results
- 7. Experimental Research
- 8. micro-CHP in the UK Market
- 9. Conclusions
- References
- Appendices

1. INTRODUCTION

Escalating energy demands, energy security issues and the current political drive to reduce carbon emissions have created an overwhelming need for innovative and future-proof decentralised energy production and management solutions to tackle the area of energy-efficient buildings (*Lovins, 2011; EC COM 677, 2010*).

The instant supply of energy is a fundamental necessity that supports modern society. This is best illustrated by the world-wide annual energy consumption per capita that stands at 17,000 kWh which is equivalent to a continuous consumption of 2000 watts per person (*Novalantis, 2005*). The source of this energy is primarily derived from fossil fuels, whether it be coal and natural gas for power and heat, or oil for transportation. Our ability to utilise fossil fuels has driven tremendous technology advancements that are themselves reliant on fossil fuels (*Figure 1-1*). These advancements have vastly improved living standards which has led to a global population boom from 1billion in 1804 to 7billion in 2011. Together these factors have resulted in an exponential growth in fossil fuel consumption over the past century. This, in essence, has demanded the beginning of the next paradigm shift to sustainability where fossil fuels can no longer be our primary source of energy. Fossil fuels currently account for more than 80% of primary energy supply (*WEC, 2013*), and current estimations see coal as the only fossil fuel to be available after 2042 and will only be available up to 2112 (*Shafiee, 2009*).

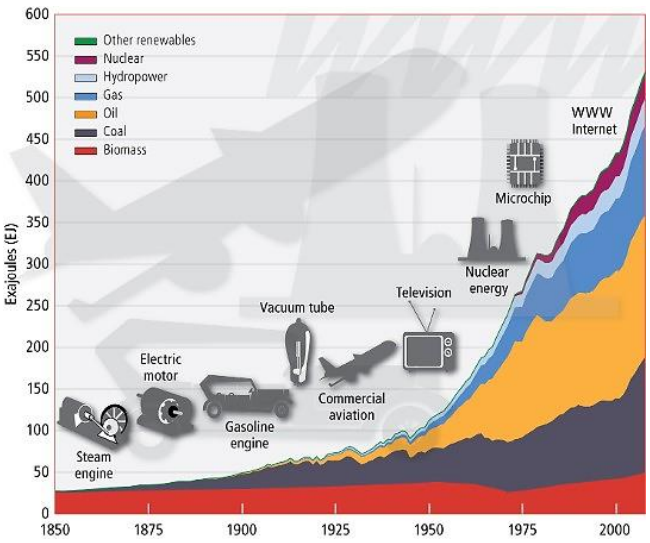

Figure 1-1: Energy consumption trends from 1850 (*IIASA, 2012*).

Diminishing reserves of fossil fuels is not the only cause to switch to more sustainable energy production and management as there is growing concern surrounding the effects of global warming. Global warming is caused by the emission of greenhouse gases (GHG) to the atmosphere and the unnatural increase of these gases is caused by the burning of fossil fuels. This has seen countries around the world sign up to the Kyoto Protocol which sets financially binding CO_2 reduction targets to be achieved within certain time constraints. The correlation between global warming and CO_2 emissions is shown in *Figure 1-2* and *Figure 1-3*.

The Kyoto Protocol requires that the UK's greenhouse gas emissions are reduced by 12.5% (from the 1990 baseline) by 2012, which equates to annual emissions of 682 million tonnes of carbon dioxide equivalent (CO_2e)(*DECC, 2013*). For the first commitment period (2008-2012) the UK has reported a 22% reduction of the six greenhouse gases covered by the Kyoto Protocol and although the commitment period is over final reporting against targets may only be published in 2016 (*DECC, 2015a*). The second commitment period (2013-

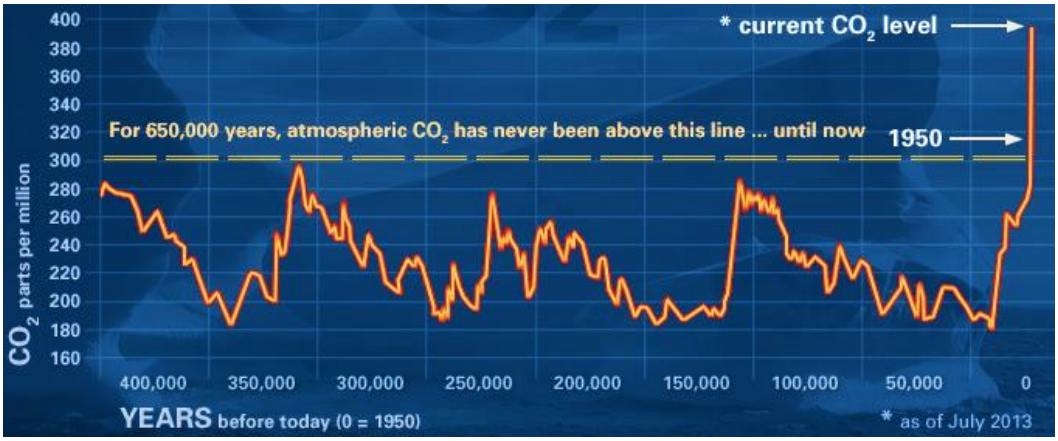

Figure 1-2: Comparison of atmospheric samples contained in ice cores and recent direct measurements measuring atmospheric CO_2 (*NASA, 2013*).

2020) the UK has identified a 20% reduction target which is yet to be ratified and made official (*DECC, 2015a*). The 2008 Climate Change Act is the framework that the UK government has put in place to direct the path towards meeting these targets, and aims to reduce the UK's emissions by 80% by 2050.

During this time the UK is also facing the rapid closure of existing grid capacity as a number of older power plants go offline. Of the reported 76GW available in 2007 an expected 22.5GW is to be close by 2020 (*Marsh, 2008*). These issues are further exacerbated by an ever growing population which places a greater demand on energy supply. The World Energy Council predicts that the global energy demand is expected to double by 2050 (*WEC, 2013*).

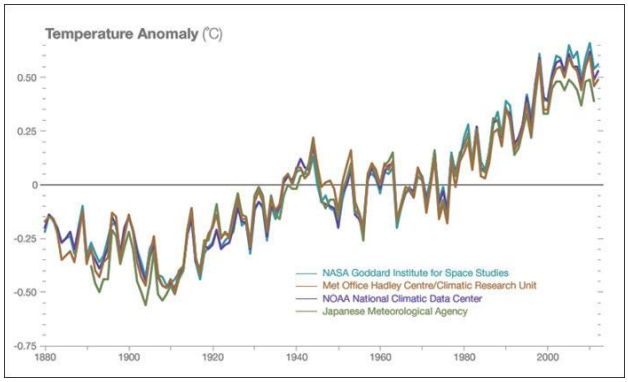

Figure 1-3: Temperature data from four international science institutions (*NASA, 2013*).

This has led to substantial interest and deployment of solar powered renewable technologies such as wind turbines, photovoltaics (PV), and biomass. As an energy resource the potential for wind energy in the UK is very strong and is considered to be the best wind resource in Europe (*Sinden, 2005*). Whilst wind and PVs are fundamentally sustainable with relatively short energy payback periods they are inherently intermittent which means the electricity grid will struggle to support their deployment at large scale. Therefore, further technologies dealing with the dynamic relationship between demand and supply will be required to support the large-scale penetration of any intermittent energy sources.

Moving forward we can identify a need for higher energy efficiency and improved connections between energy storage systems, buildings, smart grids and vehicle/mobility systems. Key challenges include energy recovery at a community level and real-time management of energy

demand and supply, and new approaches are needed to enable effective Building-to-Building and Building-to-Grid interactions as it should be in a real energy market.

At the same time Municipal Solid Waste (MSW) - rich in energy - is being produced by buildings (their inhabitants). In the EU, of the 6 tonnes of material consumed per person per year, 3 tonnes goes to landfill (*EC COM 571, 2011*). In some cases this waste is sent to large centralised waste incinerators which are unable to make full use of the waste heat (which is >65% of the total energy content) and therefore unable to fully re-capture the embodied energy. They also have disadvantages in terms of emissions and solid by-products which are often classified as hazardous. *Figure 1-4* illustrates the various routes to waste disposal employed through various regions of the EU and illustrates possible markets where better techniques may be deployed.

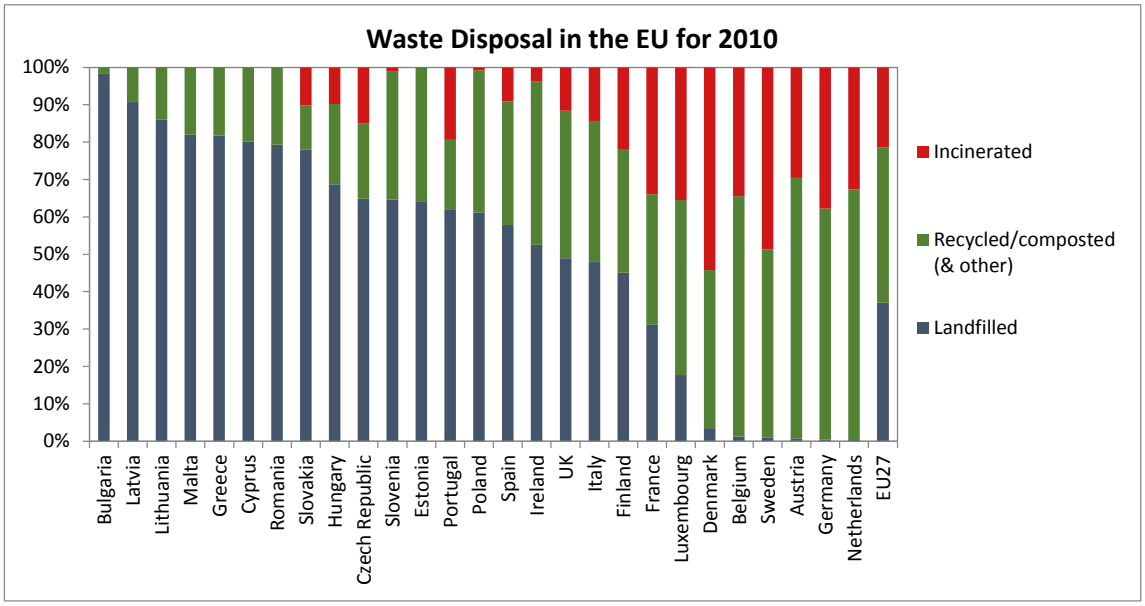

Figure 1-4: Municipal waste management in the EU for 2010 (Eurostat, 2010).

1.1 GASIFICATION OF MUNICIPAL SOLID WASTE (MSW)

The waste-to-energy (WtE) market is extremely large. In 2012 the global market for WtE was valued at USD 24 billion and is expected to rise to USD 29 billion by 2015 (*WEC, 2013b*). WtE consists of any treatment process that produces energy from waste. There are several different WtE processes that can be split into:

Thermo-chemical conversion processes

- Incineration
- Co-combustion
- Thermal gasification
- Pyrolysis

Bio-chemical conversion processes

- Anaerobic digestion (producing biogas)
- Fermentation (producing bio-ethanol)
- Dark fermentation and photo-fermentation (producing hydrogen)
- Biogas from landfill

The most common of these is incineration where excess air is used to combust the organic component releasing heat which creates a self-sustaining combustion process. During incineration the volume of waste is reduced by 85-90% (*McKay, 2002*) as the waste is broken down into gases and bottom ash. Because of the vast array of emissions that are released from incineration all incineration plants in the UK must comply with the Waste Incineration Directive (WID) 2000/76/EC which sets emission controls for any thermal processes regulated in the EU.

Apart from incineration, pyrolysis and gasification can be used for WtE but instead of directly releasing heat via combustion pyrolysis and gasification processes are used to produce secondary products which can be used to generate energy. As shown in *Figure 1-5* pyrolysis and gasification involves the breakdown of waste using heat with limited or no supply of oxygen. As the supply of oxygen decrease the demand for external heat increases as these processes generally operate at

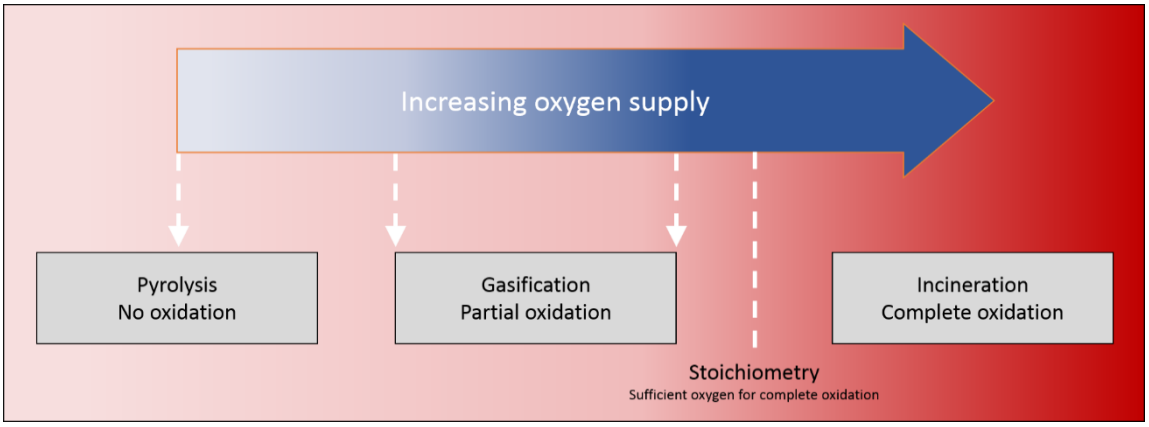

Figure 1-5: The difference between pyrolysis, gasification and incineration is identified by amount of oxygen present during the thermal treatment.

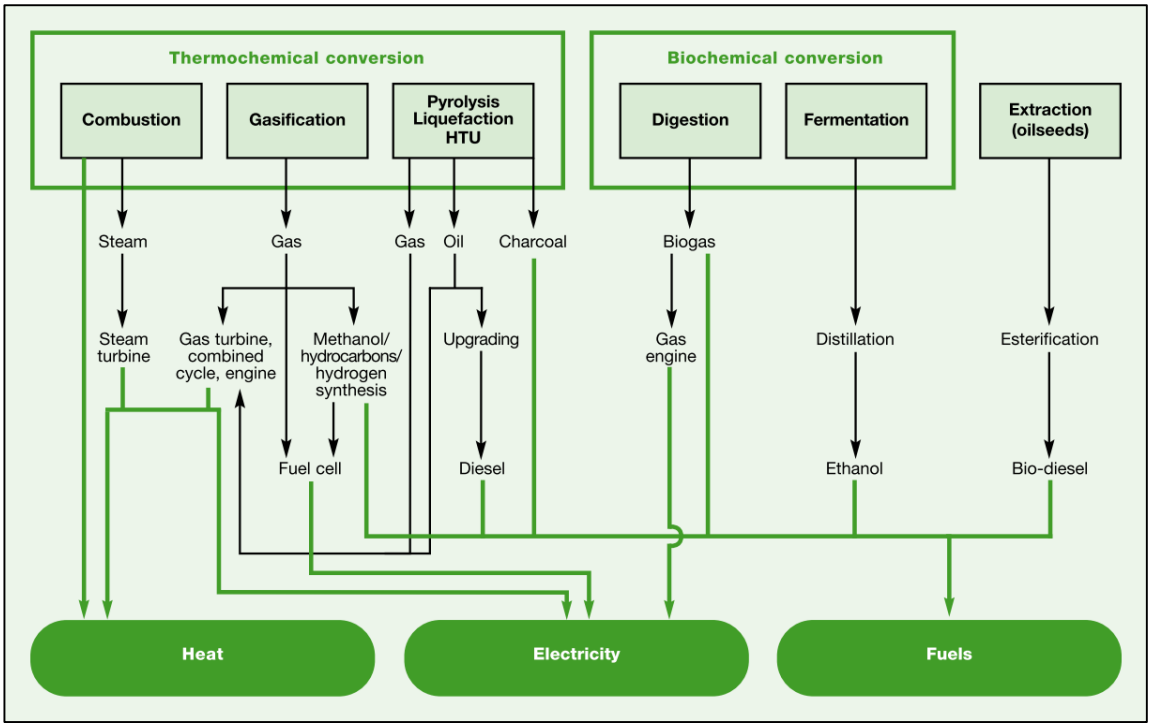

Figure 1-6: Main biomass energy conversion routes illustrating alternatives paths to producing heat, electricity or secondary products (fuels)(*UNDP, 2000*).

temperatures above 700°C. By controlling the flow of oxygen gasification systems can be designed to operate without additional external heat, the factors controlling the gasification temperature will be discussed in more detail further into this thesis. By limiting the amount of oxygen during pyrolysis and gasification the feedstock is decomposed in a reducing environment which enables the production of hydrogen which can be used to drive a fuel cell.

Figure 1-6 illustrates the various energy conversion pathways for the main thermochemical and biochemical conversion processes and shows the potential for fuel cells to produce electricity via gasification.

Of the processes identified gasification and pyrolysis are best suited to fuel cell integration as they produce a hydrogen rich syngas that is well matched to fuel cell operation. The syngas produced from the gasification of carbonaceous material is rich in hydrogen, carbon monoxide and methane that can fuel SOFCs.

Because of the external heat required to maintain pyrolysis their energy conversion efficiencies are lower than for gasification plants. There are numerous variations to gasification techniques and identification and selection of the ideal approach will be discussed in more detail in *Chapter 3*.

1.2 WASTE MANAGMENT

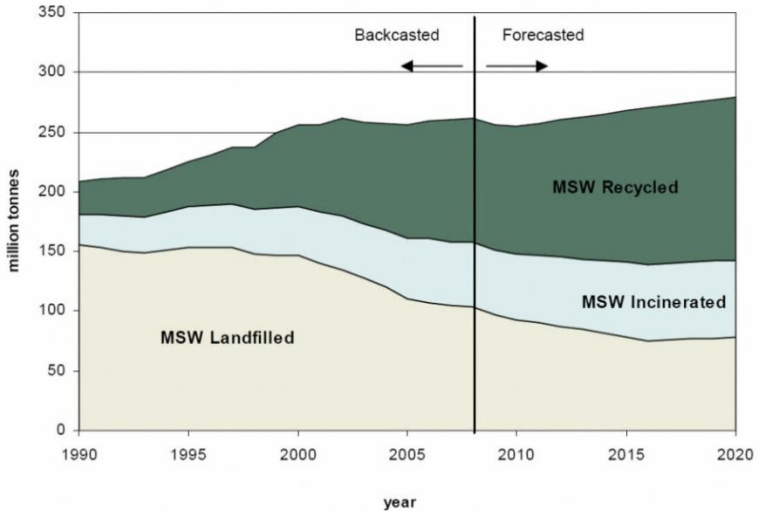

Figure 1-7: Projected generation and management of MSW in EU27 (*Bakas et al., 2011*).

Currently waste disposal is a major problem. A city of 1 million inhabitants requires approximately 1 hectare per year (to a depth of 30m) for waste landfilling (*Council of Europe, 2007*). Unprotected scavenging on landfill sites results in reduced life expectancy, and often municipalities spend considerable amounts in an attempt to disinfect sites. Landfill sites also have an environmental impact e.g. groundwater contamination and GHG emissions. Currently only 6% of the municipal waste produced in Europe is sent to incineration plants (*Eurostat, 2012*). Various schemes across the EU have been used to incentivise a reduction in waste (Polluter-Pays, Producers Responsibility, Pay-as-you-throw). The cost of municipal waste disposal to landfill can be as high as £121 per tonne (*WRAP, 2013*) and separate collection and recycling of paper is about £25 (taking into account revenue from the sale of the paper) (*Council of Europe, 2007*). The amount of waste currently sent to landfill is 192kg of the 501kg treated per capita (*Eurostat, 2009*). Whilst the EU strives to eliminate the amount of waste sent to landfill *Figure 1-7* indicates a steady decline which stalls and levels off leading into 2020 (*Bakas et al., 2011*).

In 2012/13 the amount of household waste collected in the UK was 25.2 million tonnes (*Figure 1-8*) compared with 26.6 million tonnes in 2009/10 indicating a decrease of 5.5% over the three year period (*ENV18, 2013*). This does not include the municipal component of commercial and industrial waste which in 2009 was estimated to be 24.7 million tonnes. Of the waste generated in the UK it is estimated that 40% is considered to be bio-waste (*Dohogne, 2014; Europa, 2010*). Therefore this fraction of the waste stream can be considered as a renewable source of energy providing carbon savings.

> *The renewability and sustainability credentials given to biomass stem from the fact that carbon dioxide is consumed and stored in plants through photosynthesis and released during biomass conversion (Siedlecki et al., 2011).*

As indicated in *Figure 1-9* 34% of MSW currently generated is still sent to landfill with considerable amounts already stored and available for mining. Although the trend for waste sent to landfill is falling (*Figure 1-9*) it is unlikely that waste sent to landfill will be totally eliminated. This is in part because of long term contracts between councils and waste management companies.

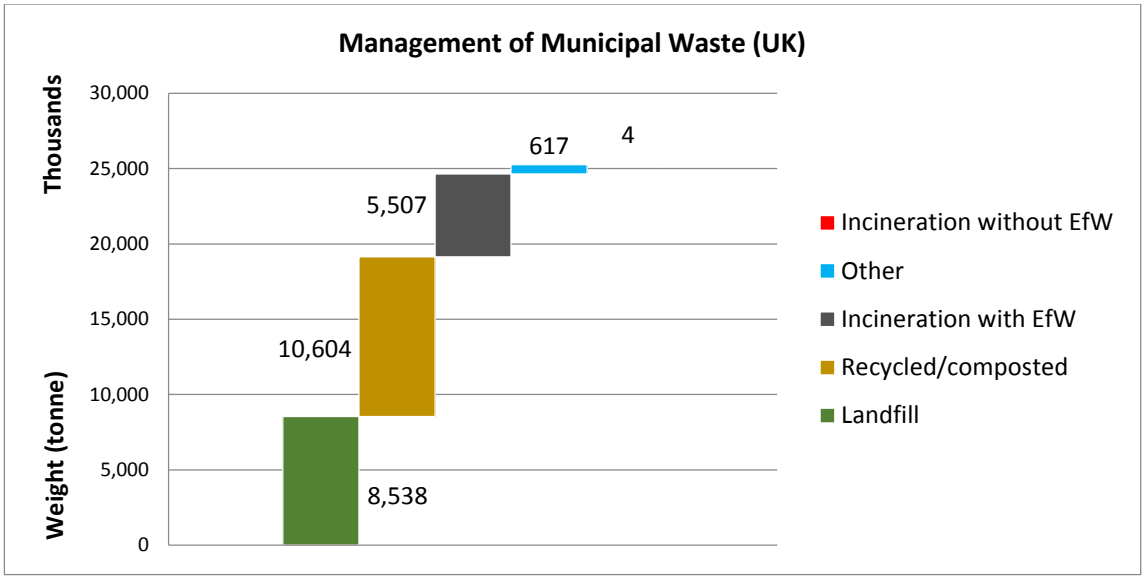

Figure 1-8: Management of MSW in the UK for 2012/13 *(ENV18, 2013)*.

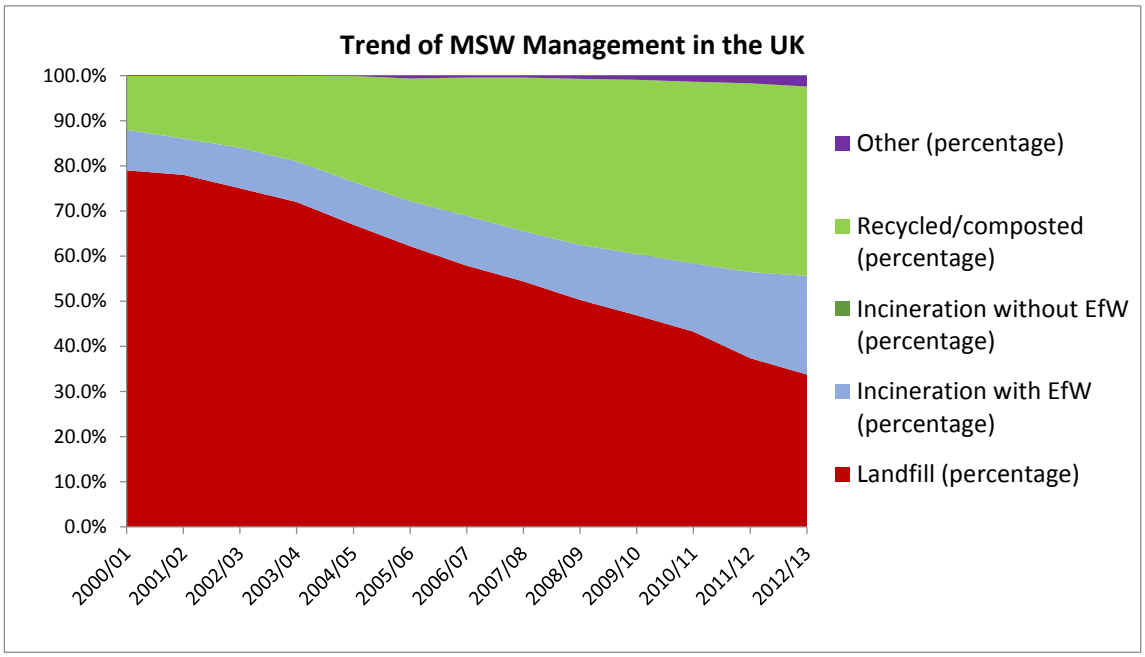

Figure 1-9: The trend of MSW management in the UK from 2000/1 to 2012/13 *(ENV18, 2013).*

The European Commission directive on waste (Directive 2008/98/EC) outlines a hierarchy by which waste must be managed, *Figure 1-10*. The benefit of this approach is that waste should now be looked at as a valued resource whilst preventing emissions, saving energy and conserving resources.The EU Landfill Directive (99/31/EC) aims to do more in terms of setting quantitative goals that will force local authorities and inevitably consumers to think more about waste management and the environmental and economic benefits that will arise from following the hierarchy. Targets for waste management have been set by the Waste, Landfill and Packaging (94/62/EC) Directives.

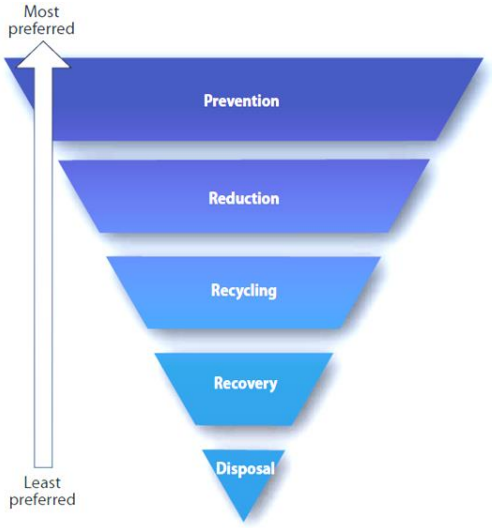

Figure 1-10: European waste hierarchy.

Targets set out in the directives:

Landfill Directive (99/31/EC)

- By 2010 to reduce biodegradable municipal waste landfilled to 75% of that produced in 1995.
- By 2013 to reduce biodegradable municipal waste landfilled to 50% of that produced in 1995.
- By 2020 to reduce biodegradable municipal waste landfilled to 35% of that produced in 1995.

Waste Directive (2008/98/EC)

- By 2020 50% of household waste is to be recycled.
- By 2020 at least 70% of construction material is to be recovered.

Packaging Directive (94/62/EC)

- By 2009 between 55 and 80% of packaging waste to be recycled, by weight.
- By 2009 material specific recycling targets by weight: glass (60%), paper and board (60%), metals (50%), plastics (22.5%), and wood (15%).

Projections of UK recycling rates show that the 50% MSW recycling target should be met by 2020, although there is no great confidence that the UK will meet the biodegradable recovery target outlined in the Landfill Directive (*Watson, 2013*). In 2009 no infringement proceedings were initiated with respect to the targets specified for packaging suggesting successful enforcement of the directive (*Europa, 2011*).

How has the Landfill Directive affected the way landfills are being managed?:

- Certain wastes banned from landfill.
- All landfill sites must be classified for the type of waste allowed.
- Pre-treatment of waste going to landfill required.
- The co-disposal of hazardous and non-hazardous waste ended in July 2004.

These requirements have led to commercial opportunities in the waste management industry, especially since the Producer Responsibility Obligations Regulations 2007 that set out obligations on producers to recover and recycle a proportion of the packaging they produce each year. Pre-treatment of waste also means consideration must be given to the recycling and recovery of waste by those collecting waste, and bans on certain substances will force operators to look for alternative solutions of waste disposal. This ties in very well with the goals set out in this research and by treating waste as a commodity there will be an economic benefit for finding sustainable solutions to waste management.

There is a clear need for mutually complementary innovative solutions to four key areas:

1.2.1 WASTE DISPOSAL

Transforming the problem of waste disposal, especially Municipal Solid Waste (MSW), into a commercially viable business which recovers the embodied energy content. Currently, on average, only 40% of the solid waste generated is re-used or recycled with the rest going to landfill or incineration (*EC COM 571, 2011*). Exploiting MSW as a principal source of energy can also mitigate the environmental impacts associated with landfill disposal and incineration.

1.2.2 CLEAN HYDROGEN PRODUCTION

Initiating the successful growth of a commercially viable distributed hydrogen infrastructure for clean (non-polluting) vehicles which do not rely on fossil fuel energy sources. Currently there are 129 hydrogen refuelling stations across 17 European countries that have been built or planned up to 2014 (*2010 Report on the European Transport H2 Refuelling Infrastructure*) with an expected 1 million hydrogen fuelled road vehicles in Europe by 2020. Through strong policy support this is expected to rise to 5 million (*HyWays, 2013*).

1.2.3 HEAT NETWORKS

Incentivising the adoption of intelligent building-to-building thermal energy supply networks to take advantage of waste energy exchange between buildings as well as to distribute energy from MSW and renewable or low carbon sources such as solar thermal, ground source heat pumps and traditional combined heat and power (CHP) schemes. Buildings are responsible for nearly 40% of energy consumption of which 67% is used for space heating. Hence by utilising the thermal energy created during the production of electricity there is considerable scope for energy savings (*EC COM 109, 2011*).

1.2.4 LOCAL ELECTRICITY PRODUCTION AND MANAGEMENT

Providing a means of local electricity generation and storage which introduces precious flexibility into the grid in order to provide a SMART means of dealing with peak production/demands as well as maximising the potential for renewable electricity grid penetration. This is in line with the 2020 goal of making 50% of the networks in Europe suitable for the integration of renewable technologies (*EC COM 519, 2009*). At present 54% of the EU's primary energy is sourced from imports (*EC COM 639, 2010*). This research, by being able to exploit the growth of renewable energy technologies, will positively assist in the securing and diversifying of indigenous EU energy supplies, in combating climate change and in helping the EU to reach the binding 20% renewable energy target for 2020. A final advantage of this approach is its future-proof character in its being able to accommodate other inflexible low-carbon sources such as nuclear energy, which will also expand, primarily after 2020.

1.3 RESEARCH AIMS AND OBJECTIVES

Although there is and has been much said about the advantages and possibilities of such advanced systems (using coal or waste) building them requires substantial levels of investments so it is the aim of this research to quantify the environmental and economic performance of an Integrated Gasification Fuel Cell Combined Cycle (IGFCC) fuelled by MSW through numerical modelling techniques and based on First Law energy conservation. Beyond this and as an ambitious contribution to knowledge this research will look to expand the original process design taking into account the real world application of these plants as well as future aspects that are already affecting the global energy market.

1.3.1 AIMS

- The overall aim of this project will be to develop a numerical model(s) with the aim to understand the flow of energy throughout the proposed IGFCC system whilst operating under varying inputs and against realistic market dynamics.
- To quantify the economic return of investment using different market economics.
- In terms of scaling important results to come from modelling will be to size the energy storage facility. This will be affected by a number of factors such as; fuel cell size, upper and lower fuel cell H_2 limits, waste composition fluctuations, maintenance downtime and also the price of wholesale electricity.
- As a numerical model primarily based on first principles the model must have the flexibility to utilise any values obtained through experimental work done in the laboratory.
- A fundamental aim will be to quantify the environmental impact and CO_2 savings of the facility.
- The feasibility of the added process of hydrogen production and storage will be measured and could prove to be a solution to some of the issues facing these IGFCC systems.

1.3.2 OBJECTIVES

This thesis aims to demonstrate the operation of an IGFCC at district scale (MW) whilst implementing various strategies that deal with current external influences impacting operational and financial performance of the plant. Some of the questions to be answered include:

- With the integration of gasification technologies with fuel cell and GT systems, along with the ancillary equipment needed for them to operate, can the plant exceed 25% electrical efficiency?
- How will variations in the waste composition affect the performance of the plant?
- How will the thermal performance of the fuel cell deal with the low hydrogen concentrations, and will the exothermic reaction be able to maintain the required operating temperature?
- How important will the implementation of large scale hydrogen storage be and can the plant feasibly produce enough hydrogen to maintain the hydrogen storage strategy?
- What is the fuel cell's tolerance to tar coming from the gasifier, and what can be done to prevent cell degradation?
- Taking into account the fluctuations of the wholesale electricity market is it feasible to build such systems?
- Can such WtE systems provide meaningful reductions in CO_2 emissions thereby helping the UK meet the 2050 reduction targets?
- Can it be economically viable to use a portion of the electricity produced to create hydrogen via electrolysis as opposed to selling it to the grid?
- Can these systems be implemented in an urban and/or industrial contexts allowing heat from the plant to be exploited as a combined heat and power supplier?
- Can combined heat and power units provide substantial CO_2 savings whilst being financially attractive?
- How much heat and power will be available for export for a plant scaled to treat 100,000 tonnes of MSW per year (based on existing commercial plant size, [APP, 2012]), and how many houses will this supply?
- Can WtE systems support the EU's waste hierarchy?

1.3.3 METHODOLOGY

The objectives will be answered using custom made numerical simulations using ChemCad chemical process simulation software, and Matlab (Simulink) numerical computing software, as well as state-of-the-art practical laboratory experiments:

- In-house development of a sophisticated Simulink model to simulate the performance of the fuel cell operating under various conditions. Outputs to include; voltage, current, utilisation factor, and cell temperature.
- Simulink model to be extended to include GT, heat exchangers, hydrogen storage, and electrolyser components.
- A custom designed ChemCad model will be used to simulate the chemical reactions within the gasifier using a typical waste composition.
- ChemCad will be used to also simulate high temperature gas filtration techniques, high and low temperature water-gas-shift reactions, and desulphurisation.
- Heat recovered from the ChemCad cycle and Simulink models will be combined to show the overall thermal output of the plant.
- Annual fluctuations of the waste composition and wholesale electricity price will be used to simulate the overall performance of the design throughout the year.
- Various hydrogen storage materials will be modelled to test the impact on energy performance.
- Laboratory testing of a GDC solid oxide fuel cell using a synthetic syngas composition including tar will be undertaken to determine effects and tolerance limits.
- Practical results and experience will be used to ensure the theoretical simulation is consistent with expected practical performance.
- Energy and financial simulation of various micro CHP (<2kW) units eligible for the UK's feed-in-tariff will be used to demonstrate commercial and environmental benefits of CHP adoption.

1.4 THESIS STRUCTURE AND ORGANISATION

Chapter 2 introduces the concept upon which this research is focused and explains the beneficial synergies that can be expected from integrating the selected technologies. The overarching benefits of the system will be to produce district scale electricity and heat close to the consumer whilst offering a sustainable solution to effective waste management that embraces the waste hierarchy and the need to reduce carbon emissions. The scale of the plant will be based on the waste supply of 100,000 tonnes per year, which equates to 60,000 tonnes per year for gasification.

Chapter 3 provides an overview of the various technologies being explored for integration in the proposed IGFCC. *Section 3.1* begins with a review of various IGFCC's that have been researched and presented in scientific publications. The results of these findings will be a guide to not only the potential design but also of the expected overall results in terms of energy efficiency and financial performance. *Section 3.2* looks at the various gasification techniques as each has their own characteristics which can determine feedstock requirements and also importantly the syngas quality. Because of the array of contaminants and impurities coming from the gasifier *Section 3.3* looks at various gas filtration techniques as well as chemical processes that may improve the syngas quality. *Section 3.4 and 3.5* looks at the various fuel cell and heat engine technologies and evaluates their potential for such system integration along with previous results of their integration in various designs. Similarly *Section 3.6* reviews various hydrogen storage techniques whilst looking with greater detail into metal hydrides which may be more advantageous when used in stationary applications where gravimetric and volumetric densities are not a priority. *Section 3.7* briefly looks at the application of large scale electrolysers.

Chapter 4 is dedicated to solid oxide fuel cells and how they operate. The chapter begins with a brief history going into the basic principles before taking an in depth look at various materials with their various advantages and characteristics. Considering the anode is exposed to gas coming from the gasifier *Section 4.4.2* looks at how some of the expected impurities could affect the cells performance and what might be done to mitigate or eliminate these effects. Throughout the chapter attention is focused on the influence of impurities at a molecular level as would be expected from integration with gasification technologies.

Chapter 5 is dedicated to explaining the fundamentals of the modelling approach used and presents the mathematical descriptors for the various components. Before each equation there is a short description justifying the chosen approach and on some occasions a choice of options is presented before an appropriate selection is chosen. As with the previous chapters the modelling is heavily concentrated modelling of the fuel cell so a large portion of the chapter is used to go into the finer details as a dynamic numerical model is developed from scratch. As the gasification process is modelled using ChemCad *Section 5.8* briefly looks at the thermodynamics behind the process and how the software recreates them. This section also presents the ultimate analysis of previously published waste compositions and describes key equations that are used to measure the gasifiers performance. *Section 5.9* looks at various approaches used for syngas filtering and purification along with the principles behind the high and low temperature shift reactions used to increase the yield

of hydrogen. The rest of the chapter looks at modelling of the gas turbine, electrolyser, hydrogen storage, combustor and the market dynamics that will affect the performance of the plant over the course of a year.

Chapter 6 presents the final results of the modelling exercise based on an annual supply of 60,000 tonnes per year of MSW to the gasifier. During the selection of the final operating conditions there is a need to compare the inlet steam and oxygen ratios to maximise the gasifier's performance whilst considering practical limitations. Modelling is carried out using two software packages so results are presented in two main sections and in the order they found in the cycle. Hot water for district heating is captured throughout the cycle and is exported at a temperature of approximately 90°C. After the overall energy performance of the complete energy system is presented calculation of the financial performance is shown along the expected overall CO_2 reduction.

Chapter 7 is published in the form of a journal publication and presents the methodology and findings of practical experiments undertaken to test and understand the performance of a typical SOFC when operating with a tar laden syngas and what the reaction pathway of the tar might be. The cell uses a GDC material at the anode for carbon deposition resilience and the synthesized syngas is made up by mixing H_2, CO, CO_2, N_2, H_2O, CH_4 and toluene (C_7H_8). After a review of common tar species present in syngas Toluene has been identified as good representative tar and is used as the model tar in these experiments. The purpose is to steadily increase the concentration of tar whilst monitoring the performance and response from the SOFC, and through monitoring the exhaust gas elucidate on reactions taking place and if the input conditions result in carbon deposition.

Chapter 8 is not directly related to the main body of work presented in this thesis but is a result of research carried out for BDSP (the EngD industry sponsor), and as such relates to building services. The chapter is presented in the form of a journal and shows the results of a research study undertaken to understand the prospect of m-CHP (>2kW) in the UK whilst benefiting from the UK's feed-in-tariff. The purpose here is to compare the various CHP systems that qualify for the feed-in-tariff whilst supplying a typical household heat and electricity demand. Results show the annual energy and financial performance of the various systems against a conventional grid supply. Systems are also operated using their optimal operating strategy (i.e. heat led or constant supply) and in the end financial and CO_2 outputs are used to identify the most attractive commercially available CHP system in the UK.

Chapter 9 is used to finalise the thesis by summing up the final results according to initial aims and objectives and offers commentary on lessons learned and future avenues for future research.

Readers Guide

2. THE WHHE CONCEPT

The concept of the integrated gasification fuel cell combined cycle (IGFCC) is derived from the same principles of the widely adopted integrated gasification combined cycle (IGCC) where coal is used as the primary fuel and the syngas is combusted to drive gas turbine and/or steam turbine (CCGT) to produce electricity. By introducing a high temperature fuel cell in a hybrid configuration with a gas turbine electrical efficiencies are expected to improve substantially (*Sadhukhan et al., 2009; U.S. D.O.E., 2012; Singhal, 2000; Grol, 2009*), and similar to the IGCC process the energy conversion devices are protected by filtering particulates, tars and sulphur prior to entry. Fuel cell's are not limited by the Carnot efficiency restrictions meaning greater electrical efficiencies can be achieved.

These processes have the advantage of easily applying carbon sequestration methods as the gas flows are kept in a controlled environment until being exhausted. Due to the thermo-chemical process created by the gasifier we can extend this technology to extract the embodied energy contained within general waste that is currently sent to landfill or incinerated. As illustrated above, the business of waste management is an environmental issue and legislation such as the EU Landfill Directive (formally Council Directive 1999/31/EC) is forcing businesses and local authorities to look for alternatives to sending waste to landfill. To comply and facilitate the EU waste hierarchy of recycling and recovery before disposal material recycling facilities (MRF) must be implemented on the front-end of any IGFCC facilities.

This project proposes to develop and expand on the original concept of IGCC by including MSW as a primary fuel and using elements of hydrogen production and storage in order to complement and improve the performance of the original design. A schematic of the system can be seen in *Figure 2-1*.

This research proposes to demonstrate the theoretical performance of an integrated Waste management, Hydrogen production and storage, Heat and Electricity Energy Centre - WHHE Energy Centre using a numerical simulation based on experimental research and well developed mathematical algorithms.

WHHE Energy Centres support four key areas:

1. Ultra clean waste disposal and high efficiency energy recovery.
2. High efficiency hydrogen production to supply infrastructure for local clean vehicles.
3. Waste heat energy supply to boost the uptake of intelligent thermal energy networks which efficiently exchange heat between local buildings.
4. Local high efficiency electricity production and management (hydrogen storage backup and robust sequential controllers for fast load following and fuel efficiency) to maximise local decentralised renewable energy penetration and enable a low-carbon, flexible, smart electrical grid.

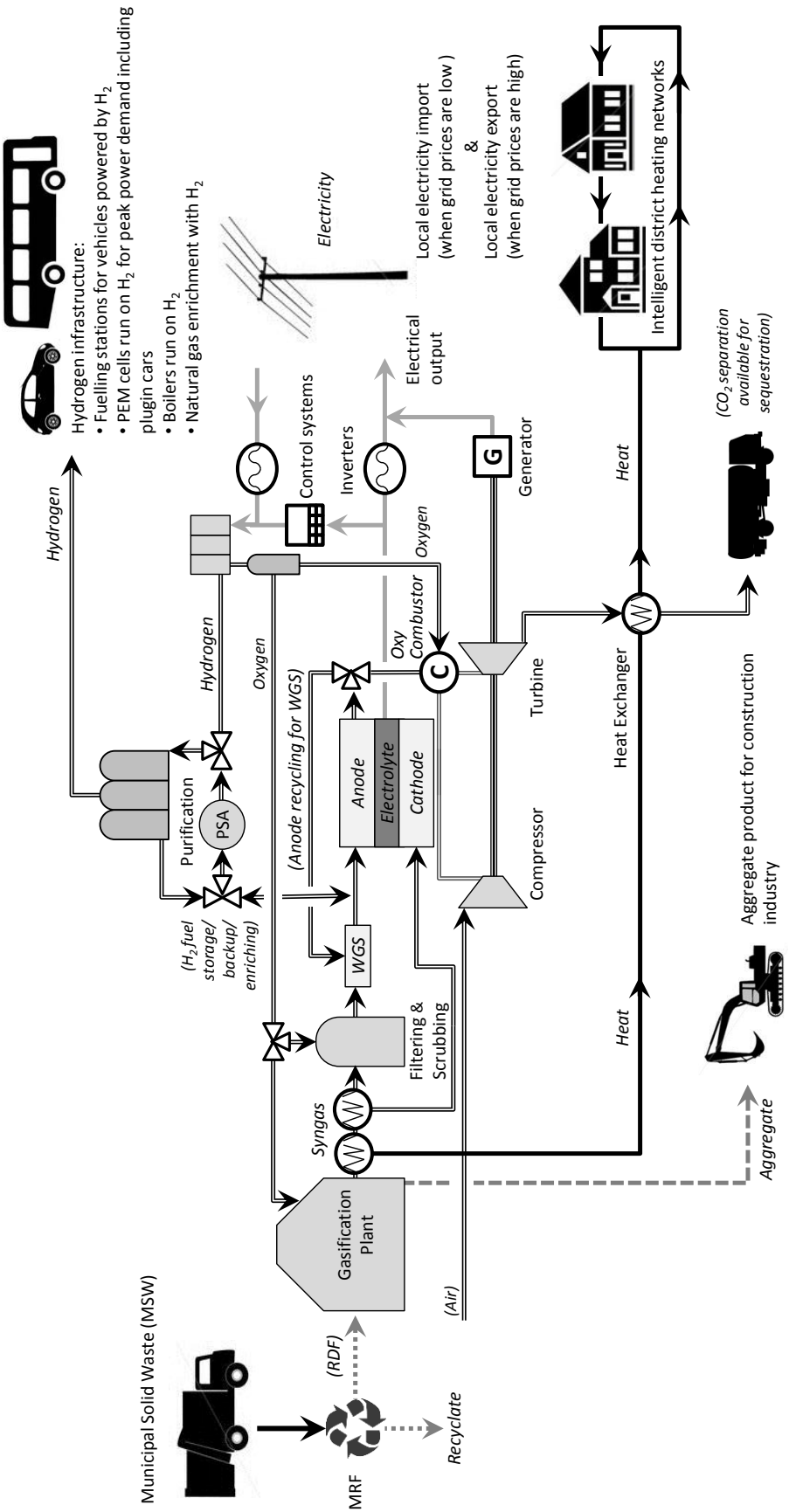

Figure 2-1: Dual fluidised bed/plasma gasification – SOFC/GT hybrid system schematic.

This research aims to investigate the integration of proven cutting-edge fuel processing, energy production and energy storage technologies in an innovative manner to achieve a highly efficient and flexible decentralized energy system for the building industry. These technologies include: thermal plasma gasification processes, gas filtering, hybrid fuel cell/heat engine combined cycle, hydrogen production (electrolysis), hydrogen storage (nanostructured high capacity metal hydrides), enhanced heat exchange and effective thermal management systems, *Figure 2-1*. High temeperature SOFCs are included as they offer higher electrical efficiencies compared to combustion engines - this further discussed later in this paper.

This project represents an ambitious step in the direction of energy decarbonisation and security by providing decentralised energy centres for the long term, comprehensive management of heat, electricity, hydrogen and waste.

2.1 BENEFITS

WHHE Energy Centres have been conceived to directly address the obstacles to delivering high efficiency energy networks in the built environment. These networks are authentic energy system designs driven by conserving fuel and power, minimising electricity and heat generation costs and reducing emissions. In essence, WHHE Energy Centres are able to address these obstacles by simultaneously and holistically tackling all four problem areas of waste, hydrogen, heat and electricity. This is because they are based on, and hence give leverage to, the inherent synergies between the integrated systems. The commercial potential is supported by income from gate fees for accepting waste for waste to energy and recycling activities, renewable obligation certificates (ROCs) applicable to the bio-fraction of the waste used to produce electricity, and government support through incentives such as the UK's renewable heat incentive (RHI).

Overall benefits:

a. **Waste-to-energy sites can be cleaner, smaller and located more centrally, offering district heating opportunities**

   The two-stage thermal fluidised-bed plasma waste gasification techniques used in the Centre have been demonstrated to significantly reduce emissions over other incineration methods as the high temperatures (~1200°C) (*Morrin et al., 2011*) break down pollutants such as dioxins into their elementary constituents. Current treatment of MSW requires a MRF to extract the dry recyclable material, such as paper, card, glass and metals. A WHHE Energy Centre can be designed to be housed in an architecturally appealing warehouse with a modest ventilation stack limited to 10m. Consequently, the public reaction is likely to be much more favourable than for incineration or landfill. Also, because for planning permission waste treated by plasma is classed as "waste recovery" rather than incineration, WHHE Energy Centres can be located more centrally in the built environment. This allows commercial intelligent waste heat networks to be developed to take advantage of the significant amounts of waste heat from the MSW processing (as well as minimising

transmission losses and emissions from transport). Making use of the waste heat not only improves the carbon footprint but adds an extra dimension of commerciality over waste-to-energy sites limited to producing electricity only. In addition, the solid by-product (Plasmarok®) from the thermal plasma system is benign and certified to be sold as an aggregate in the construction industry. This is a distinct advantage over standard incineration of MSW, where the solid waste by-product is classified as hazardous and represents an externality requiring disposal.

b. **Hydrogen infrastructure can be introduced into the built environment**
In WHHE Energy Centres, hydrogen is produced and stored onsite to facilitate commercial electricity production, and to help regulate the energy content of the syngas from the gasification system and provide back up during planned plasma lining maintenance downtime. The advanced, compact solid-state hydrogen storage system employed on site requires a heat source for the endothermic hydrogen desorption kinetic. This disadvantage is counteracted by taking advantage of local waste heat. Ultimately the system provides a local source of hydrogen to boost the uptake of clean fuel cell and plug-in electrical vehicles. This can be scaled up as demand increases and will provide the centre with another valuable future revenue stream.

c. **District heating infrastructure can be introduced into the built environment**
WHHE Energy Centres turn the problem of waste disposal into a beneficial means of providing district heating as both plasma gasification and solid oxide fuels cells operate at high temperatures. This thermal energy can be utilised when WHHE Energy Centres connected to distributed heating networks. In Europe there are more than 5,000 district heating systems supplying more than 9% of total European heating demands equating to approximately 556TWh of heating and this is forecast to double by 2020 (*DHC+ Technology Platform, 2009*). District heating penetration is most prevalent in northern, central and eastern European states with Germany, as one of the leaders, having a capacity of 51.5GW (*Euroheat & Power, 2009*).

d. **High efficiency electricity production and flexibility can be introduced into the grid**
Standard decentralised electricity generation systems that run on syngas suffer from relatively low levels of efficiency (<35% with syngas). Solid oxide fuel cells (SOFCs) achieve 45% electricity generation efficiency with syngas (and combined heat and power overall efficiency of >80% LHV). SOFCs also allow minor impurities to be tolerated, thus avoiding the expensive gas purification associated with PEM fuel cells. However, the actual level of electrode phases interconnectivity and the rate of electrochemical reactions of SOFC do not allow rapid responses to dynamic load fluctuations experienced in buildings. The introduction of electrolysis and hydrogen production allows for excess power to be stored in the form of hydrogen enabling the system to manage fluctuations in supply or demand whilst allowing the SOFC to operate at its highest efficiencies. Oxygen produced from the electrolyser also provides the benefit of feeding the gasification process thereby eliminating the need and expense of an air separation unit. Pure oxygen can also be used to burn any excess hydrogen in the exhaust stream supplying further heat without the risk of producing

NO_x emissions. Hydrogen storage in metal hydrides offers a safe, efficient, compact and long cycling-life means of storage. The materials of interest are nanostructured magnesium composites and room-temperature TiMn-alloy hydrides which, can provide reversibly 6.5 H-wt% at 250°C and up to 20 scm^3/min/g H_2 desorption flow rate (*Dehouche et al., 2009*), and 1.5 H-wt% and up to 45 scm^3/min/g H_2 flow rate (*Dehouche et al., 2005*), respectively. The introduction of a combined-cycle heat engine will boost total electrical efficiency. The SOFC/GT hybrid system relies on close coupling of subsystems (GT recuperates the energy left in the SOFC exhaust) to achieve its high electrical efficiency (potentially exceeding 50%).

2.2 CHALLENGES

The obstacles to achieving a step change in effective energy supply and management in the built environment may be summarised as follows:

a. **Waste-to-Energy commerciality, environmental impacts, safety concerns and public perception**

WtE solutions avoid recourse to landfill and liberate energy in a manner that can be commercially viable. However, many current solutions require extensive gas cleaning to limit their emissions (particulates, heavy metals, trace dioxins, acid gas, nitrogen oxides, carbon dioxide and volatile organic compound emissions). These gas cleaning techniques do not eliminate pollution but merely transfer the problems from gas to liquid which is not a satisfactory long term environmental solution. At the required scale the safety concerns will need to be satisfied by following local legislation and the challenges would be the same for any WtE plant. The inherent nature of the hydrogen storage will provide a higher level of safety compared to equivalent high pressure solutions. The presence of large vent-stacks often precludes locating sites in built environments. Consequently, sites located at significant distances from thermal energy end-users have a low viability for the use of waste heat.

b. **Electricity grid flexibility**

One of the key problems facing new technologies is supply and demand matching. In fact the only current large-scale method of storing clean energy - pumped hydropower (Global ca.104,000MW_e and Europe ca.44,000MW_e [*EIA, 2013; 2012; ESA, 2014*]) - is limited to certain regions and in many cases has significant environmental impacts. The second largest solution - compressed air energy storage (Global ca.440MW_e and Europe ca.290MW_e [*Setis, 2012*]) - has a very small contribution with remaining technologies totalling less than 426MW_e [*EPRI, 2010*]. The challenge is to develop a solution that is technically, economically and environmentally feasible, whilst being adaptable to a variety of climatic and regional needs.

c. **Hydrogen transportation, storage and low carbon sourcing**

In the built environment, hydrogen infrastructure development is hindered by two major obstacles. The first is the transportation and storage of relatively high volumes of hydrogen

which normally requires liquefying hydrogen at -252°C or through high pressure containers with reduced capacity. These processes can be very expensive (30% of the heating value of hydrogen is needed for liquefaction) or infeasible due to the low energy density and can also experience significant losses with added safety concerns. The second relates to the inherent problem of producing hydrogen from fossil fuels. Vehicles fuelled from hydrogen reduce local pollution levels in areas with high traffic density. Furthermore, studies have shown that vehicles running on hydrogen derived from natural gas can reduce overall GHG emissions by as much as 50% (*Brinkman et al., 2005*). However, there are still significant opportunities to reduce emissions further by deriving hydrogen from excess grid electricity produced, for example, by wind turbine farms in periods of high wind speeds.

d. **Heat network energy commerciality**

Standard CHP district heating schemes have been proven to have a particularly low carbon footprint as both electricity and waste heat are used locally. However, the main obstacle to the uptake of traditional district heating schemes is the financial profitability which only accrues over the long term – typically 40-50 years (*LGA, 2013*). This often proves unattractive for companies aiming for short-term returns on investment.

Using the latest commercially available products and leveraging recently developed hydrogen storage nanomaterial and high surface area catalysts technology, this interoperable system can be optimised in response to local climates and context (tuned to local heating, cooling and electricity needs and adapted to manage local waste flows as discussed below).

Specific end-user benefits

The WHHE Energy Centres have been conceived to interface with a wide variety of end-user scenarios which may arise from local contextual circumstances. The system can be tuned (as will be demonstrated by the validated mathematical models which will be produced) to accommodate specific contexts and end-user needs since the heat and power streams are readily scalable through careful consideration and tailoring of the various energy systems and how the fuel is utilised.

End-user Context 1 – Electricity demand bias

WHHE Energy Centres can be focused on electricity production via the fuel cell/heat engine combined cycle. This is particularly relevant where advantage can be taken from incentives for local renewable electricity production (e.g. through the organic waste content). An electricity-only energy scenario is likely to become increasingly relevant in certain regions in the coming decades as space heating demands decrease (due to improved building standards in terms of structure insulation, air tightness and air heat recovery systems) and electricity becomes the dominant energy to power buildings via electrical boilers/heater. Also the demand from electric vehicles will increase.

End-user Context 2 – Heat demand bias

WHHE Energy Centres in cold climates, where high heating demands exist, can focus on meeting the fluctuating energy profiles using stored hydrogen derived directly from purified syngas via a pressure swing absorption unit. Heat fluctuations can be met using conventional boiler systems running on pre-purified hydrogen. District heating networks can also capitalise on any significant thermal energy sources such as waste heat from industrial processes. WHHE Energy Centres can be tuned to deliver specific heat grades depending on the available/required exergy levels via intelligent building-to-building waste heat networks. The WHHE Energy Centre provides a commercial impetus for new district heating schemes but equally can be added to supplement existing district heating networks.

End-user Context 3 – Increasing hydrogen infrastructure

The proposed hydrogen storage backup system in WHHE Energy Centres is modular. This allows for expansion to accommodate future increases in demand for hydrogen (as indicated by the SET plan described in section 1.1.6). The Pressure Swing Absorption unit can also be used to purify syngas for hydrogen storage in order to cater for an increased demand. The challenge of safely storing hydrogen is better solved through solid state hydrogen materials as the staorage mechanism relies on chemical bonds that that allows storage to be achieved at relatively low pressures and less leakage compared to convetional high pressure solutions.

End-user Context 4 – High renewable grid penetration

As grid penetration by renewables (e.g. wind, solar) increases, grid management becomes an issue compounded by demand profiles, such as low demand periods at night-time. The same is true for regions with high penetrations of nuclear power which being base load in character is inflexible to demand fluctuations. In the UK, for example, there have already been instances of negative wholesale electricity prices. During such times electricity can be used to generate and store hydrogen in WHHE Energy Centres and then sold back to the grid during peak demands/prices. Recent studies by Brunel University have shown that solid hydrogen storage balancing systems can achieve lower electricity generation costs than a power system without storage (*Lohner et al., 2012*).

End-user Context 5 – Biomass enriched MSW

The energetic content of MSW can be increased by including other waste streams which may be available locally such as sludge or waste from the food industry, forestry and agriculture. Increasing the biogenic fraction of fuel will in some case increase the renewable energy incentives that can be claimed and thereby boost commerciality.

End-user Context 6 – Land fill clean-up program

MSW fuel streams can also be supplemented by material reclaimed from local landfill as part of new landfill clean-up contracts/programmes. The WHHE Energy Centre can be tuned to ensure the hydrogen storage loops are able to enrich the syngas derived from a waste stream with lower or variable energetic content to ensure the fuel cells are optimally loaded and running at their highest efficiency. Specialist waste, e.g. from hospitals, can also be treated. For this case, a hospital's heat and electricity can be provided as well as hydrogen

for future hospital vehicles. Difficult waste streams such as hazardous materials, which represent 3% of the total waste produced in the EU (*EC Environment, 2012*), as well as construction, industrial and tyre waste could also be processed in the WHHE Energy Centre.

Readers Guide

Overview

1. Introduction

2. The WHHE Concept

3. Literature Digest

Gasification
- Reactions
- Waste variations

IGFCC
- General

Fuel Cells
- Basic principles
- Types
- SOFCs
- Status

Filtering and Gas Processing
- Tars
- Acid gas
- The Claus process
- PSA
- Membranes
- Ceramic filters
- WGS
- ASU

Heat Engine
- General

Hydrogen Storage
- General

Electrolysers
- General

4. SOFCs

5. Modelling

6. Modelling Results

7. Experimental Research

8. micro-CHP in the UK Market

9. Conclusions

References

Appendices

3. LITERATURE DIGEST

As an overview, this research and proposed system advances the state-of-the-art of energy management centres by:

1. Modelling a state-of-the-art 2-stage plasma gasification process to meet the required gas purity via the introduction of a bespoke pressure swing absorber (PSA) unit to deal with fluctuation in syngas composition and syngas flow rate.
2. Including a state-of-the-art solid-oxide fuel cell (SOFC) operating on syngas.
3. Introducing a combined cycle heat engine to boost electrical efficiencies to >25%.
4. Introducing a PEM electrolyser to allow the SOFC to run at continuous optimum conditions and the system to operate in multiple modes, e.g. to import/export electricity in order to take advantage of the frequent/large grid price fluctuations and introduce precious flexibility into the grid.
5. Utilising state-of-the-art high efficiency solid state hydrogen storage materials and system for use with the PSA and electrolyser. Gravimetric energy density is less of a concern for stationary applications as volume is much more at a premium than weight. Furthermore, low pressure storage is preferred due to reasons of system safety and lower costs for compression.
6. Create state-of-the-art mathematical models, such as dynamic simulations, reactor network modelling and financial simulation, in order to optimise the system at end-user scales - which include intelligent district heating networks.

This research is very timely and a similar system is already being trialled in Korea. In October 2011, Ballard & GS Platech's South Korean Waste-to-Energy Fuel Cell Plant was commissioned to demonstrate a plasma gasification waste-to-energy plant which uses a 50kW PEM fuel cell system to supply power to the local Cheongsong grid (*Fuel Cells Bulletin, 2011*). No details of the plant plant have been published and no updated records are avaible so it is not known if this project is ongoing or if it still exists. Taking inot consideration the requirements and differences between the two fuel cell technologies (SOFC and PEM) the following implications can be assumed; its gas clean-up is much more costly and space consuming than that of a WHHE Energy Centre which uses a more robust (and more efficient) SOFC combined cycle. In addition, it would be less flexible than the WHHE Energy Centre which is able to dynamically interact with the grid (via the hydrogen storage system) in order to benefit commercially from the variations in wholesale electricity prices.

This section will examine the current state-of-the-art that has been published in the academic arena.

3.1 GASIFICATION

Gasification is a process whereby carbonaceous materials are heated in the presence of an oxidising agent to produce a gaseous fuel with a low to medium heating value (commonly referred to as syngas). The process does not involve combustion (complete oxidation) but is rather a partial oxidation reaction. Heat can be provided directly through the partial oxidation process by allowing limited amounts of oxygen or steam, or indirectly by supplying superheated steam, heated bed materials, or by burning some of the gases separately. Syngas comprises mainly of CO, CO_2, and H_2 along with smaller concentrations of CH_4, steam (H_2O), nitrogen (N_2)(if air is used for gasification), and trace amounts of tar, volatile alkali metals, nitrogen compounds, sulphur compounds, chlorine compounds and particulates (*Coll et al., 2001; Higman and van der Burgt, 2003; Lorente, 2013*).

The general definition of a tar is reported in *Milne et al.* (1998) as: "The organics, produced under thermal or partial-oxidation regimes (gasification) of any organic material, are called "tars" and are generally assumed to be largely aromatic."

The quality and composition of the syngas depends on a number of factors that include; type of gasifier, feedstock, feedstock size, moisture content, temperature, pressure, gasification agent, residence time and the presence of bed catalysts. Syngas can be used for various applications; as raw material for synthesis of ammonia, liquid fuel (via Fischer-Tropsch), and methanol, or methanation to produce synthetic natural gas, or to generate power as syngas is burnt to provide heat to drive a gas or steam turbine. The efficiencies of these plants are thus constrained by the limits of the Brayton or Rankine thermodynamic cycle. Therefore to improve the electrical output of these plants we must look to technologies such as fuel cells that move beyond these limits.

There are several types of gasifier and they include the updraft and downdraft fixed bed, entrained flow, bubbling and circulating fluidised bed, duel fluidised bed and plasma. Each type of gasifier has inherent characteristics and requirements in terms of the type and size of feedstock, quality of gas produced and gasifier efficiency.

An entrained flow system (*Figure 3-1*) requires feedstock with a small particle size (<1mm) and low moisture content (<15%), as particles are suspended in the chamber during vaporisation. This results in short residence times and reduced amounts of methane and tars in the syngas. Because of the short residence times high temperatures are requires to ensure good conversion of the feedstock. This means, to maintain these higher operating temperatures, oxygen consumption is high. Entrained flow systems can handle a diverse range of feedstock although the quality and composition needs to be kept consistent with biomass being preferred (*E4Tech, 2009*). Pre-treatment of the feedstock to the required size and moisture content can be energy intensive and costly to the efficiency of the plant.

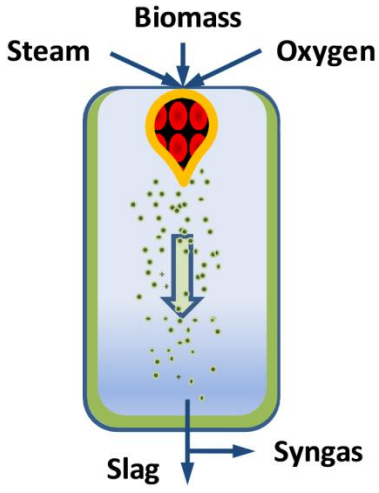

Figure 3-1: Entrained flow gasification (*E4Tech, 2009*).

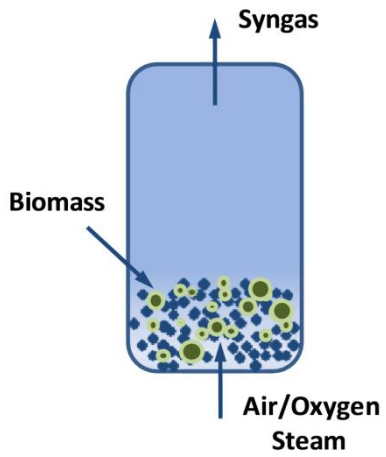

Figure 3-2: Bubbling fluidised bed gasification (*E4Tech, 2009*).

Bubbling fluidised bed gasifiers (*Figure 3-2*) can operate using a wide variety of feedstock, although, feedstocks with low ash melting temperatures can lead to bed agglomeration. This can be countered by the addition of feedstocks with higher ash melting temperatures and/or the inclusion of a mineral binding product such as dolomite to the bed material. Feedstock sizing and moisture tolerance is more generous with a range between 50-150mm in size and 10-55% moisture content. The quality of the syngas depends strongly on whether pure oxygen or air is used as nitrogen will highly dilute the syngas composition. The syngas contains a large amount of particulates along with increased amounts of methane and tars (*E4Tech, 2009*).

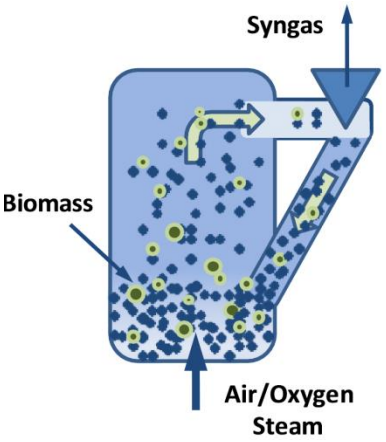

Figure 3-3: Circulating fluidised bed gasification (*E4Tech, 2009*).

Circulating fluidised bed (*Figure 3-3*) systems like entrained flow systems prefer biomass feedstocks but can handle a diverse range that includes MSW. Feedstock is required to be smaller than 20mm and the moisture content can vary between 5-60%. Similar to the bubbling system circulating fluidised bed gasifiers suffer from nitrogen dilution along with increased amounts of particulates and hydrocarbon species in the syngas (*E4Tech, 2009*).

Plasma gasification systems (*Figure 3-4*) are the most diverse and can accept almost any material as feedstock as inorganic materials are vitrified. The ability to control the temperature of the gasifier through the power input to the plasma torch means there are no limitations to feedstock size and moisture content. However, the characteristics and composition of the feedstock directly influence the quality and heating value of the syngas so considerations should be made according to the overall outputs required. Gasification can be achieved without the presence of a gasifying agent, instead, external gas (air, oxygen, steam, nitrogen, argon) is required to maintain the plasma field. The temperature of the plasma core can reach ca. 30,000°C thereby providing an average reactor temperature of up to 5,000°C (*E4Tech, 2009*). These high temperatures ensure efficient breakdown of molecules, and any formation of hydrocarbons such as tar are cracked, thereby producing a very high quality syngas (*Galeno et al., 2011*).

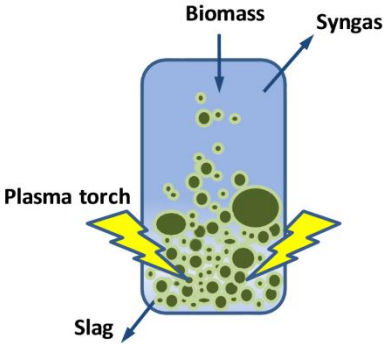

Figure 3-4: Plasma gasification (*E4Tech, 2009*).

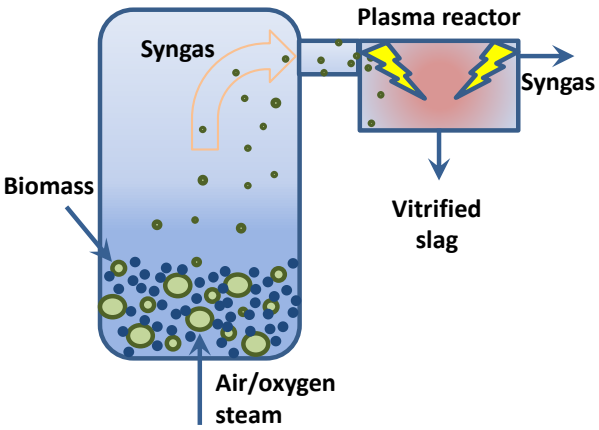

Figure 3-5: Dual bubbling fluidised bed/plasma gasification.

A concept called Gasplasma® presented in (*Morrin et al., 2012*)(*Figure 3-5 and 3-6*) employs a two stage fluid bed-plasma gasification process developed by Advanced Plasma Power (APP) and uses a conventional bubbling fluidised bed gasifier from Energy Products of Idaho (EPI) (*E4Tech, 2009*), and is combined with a subsequent in-house plasma chamber. The gasifier operating at ca.850°C and using steam and oxygen as gasifying agents produces a raw syngas, containing particulates and tars, which is passed to the plasma converter operating at ca.1200°C which serves to crack the remaining organic molecules (including tars). From the vitrification of ash and inorganic materials the plasma converter produces an inert slag (called Plasmarok®) and is a suitable material for construction aggregate. The result is a high quality syngas with virtually no tar products.

In the APP design the MSW feedstock is first treated in a materials recycling facility (MRF) which serves not only to promote the waste hierarchy but also to remove moisture to 10-17%, and to homogenise the waste (*Morrin, 2011*). This concept drastically reduces the parasitic loads associated with single stage plasma gasification whilst producing the same quality syngas.

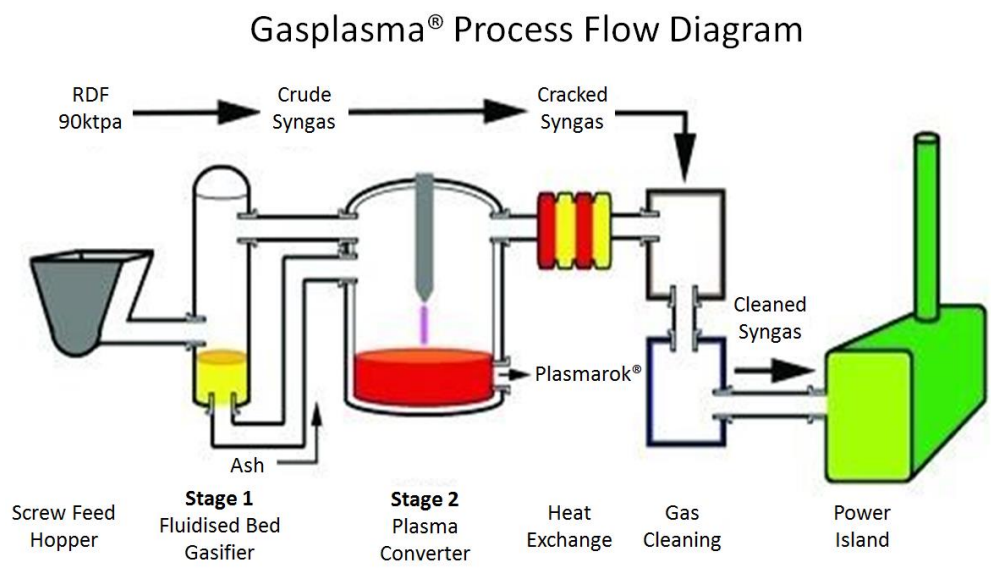

Figure 3-6: Gasplasma® process developed by Advanced Plasma Power including a plasma converter in order to breakdown tar (*APP, 2012*).

3.1.1 REACTIONS

The process of gasification involves the breakdown of materials and the principle chemical reactions involve carbon, hydrogen, carbon monoxide, carbon dioxide, steam and methane and can be represented through the following reactions (*Higman et al., 2003*) (standard enthalpies of formation [$\Delta_r h$ at 298K]):

$C + \frac{1}{2}O_2 \rightarrow CO$	-111 MJ/kmol
$CO + \frac{1}{2}O_2 \rightarrow CO_2$	-283 MJ/kmol
$H_2 + \frac{1}{2}O_2 \rightarrow H_2O$	-242 MJ/kmol
$2CO \leftrightarrow C + CO_2$ **(Boudouard)**	-173 MJ/kmol
$C + H_2O \leftrightarrow CO + H_2$ **(Water gas)**	+131 MJ/kmol
$CO + H_2O \leftrightarrow CO_2 + H_2$ **(CO shift)**	-41 MJ/kmol
$C + 2H_2 \leftrightarrow CH_4$	-75 MJ/kmol
$CH_4 + H_2O \leftrightarrow CO + 3H_2$ **(Steam methane reforming)**	+206 MJ/kmol

The temperatures used for gasification are sufficiently high that no hydrocarbons can be present in any significant quantity (apart from methane) (*Higman et al., 2003*), and the gas phase reaction rates are sufficiently high at the normal gasification temperature that the main gaseous components achieve thermodynamic equilibrium (*Liu et al., 2009*).

The introduction of oxygen will promote exothermic oxidation whereas if steam, carbon dioxide, or nitrogen is used along with oxygen as an input to the gasifier these compounds are used as moderators. Moderators are used to control the temperature of the reactor as their reactions are endothermic and they serve to remove heat from the reactor. These moderator gases are used to maintain fluidisation within the unit keeping the fuel and inert bed material suspended allowing fluid movement of these solids. The influence of oxygen and steam to control the temperature of the gasifier will be looked at in greater detail further into the text.

3.1.2 VARIATION IN WASTE COMPOSITION

The composition of waste is never fixed and understanding these variations can be very important for waste management planning. There is a number of factors that contribute to these variations and they include; seasonal variations, different regional areas, cultural and ethnic diversity, socio-economic profile, urban context and many other factors that influence consumer trends (*EB Nationwide, 2004; NWRWMG, 2010; Jones et al., 2008*).

Table 3-1: Seasonal variation of kerbside waste (NWRWMG, 2010).

Primary Categories	Summer Sampling			Winter Sampling		
	Mean	*Lower Bound*	*Upper Bound*	*Mean*	*Lower Bound*	*Upper Bound*
Paper	5.63%	1.18%	10.08%	8.10%	*3.22%*	*12.99%*
Card	2.42%	0.00%	5.80%	4.09%	*2.66%*	*5.52%*
Dense Plastic	5.68%	2.08%	9.29%	6.55%	*4.91%*	*8.20%*
Plastic Film	6.27%	2.62%	9.92%	9.85%	*8.65%*	*11.05%*
Textiles	3.69%	0.00%	8.205	3.53%	*1.49%*	*5.57%*
Glass	8.84%	3.47%	14.21%	7.01%	*1.60%*	*12.41%*
Miscellaneous Combustibles	6.92%	1.78%	12.07%	6.37%	*4.38%*	*8.36%*
Miscellaneous Non-combustibles	2.50%	0.86%	4.15%	1.37%	*0.48%*	*2.25%*
Ferrous metal	1.74%	0.79%	2.70%	0.99%	*0.06%*	*1.93%*
Non-Ferrous Metal	1.08%	0.19%	1.97%	2.01%	*1.44%*	*2.59%*
Waste Electrical & Electronic Equipment	0.09%	0.00%	0.18%	0.38%	*0.11%*	*0.64%*
Hazardous Household Waste	0.35%	0.00%	0.72%	1.81%	*0.56%*	*3.06%*
Organic Non-Catering	9.78%	3.31%	16.25%	6.86%	*3.72%*	*10.0%*
Organic Catering	39.82%	20.18%	59.46%	30.78%	*21.14%*	*40.41%*
Fines (Less than 10 mm)	5.19%	2.40%	7.97%	10.30%	*3.09%*	*17.51%*

Table 3-2: Variation in waste composition according to different socio-economic groups (NWRWMG, 2010).

Primary Categories	Wealthy Achievers	Urban Prosperity	Comfortably Off	Moderate Means	Hard Pressed
Paper	6.6%	15.3%	5.2%	7.1%	8.9%
Cardboard	2.9%	6.8%	4.2%	5.9%	3.3%
Dense Plastic	5.45%	7.04%	8.00%	7.00%	6.22%
Plastic Film	8.94%	11.39%	9.23%	8.81%	7.14%
Shoes and Textiles	2.98%	3.06%	5.11%	7.32%	3.25%
Glass	8.8%	16.5%	9.1%	6.5%	6.6%
Miscellaneous Combustibles	7.5%	8.5%	8.2%	6.6%	4.1%
Miscellaneous Non-Combustibles	2.4%	0.6%	2.5%	1.7%	0.7%
Ferrous Metal	1.0%	0.0%	2.0%	1.0%	1.6%
Non-Ferrous Metal	1.2%	2.2%	1.9%	2.4%	2.0%
Waste Electrical & Electronic Equipment	0.5%	0.5%	0.0%	0.1%	0.1%
Hazardous Household Waste	2.0%	0.0%	0.0%	0.6%	0.7%
Organic Non-Catering	8.1%	2.3%	8.1%	2.5%	10.3%
Organic Catering	34.3%	24.5%	30.9%	40.1%	34.4%
Fines (Less than 10 mm)	7.4%	1.4%	5.7%	2.5%	10.7%
Total	**100.0%**	**100.0%**	**100.0%**	**100.0%**	**100.0%**

Table 3-3: Statistical summary of variation in waste categories in 2008 (*Jones et al., 2008*).

WASTE CATEGORY	mean of all hhs (kg/hh/wk)	% of hhs disposing of waste category	households disposing of waste category				
			arithmetic mean (kg/hh/wk)	median (kg/hh/wk)	standard deviation (kg/hh/wk)	range (kg/hh/wk)	coefficient of variation
cardboard & paper packaging	0.9	95.7%	0.9	0.8	0.7	3.4	0.7
non-packaging paper	1.8	94.7%	1.9	1.3	1.7	7.3	0.9
dense plastic packaging	0.6	97.9%	0.6	0.5	0.5	2.1	0.8
miscellaneous plastic	0.4	93.6%	0.4	0.3	0.4	1.9	0.9
ferrous packaging	0.3	89.4%	0.4	0.3	0.5	3.0	1.2
aluminium packaging	0.2	86.2%	0.2	0.1	0.3	1.5	1.3
miscellaneous metal	0.3	31.9%	0.8	0.1	1.4	5.0	1.8
glass packaging	1.4	94.7%	1.5	1.1	1.3	5.9	0.9
textiles	0.4	63.8%	0.6	0.1	1.3	9.0	2.3
putrescible kitchen waste	2.8	93.6%	3.0	2.3	2.7	12.3	0.9
garden waste	3.3	64.9%	5.0	1.6	7.4	40.0	1.5
sanitary wastes	0.3	9.6%	3.5	2.8	3.5	9.5	1.0
misc. combustible waste	1.4	73.4%	2.0	0.2	5.9	43.2	3.0
misc. non-combustible waste	0.6	43.6%	1.4	0.2	3.6	19.0	2.6
fines	0.1	47.9%	0.2	0.1	0.2	1.0	1.3
TOTAL WASTES	14.7	100.0%	14.7	10.6	11.2	45.0	0.8

In a study published by *Chester et al. (2008)* the variation in oxygen and hydrogen content is influenced by the perturbations to the waste stream's composition. Results of a Monte Carlo simulation showed that for household waste the hydrogen content has a mean of 9.87% with a standard deviation of 0.49. Therefore, indicating with 95% confidence that the hydrogen content varies between 8.94% and 10.87%.

3.2 IGFCC

Due to the number of components being integrated a search of publications produces a variety of configurations where authors have looked at different gasification technologies, primary feed stocks, fuel cells, filtering techniques etc. In order to gain a comfortable perspective of the current state of published knowledge only papers with direct similarities will be discussed.

Galeno et al. (2011) carried out modelling research on the integration of a SOFC with a plasma gasification unit operating on MSW. The research was carried using the Aspen Plus code environment where the authors used a previously self-developed thermochemical model which was titled 'EquiPlasmaJet' (EPJ) for the modelling of the gasification unit. The SOFC was modelled at a one dimensional system level where the following assumptions were made: steady state and isothermal operation, fuel composition only varied on outlet, all gases were ideal, all reactions were in chemical equilibrium and uniform cell voltage was produced by each cell. The overall results showed a net power output of 4.2MW per kg of refuse derived fuel with an electrical efficiency of 33% compared with a quoted 20% efficiency of conventional incineration technologies producing electricity.

An earlier paper published by the same department authored by *Minutillo et al. (2009)* focusses on the development of the EPJ model, created using Aspen Plus, and applied to the modelling of an integrated plasma gasification combined cycle power plant without the fuel cell. In this research syngas derived from MSW with a LHV of 9 MJ/kg was used to drive a gas turbine where the system efficiency was calculated at 31%.

Sadhukhan et al. (2009) published a paper on the performance analysis of an integrated biomass gasification fuel cell (BGFC) system against that of a conventional biomass gasification combined cycle (BGCC), whilst using Aspen Plus as their simulation platform. The process studied included syngas filtering using Rectisol. Steam and unspent fuel from the SOFC was fed back to the gasifier as a means of promoting the gasification process and increasing hydrogen production. The simplified model for the fuel cell predicted a performance efficiency of 85% whilst producing 652kW of electricity based on a LHV of 14.6 MJ/kg for the raw biomass and an 85% fuel utilisation factor. The overall system electrical efficiency for the BGFC cycle was reported at 64.41% and at 83.4% when running in CHP mode. Corresponding, the electrical efficiency for the BGCC was calculated at 32.14% and 42.23% in CHP mode.

An interesting study carried out by *Meerman et al. (2010)* looked at the performance of an integrated polygeneration gasification facility which aims to produce electricity during peak hours whilst switching to the production of chemicals during off-peak hours. This concept is similar to one of those in this research, and that is to deal with load fluctuations through the production of a secondary fuel. Although *Meerman et al. (2010)* do not make use of fuel cell it is interesting to understand their findings. Again modelling was done using Aspen Plus. When producing only electricity the facility demonstrates an efficiency of 40%, but when the gas turbine is run at 64% part load and the remaining gas going to chemical production the overall efficiency was seen to be as high as 59%.

A numerical study which looks at an integrated gasification fuel cell combined cycle fuelled by coal was carried out by *El-Emam et al. (2011)* where the heat from a SOFC was used to drive a gas turbine and steam turbine. The main outcome to come from this study, which analysed the performance of the system using two types of coal, was that the overall system efficiency varied between 38.1% and 36.7%. A very simplified model was used to calculate the partial pressures which were applied to the Nernst equation where a constant value of 1.19V was used for the maximum reversible voltage. The Nernst equation is used calculate the theoretical potential for an electrochemical reaction as a function of the partial pressures of the reactants and products and is further explained in *Chapter 4*.

Nagel et al. (2009) performed a technical analysis, using Aspen Plus, of a biomass integrated gasification fuel cell system scaled to 1MWe. Here the SOFC ran with predefined values for fuel utilisation at 85% and 46% electrical efficiency whilst providing a voltage of 0.6V. No tar removal techniques were applied and were assumed not to have an impact on the performance of the fuel cell. Organic sulphur compounds were also assumed not to have an impact on the fuel cell. No overall system efficiencies were measured but the conclusions were concentrated rather on the effects of various gasification technologies on the thermal gradients of co-current and counter current fuel cell designs. The gasification techniques studied were; updraft gasification, downdraft gasification and fluidised bed gasification which produced syngas with LHVs of 5.193, 4.797 and 7.288 MJ/m^3 respectively. Concluding remarks from the authors stated that for co-current cell designs thermal stresses increased with increasing internal reforming potential, and in contrast counter-current cells are comparably insensitive to varying fuel gases.

A further study using Aspen Plus was conducted by *Panapoulos et al. (2005)* where a modelling and feasibility study was performed for a SOFC when integrated with an allothermal biomass gasification unit. The author mentions the advantages of building these facilities in regions where heat can be utilised thereby operating the plant as a CHP facility. The research also concentrates on using optimal filtering techniques which remove particulates, sulphur compounds as well as any tar compounds. The SOFC model uses equations for; molecular and Knudsen diffusion, and all three losses where individual material properties such as resistance are included. Overall the fuel cell modelling seems to be very well constructed with sound explanations for the approach taken. Results of the study concluded a system efficiency of 36% producing 140kWe with a fuel utilisation of 70%. Heat from the fuel cell is recycled to feed the gasifier and the overall thermal efficiency was calculated at 14%.

3.3 FILTERING AND GAS PROCESSING

A major obstacle in the successful application of gasification technologies is the relative inability to clean the syngas efficiently and reliably. As mentioned, raw syngas coming from the gasifier invariably contains significant amounts of fluid and solid contaminants such as ash and char, tars (organic hydrocarbon molecules), volatile alkali metals, nitrogen compounds, sulphur compounds, chlorine compounds and others (*Coll et al., 2001; Higman and van der Burgt, 2003; Lorente et al., 2013*). To maximise the overall cycle efficiency gas filtering and processing must be accomplished at the highest possible temperature.

3.3.1 MEMBRANE SYSTEMS

Polymer membranes can be used to selectively separate gas compounds by utilising the difference between solubility and diffusion properties of different gases. Permeation through the membrane is controlled by the difference in partial pressure of the gas component either side of the membrane. Because permeation is controlled by partial pressure it is difficult to control selectivity, a list of typical syngas components and their relative permeability rates is shown in *Table 3-7*. This means during hydrogen separation purification levels can be low. Although, in application these systems can be useful if placed before the PSA thereby allowing the PSA to operate at better efficiency and means the PSA unit can be much smaller.

Table 3-4: Relative permeability rates of typical syngas components (*Higman et al., 2003*).

Quick	Intermediate	Slow
H_2	CO_2	CO
He		CH_4
H_2S		N_2

3.3.2 CERAMIC FILTERS

Hot gas filtration using ceramic filters with a mirco-porous surface with the ability to trap sub-micron particles operating at temperatures from 400 - 1100°C have many benefits in filtering syngas (*Glosfume, 2013*)(*Figure 3-7*). These filters (also called candle filters) effectively replace conventional bag filters used to capture particulates, and filtering at elevated temperatures prevents condensation of products on the filters and maintains energy otherwise lost during excessive cooling. These filters are also used to reduce emissions of HCl and SO_2 by injecting sodium bicarbonate ($NaHCO_3$) into the incoming gas allowing the following reactions to take place (sodium bicarbonate remains active at 450°C):

$$NaHCO_3 + HCl \longrightarrow NaCl + H_2O + CO_2$$

$$2NaHCO_3 + SO_2 + \frac{1}{2}O_2 \longrightarrow Na_2SO_4 + 2CO_2 + H_2O$$

Figure 3-7: Hot gas ceramic filter module (*Glosfume, 2013*).

3.3.3 DEALING WITH TARS

A drawback even when gasifying at high temperatures between 800-1000°C is the formation of a significant amount of tar within the synthesised gas. The formation of tar is problematic to the system as this will cause build up and blockages of the equipment, therefore a secondary reactor is required to further purify and clean the gas. The formation of tar is a major obstacle in utilising gasification for power generation and there are various methods for reducing or eliminating the production of tar.

Asadullah et al. (2008) have shown that by using a catalytic process with $Rh/CeO_2/SiO_2$ as a catalyst we can improve the reforming and combustion reactions at lower temperatures, and cellulose products such as tar can be completely converted to gas at 500°C. Further tar removal techniques are explored and explained in a paper published by *Han and Kim (2008)*. There are mechanical methods that are employed to capture the particles from the product gas and these include scrubber, filter, cyclone and electrostatic systems. These systems have tar separation efficiencies ranging from 51-91%, but from the removal the energy embodied within the tar is lost. These systems are fairly expensive and produce a large amount of contaminated water which introduces a new waste management problem. The Energy Research Centre of the Netherlands have successfully demonstrated a tar removal system called 'OLGA' (oil-based gas washer) where the tar could be selectively and completely removed, whilst reducing the water-soluble tar compounds and preventing excessive waste water contamination, seen in *Figure 3-8*.

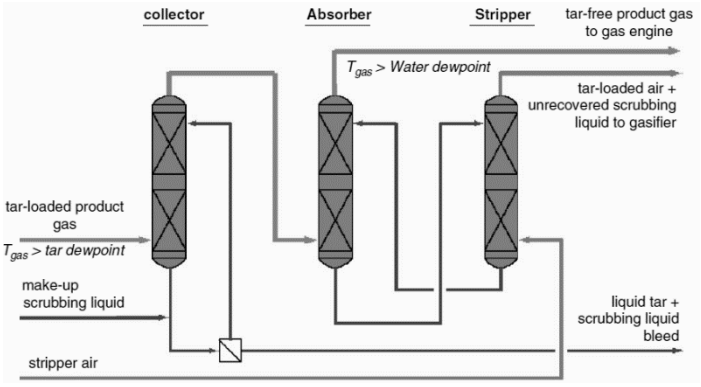

Figure 3-8: The outline of the OLGA process

Electrostatic precipitation is a particle collection device that can completely remove the heavy tar in the product gases, and is applied in coal fired power plants, metallurgical industry and the cement industry due to its high efficiency.

Activated carbon filters have also been shown to obtain good tar separation efficiencies but over time the tar is deposited and builds up on the filter surface that would eventually lead to plugging.

Table 3-5: The reduction efficiency of particle and tar in various gas cleaning systems (*Hasler and Nussblaumer, 1999*)

Gas Cleaning System	Particle reduction (%)	Tar reduction (%)
Sand bed filter	70-99	50-97
Wash tower	60-98	10-25
Venturi scrubber		50-90
Wet electrostatic precipitator	>99	0-60
Fabric filter	70-95	0-50
Rotational particle separator	85-90	30-70
Fixed bed tar absorber		50

The operating conditions also play an important role in the formation of tar and the parameters that affect this are: temperature, equivalence ratio, pressure, gasifying medium, residence time and the type of feedstock. Research on the influence of temperature has been conducted by *Li et al*. (2004) who reported that tar yield from biomass gasification decreased from 15.2 to 0.4g/Nm^3 as the temperature increased from 973K to 1088K, and further studies by *Narváez et al.*, (1996) showed tar content at 700°C was 19g/Nm^3 and at 800°C it was 5g/Nm^3, how the has been varied is not mentioned and if done by increasing the exothermic oxidation it is difficult to conclude which change is causing the tar variation. It has also been shown that the tar yield increased with temperature until 600°C is reached at which point the yield begins to fall away (*Fagbemi et al., 2001*). This is explained by the temperature at which tar cracking begins and the tar begins to decompose.

The lambda ratio (λ) which describes the actual air fuel ratio against the air fuel ratio for complete combustion, and increasing this ratio has shown to have a beneficial effect on the reduction in tar formation, but also results in a decrease in the heating value of the gas produced. A study done in increasing the λ in two stages; 0.19-0.23 and 0.23-0.27, showed an increase in gas yield from 2.13 to 2.37 Nm^3/kg and the Lower Heating Value (LHV) increased from 8,817 to 8,839 kJ/Nm^3 in the first stage, whilst the second stage caused a decrease in the LHV (*Bhavanam et al. 2011*). It has been reported that the λ producing the highest yield in H_2 (9.3%vol) is 0.59 (*Bhavanam et al. 2011*).

Singh et al. (2014) studied the various conditions under which carbon deposition through the build-up of tar could be limited and what are the contributing factors to tar formation. These parameters were extended to the operation of the SOFC and how factors such as: material of the anode, current density, temperature and steam/carbon ratio, effect the carbon deposition due to tar build up at the SOFC.

It was shown that as the current density increases the amount of carbon deposited reduces until a point where it reaches zero, and this varies depending on the composition of tar within the syngas at 750°C. Increasing the steam content has also been shown to have a favourable effect on carbon deposition, making the fuel cell more resilient and less susceptible to tar degradation as a result.

A 150hr test of a commercial high temperature single planar SOFC operating on wood gas from the Viking two-stage fixed-bed down draft gasifier at the Technical University of Denmark has been performed and presented in a paper by *Hofmann et al. (2007)*. The results showed that with a steam/carbon ratio of 0.5 and an operating temperature of 850°C the fuel cell operated with a fuel utilisation factor around 30% and a current density of 260 mA/cm^2 providing an average power density of 207mW/cm^2 with no signs of carbon deposition or any contamination of the anode. The Viking gasifier's two stage process limits the formation of tar by separating the pyrolysis and gasification stages, where pyrolysis products are partially oxidised and heated to 1100°C, significantly reducing the formation of tar, before passing through the char bed created in the gasification chamber, further reducing the tar composition. The gas is then cooled to 90°C through several heat exchangers which recover the heat to be used further in the system, soot particles are then removed using a bag house filter before the moisture is extracted through condensation. Prior to entering the fuel cell an activated carbon filter is used to remove the sulphur and polycyclic aromatic hydrocarbon content, and the steam/carbon ratio is controlled by a condenser/heater before the gas is reheated for entry into the fuel cell.

The Gasplasma® process developed by APP uses a conventional fluidised bed gasifier operating at a temperature between 700-850°C and uses a mixture of steam and oxygen as the gasification medium (*Ray et al., 2012*). This produces a raw syngas with significant amounts of char, ash, tars and other liquid organic contaminants (*Chapman et al., 2010*). This gas is then treated in a single carbon electrode plasma converter where the temperature of the gas is increased whilst being exposed to intense ultra violet light which aids the breakdown of the tar and char products (*Ray et al., 2012*). The plasma chamber is operated at temperatures between 1100-1200°C (*Materazzi et al., 2013*). Particulates in the chamber are trapped and vitrified into an environmentally stable slag the company have called Plasmarok® (*Chapman et al., 2010*).

The role of the plasma converter to reduce the levels of tar is demonstrated in *Figure 3-9*, and the impact of temperature on the cracking of benzene is shown in *Figure 3-10*.

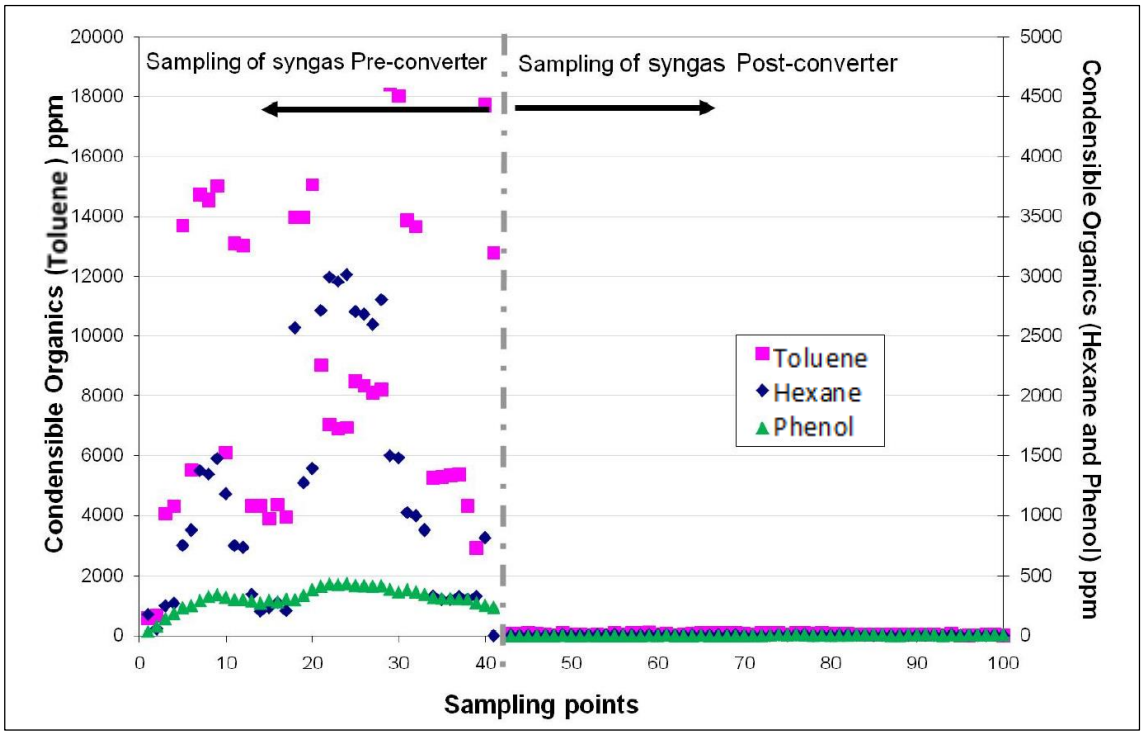

Figure 3-9: Demonstrating the role of the plasma chamber by measurements of tar products before and after exposure to the thermal plasma (*Chapman et al., 2010*).

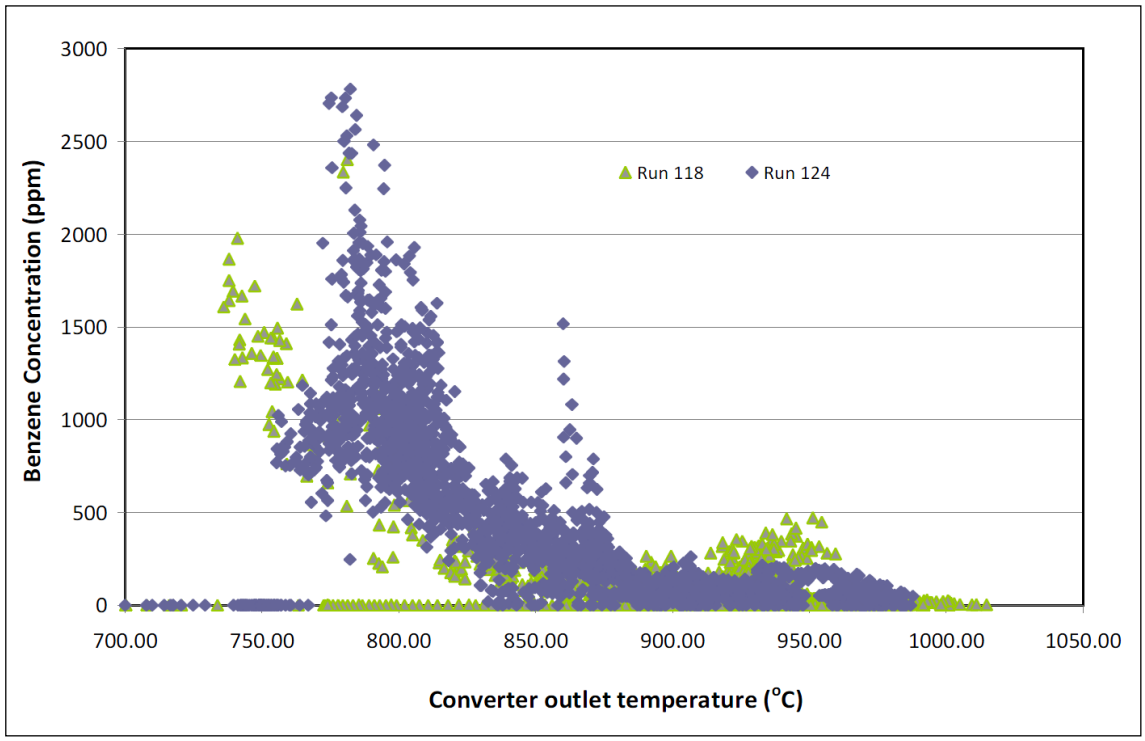

Figure 3-10: The influence of the plasma chamber outlet temperature on the concentration of benzene (*Chapman et al., 2010*).

3.3.4 ACID GAS REMOVAL

There are a number of commercial processes currently available for the removal of acid and all are based on the following principles (*Higman et al., 2003*):

- Absorption in a solvent
- Adsorption onto solid particles
- Diffusion through a permeable membrane
- Chemical conversion

The application of these processes requires cooling of the gas resulting in overall efficiency losses to the plant. The selection of one of the above processes depends on; purity requirements, raw gas composition, and selectivity.

Absorption in a solvent requires washing the syngas in a column where acid components are selectively removed. The rich solvent is then regenerated and recycled back to the absorber, seen in *Figure 3-11*. Generally regeneration through reboiling the solvent leads to the release of the acid components in their original form. A class of oxidative washes can be used to regenerate the solvent by oxidising the active component thereby recovering the sulphur in elemental form.

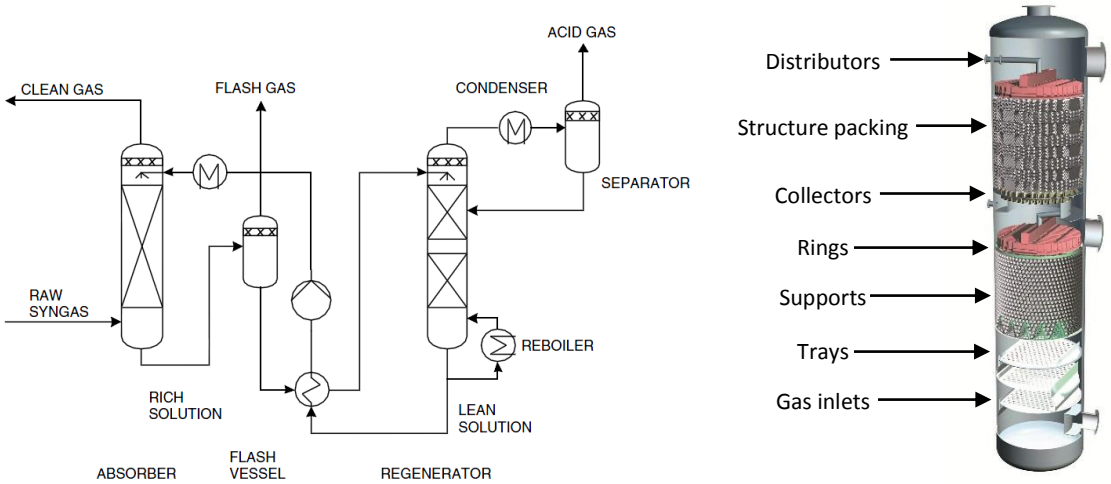

Figure 3-11: Typical absorber flowchart including regeneration (*Higman et al., 2003*), and illustration of tower with different types of internals (*Sulzer, 2014*).

Selexol™ is often used as a physical solvent wash used to primarily remove H_2S, and will also absorb COS and CO_2 but at lower ratios. Selexol™ has the benefit of working at near ambient conditions which eliminates the heavy refrigeration demands of other solvents, such as Rectisol® which requires a temperature of about -40°C to -62°C (*Song et al., 2009*), although lower operating temperatures will increase solubility (*Higman et al., 2003*). Selexol™ is a mixture of dimethyl ether of polyethylene glycol (DEPG) ($CH_3O(C_2H_4O)_nCH_3$ (n between 2 and 9), a comparison of solubilities of various gases in Selexol™ solvent is shown in *Table 3-5*. After regeneration H_2S is often processed in a Claus unit to produce elemental sulphur.

Table 3-6: Relative solubility of various gases in Selexol™ (*Song et al., 2009*).

Component	R=K[CH_4]/K[component]
H_2	0.2
N_2	0.3
CO	0.43
CH_4	1
C_2H_6	7.2
CO_2	15.2
C_3H_8	15.4
COS	35
NH_3	73
H_2S	134
C_6H_{14}	167
C_7H_{16}	360
CS_2	360
SO_2	1400
C_6H_6	3800
C_2H_5OH	3900
CH_2Cl_2	5000
CH_2Cl_3	5000
C_4H_4S	8200
H_2O	11,000
HCN	19,000

Amine solutions in water are also extensively used for acid gas removal. Amines used for syngas treatment are mono- and diethanolamine (MEA and DEA), methyldiethanolamine (MDEA), and di-isopropanolamine (DIPA). MDEA is the most widely used in syngas applications as CO_2 is absorbed more slowly than H_2S (*Higman et al., 2003*). MDEA also has the potential to absorb COS albeit at lower solubility rates so it is recommended to use a hydrolyser to convert COS to H_2S using the following reaction:

$$COS + H_2O \longrightarrow H_2S + CO_2$$

The process for MDEA absorption and regeneration is similar to the process described in *Figure 3-11* above.

3.3.5 THE CLAUS PROCESS

Once sulphur compounds are removed from the syngas it is unacceptable to release H_2S to the atmosphere so it is necessary to convert the sulphur compounds into secondary products which are more benign. The preferred choice is to produce elemental sulphur which has a market value and is also easy to transport in bulk. In order to produce elemental sulphur from H_2S and SO_2 a reaction defined as the Claus process is used and follows the following set of reactions:

$$H_2S + \frac{3}{2}O_2 \leftrightarrow SO_2 + H_2O$$

$$2H_2S + SO_2 \leftrightarrow 2H_2O + \frac{3}{8}S_8$$

$$Overall\ reaction \implies \quad 3H_2S + \frac{3}{2}O_2 \leftrightarrow 3H_2O + \frac{3}{8}S_8$$

3.3.6 PRESSURE SWING ADSORPTION

Pressure swing adsorption (PSA) units are used to separate gas species from a mixture under pressure. This technology relies on a species molecular characteristics and affinity to adsorb to a solid surface and once the pressure is reduced the gas species is released. Gas selectivity is controlled as different gases have a tendency to be attracted to different materials at varying degrees. Unlike cryogenic separation these units tend to operate at near ambient conditions (*Jaya, 2013*). When used for hydrogen purification the pressure range is in the range of 15-30 bar, with typical yields between 80-92% and purities can range from 99-99.999% (*Higman et al., 2003*). In the application of gasification systems it is useful to compare the performance of likely impurities as shown in *Table 3-6*.

Table 3-7: Relative strength of adsorption of typical syngas impurities (*Higman et al., 2003*).

Non-absorbed	Light	Intermediate	Heavy
H_2	O_2	CO	C_3H_6
He	N_2	CH_4	C_4H_{10}
	Ar	C_2H_6	C_5+
		CO_2	H_2S
		C_3H_8	NH_3
			H_2O

3.3.7 WATER GAS SHIFT

Due to the high levels of CO produced from gasification there is an opportunity to increase the amount of H_2 in the syngas by shifting the CO to CO_2 through the following exothermic reaction:

$$CO + H_2O \leftrightarrow CO_2 + H_2 \qquad \text{-41 MJ/kmol}$$

As shown the WGS reaction produces an extra mole of hydrogen from the reaction of carbon monoxide with water. Reducing the amount of carbon monoxide is also advantageous as carbon monoxide can poison downstream catalysts. The process often uses a catalyst to facilitate the reaction and is controlled using temperature, *Figure 3-12* shows it is more favourable to run the WGS reaction at lower temperatures.

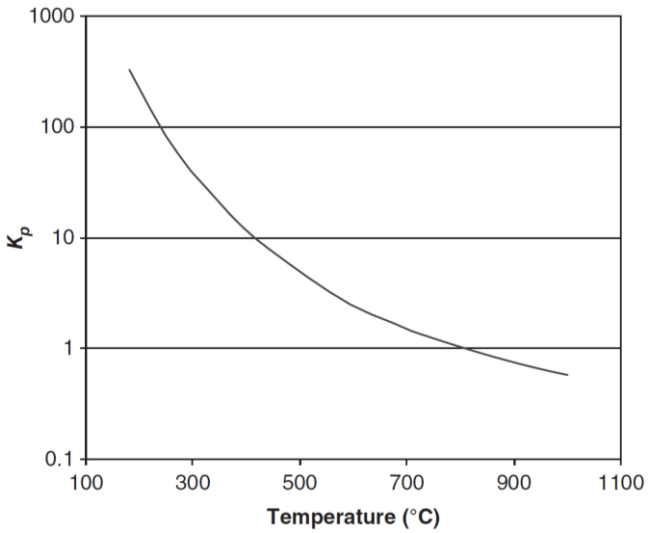

Figure 3-12: Variation of the WGS equilibrium constant as a function of temperature (*Song et al., 2009*).

Generally the WGS reaction is carried out in two steps, first a high temperature shift reaction (>300°C), followed by a low temperature shifts that takes advantage of the favourable equilibrium below 250°C (*Song et al., 2009*).

- **HIGH TEMPERATURE SHIFT**

The conventional high temperature shift reaction normally uses an iron oxide based catalyst operating at a temperature range between 300-500°C. The catalyst comprising of 90% Fe_2O_3 and 10% Cr_2O_3 is generally used. The catalyst is tolerant to sulphur and chlorine compounds, although sulphur may accumulate as FeS which is less active (*Song et al., 2009*). There is also a danger that sulphur fluctuations in the gas can damage the mechanical strength of the catalyst. Heat management in the reactor is a concern as the reaction is exothermic so shifting is often done in stages which limits excessive catalyst temperatures and promotes equilibrium of the reaction. Stages are normally separated by heat exchangers which serve to control inlet temperatures.

Another catalyst that offers very good tolerance to sulphur and functions above 300°C is Molybdenum disulphide (MoS_2) (*Reddy and Smirniotis, 2015*) and the resistance to both H_2S and HCl has been presented by *Torkelson et al. (2008)* where no irreversible degradation was seen at 3000ppm and 350ppm of H_2S and HCl respectively.

- **LOW TEMPERATURE SHIFT**

These reactions operate in the temperature range of 200-250°C and typically use a copper-zinc-aluminium catalyst, although, ZnO has an affinity to sulphur. Again the challenge is to control the temperature of the reaction as above 270°C the copper catalyst will begin to recrystallize.

3.3.8 AIR SEPARATION UNIT (ASU)

When oxygen is used instead of air for gasification plants must include an air separation unit (ASU) to provide oxygen from air. The most widely used technique for separating oxygen from air is cryogenic liquefaction whereby oxygen is compressed and condensed to its liquid state thereby distilling air into nitrogen gas and liquid oxygen. This is a mature technology that is proven and reliable which is important for gasification processes as the oxygen feed is at the start of the cycle and very much controls the performance of the plant.

Other technologies such as PSAs can be used where smaller capacities may be required but can only reach purities of approximately 95%. Polymer membranes can also be used although purities are much lower at approximately 40%.

Ceramic ion transport membranes are another alternative for providing high purity oxygen and offer some benefits over cryogenic distillation in terms of size and water consumption and can be 100% selective towards oxygen. These membranes operate at high temperatures (700°C) where oxygen molecules are converted to ions and transported through the membrane (*Smith and Klosek, 2001*).

For gasifier plants where syngas is used to produce other chemical products oxygen purities can be very important, but for small scale systems small levels of impurities may not be too much of a concern. Also, the proposed system will benefit from producing hydrogen from an electrolyser as the electrolyser will inherently be a source for pure oxygen thereby reinforcing the synergies between the technologies being integrated.

3.4 FUEL CELLS

3.4.1 BASIC PRINCIPLES

Fuel cells can be referred to as voltaic cells because chemical energy is directly converted to electricity without the need to produce intermediary heat. Therefore these systems are not constrained by the Carnot efficiency:

$$\eta_{carnot} = \frac{T_H - T_C}{T_H}$$

The difference between fuel cells and batteries is that batteries expend stored energy and once used are either discarded or recharged via an electric charging current. Fuel cells on the other hand are replenished via a supply of fuel which in most cases is hydrogen.

The electrochemical process that produces electricity from the chemical reaction consists of reduction-oxidation reaction where one side loses electrons (oxidation) whilst the other gains electrons (reduction). The formula showing the reaction of a SOFC is expressed as:

$$H_2(g) + O^{2-} \rightarrow H_2O(g) + 2e^- \implies \text{oxidation}$$

$$\frac{1}{2}O_2(g) + 2e^- \rightarrow O^{2-} \implies \text{reduction}$$

The transfer of electrons in the reaction are utilised by separating the fuel and air supplies using an electrolyte material which conducts ions but not electrons, and by connecting either side to an external electrical circuit. Therefore the only way for the chemical reaction to be completed is for the electrons (from the oxidation reaction) to complete the electrical circuit in order to feed the reduction reaction which creates the ions that are transferred through the electrolyte.

3.4.2 TYPES

There are five principle types of fuel cells available and they are distinguished by the type of electrolyte material used between the anode and cathode. Each have their own advantages. *Table 3-8* and *Figure 3-13* provide a review of the main differences between the technologies.

AFC's- Alkaline fuel cells, uses alkaline salt as an electrolyte.
PEMFC's- Proton exchange membrane fuel cells, uses a solid polymer as an electrolyte and operate at low temperatures.
PAFC's- Phosphoric acid fuel cells, uses phosphoric acid as an electrolyte; the only commercially available fuel cell.
MCFC's- Molten carbonate fuel cells, uses a carbonate salt electrolyte that becomes molten at about 650^{o}C.
SOFC's- Solid oxide fuel cells, uses ceramic materials as an electrolyte and operate between 500-1000^{o}C.

Table 3-8: Comparison of available fuel cell technologies

Fuel Cell Type	Electrolyte Material	Mobile ion	Operating Temperature	System Output	Electrical (CHP) Efficiency	Power Density	Advantages
AFC's	Alkaline salt	OH^-	90 - 100°C	10kW-100kW	40-60% (>80%)	150-400 (mW/cm^2)	• Cathode reaction faster in alkaline electrolyte. • Can use variety of catalysts.
PEMFC's	Solid organic polymer	H^+	50 - 100°C	<1kW-250kW	25-35% (70-90%)	300-1000 (mW/cm^2)	• Solid electrolyte reduces corrosion & electrolyte management problems. • Low Temperature. • Quick start-up.
PAFC's	Phosphoric acid soaked in a matrix	H^+	150 - 200°C	50kW-1MW (modular)	>40% (>85%)	150-300 (mW/cm^2)	• High overall efficiency with CHP. • Increased tolerance to impurities in hydrogen.
MCFC's	Lithium, sodium or potassium soaked in a matrix	CO_3^{2-}	600 - 700°C	<1kW-1MW (modular)	45-47% (>80%)	100-300 (mW/cm^2)	• High efficiency. • Fuel flexibility. • Suitable for CHP.
SOFC's	Yttria stabilized zirconia	O^{2-}	500 - 1000°C	<1kW-3MW	35-60% (<90%)	250-350 (mW/cm^2)	• High efficiency. • Fuel flexibility. • Solid electrolyte reduces corrosion & electrolyte management problems. • Suitable for CHP. • Hybrid/GT cycle.

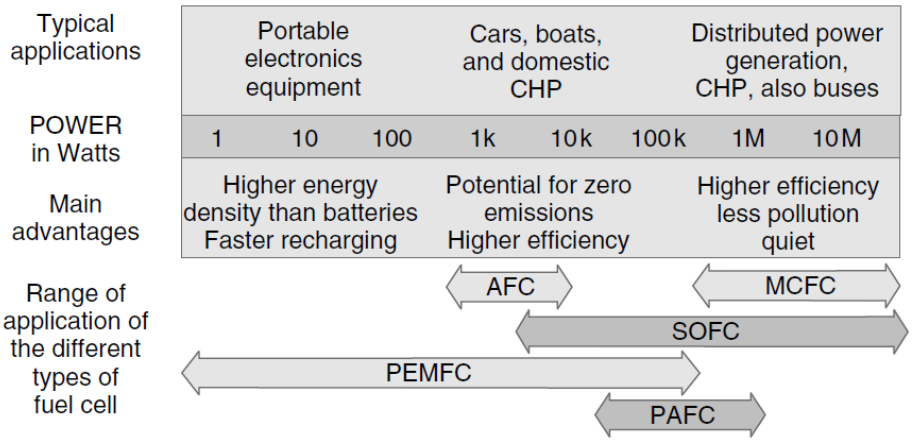

Figure 3-13: Fuel cell systems shown according to suitable scale and application (*Larminie et al., 2003*).

3.4.3 SOFCs

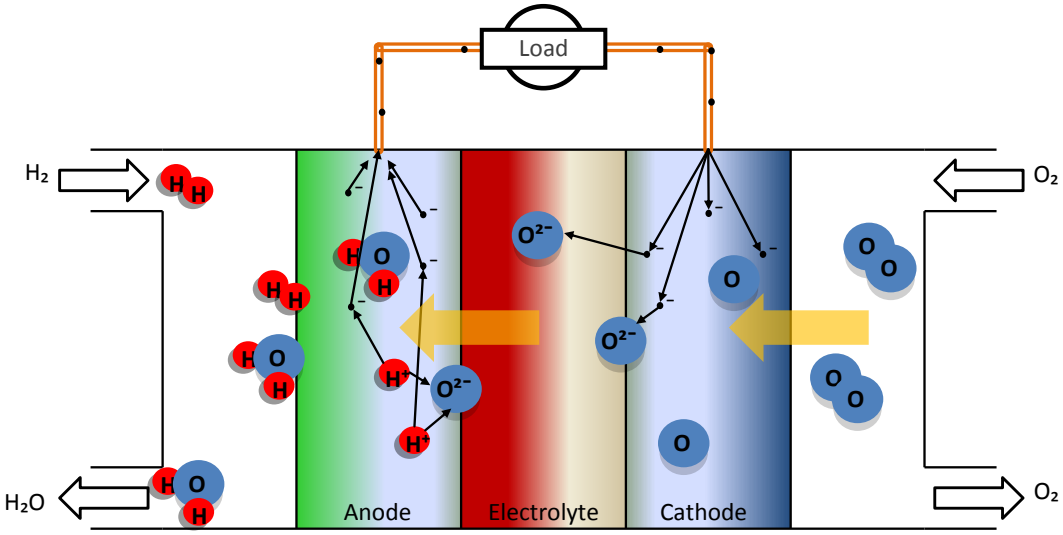

Figure 3-14: Graphic representation of the transport processes within a SOFC showing the flow of oxygen ions through the electrolyte and the flow of electrons from the anode to the cathode via an external load.

3.4.4 STATUS

Of all fuel cell technologies it is Solid Oxide Fuel Cells (SOFCs) that offers by far the greatest potential for the future of high efficiency stationary power supply. Although other technologies are more progressed in terms of large-scale commercial applications, SOFCs have made significant advances along the technology development cycle over the last 5 years. Currently they are commercially available from several companies at very small scale (domestic application 1-2kW) with electrical efficiencies of 60% (*CFCL, 2009*). Sunfire has released 1.1kW and 1.4kW and now 1.7kW versions of its SOFC unit with companies such as Valliant now offering wall mounted versions. Unlike other leading SOFC commercial companies such as CFCL, Sunfire have committed to a programme of larger scale commercial offering starting from a successful release of 5kW units in 2012. Furthermore Sunfire have already achieved 85% fuel utilisation rate in their commercial products. In the medium term, for smaller-scale installations <250kWe, high-temperature fuel cells can be expected to compete commercially with gas engines and micro gas turbines (*Restmac, 2008*).

Figure 3-14 illustrates the transport processes within a SOFC and shows how the electrons must pass through an external load to complete the redox reaction.

There is considerable potential in combing high temperature SOFCs with gas turbines in a hybrid configuration where heat from the fuel cell is used to charge the air coming from the compressor on its way to the expander. The two technologies share favourable synergies as the hot exhaust gases coming from the fuel cell still contain unutilised fuel which can be burnt to reach temperatures that are ideally suited to gas turbine temperature. Also, when directly integrated the fuel cell performs better when run on pressurised air coming from the compressor as pressurised SOFCs offer higher efficiencies according to the Nernst equation (*Bove et al., 2008*). Pressurised also carry

several challenges that must be overcome mainly; achieving a sufficint seal between interconnects at high temperature, and preventing damage to brittle ceramic cells in high pressure and high temperature environments.

Although research is being done to lower the operating temperatures of SOFCs (commonly around 800°C), in the context of a fully integrated energy centre (especially with heat engine hybridisation and links to intelligent district heating networks) there is strong case keeping the operating temperature as high as possible.

Commercial SOFC fuel cells are typically run on steam-reformed methane. However, the potential to run on syngas is clear.

SOFCs and Syngas: SOFC, unlike alternatives such as PEM cells, have a high tolerance to impurities. However, syngas composition from plasma converters is a complex mixture of many species besides H_2(g) which include CO(g) CO_2(g) H_2O(g) N_2(g) and, in trace amounts: HCl(g), C_3H_8(g), CH_4(g), SO_2(g), H_2S(g), COS(g), C_2H_2(g), C_6H_6(g), C_2H_4(g), C_6H_5OH(g), HCN(g), NH_3(g), NO(g), NO_2(g), N_2O(g), O_2(g), HF(g) (as well of potential traces of As, Ba, Cd, Cr, Mn, Mo, Ni, Pb, Sb, Co, Cu, V, Hg, Zn).

Electrical efficiencies of typical gas engines operated with syngas are usually 20-25% (*Florez-Escobar et al., 2015*). Micro gas turbines show electrical efficiencies of 29% for smaller units and 33% in the 200 kW range. Compared to that, high temperature fuel cell (HTFC) systems achieve 35-45% electrical efficiencies as stand-alone units operated with syngas. The high power-to-heat ratio of high temperature fuel cells makes an application in the CHP market attractive.

Among the HTFC types, the molten carbonate fuel cell (MCFCs) benefits from advanced field experience and a more consolidated scientific background. Several developers have demonstrated the MCFC's performance and flexibility in decentralized and niche applications, and an increasing number of small-to-medium-scale plants (250kW - 2MW) are being installed around the world, particularly where stringent environmental constraints are in place (e.g. California) or strong government backing and vision provide impetus to their implementation (e.g. South Korea). Due to the tendency of the electrolyte to evaporate over long periods of operation, commercial MCFC systems are always fairly large (>100kW) in order to maximize the volume-to-surface ratio and minimize the evaporation effect.

The wide variety of possible catalyst materials and the absence of liquid components make SOFCs a promising technology for many applications. SOFCs are operated in a wide range of temperatures (600-1000°C) with a wide range of catalysts, which make strict categorization of contaminant effects very difficult. The critical values of the contaminants mentioned are higher than for the MCFCs but this is to be verified case-by-case.

In practice, SOFCs can tolerate widely varying H_2/C_xH_y/CO compositions; however, the performance optimisation may require significant system design changes (*Yi et al., 2005*). Several groups have studied SOFC fuel flexibility, using theoretical analysis (*Marsano et al., 2004; Eguchi et al., 2002; Coutelieris et al., 2003; Douvartzides et al., 2003; NETL, 2000*). A thermodynamic simulation study, supported by experimental investigation of a variety of fuels in a 25kW tubular SOFC, was reported by Singhal in 2000 (*Singhal, 2000*). Sunfire's stack show only a small deviation in power if fuels

derived from catalytic partial oxidation or steam reforming are compared to its benchmark 40% H_2 / 60% N_2 mixture (*Schimanke et al., 2010*).

Many thermodynamic system analyses of gasification integrated with SOFCs are published, where the theoretical feasibility of the system is proven (*Aravind et al., 2008; Vasileiadis et al., 2004; Panopoulos et al., 2005*). Applications of thermodynamic equilibrium modelling to gasification processes have been reported, especially with reference to coal conversion and to a number of specific biomass gasification processes. The latter have been mainly concerned with parametric studies of the influence of operating conditions and fuel characteristics on the heating value of the product gas and on the overall behaviour of particular gasification plant installations. They have not addressed the potential predictive capability of such methods with regard to such objectives as, say, the enhancement of the product-gas hydrogen content or the production of a syngas with a given CO/H_2 ratio.

A municipal waste gasifier and a SOFC have been tested by the Energy Research Centre for the Netherlands (ECN). ECN connected a two-stage gasifier with a 1 kWel SOFC stack from Hexis. The gasifier was operated with willow and pelletised paper recycling rejects (a rather homogeneous municipal waste). The achieved SOFC efficiency was 41% LHV. However, the stack was operated for no more than 48 hours and some degradation due to soot formation was observed (*Oudhuis et al., 2004*). Later, a 30-cell stack of Staxera's early technology Mk-100 was operated for 5500 h with a H_2/N_2 mixture and several 100 hour tests with different types of cleaned gasifier gases (*Rietveld et al., 2009*).

Extended research has been performed using biomass gasifiers and gas cleaning appropriate to SOFC requirements. The results are largely transferable to gasifier operation with municipal waste. Differences can occur according to the gasifier technology and contaminants in the feedstock like heavy metals, chlorine or alkalines. Gas clean-up was the main focus of SOFC projects like Biocellus and Green Fuel Cell (*EC, 2004*). In the FP6 project Biocellus, a Ni/GDC anode based SOFC was connected to a gasifier for 150h without any significant problem (*Hofmann et al., 2007*). Experiments were also carried out with similar SOFCs connected to a circulating fluidized bed gasifier (CFBG) using real gas with several thousand ppms of tar fed to the SOFCs. No significant degradation of SOFC voltage was observed. It was shown in Green Fuel Cell, that a 30-cell Staxera stack could be operated over several thousand hours including 5 periods of 100h continuous operation directly connected to a biomass gasifier or pyrolysis reactor without an increase of the degradation in comparison to hydrogen operation.

Recently, significant work has been done in relation to SOFC operation with syngas from gasifiers, including testing of the tolerance of the SOFC against impurities and development of hot-gas cleaning technologies. Even if not all of the impurity reactions of the stack have been revealed, the stability and robustness of Sunfire's stack technology provides the basis for a fast advancement. A complete self-sustained SOFC demonstration system fuelled with syngas, would be an innovation towards being able to adopt SOFC technology in power generation units fuelled by renewables and municipal waste.

A map of companies developing and advancing fuel cell technologies as commercial products is presented in *Figure 3-15.*

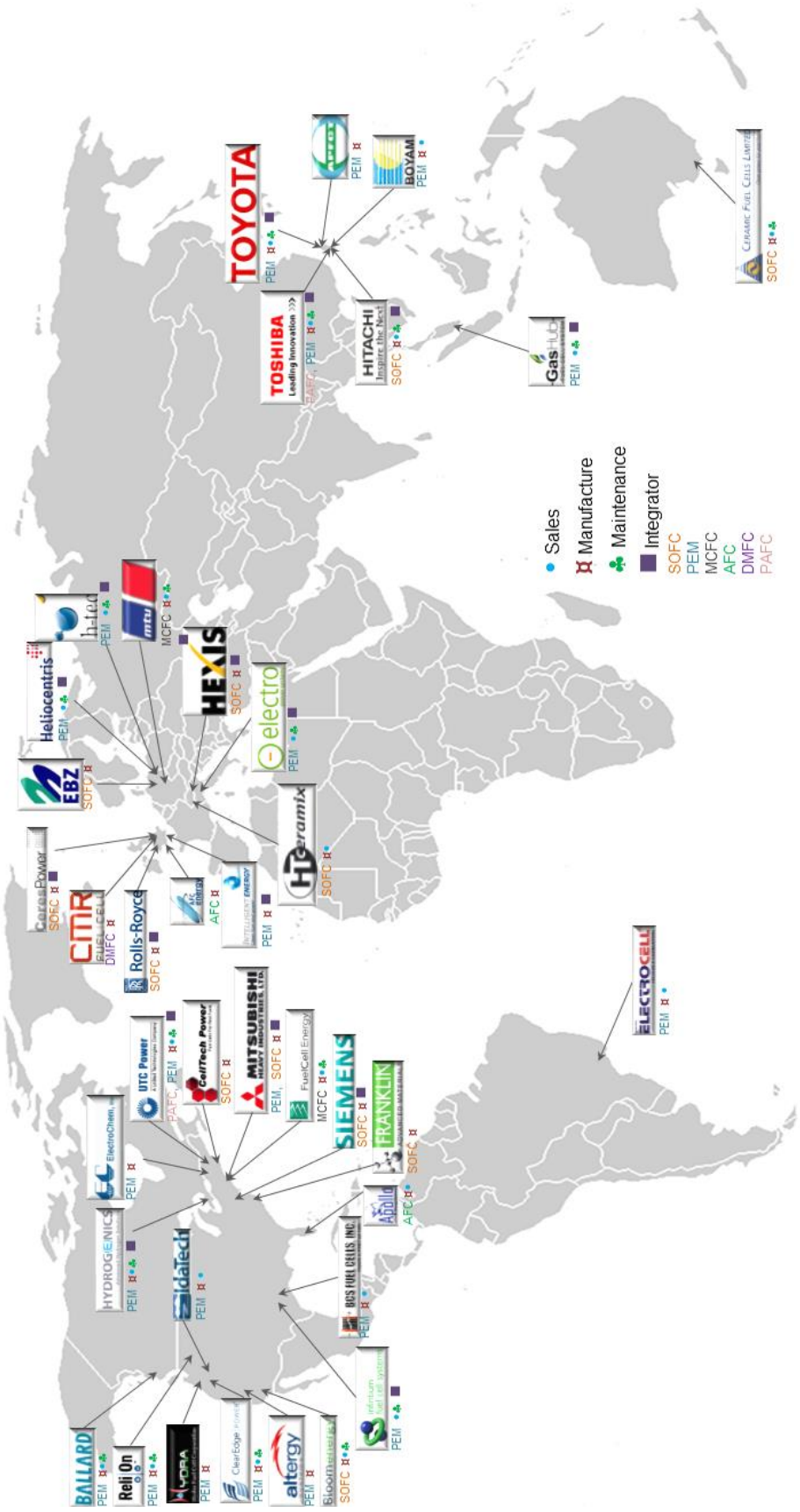

Figure 3-15: Global map of companies making commercial advancements in various fuel cell technologies.

3.5 HEAT ENGINE

The WHHE Energy Centre will use a gas turbine (GT) in a SOFC-GT hybrid configuration. The introduction of a heat engine coupled with high temperature SOFC has received much interest due to the inherent synergies and the promise of improved electrical efficiencies. The type of heat engine applied can vary between gas turbines, steam turbines and Stirling engines, but the combination with the most promise for large scale application (MW scale) is the SOFC-GT. There are two possible integration strategies for this configuration - direct or indirect. The direct approach requires the cathode of the fuel cell to run on the outlet of the compression stage of the gas turbine cycle (Brayton cycle) whereby the heat from the fuel cell is used to drive the expander. This approach is advantageous as the fuel cell's performance is directly influenced by the partial pressure of the reactants so increasing the operating pressure will increase the electrical efficiency. The indirect approach requires heat from the fuel cell to be transferred to the gas turbine via a heat exchanger between the compressor and expander making these systems safer and less complex. Simulations studying the electrical efficiencies of these SOFC-GT systems have shown to be as high as 60% where approximately 20% of the electrical output is expected to come from the GT (*Bang-Moller et al., 2011; Komatsu et al., 2010; Calise et al., 2006*). Commercial SOFC/GT hybrid systems have been developed by Siemens, Rolls-Royce, and Mitsubishi Heavy Industries (*Mueller et al., 2008*), and in 2013 Mitsubishi Heavy Industries operated a 200kW pressurised system for 4,000 hours and achieved a thermal efficiency of 50.2% (*Mitsubishi, 2013*). A pressurised 220kW SOFC-GT system was also developed and tested by Siemens Westinghouse where the system achieved an electrical efficiency of 52% (from their target of 57%) and the GT provided 11% of the overall electrical output.

But when considering smaller scale systems where GT units become less efficient and unfeasible (<25kW)(*Komatsu et al., 2010*) the application of Stirling engines become attractive, and more so if the operating temperature of some SOFCs is lowered as envisaged. In a thermodynamic analysis of a 10kW SOFC-Stirling engine reported in *Rokni* (*2013*) the hybrid system achieved an electrical efficiency of ca. 60% where 11% of the electrical output of the system comes from the Stirling engine. The same author reported in *Rokni (2014)* that a SOFC-Stirling engine configuration fuelled by biomass gasification achieves a thermal efficiency of 42% where 21% of the electrical output comes from the Stirling engine.

3.6 HYDROGEN STORAGE

When considering solutions for hydrogen storage there are several characteristics that should be considered:

- Gravimetric energy density - the amount of energy stored per unit weight (*Figure 3-16*).

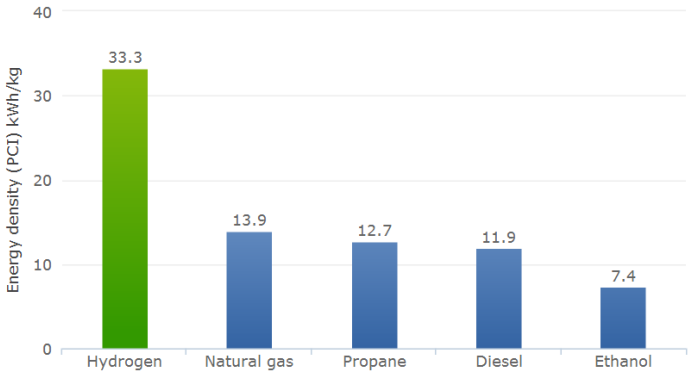

Figure 3-16: Comparison of gravimetric energy densities for the most common fuels using LHV (*McPhy, 2014*).

- Volumetric energy density – the amount of energy stored per volume (*Figure 3-17*).

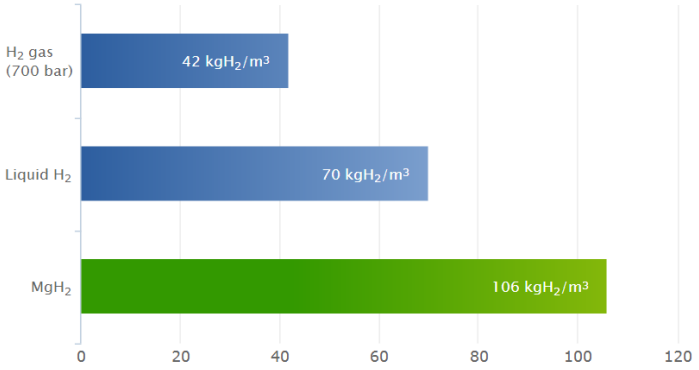

Figure 3-17: Comparison of various hydrogen storage technologies (*McPhy, 2014*).

- Turnaround efficiency – the ratio of the amount of hydrogen retrieved versus amount stored, or the amount of energy retrieved versus amount input.
- Dormancy – the ability to store hydrogen over long periods of time.

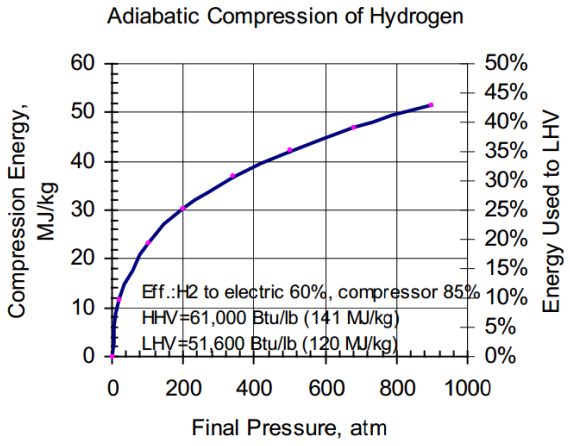

Figure 3-18: Energy consumption of compressing hydrogen shown also as a percentage of the hydrogen energy content (*Heung, 2003*).

There are many forms of gas, liquid and solid state hydrogen storage techniques. WHHE Energy Centres will employ solid-state metal hydrides as solid-state metal hydride storage units are ideally suited for stationary applications with readily available local heat sources. They are compact with storage densities of 120g/l as compared to 70g/l for liquid hydrogen storage. They offer the ability for rapid charge and discharge and, importantly they operate at relatively low pressures (10bar compared to 700bar for compressed storage as used in prototype vehicles (*H2Mobility, 2011*)). Solid-state units can also store hydrogen without any leakage. A cost driver model developed at HZG (*Jepsen et al., 2012*) shows the advantages of solid state hydrogen storage against high pressure hydrogen storage systems with respect to lower energy consumption necessary for compressing the hydrogen. Furthermore a suitable solid state hydrogen tank can be directly coupled to an electrolyser, thus saving investment and maintenance cost of compression. Compression and liquefaction are also energy intensive as illustrated in *Figure 3-18* where compression to 700 bar which requires more than 35% (of the LHV) of the energy being stored. Liquifying hydrogen to 20K will require approximately 39% of the LHV (*Heung, 2003*). Compared to the operation of a metal hydride storage system which requires approximately 13-30% LHV (*Heung, 2003; Zuttel, 2003*).

Stationary prototype solid state storage of hydrogen produced from solar and wind energy via electrolysis has been demonstrated in room temperature hydrides (*CRES, 2011; Lucero et al., 2011*). From the point-of-view of volumetric compactness these tanks are very attractive. However, their heavy weight prevents further commercialisation especially for portable applications. Furthermore, today, commercially available tanks made from these materials and containing only some tens of grams of hydrogen are sold at market prices of >1,000 €. In an attempt to improve weight related capacity *Akiba et al*. (2010) demonstrated the potential of BCC alloys together with Toyota in a combined metal hydride – 350 bar compressed hydrogen gas tank, confirming a capacity of 2.2 wt% and 51 kg/m^3 on system level (*Akiba, 2010*).

Recently, a novel concept to overcome energetic H-sorption obstacles has been suggested by *Dehouche et al*. (*2005*)(*2006*), *Liang et al*. (*2005*), *Kojima* (*2006*), and *Wang et al*. (*2006*) through structural destabilization and hybridization approaches allowing to lower the reaction enthalpy and increase the sorption kinetics of high capacity hydride materials. More recently, *Dehouche et al.* (2008), reported that metastable alloy phases of Zr-Ni compounds prepared by the arc-melting technique have a significant effect in enhancing the sorption kinetics of ball milled MgH_2 at 250°C. Hydrogen unloading results demonstrate that doping nanostructured Mg-hydride with activated alloys yields increased desorption kinetics and substantial reduction of discharge temperature of

MgH_2 nanocrystals. Magnesium-based metal hydrides are benign, cheap, have high gravimetric and volumetric densities as well as good sorption reaction kinetics.

Preliminary findings (*Lohner et al., 2013*) of the decentralized combined heat and power system modelling performed in Matlab has shown that solid hydrogen storage configurations without operational restrictions have better characteristics than the gaseous hydrogen storage configurations. Also, a comparison of power balancing plants with and without storage shows much higher load factors and efficiency levels (>60%) for the installation with backup hydrogen storage unit. Moreover, from an economic point of view, the solid hydrogen storage balancing system configuration can achieve lower electricity generation costs than a power system without storage, which simply increases its power unit capacity to meet high electricity demand (*Lohner et al., 2012*).

3.7 ELECTROLYSERS

A PEM electrolyser will be modelled to convert electricity produced by the fuel cell combined cycle to hydrogen during periods when the wholesale value of grid electricity is below a threshold value. It can also be used to convert cheap grid electricity into hydrogen. PEM cell electrolysers, unlike traditional units such as alkaline electrolysers, have very low maintenance requirement (no corrosion) and are very simple to set up. They also produce hydrogen at 15bar which is ideal for metal hydride hydrogen storage units. A PEM cell electrolyser therefore removes the need for a compressor which has associated energy losses and maintenance requirements. The cell efficiencies of both PEM electrolyser and alkaline electrolysers are up to 70% (4.9 kWh/Nm^3). However, PEM electrolysers can produce higher H_2 purities for greater compatibility with the hydrogen storage system. They are also extremely compact and have very long lifetimes (>20years). Currently PEM cell electrolysers cost just under 6 times more than alkaline fuel cells (3750$/kW compared to 640$/kW) although this gap is expected to close significantly as PEM cell manufacturing technology develops and uptake increases.

Although the scale of the demonstration system is relatively small it is worth noting that large-scale commercially viable electrolyser projects are currently underway. An example is the Hydrogenics' 1MW electrolyser for Renewable Energy Project using their HySTAT® electrolyser for a large scale renewable energy storage. The project is the largest of its kind in Germany with the capacity to store sufficient hydrogen to produce up to 27 MWh of energy. Known as RH_2-WKA, the project will be based in Mecklenburg-Vorpommern in northern Germany which has favourable wind regimes. The owner of the wind-hydrogen system is German-based WIND-projekt GmbH (www.wind-projekt.de). It is powered by a 140 MW wind farm, comprising an array of 7.5 MW wind turbines. By incorporating hydrogen generation and storage in the system design, the fluctuating wind energy can be smoothed, guaranteeing the supply of renewable power. The stored hydrogen will be used for a variety of purposes, including electricity generation, for transport and can also be fed to the natural gas network. There is also much interest in converting any hydrogen for export into synthetic natural gas through a process of methanation, this would make the gas better suited for export and eliminate some of the challenges associated with transporting hydrogen.

Readers Guide

Overview

1. Introduction

2. The WHHE Concept

3. Literature Digest

4. SOFCs

Introduction and History

Manufacture
- General

Basic Principles
- General

Materials
- Electrolytes
- Electrodes
- Interconnects
- Seals

5. Modelling

6. Modelling Results

7. Experimental Research

8. micro-CHP in the UK Market

9. Conclusions

References

Appendices

4. SOLID OXIDE FUEL CELLS

4.1 INTRODUCTION AND HISTORY

Fuel cells in essence are devices that convert chemical energy into electrical energy through an electrochemical reaction. The high efficiencies and high operating temperatures obtained from SOFC's have led to much interest in the development of the technology in combined cycles.

Fuel cell technology was first demonstrated by the work of Sir William Robert Grove in 1838 when during an electrolysis experiment where he discovered a flow of electricity when the two electrodes were connected, and went on to publish a diagram of the "Grove Gas Battery" in 1843 (*Figure 4-1*).

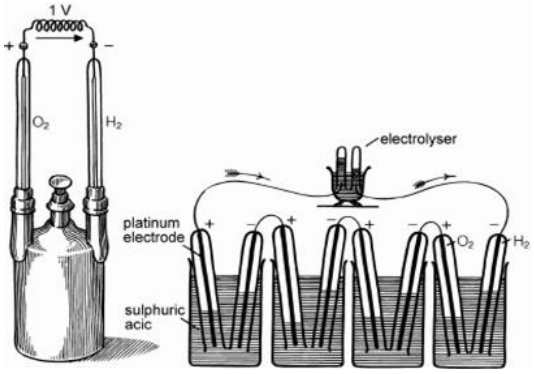

Figure 4-1: Grove gas battery (*strath.ac.uk, 2014*).

After this the next big advancement came from Francis Thomas Bacon at Cambridge University who developed a 5kW alkaline system in 1950. Then in the 1960's NASA used a 1.5kW alkaline fuel cell system that was used in the Apollo spacecraft and provided both electricity and drinking water.

Research on SOFC's started in the 1930's by Baur and colleagues (*Bove et al., 2008*) which were driven by the discovery of appreciable ionic conductivity of the Nernst mass – doped zirconia.

How the SOFC works is by making use of an electrolyte made from a ceramic material such as yttria-stabilised zirconia (YSZ) which acts as a conductor of oxide ions at temperatures from 600°C to 1000°C. The ceramic material allows for oxygen atoms to be reduced on its porous cathode surface by electrons thereby creating oxide ions which are then transported through the ceramic body to a fuel rich anode surface. Here the oxide ions react with hydrogen giving up electrons to an external circuit, as can be seen graphically in *Figure 4-2*, and the chemical reactions are represented by the chemical equations:

$$H_2(g) + O^{2-} \rightarrow H_2O(g) + 2e^- \implies \text{oxidation}$$

$$\frac{1}{2}O_2(g) + 2e^- \rightarrow O^{2-} \implies \text{reduction}$$

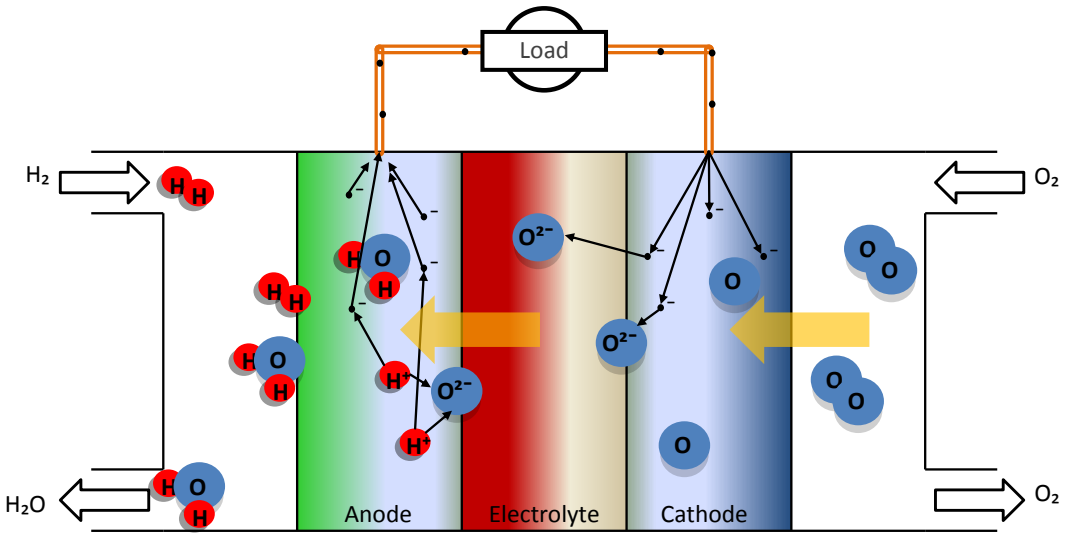

Figure 4-2: Graphic representation of the transport process within a SOFC.

One of the strongest advantages of solid oxide fuel cells is their fuel flexibility, which is a result of the internal reforming capabilities (catalysts such as Nickel are often used to promote reforming). Solid oxide fuel cells may consume hydrogen produced by the reforming of natural gas, the process of reforming is endothermic and is fed by heat generated through the exothermic reaction taking place at the electrolyte. The chemical reactions include a methane reforming process followed by a gas-shift and occur as follows:

$$CH_4 + H_2O \rightarrow CO + 3H_2 \qquad \text{Steam-reforming}$$

$$CO + H_2O \rightarrow CO_2 + H_2 \qquad \text{Gas-shifting}$$

Going beyond hydrogen consumptions studies reported in *Zhang et al. (2009)* have shown the possibility of solid oxide fuel cells being directly fuelled with dry hydrocarbon. The electro-oxidation of hydrocarbons at the anode produces:

$$C_nH_{(2n+2)} + (3n+1)O^{2-} \rightarrow nCO_2 + (n+1)H_2O + (6n+2)e^-$$

But as a further source of hydrogen this project utilises the gasification of waste to produce a hydrogen rich syngas which will be used to fuel a SOFC.

SOFC's can be designed to operate at temperatures ranging from 1000°C down to as low as 500°C. The operating temperature is normally dependent on the electrolyte thickness, cell configuration and the materials being applied. Higher temperatures are required for YSZ electrolytes with a thickness >25µm - this is to limit ohmic losses. *Figure 4-3* illustrates the single cell performance of an YSZ electrolyte operating at reduced temperatures, and although there is a drop in performance it is important to measure the feasibility of the various temperature ranges and the benefits that may be achieved through lowering the operating temperature, this will be discussed further into the paper.

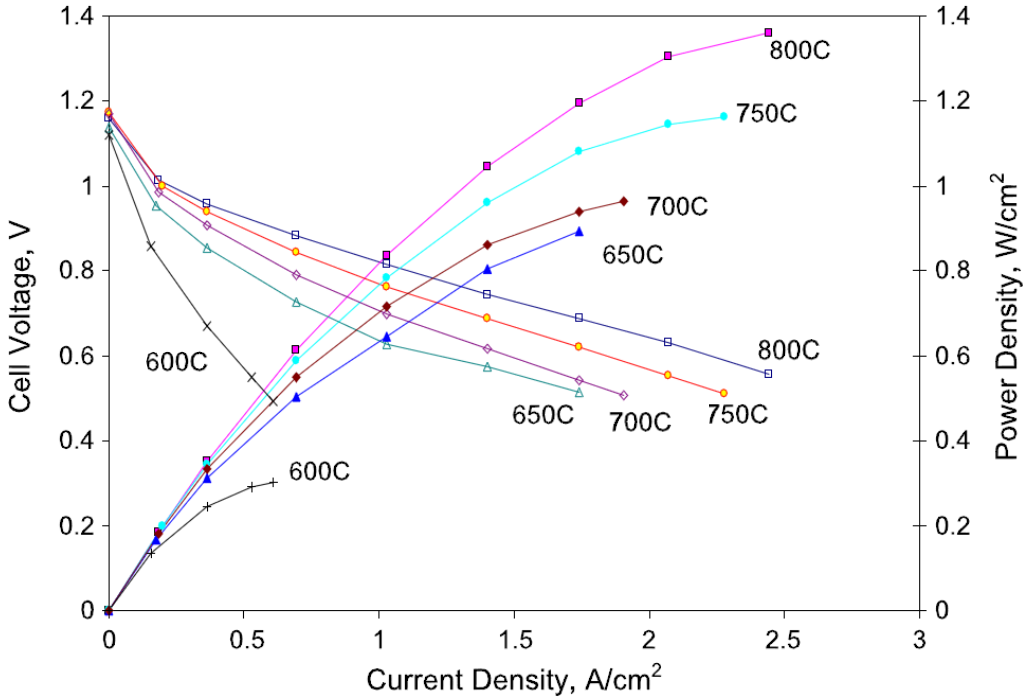

Figure 4-3: Example of a SOFC single cell performance at reduced temperatures.

Research is also being conducted in producing proton-conducting SOFC (H-SOFC), as opposed to oxygen-ion-conducting SOFC the latter is what we have when using YSZ as an electrolyte. H-SOFC's have been shown to improve electrochemical reactivity whilst withstanding high operating temperatures and complete hydrogen utilisation is also plausible. These advancements will allow for lower running temperatures which is favourable in terms of productions cost and cell degradation.

The promise of SOFC's comes from the extremely attractive levels of efficiency potentially available to these devices, some as high as 60% (*Payne et al., 2009; CFCL, 2009)*. There is also potential for this technology to be incorporated into transport applications and will be further discussed during the research of the hybrid systems.

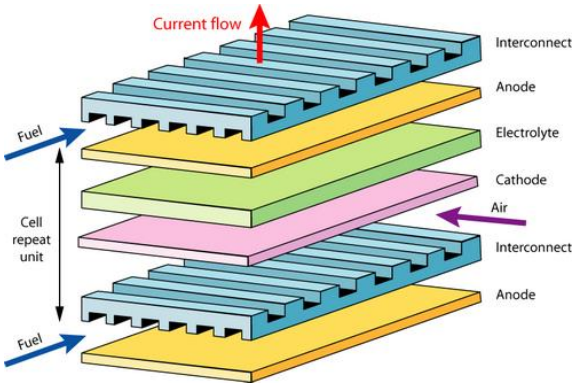

Figure 4-4: Single cell assembly showing interconnects sandwiching the PEN (*University of Cambridge, 2012*).

The physical properties of the fuel cell are built as displayed in *Figure 4-4* where the cathode, electrolyte and anode are collectively referred to as the PEN (positive electrode, electrolyte, negative electrode). Each cell provides a theoretical and reversible open circuit voltage (OCV), which will be discussed and used in great detail further into the modelling and experimental research presented.

The actual OCV will often fall below the theoretical value. This is because of losses in potential due to residual electronic conduction in the electrolyte and also from the cross-over of

gases caused by micro cracks and fissures in the electrolyte. The amount of voltage available to system depends on the fuel used and the operating temperature and pressure.

The area specific resistance of the overall system whilst operating at 1000°C can be reasonably limited to about 0.50Ωcm^2 and about 1.5 Ωcm^2 when running at 800°C, therefore the operating temperature, which is dependent on mass transfer, energy activation and fuel utilisation, is an extremely important factor to be taken into account when looking at overall efficiencies and optimisation of the fuel cell. This will also lead to the conclusion that the fuel cell, in order to be viable, will need to be run at constant optimum temperature which will indicate the desired mass flow rate through the system and will need to be balanced with the desired OCV and the overall size of the fuel cell. By stacking several cells in parallel or series we will be able to attain the voltage and power required by the system design, and this will be termed the cell stack.

4.2 BASIC PRINCIPLES

In the past SOFCs using YSZ as an electrolyte would be required to operate at temperatures between 800-1000°C in order to maintain power density levels around 1W/cm^2, whilst also assisting the fuel flexibility of these systems through internal reforming. Temperature also has an effect on the ionic conductivity and internal resistance which can be limited to 0.5 Ωcm^2 at 1000°C and 1.5 Ωcm^2 for the overall current collector assembly (*Bove et al., 2008*). There are problems that arise from operating at such high temperatures and these are mainly in the area of material compatibility, and unlike heat engines whose efficiency is derived from the theoretical Carnot Cycle where higher operating temperatures means higher efficiency; fuel cells actually display a theoretical increase in efficiency from a reduction in temperature and are not constrained by the difference in temperatures but rather by the relative change in the stored chemical energy.

$$\eta_{carnot} = \frac{T_H - T_C}{T_H}, \qquad \eta_{FC_{elec}} = \frac{\Delta_{rev}G}{\Delta_{rev}H} = 1 + \frac{T\Delta_{rev}S}{|\Delta_{rev}H|}.$$

Figure 4-5 illustrates a comparison of the efficiency limits between fuel cells (showing both water and steam at the exhaust) and the theoretical Carnot cycle using 50°C at the exhaust (T_C).

To better understand the chemical energy available to the fuel cell and how to calculate the amount of energy available to do work we should look at the Laws of Thermodynamics (presented in more detail in *Section 5.3*).

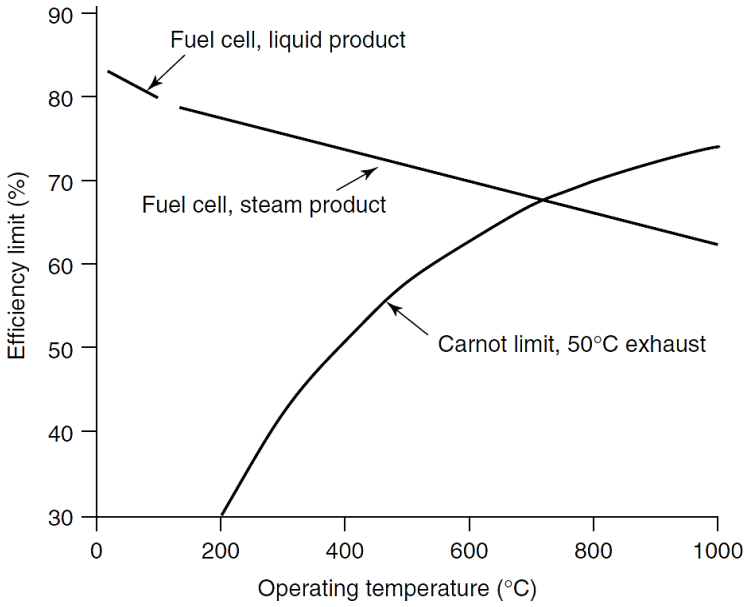

Figure 4-5: Maximum fuel cell efficiency (using H_2) at standard pressure, with reference to the HHV. Compared with the theoretical Carnot limit, with an exhaust temperature of 50°C (*Larminie et al., 2003*).

4.3 MANUFACTURE

There are many considerations to be made before one can consider making a solid oxide fuel cell. Whilst the fundamental principle of what makes the fuel cell work is the electrochemical characteristics of the electrolyte, it is the entire PEN that must be designed towards finding the optimal performance within the material constraints taking into account the thermal, electrical, and mechanical properties of each layer. The typical performance targets for single cells are about 0.5 W/cm^2 at 0.7 V and 0.7A/cm^2 for 85% fuel utilisation (*Steele, 1996*), and conductivity of ions through the electrolyte are targeted at 0.1 S/cm (*Molenda et al*., 2007).

Table 4-1: SOFC material requirements

	Anode	Cathode	Electrolyte	Interconnect
Conductivity	High electron + ion		High ionic	High electron
Porosity	Porous		Fully dense	
Stability	Chemical, phase, morphological and dimensional			
Compatibility	No interdiffusion between adjoining layers and no damaging chemical interactions			
Thermal Expansion	Must match adjoining layers			

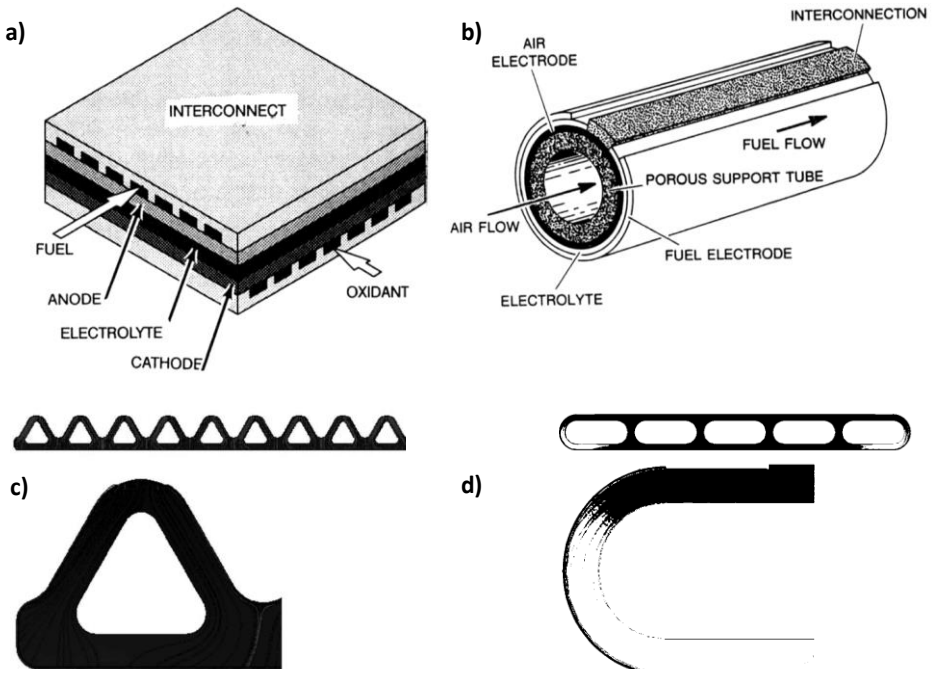

Figure 4-6: Various SOFC geometry designs a) planar, b) tubular, c) delta and d) high power density

SOFCs can also be grouped into two main geometry groups; planar and tubular designs are the most popular designs whilst there are further configurations such as the delta and high power density designs being researched by some companies. *Table 4-2* and *Figure 4-7* summarise and illustrate various configurations that are used to support the cell and its very thin and fragile layers. Commonly when manufacturing the PEN a substrate which is thicker is used for mechanical strength enabling the remaining layers to be applied onto. As shown in *Figure 4-7* any of the layers can serve this purpose but because the thickness of the electrolyte has an influence on the ion conductivity the electrolytes are often made as thin as possible. But there are manufacturers who still use electrolyte supported cells. Cells can also be externally supported via the bipolar interconnect plates or by using a porous substrate at one of the electrodes.

Table 4-2: Various cell configurations and their characteristics.

Cell Configuration	Advantage	Disadvantage
Self-Supporting		
Electrolyte Supported	Strong support from dense electrolyte Less susceptible to failure due to anode re-oxidation and cathode reduction	Higher resistance due to electrolyte conductivity Higher operating temperatures to minimize ohmic losses
Anode Supported	Highly conductive anode Lower operating temperatures	Potential anode re-oxidation Mass transport limitations due to anode thickness
Cathode Supported	Potential cathode reduction Lower operating temperatures	Lower conductivity Mass transport limitations due to anode thickness
External Supporting		
Interconnect supported	Lower operating temperatures Stronger structures	Interconnect oxidation Flow-field design limitations
Porous Substrate	Lower operating temperatures Potential to use non-cell materials for support	Increased complexity Potential for electrical shorts

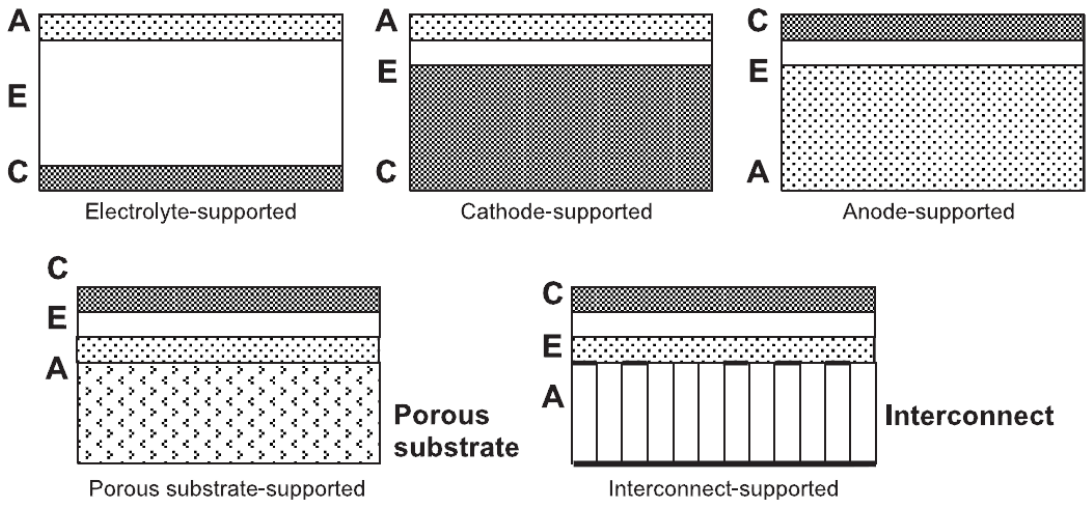

Figure 4-7: Graphic representation of cell configurations.

Different processes are used for low cost fabrication of the SOFC's electrolyte and electrodes. Components must be fabricated according to specific properties to enable cycling and long term stability (*Tietz et al., 2002*). Manufacturing techniques vary greatly depending on the cell geometry and substrate support configuration. *Table 4-3* is a summary of the fuel cell layers, material and manufacturing process.

Table 4-3: Typical SOFC materials and manufacturing processes.

Layer	Material	Manufacturing process
Electrolyte	Yttrium-stabilized Zirconia (YSZ)	Tape casting, screen printing, CVD. Sintering >1400°
Anode	Yttria-doped zirconia cermets with 10-50% nickel (Ni/YSZ)	Tape casting, buffer solution, pressing
Cathode	Strontium-doped lanthanum magnetite LSM($La_{1-x}Sr_xMnO_{3-\delta}$)	Screen printing, electro-deposition, extrusion
Interconnect	Lanthanum chromites ($LaCrO_2$)	Machining

4.4 MATERIALS

The high operating temperatures of SOFC's represents a problem concerning the chemical and thermochemical stability of the materials being applied, satisfying these conditions also limits the number of materials available for the various components, whilst maintaining performance.

4.4.1 THE ELECTROLYTE

The electrolyte in any fuel cell must display the ability to conduct ions whilst at the same time showing a resistance to the transfer of electrons, and for SOFC's this must be maintained at elevated operating temperatures. The electrolyte in a SOFC is ceramic in nature and normally very thin, depending on; the support configuration, manufacturing process used and performance required. One of the challenges when creating a ceramic layer, which can be as thin as 5µm thick, is to keep it free of porosity and uniform in thickness. A reduction in thickness is used to compensate for the increase in resistance caused by a reduction in temperature, but the resistance is not only dependant on thickness but also on the contact geometry at the electrolyte/electrode interfaces, and there is a point where this constrictive resistance becomes dominant and thickness is no longer important (*Somiya et al., 2003*).

Some of the complications associated with the application of a ceramic electrolyte is, the lack of chemical or mechanical strength and the energy losses caused by current flow. These brittle high temperature ceramics are susceptible to failures caused by mechanical or thermomechanical stresses and through better material selection and engineering need to be managed within tolerable limits.

Fluorite-structured[1] oxide materials such as yttria stabilized zirconia YSZ (Y_2O_3-ZrO_2), scandia-stabilized zirconia ScSZ (Sc_2O_3-ZrO_2), rare earth doped ceria (CeO_2), rare earth doped bismuth oxide (Bi_2O_3) and lanthanum gallate ($LaGaO_3$) have been widely investigated as solid electrolytes for a fuel cell. From these YSZ has been most successfully employed. This is because of the dual roles played by the yttrium oxide dopant (Y_2O_3); it stabilises the high temperature cubic phase in zirconia, and also generates an oxygen vacancy for every mole of yttrium dopant. As indicated by the Kroger-Vink notation[2]:

$$Y_2O_3 \xrightarrow{ZrO_2} 2Y'_{Zr} + 3O_O^{\times} + V_O^{\cdot\cdot}$$

Zirconia ZrO_2 exists in three crystalline forms; monoclinic, tetragonal, and cubic. Zirconia in the cubic phase only exists in the cubic phase at temperatures above 2370°C, and is not encountered in sintered products which are processed at much lower temperatures. Pure zirconia spontaneously

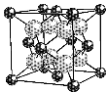

[1] In the fluorite structure, the cations (smaller, darker atoms) occupy the ccp positions and the oxygen ions occupy the tetrahedral sites.< http://neon.materials.cmu.edu/rohrer/defects_lab/defect_comp_bg.html>

[2] Y'_{Zr} = yttrium cation on a zirconium site, caused by doping.

disintegrates during cooling after sintering above 1170°C this is because of the tetragonal to monoclinic transformation that involves an increase in density from 5.7 to over 6g/cm^3. Therefore for applications involving temperatures over 1000°C the zirconia must be stabilized to prevent the destructive phase inversion. By stabilising the zirconia the cubic structure of the composition is maintained and has no phase transformation from room temperature to about 2500°C, (Harper, 2001). The crystalline phase of sintered 2mol% Y_2O_3 Y_2O_3-doped zirconia have been found to be tetragonal and cubic in 6mol% Y_2O_3-doped zirconia, and intermediate compositions have a mixture of the two crystalline phases, this can be referred to as partially stabilized zirconia.

YSZ is created by doping ZrO_2 with Y_2O_3 at a certain percentage, normally 8mol%, lower doping levels i.e. 2-3mol%, the metastable tetragonal zirconia exhibits improved fracture toughness and strength but lower ionic conductivities (*Somiya et al., 2003*). Whilst doping the zirconia fluorite structure two zirconium cations (Zr^{4+}) are replaced by two yttrium cation (Y^{3+}), and in order to maintain the charge balance one oxygen site (O^{2-}) is left vacant. It is this vacant oxygen site that promotes ion conductivity, and the more vacancies that are made available the more oxide ions can be conducted through the material. There is an upper limit to the amount of doping before which the conductivity begins to decrease rather than increase due to the interaction of defects, 8 molar % of doping will cause about 4% of the oxygen sites to be vacant. The material's conductivity is therefore dependant on the concentration of the charge carriers, in this case the oxygen vacancies, and the carrier mobility which is characterised by the materials diffusivity. The ionic diffusivity (*D*) of ceramic electrolytes is exponentially dependant on temperature which is one of the reasons these electrolytes perform better at higher temperature:

$$D = D_0 e^{-\Delta G_{act}/(RT)}$$

where D_0 is a constant and is material dependant (cm^2/s), ΔG_{act} is the activation barrier for the diffusion process (J/mol), R is the gas constant and T is temperature (K).

Another zirconia based electrolyte which has shown to display improved ionic conductivity suitable for intermediate temperature operation is scandia-stabilized zirconia (ScSZ), which has shown to have a conductivity of 0.3 S/cm at 1000°C (*Somiya et al., 2003*). The improved performance is attributed to the smaller ionic radius of Sc^{3+}, and the grain refinement has been shown to significantly increase the conductivity of solid electrolytes (*Mondal et al., 1998; Vijaya et al., 2010*). There are however concerns over the stability of the ionic conductivity over time, although degradation has been shown to improve with 10mol% Sc doping, and Sc is more costly than yttrium (*Kharton et al., 2004; Badwal et al., 2000*). In studies using Sc_2O_3 content have been studied between 7 and 11mol% at a temperature of 850°C, with a further comparison study at 1000°C. Results all indicated conduction degradation as a function of time, but much lower for compositions between 9 and 11mol%. The cell containing 9.3mol% Sc_2O_3-ZrO_2 showed the lowest rate of degradation at both 850 and 1000°C which measured an increase in resistance of 3.0 and 1.7% respectively after 5000min (*Badwal et al., 2000*). The major cause of cell degradation between 7 and 9mol% Sc_2O_3-ZrO2 has been attributed to transformation of a distorted fluorite-type phase present to a cubic phase on annealing, and low degradation rate from compositions above 9mol% is due to the

absence of the distorted fluorite-type phase. For compositions above 10mol% the material has been seen to exhibit a rhombohedral[3] cell structure which transforms to a cubic phase between about 500 and 600°C upon heating and reappears on cooling. The 9.3mol% specimen showed no indication of the rhombohedral or distorted fluorite phases and was therefore the reason why the maximum stability over time was seen in this sample (*Badwal et al., 2000*).

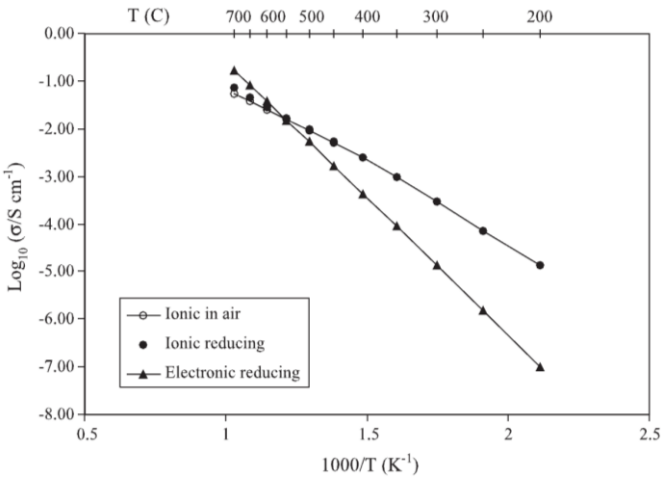

Figure 4-8: Ionic and electronic conductivities of GDC10 in a reducing atmosphere

Similarly doped ceria is a fluorite structured oxygen ion conducting material applied to SOFCs. Here ceria (CeO_2) is doped with an aliovalent lanthanide metal yielding $Ce_{1-\delta}(Ln)_{\delta}O_{2-1/2\delta}$. The advantage this material has over YSZ is that it shows higher ion conductivity, which therefore means the system can be run at lower temperatures whilst keeping the performance on par with YSZ. Doping materials yielding the highest levels of conductivity are samaria and gadolinia often abbreviated to SDC and GDC respectively and their concentration levels are normally in the range of 10-20%. GDC10 ($Ce_{0.9}Gd_{0.1}O_{1.95}$) has an ion conductivity of 0.01 S/cm at 500°C (*Kharton et al., 2004),* and 0.25S/cm at 1000°C *(Somiya et al., 2003*). The reason for this improved performance can be explained by studying the relevant sizes of the dopant ions compared to the primary ions they replace. The concentration limit of the doping material is the point where ion conductivity begins to drop instead of continuing to increase, this is caused by the interaction between the dopant ions and the oxygen vacancies, and because of their opposite charges it was thought this phenomenon was a result of the Coulomb effect. However if this were the case all dopants of the same charge would result in the same level of conductivity, it turns out that it is size that is of importance and not charge. It has been shown that the interaction between these defects is through the elastic strain experienced by the crystal lattice structure when there is a variation in the size of the dopant ion that replaces the original. The most favourable conductivity performance is found when the dopant ion closely matches the ion being replaced, thereby leaving the structure as undisturbed as possible. This explains why GDC shows higher levels of ion conductivity, as the dopant ions are more closely matched in terms of size compared to that of YSZ.

The disadvantage of using ceria materials in SOFC applications is that ceria tends to partially reduce from Ce^{4+} to Ce^{3+} under the reducing conditions at the anode. This produces n-type electronic

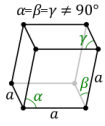

3 Illustration of the rhombohedral cell structure

conductivity causing partial internal electronic short circuits, and also it generates nonstoichiometry and expansion of the lattice structure which can lead to mechanical failure *(Kharton et al., 2004; Mogensen et al., 2000; O'Hayre et al*., *2009)*. When comparing the electronic conductivity against the ionic conductivity it is indicated that the electronic conductivity will be greater than the ionic conductivity at temperature greater than 550°C, as seen in *Figure 4-8* (*Steele et al., 2000*). The problems facing doped ceria can be mitigated by applying other solid electrolytes such as YSZ in a multilayer cell, but this too has its draw backs coming from differences in expansion coefficients and the formation of reaction products. There is also a problem when considering the manufacture of GDC electrolytes onto Ni-YSZ anode supported electrodes as these materials are sintered at 1300°C the formation of $Gd_2Zr_2O_7$ and Gd_2NiO_4 have been observed and will have a negative effect on cell performance (*Mogensen et al., 2000*).

Yttria doped ceria ($Ce_{0.8}Y_{0.2}O_{1.9}$) has been investigated as an electrolyte material due to its high ion conductivity and compatibility with more active electrodes such as lanthanum cobaltites, thereby allowing for a reduction in operating temperature (*Peng et al., 2002*). The problem with this approach, as mentioned above, is the tendency for ceria to reduce from Ce^{4+} to Ce^{3+} resulting in electronic conduction (*Mitsuyasu et al., 1998*). A solution to overcome this problem is to introduce a bi-layer where YSZ is coated on the anode side of the electrolyte, thereby eliminating ceria's exposure to the reducing atmosphere of the anode. Although this has also seen to have ill effects on the performance of the electrolyte as these two fluorite structures undergo a solid state reaction at elevated temperatures of about 1600°C, where there is a dissolution of ceria into zirconia (or vice versa), to form a new fluorite phase (CeO_2-ZrO_2-Y_2O_3) with poor ion conductivity (*Mitsuyasu et al., 1998; Kim et al., 2002)*.

Bismuth oxide (Bi_2O_3) based electrolytes have shown high levels of ion conductivity compared to zirconia based electrolytes at comparable temperature, and would be ideal for intermediate temperature applications. The problem with bismuth oxide is that it has been reported to transform between four polymorphs; α, β, γ, and δ-phases, with each having an effect on the electrical and thermal expansion properties of the material. The transition from monoclinic α-Bi_2O_3 to the high temperature cubic δ-Bi_2O_3 occurs at approximately 730°C and the δ-phase has been shown to be stable up to 825°C before it melts. A high level of hysteresis has been observed upon cooling from the high temperature δ-phase with a the possibility of two intermediate metastable phases forming: the tetragonal β-phase occurs at approximately 650°C, and the body centred cubic (bcc) γ-phase that forms at approximately 640°C. The γ-phase has shown to persist to room temperature when the cooling rate is kept suitably low, the β-phase however decomposes back to the α-phase (*Sammes et al., 1998*). It is also important to understand the thermal expansion characteristics of each of these phases as they would directly affect the mechanical integrity of a layered assembly. The thermal expansion co-efficient of α-Bi_2O_3 has been found to be approximately $11.0x10^{-6}K^{-1}$, β-phase $23.0x10^{-6}K^{-1}$, γ-phase $20.0x10^{-6}K^{-1}$, and δ-Bi_2O_3 $24.0x10^{-6}K^{-1}$ (*Sammes et al., 1998)* and of biggest concern is the large volume change between the α-phase and the other three phases. It is the δ-Bi_2O_3 that illustrates the highest levels of ion conductivity (1 S/cm at 750°C *, O'Hayre et al., 2009*), but due to its instability various approaches have been applied in order to stabilise this material down to temperatures below the α→δ transition temperature. This can be achieved by

substituting the bismuth with rare-earth dopants such as Y, Dy or Er, alternatively higher valency cations such as W or Nb can be used. Because the Bi^{3+} cations are relatively large the ionic conduction increases with increasing rare-earth dopant radius, therefore the maximum conductivity is observed for Er and Y dopants; $Bi_{1-x}Er_xO_{1.5}$ ($x\approx0.20$) and $Bi_{1-x}Y_xO_{1.5}$ ($x\approx0.23$-0.25). But these fluorite structures are metastable below 770-870K and undergo a slow phase transformation over time, which also affects conductivity.

4.4.2 THE ANODE

The basic requirements of anode materials are that they should have high electron conductivity, electrocatalytic activity for fuel oxidation, chemically stable, thermal compatibility and sufficient porosity for efficient gas transportation, as a further bonus catalytic activity towards hydrocarbon reforming may be preferable. Metals such as Ni, Co, Fe, Pt, Mn, and Ru have been studied (*Jiang et al., 2004*) as anode materials and the electrochemical activity of Ni has shown to be the highest. The melting point of nickel is 1453°C with a thermal expansion coefficient of $13.3x10^{-6}K^{-1}$ and the electronic conductivity varies from $138x10^{4}$S/cm to ~$2x10^{4}$xS/cm between 25°C and 1000°C respectively and is the most common applied metal in a YSZ-Ni cermet.

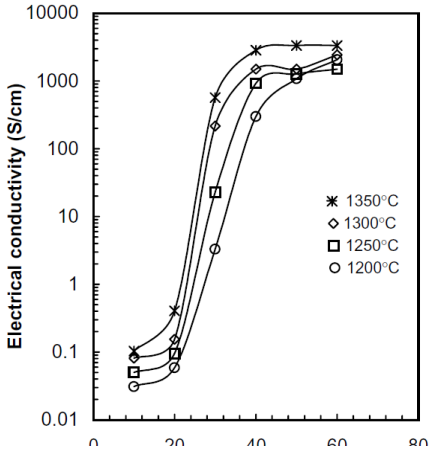

Figure 4-9: The variation of electrical conductivity as a function of nickel concentration in YSZ-Ni cermet fired at the temperatures indicated, measurements taken whilst operating at 1000°C (*Zhu et al., 2003*)

Due to the reducing atmosphere at the anode the layer could be made of porous nickel, were it not for the high thermal expansion co-efficient. This is corrected by dispersing the nickel in a matrix of YSZ forming a cermet. This is done by sintering YSZ powder and NiO_2 to form a NiO/YSZ composite material, the NiO is then reduced *in situ* thereby dispersing the nickel and leaving behind a porous ceramic. Cermets made of YSZ-Ni (Ni/ Y_2O_3:ZrO_2) typically contain 30-50% mol-% nickel. 30% nickel cermets exhibit thermal expansion coefficients in the region of $12.5x10^{-6}K^{-1}$, compared to the thermal expansion coefficient of nickel we can see how the application of YSZ is used to bring down the overall characteristics to make the anode more compatible with the YSZ electrolyte. But consideration for electrical conductivity must also be taken into account when selecting the nickel content, as can be seen in *Figure 4-9*.

When designing a system to be run on hydrocarbon fuels where a process of reforming to produce hydrogen must be included there is often a problem of carbon deposition which must be considered and dealt with. This is a concern at the anode, as this is where the fuel is introduced into the fuel cell and the reformation process is often done within the anode chamber, which is a distinct advantage inherent to SOFC's. In order to combat this carbon formation and build up high steam/carbon ratios are varied, but this has an adverse effect on the electrical efficiency as the fuel is diluted with steam. The reforming process is an endothermic reaction which can also cause areas of cooling therefore introducing thermal gradients that can cause mechanical damage to the cell stack. When using nickel based cermets in systems operating on natural gas there is a risk of sulphur poisoning as well as carbon deposition which could cause metal dusting of the nickel, this causes the disintegration of bulk metals and alloys at high temperatures.

Nickel has a tendency to go through a process of re-oxidation when exposed to oxygen at elevated temperature. The phase change of Ni to NiO produces a volumetric expansion of 69% (*Pihlatie et al., 2009*) if this expansion exceeds the mechanical limits of the electrolyte it will cause fracture leading to cell failure, the volume change experienced by the anode material is somewhat reduced because of the porous nature of the material. In a study performed by *Waldbillig et al. (2009)* it was shown that course structured anode substrate material experienced no volume change or cracking during redox cycling whereas fine structured anode functional material experienced no volume change during reduction but expanded between 0.9% and 2.5% during oxidation, please refer to *Figure 4-10* for an example of an anode supported cell structure. This is an important consideration to be made when developing anode supported cells using nickel, not only does redox cyclic risk mechanical failure of the electrolyte but the oxidation of nickel will have a significant degrading effect on fuel cell performance as the interface between the layers is affected, and the nickel will need to be re-reduced in order to function. Understanding the reduction behaviour of the cell is an important element to quantify as this can be used to design start-up strategies and information on the re-oxidation kinetics is fundamental to limiting performances losses as well as mechanical failure. *Jeangros et al. (2013)* studied the reduction of NiO by hydrogen and found that the reduction of NiO to α-phase Ni reaches a fraction of 0.6 very quickly in the range 350°C < T < 420°C after which the particles slowly to tend towards complete reduction at 600°C.

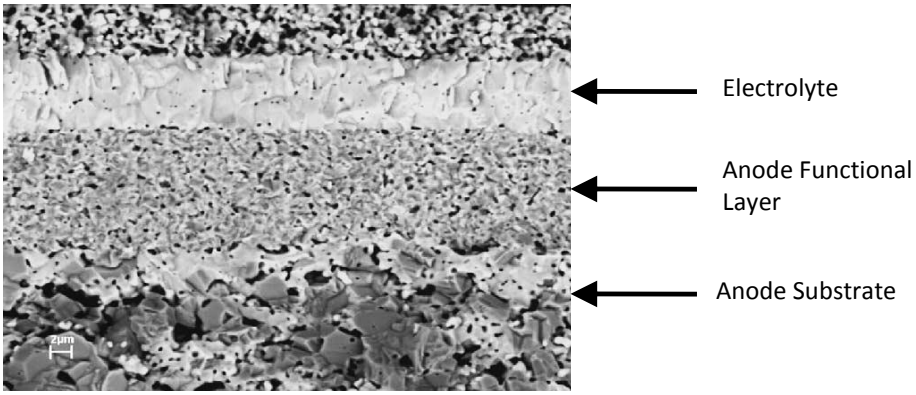

Figure 4-10: Scanning electron microscopy image of an anode supported cell showing course structured anode substrate and fine structured anode functional layer.

With SOFC's inherent ability to reform methane an important advantage of this system is to integrate this technology using the existing natural gas infrastructure. Natural gas is however odorized by distributors by the addition of organic sulphur, allowing for the fast detection of leaks. However sulphur has a detrimental effect on the electrochemical functionality of nickel as sulphur is absorbed by the nickel thereby blocking the available active nickel sites. As presented by *Nagel et al. (2009b)*, 1ppm of H2S caused a 15% drop in performance, but these effects can be reversed and the nickel catalyst regenerated by merely switching to a sulphur free fuel. There may be some permanent damaged caused as the sulphur reacts with nickel to form nickel sulphide ($Ni3S_2$) which melts at 806°C causing enhanced nickel particle sintering. Excessive concentrations of sulphide can also cause permanent degradation as the sulphur causes the nickel to coarsen to form large nickel clusters, thereby reducing the active area and hence the triple phase boundary region causing an increase of the activation polarisation. Also by isolating the nickel particles there will be an effect

on the conductivity of the anode whilst increasing the ohmic losses. These mechanisms can contribute to the permanent functionality of a nickel based anode (*Nagel et al., 2009b)*. However in *Haga et al. (2008)* it is revealed that nickel sulphide is only stable at 1000°C when the concentration of hydrogen sulphide is at approximately 8000ppm, thereby indicating no formation of nickel sulphide when working with such small concentrations of hydrogen sulphide. *Haga et al.'s (2008)* further study in the effects of sulphur went on to quantify the voltage drop after the introduction of 5ppm hydrogen sulphide at 800, 900 and 1000°C and were found to be 80, 35 and 15mV respectively, which seem to coincide with the results found in *Nagel et al. (2009b).* It was also found that sulphur compounds CH_3SH and COS showed almost identical performance drops as hydrogen sulphide when initially introduced but where hydrogen sulphide tends to remain in a quasi steady state CH_3SH showed a further gradual decrease in voltage, please refer to *Figure 4-11*. Further studies by *Matsuzaki et al. (2000)* on how the effects of sulphur poisoning are influenced by lower temperatures, results indicated that detectable degradation occurred at concentrations of 2, 0.5 and 0.05ppm at 1000, 900 and 750°C respectively. This is of serious concern as efforts are made to reduce the operating temperature of these systems to intermediate levels, in order to ease the requirements made on material compatibility whilst running on natural gas supplies.

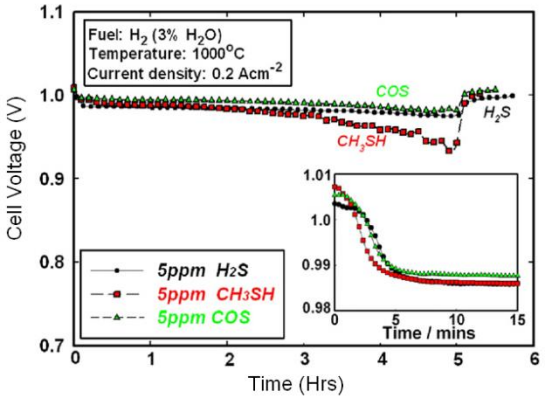

Figure 4-11: Cell voltage fluctuations as a result of poisoning by H_2S, CH_3SH and COS for 5 hrs followed by recovery without impurities (Haga et al., 2008).

As the effects of sulphur poisoning are fairly well understood when employing nickel as a catalyst in the reducing atmosphere of the anode work has been carried out to find materials that mitigate these effects, this may lead to materials that replace nickel or the ceramic composition of the electrolyte. An alternative to applying cermets is to apply oxides as the backbone of the anode, thereby satisfying the ion and electron conductivity requirements whilst catalytic materials are dispersed within this structure in order to facilitate the oxidation and reforming of hydrocarbon fuels. *Kurokawa et al. (2007)* tested a Y-doped $SrTiO_3$(SYTO)-yttria stabilized zirconia porous electrode backbone infiltrated with catalytic ceria (Ce) and ruthenium (Ru). SYTO is a chemically stable perovskite that is a mixed ionic and electronic conductor (MIEC) with a tested conductivity of 80 S/cm, and ruthenium and cerium are known to be good anode catalysts. One of the advantages of this approach is an increase in the catalytic active area as the catalytic material is deposited onto the oxide and the YSZ. This approach was tested against H_2S concentrations between 10-40ppm and the results showed from an initial power density of 510mW/cm^2 there was an initial drop until maintaining a constant maximum power density of 470mW/cm^2 at 1073K at 10ppm, but completely recovered after the supply of H_2S was stopped. Analysis of this cell was also made at varying temperatures without the application of sulphur and showed power densities of 510mW/cm^2 at 1073K at 0.85mA/cm^2 and 240mW/cm^2 at 973K at 0.5mA/cm^2. This paper however fails to report on the effects when the concentration of H_2S is increased to 40ppm, besides stating that the cell did

not fully recover after this higher concentration. Also, it would be beneficial if they could test this cell at their lower temperature range whilst running at 10ppm, as part of their original motivation was to show improved performance over the nickel based anodes at lower temperatures.

In *Haga et al. (2008)* the authors go on to study the effects of chlorine and the formation of nickel chloride ($NiCl_2$) which is stable when 100ppb and 10ppm of Cl_2 are contained in the fuel gas at 800°C and 1000°C respectively. The formation of nickel chloride can have a permanent effect on the durability of the anode as the sublimation temperature of nickel chloride is 985°C, and should definitely be considered when designing a system that operates close to this temperature. Test carried out using levels of 5, 100 and 1000ppm of chlorine caused a continuous decline of the cell voltage with the 100ppm and 1000ppm showing 1.7% and 13% degradation over 100 hours of exposure respectively. With 5ppm of chlorine exposure cell degradation was observed to be minimal but still measurable.

4.4.3 THE CATHODE

The function of the cathode is to promote oxygen reduction, absorption and diffusion at the triple phase boundary. This is done by selecting materials that provide active sites for oxygen absorption (*Shih et al., 2011*).

The most popular material which is compatible with the YSZ electrolyte, and provides long-term stability and good performance at temperatures above 850°C is strontium-doped lanthanum magnetite LSM ($La_{1-x}Sr_xMnO_{3-\delta}$), typically with *x=0.10-0.25* and exhibits a thermal expansion of about $11x10^{-6}K^{-1}$ (*Jiang, 2008; Bove et al., 2008*). LSM cathodes show good catalytic activity and electronic conductivity but have very low ionic conductivities. Therefore the reduction and transport of the oxide ions can only be achieved at the triple phase boundary. In order to extend the reaction zone to include the bulk of the cathode material LSM is often mixed with a good ionic conductor to produce a MIEC. Electronic conductivity of these materials is achieved due to the hopping of electron holes between Mn^{3+} and Mn^{4+} valence states.

Calcium (Ca^{2+}) can also be used as a dopant at concentrations between 10-30 mol%. Strontium or calcium doping is used to increase the electronic conductivity. In LSM the oxide ions are conducted via oxygen vacancies incorporated by adding lower valence ions such as Sr to the La sub-lattice providing for the deviation δ from stoichiometry. This material belongs to the ABO_3 perovskite oxide[4] family. Below 800°C these LSM materials show poor catalytic activity towards oxygen reduction and electronic conductivity is also reduced. Therefore for intermediate temperature SOFCs require different cathode materials such as $La_{1-x}Sr_xFe_{1-y}Co_yO_{3-\delta}$ (LSCF) where Mn is substituted by Co or Fe on the B-sites (*Taroco et al., 2011*). Although strontium cobalt oxides have higher catalytic activity than conventional lanthanum strontium manganese oxides they have severe problems in compatibility with zirconium based electrolytes (*Sakai et al., 2007*). The formation of a

4 The larger rare-earth ions occupy the A-sites, and the transition metal ions occupy the octahedral B-sites. Doping is accomplished on the A-sites where La^{3+} is replaced by a Sr^{2+}.

secondary phase $La_2Zr_2O_7$ behaves like an insulating material therefore negatively impacting the performance of the cell. To prevent the formation of this secondary phase a doped ceria layer such as samaria-doped ceria (SDC) is inserted between the LSCF and the electrolyte. This approach is widely adopted for SOFCs operating at lower temperatures (*Sakai et al., 2007*).

Cathodic overpotentials of manganite cathodes can be greatly modified by replacing different rare-earth cations at the A site i.e. $Ln_{0.6}Sr_{0.4}MnO_3$ (Ln=La, Pr, Nd, Sm, Gd, Yb, Y) (*Sun et al., 2010*). The selection of smaller lanthanoids can suppress the formation of $Ln_2Zr_2O_7$ such as $Pr_{1-x}Sr_xMnO_3$, $Nd_{1-x}Sr_xMnO_3$ and $Sm_{1-x}Sr_xMnO_3$ systems. And increasing the Sr substitution combined with lanthanides with higher atomic numbers is beneficial when matching the thermal expansion coefficient (*Sun et al., 2010*).

Strontium doped lanthanum ferrite ($La_{0.8}Sr_{0.2}FeO_3$)(LSF) cathodes have shown promising stability and performance at 750°C, and these iron based cathodes more chemically stable in the presence of YSZ (*Simner at al., 2003; Sun et al., 2010*). The addition of Sr causes a charge unbalance by forming Fe^{4+} ions creating oxygen vacancies and at high temperatures LSF will lose oxygen to form oxygen vacancies at the expense of decreasing hole concentration (*Sun et al., 2010*). Therefore maintaining ion conduction at the expense of electron conductivity.

As will be discussed in the next section the use of chromium alloys as intermediate temperature SOFCs can lead to poisoning of the cathode. Therefore the selection of cathode material should take this into account and a material that has shown to be unaffected by chromium evaporation is $LaNi(Fe)O_3$ (LNF)(*Zhen et al., 2007; Komatsu et al., 2010b; Taguchi et al., 2013*). LNF is attractive as the material exhibits high oxygen reduction activity at 800°C, high electronic conductivity, and an expansion coefficient close to that of zirconia electrolytes. At 800°C the LNF material has shown to have an electronic conductivity which is three times greater than that of traditional LSM cathodes (*Huang et al., 2011*). A draw back of the material is that during sintering with the zirconia electrolytes a layer of $La_2Zr_2O_7$ tends to form at the interface (*Chiba et al., 2008*). Again, to overcome these issues composite active layers have been used between the electrode and electrolyte. Some materials used include; Pr-doped ceria ($Ce_{1-x}Pr_xO_{2-\delta}$ (x=0.1-1.0) (*Taguchi et al., 2013*), $Ce_{0.8}Sm_{0.2}O_{1.9}$ (*Chiba et al., 2008*), and $Ce_{0.9}Gd_{0.1}O_{1.95}$ (*Nishi et al., 2014*).

4.4.4 INTERCONNECTS

The interconnect serves to separate the gas streams whilst at the same time serving as a current collector, for this reason interconnects are often referred to as bipolar plates. Interconnects must be chemically compatible with electrode materials and must have good electronic and thermal conductivity characteristics, resistance to corrosion in oxidising and reducing environments, and must have a close thermal expansion coefficient with the other cell components. The two materials most commonly used as interconnects are ceramic and metallic. Ceramic materials are generally required at very high operating temperatures but with the trend for lowering the operating temperatures increases the use of metallic interconnects becomes more favourable.

Ceramic interconnects are conventionally based on $LaCrO_3$ type materials as they do not decompose when exposed to typical SOFC environments (*Menzler et al., 2010*). This material exhibits excellent

electric conductivity under SOFC conditions when compared with other ceramics, could be improved by doping with Mg, Sr, or Ca (*Wu et al., 2010*). A drawback of these materials is that they cannot be used at temperatures below 800°C as the chromium reduces from Cr^{4+} to Cr^{3+} in reducing atmospheres. This reduction of the material causes the formation of oxygen vacancies and expansion of the material that can lead to cracking. The fact that these materials are expensive to manufacture makes the choice of metallic interconnects more favourable. $LaCrO_3$ also behaves as a p-type semiconductor and conductivity decreases with decreasing oxygen partial pressure as the lanthanum chromite becomes oxygen deficient (*Fergus, 2004; Wu et al., 2010*). $LaCrO_3$ has very poor sinterability which is attributed to the formation of CrO_3 which is then reduced to Cr_2O_3 (as described above) which again can be improved by doping with Sr or Ca (*Fergus, 2004*).

Metallic interconnects are cheap, easy to manufacture and provide very high electrical conductivities. However, they have the disadvantage of corrosion. Generally the materials used are chromium alloys but also include some ferritic steels specially developed for SOFC operation. Unfortunately chromium in the chromium alloys has a tendency to evaporate causing poisoning of the cathode where the production of $CrO_2(OH)_2$ can accumulate at the porous electrode thereby blocking the diffusion pathways (*Zhen et al., 2007; Schuler et al., 2012*). Chromium vapour also reacts with LSM to form $(Mn,Cr)_3O_4$, and in the case of LSCF chromium vapour leads to the formation of $SrCrO_4$ (*Shaigan et al., 2010; Park et al., 2014*). Chromium evaporation can also produce surface stress that can cause the material to crack (*Fergus, 2005*). To address these issues chromia forming alloys are being developed. Increasing chromium content has been used to offset the loss due to volatilisation. Volatilisation can be reduced through the alloying of elements such as manganese and titanium (*Fergus, 2005*). Also to be considered is the amounts of aluminium and silicon as the formation of their insulating oxides (alumina and silica) that will have a negative impact on the performance of the interconnects.

Another approach to modifying these metallic materials to meet the requirements of an interconnect is to apply coatings to existing alloys. A number of coating materials have been applied and include perovskite oxides such as; (La, Sr)MnO_3, (La,Sr)CoO_3, (La,Sr)CrO_3, and spinels such as $(Co,Mn)_3O_4$ and $(Mn,Cr)_3O_4$, and also metallic coatings of Co, Ni, and Cu (*Lacey et al., 2010*). Coating techniques include sol-gel, chemical vapour deposition, pulsed laser deposition, plasma spraying, screen printing, slurry coating, radio frequency magnetron sputtering, large area filtered arc deposition, and electrodeposition (*Shaigan et al., 2010*).

To achieve good contact for current exchange a metallic mesh (often nickel) is used between the interconnect and the electrode.

A summary of thermal expansion coefficient (TEC) for some of the materials discussed is presented in *Table 4-4*.

Table 4-4: Thermal expansion coefficients for various SOFC materials.

Compound	TEC ($x10^{-6}K^{-1}$)	Reference
YSZ	~10.5	*Singhal et al., 2003*
Ni-YSZ	~12.5	*Singhal et al., 2003*
ScSZ	~10.7	*Sun et al., 2010*
GDC	~12.5	*Sun et al., 2010*
CeO_2	~11.5	*Mogensen et al., 2000*
LSM	~11.0	*Singhal et al., 2003*
LSCF	~12.0	*Singhal et al., 2003*
LSF	~12.5	*Simner et al., 2003*
LNF	~11.4	*Sun et al., 2010*
$LaCrO_3$	~9.5	*Wu at al., 2010*
Metallic interconnects	~11.5-12.5	*Bove et al., 2003*

4.4.5 SEALS

Another concern for SOFCs that employ a planar design configuration is to obtain an air tight seal between ceramic cells and interconnects. The requirements for sealing are extremely stringent as they are required to maintain air tightness at very high and varying temperatures in reducing and oxidising environments. To avoid mechanical stress seals must have closely matched thermal expansion coefficients ($10x10^{-6}K^{-1}$ to $13x10^{-6}K^{-1}$). Chemical compatibility is also a concern that must be considered. Importantly seals must be electrically insulating to avoid short circuiting within the stack. A schematic of the seal requirements between the cells and the stack manifold is shown in *Figure 4-12*.

Seals have been conventionally based on bonded, rigid seals primarily made from glasses and glass-ceramics and serves to bond the stack together (*Simner et al., 2001*). The advantages of using glass seals is that they can be designed to soften at elevated temperatures allowing viscous movement so when the temperature is lowered to typical SOFC operating temperatures the glass recrystallizes to form a rigid, bonded hermetic seal. Glass compositions can also be tailored to match the thermal expansion coefficient according to the rest of the materials used in the cell. The viscous movement of the glass seals can negatively affect the electrodes through solid state diffusion into the electrode, and the brittle nature of the crystalized glass can also lead to cracking. Thermal cycling using glass seals can cause thermal shock as the bonded seals turn the stack into a solid unit (*Simner et al., 2001*). Glass seals are normally applied by mixing glass powder with an organic paste which when heated evaporates before the glass ultimately melts to form the seal.

Glass-ceramics use glasses that are amorphous when melted but are specifically designed to partially or fully crystalize and become opaque at a high temperature range below the melting temperature range (*Lessing, 2007*). Glasses based on silica are often preferred over phosphate as phosphate has shown to volatise and react with nickel-zirconia to form nickel phosphide and zirconiumoxyphosphate. Barium aluminosilicate based compositions will eventually react with chromium oxide or aluminium oxide scales on the metal interconnects to form barium chromate or a celesian phase at the interface which can lead to delamination. Also, boron based compositions can react with water over time to produce $B_2(OH)_2$ or $B(OH)_3$ gas leading to decomposition of the seal (*Lessing, 2007*). Composites are often proprietary compositions which are well protected by researchers and manufacturers.

An alternative to bonding glass glass-ceramic seal materials are compressive sheet-structured silicate materials that act as gaskets which seal the units under compressive pressure. This does require that the stack design must be able to maintain the desired compressive load during operation. These micas belong to a class of minerals known as phyllosilicates composed of sheets of silicate tetrahedrons (*Simner et al., 2001*). These seals have shown stable thermal cycling performance although with enhanced leakage rates (*Bram et al., 2004*).

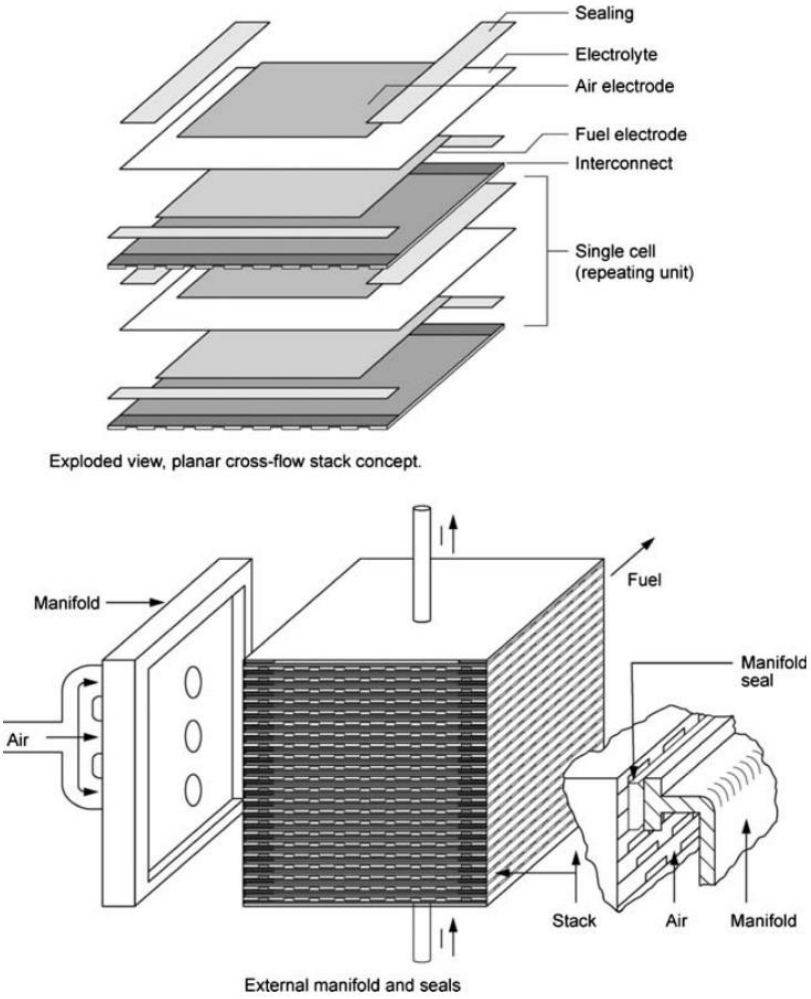

Figure 4-12: Schematic of edge sealing of planar cells and external stack manifold (*Lessing, 2007*).

Readers Guide

Overview

1. Introduction

2. The WHHE Concept

3. Literature Digest

4. SOFCs

5. Modelling

Introduction
- The need
- Model validation

Model Development
- Real World problem
- Goal defining
- System boundaries

Matlab
- Mathematical descriptors
- Fuel cell
- Combustor
- Heat engine
- Electrolysis
- Hydrogen storage
- Fuel and market dynamics

ChemCad
- Gasification
- Filtering and processing

Economics and Environment
- Feasibility
- CO_2 savings

6. Modelling Results

7. Experimental Research

8. micro-CHP in the UK Market

9. Conclusions

References

Appendices

5. MODELLING

5.1 INTRODUCTION

The purpose of system modelling is to enable users to simulate physical systems without the need to build the real product, and in some cases where systems are of global scale cannot be reproduced. This enables us to study these systems without the expense and effort required to build or change the physical product. Models are developed using a sequence of mathematical equations that predict and explain the performance of the system, and are primarily studied over a continuous period of time through the simulation of predicted dynamics.

A system can be defined as a collection of functioning units whose relationship can be described within a defined environment and boundary. Every system consists of subsystems that make up the hierarchy of the defined system and it is important to pay careful attention to understand the influences of these sub-systems. This will help to define the extent and sensitivity of the study with respect to the required results. It is also necessary to determine what falls within the system boundary. System boundaries are very often dependent on the user, on time, and on the system. Systems exchange inputs and outputs over the system boundary with the environment, for instance in this study MSW will be input and heat, electricity and by-products will be output.

The mathematical equations used to construct and describe the system are derived from physical laws and are written as difference or differential equations. Simulations are generally iterative in their development as illustrated in *Figure 5-1*. During model development revisions are made after studying results derived from simulations until an adequate level of understanding is obtained and validated.

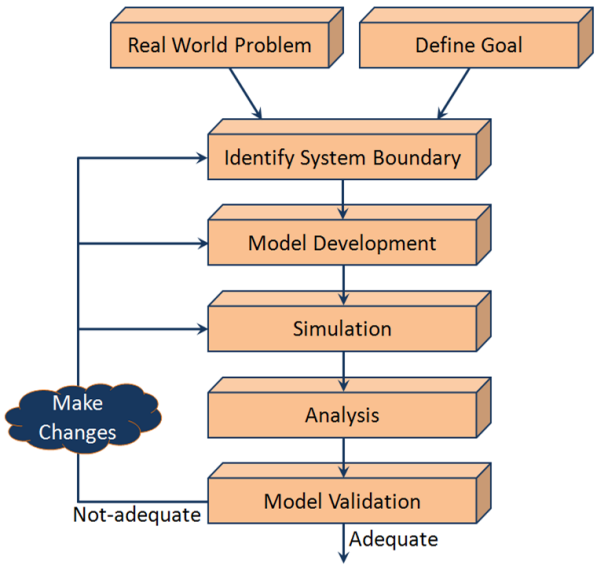

Figure 5-1: Illustrative description of the modelling process.

System Classification

Systems can be classified through a number of parameters such as:

- Time
  - Discrete: a discrete-time model is usually made up of difference equations describing the behaviour of a system over time. Difference equations relate one system parameter with another from an earlier time.
  - Continuous: continuous models usually consist of algebraic or differential equations describing the behaviour of a system over time. These dynamic equations often involve the rate change of a time dependent parameter.
  - Hybrid: hybrid models incorporate both discrete and continuous system behaviour and benefits the system by allowing more flexibility.
- Complexity
  - Physical systems: can be defined as systems that can be measured using physical devices such as electrical systems, mechanical systems, computer systems etc.
  - Conceptual systems: are systems whose measurements are conceptual/imaginary and qualitative such as social systems, economic systems etc.
  - Esoteric systems: are systems where physical measurements cannot be taken and their complexity is of the highest nature.
- Interactions
  - Independent: where events have no effect upon another.
  - Cascaded: where the effects of an event are unilateral ie. A→B, B→C etc.
  - Coupled: where events mutually affect each other.
- Uncertainties involved
  - Deterministic: there are no uncertainties in any variables.
  - Stochastic: where some variables are random.
  - Fuzzy systems: where the nature of the variables is fuzzy and are quantified using linguistic terms.
- Nature and type of components
  - Static or dynamic.
  - Linear or non-linear.
  - Time-variant or time-invariant.
  - Deterministic or stochastic.
  - Discrete or continuous.

Hence, when developing a mathematical model consideration must be given to the system boundary, components and their interactions. Model development will also depend on the type of analysis trying to be performed i.e. steady state or transient. The assumptions made during modelling will also play an important role in determining the complexity of the model and also the accuracy. Fewer assumptions may make the model more complex but the accuracy of the results will be better. Therefore the two things to be considered when optimising the outcome of your simulation are:

i) Simplicity of the model, and
ii) The accuracy of the model.

Through the use of variables in the mathematical model descriptive models are built as a hypothesis of how the system would work and estimations are made to describe how different events could affect the system. These mathematical models can be classified into 'black-box' models where no prior information is available and the functional relationship between variables and the numerical parameters is estimated, whereas 'white-box' models have all the necessary information available. Generally all models fall between these two distinctions and the more prior information available the more accurate the model will be.

5.1.1 THE NEED FOR MODELLING

Real systems are generally modelled for the following reasons:

- Experimenting with real systems is too expensive,
- There is an element of risk involved,
- Designers want to design new systems using abstract specifications,
- Modelling can force us to think through the process before physical models are built,
- Modelling improves the understanding about a system,
- To drive improvements to system performance,
- Explore various economical solutions,
- For training or entertainment using virtual environments.

5.1.2 MODEL VALIDATION

One of the biggest questions we need to face throughout the modelling process is; *Are the results reliable and realistic?* Usually an engineer will have a set of measured results from the real system which can be used to validate the final result, but when the system uses a number of interacting sub-systems the problem then extends to validating the output of these lower-level components. Here, published data from similar research will be used along with results from experimental research. This in itself poses its own problems as depending on the assumptions made the publisher may not be addressing the problem with the same level of complexity sought, which rely on initial assumptions.

5.2 MODEL DEVELOPMENT

There are a number of tools that can be used for mathematical modelling and in this study Simulink, which is a graphically based application of the MatLab, will be used to carry out selective modelling of most of the processes. Simulink enables users to develop models in the form of block diagrams. With a library of standard components block diagrams can be developed where simulation algorithms and parameters can be accessed and manipulated with minimal effort producing intuitive results and speeds up the iterative modelling process.

For those processes where Simulink modelling is not best suited ChemCad (*Chemstations, 2014*) will be used. ChemCad is ideally suited to modelling of chemical processes such as gasification, gas filtration and separation, and heat management.

5.2.1 REAL WORLD PROBLEM

- A need for new supplies of heat and electricity that is not reliant on traditional fossil fuels.
- New techniques for producing energy more efficiently with reduced CO_2 emissions.
- Solutions for extracting the embodied energy going to landfill in the form of waste.
- Solutions for the problem of waste management and the elimination of landfill.
- Understanding how high temperature SOFCs can be utilised and integrated to provide decentralised heat and power.
- Can hydrogen be used for viable energy storage providing further opportunities for the penetration of renewable energy produced via wind or PVs?

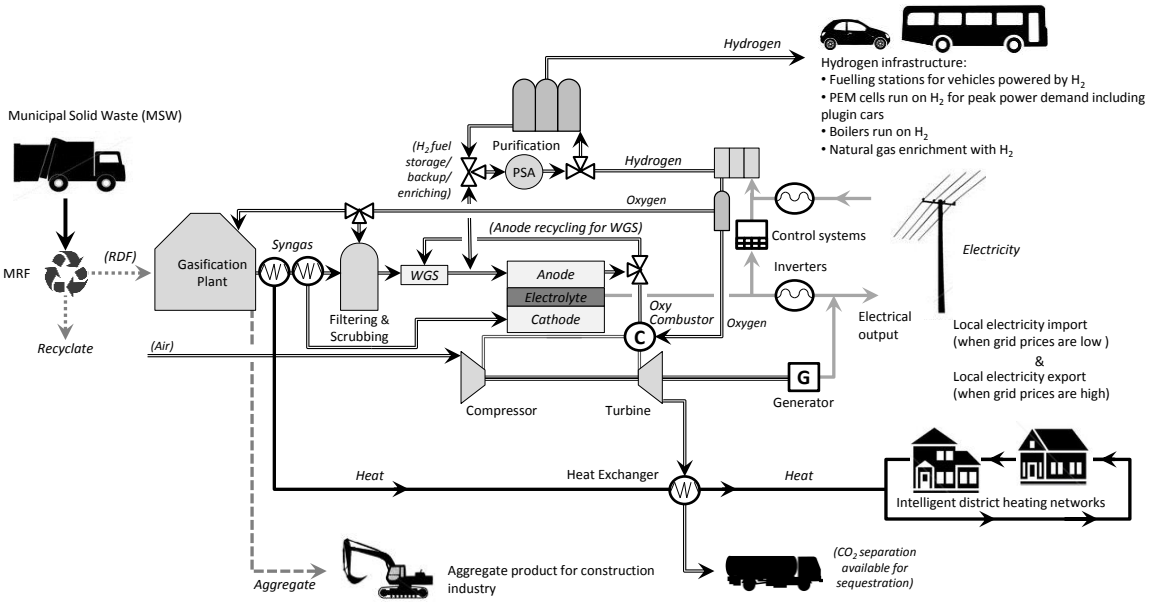

Figure 5-2: Schematic of proposed system illustrating the real world problem.

5.2.2 DEFINE GOAL

- Produce and validate a model that describes the operation of a SOFC whilst running on purified syngas.
- Describe the flow of energy as inputs and outputs for plasma gasification, filtering, SOFC, heat engine, electrolyser, hydrogen storage, and the heat and electricity available/required from the grid.
- Apply a real heat and electrical load profile to be supplied a numerical model describing this system.
- Do a cost/benefit analysis as a parametric study using variations of the included components of this system along with alternatives.
- Study the expected CO_2 and other emissions produced by this system.
- Provide a model where variable material characteristics of the fuel cell, electrolyser and hydrogen storage can be changed as a means of optimisation.
- Develop a model capable of providing information that will help users understand the integration of these various components.

5.2.3 IDENTIFY SYSTEM BOUNDARIES

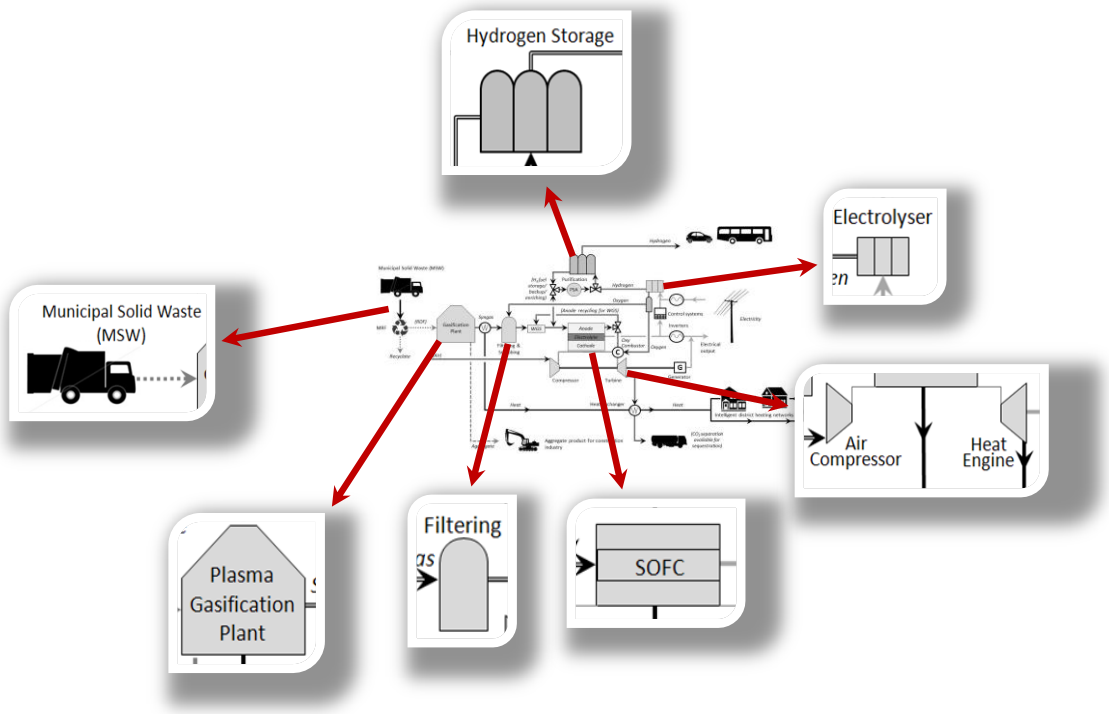

Figure 5-5: Highlighting the system boundaries of the real world problem.

5.3 SOFC - MATHEMATICAL DESCRIPTORS

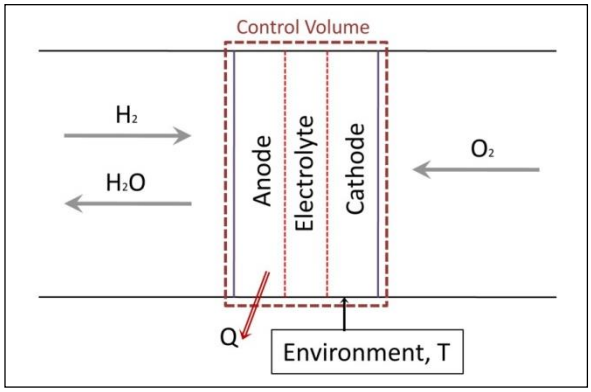

Figure 5-6: Graphical representation of the control volume surrounding the PEN

Mathematical descriptors will be used to describe the mass transport and electrochemical reactions occurring within the fuel cell. In order to accurately describe the effects of changes in syngas composition it is important to model how the changes in partial pressure will influence the performance of the fuel cell. This means it would not be sufficient to model the fuel cell at a system level but rather this research will be carried out at cell level where material properties such as porosity, tortuosity, thickness, energy activation and conductivity are accounted for.

In order to simplify the modelling approach a file containing all variables has been compiled as an m-Code Matlab file and is presented in *Appendix A.1.*

5.3.1 THE FIRST LAW OF THERMODYNAMICS AND THE STEADY FLOW ENERGY EQUATION (SFEE)

Considering the control volume in *Figure 5-4* we can see that the molar flow rate is governed by the electrochemical reaction:

$$H_2 + \frac{1}{2}O_2 \longrightarrow H_2O$$

$\therefore$ the molar ratio per mole H_2 is: $n_{H_2} = 1mol, \quad n_{O_2} = \frac{1}{2}mol, \quad n_{H_2O} = 1mol$

Other gases such as N_2 may be present but are not part of the reaction and do not transfer through the membrane and therefore are not regarded.

So it follows that the SFEE takes the form (ignoring the terms for kinetic and potential energy):

$$q + w = \sum n_i H_i - \sum n_j H_j$$

Where q is the heat transferred into the control volume and w is the work transferred out, $\sum n_i H_i$ is the enthalpy of reactants delivered and $\sum n_j H_j$ is the enthalpy of the products leaving the fuel cell.

5.3.2 THE SECOND LAW OF THERMODYNAMICS

The Second Law of Thermodynamics introduces the concept of entropy which is an amount of energy that is not available to do work as this energy is lost as a result of the rearrangement of atoms within the system (*Thompson, 1967*), and can be defined as:

$$\mathrm{d}S = \frac{\mathrm{d}Q}{T}\Big|_{\mathrm{rev}}; \qquad \mathrm{d}S \geq \frac{\mathrm{d}Q}{T}\Big|_{\mathrm{cyclic}}$$

The maximum available electrical work obtainable by the system is given by the change in Gibbs free energy ΔG of the electrochemical reaction and is expressed as:

$$\Delta G = \Delta H - T\Delta S$$

Where ΔH corresponds to the total thermal energy available in the system and $T\Delta S$ refers to the change in entropy which is the amount of energy not available to do work. Therefore ΔG is a measure of the amount of "free" energy available to do work.

Then by combining these expressions we find:

$$W_{max} = \left(H_{H_2O} - H_{H_2} - \frac{1}{2}H_{O_2}\right) - T\left(S_{H_2O} - S_{H_2} - \frac{1}{2}S_{O_2}\right)$$

Now by splitting the terms into standard conditions and system conditions i.e. (p_0, p) and considering the Entropy change of an ideal gas derived from $TdS \rightarrow dS = c_v\frac{dT}{T} + R\frac{dv}{v}$ we find:

$$W_{max} = \Delta G = -\Delta G_T^o + T\left[-Rln\left(\frac{p_o}{p_{H_2}}\right) - \frac{1}{2}Rln\left(\frac{p_o}{p_{O_2}}\right) + Rln\left(\frac{p_o}{p_{H_2O}}\right)\right]$$

$$\Delta G = -\Delta G_T^o + RTln\left[\left(\frac{p_{H_2}}{p_{H_2O}}\right)\left(\frac{p_{O_2}}{p_0}\right)^{1/2}\right]$$

Where ΔG_T^o is the Gibbs change in energy for one mol of H_2 at temperature T and a standard pressure p_0=101kPa .

Further, in an electrochemical reaction the electrical work can be considered as the energy provided by the reaction. Therefore we can define:

$$\Delta G = -W_e = -n_eFE$$

Which provides us with an expression called the Nernst equation:

$$E = E^o + \frac{RT}{nF}ln\left[\left(\frac{p_{H_2}}{p_{H_2O}}\right)\left(\frac{p_{O_2}}{p_0}\right)^{1/2}\right]$$

$$c_p = a + bT + cT^2 + dT^3 + eT^4$$

5.4 SOFC - MASS TRANSPORT

5.4.1 GAS DIFFUSION AT THE ELECTRODES

The anode and cathode electrodes are assumed to be made of porous materials that conduct both electrons and ions. Therefore these regions experience the transport of gas species, electrons and ions, and at the triple phase boundary (TPB) these elements combine. For this reason the electrodes are the most complex regions to model. Because the electrodes tend to conduct ions slower than the electrolyte, and because they readily conduct electrons, the oxygen ions tend to combine with hydrogen very close to the electrolyte-anode boundary. Similarly the O_2 molecules tend to dissociate and liberate their electrons at the electrolyte-cathode boundary. For simplification these regions can be modelled as another layer called the reaction zone which is continuous in nature, unlike the true non-continuous nature of the TPB. So, at the anode there is a flux of hydrogen to the reaction zone and a water flux from the reaction zone to the gas channel, and the cathode experiences a one-way flux of oxygen to the reaction zone.

Due to the thickness of the anode supported cell reactant gases are prevented from freely reaching the reaction zone and the momentum of the fuel gas is nearly zero (*Yakabe et al., 1999*). This causes significant voltage losses due to high concentration polarization at high current densities. This essentially means during periods of high demand (high current density) the supply of reactant to the reaction zone is restricted by the molecule's ability to diffuse through the electrode, which in this case is the thick supporting anode. The diffusion rates are affected by the structural characteristics of the anode e.g. pore size, volume fraction of the pores, and the tortuosity. The concentration polarization is also not uniformly spread across the anode as the feed rate is a function of the position along the length of the fuel channel. As this level of detail is not required by our system the concentration polarization will be measured as an average value over the full anode, and because concentration polarization values can have a dramatic effect on the performance of the fuel cell it is an important calculation to get right.

Mass transport calculations are required to estimate the gas concentrations at the reaction zone and a suitable model will need to take into account the above mentioned material characteristics as well as parameters such as; pressure, temperature, and gas concentrations. Diffusion through a porous media can be defined as either ordinary or Knudsen diffusion and the difference between the two can be attributed to the pore size of the material and the interaction of the molecules (*O'Hayre et al., 2009*). If the pore diameter is large compared to the free path of the molecules and the collision of gas molecules is dominated more between themselves than the pore walls the diffusion is classed as ordinary. But if the size of the pores is small compared to free path and the molecules collide mainly with the walls the diffusion is deemed to be Knudsen diffusion.

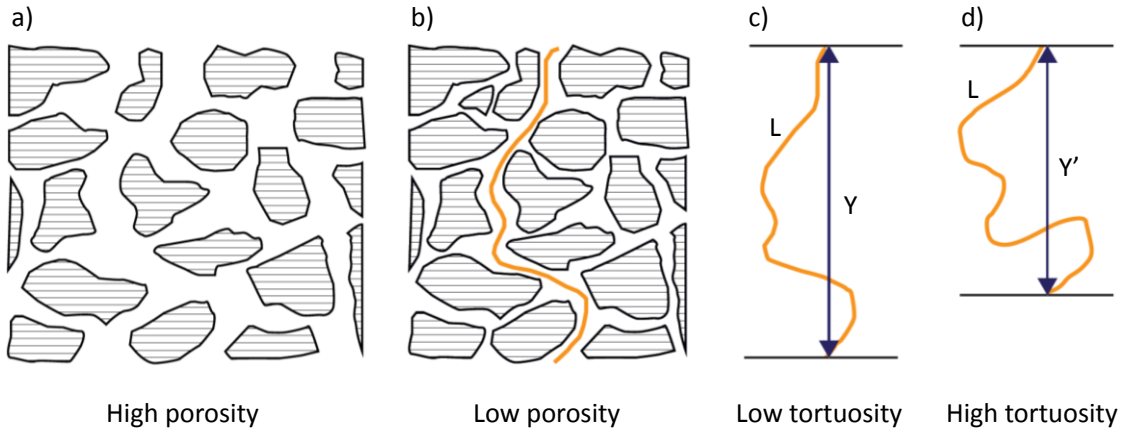

Figure 5-7: Illustrative comparison between a) high porosity, b) low porosity, and tortuosity which describes the path through a porous structure and is a function of the pore length (L) and the displacement Y. Reducing the displacement Y to Y' seen in c) and d) describes an increase in tortuosity.

Extensive studies have been published on this topic over the years and generally there are three models that have been used and reasons for individual choices are determined by the expected outcomes and the assumptions made. Mass transport of gases through a porous media can be described using; the extended Fick's model, the dusty-gas model as well as the Maxwell-Stefan model, and a comparison of the three models was done by *Suwanwaragkul et al*. (2002)(the three models are described in more detail below).

5.4.2 THE ORDINARY DIFFUSION COEFFICIENT

From solving the Boltzmann equation the following equation was derived by Chapman and Enskog, further simplification has been made using the ideal gas law (*Murzin et al., 2005; Poling et al., 2001*):

$$D_{ij,m} = \frac{0.00266T^{\frac{3}{2}}}{PM_{ij}^{\frac{1}{2}}\sigma_{ij}^{2}\Omega_{D}},$$

where

$$M_{ij} = \frac{2}{\frac{1}{M_i} + \frac{1}{M_j}},$$

and P is the pressure, M_i is the molecular weight of the i^{th} species, T is temperature, σ is the characteristic length of the intermolecular force law. Ω_{D} is the collision integral for diffusion which is dependent on temperature and is approximated by the Lennard-Jones 12-6 Potential:

$$\psi = 4\varepsilon\left[\left(\frac{\sigma}{r}\right)^{12} - \left(\frac{\sigma}{r}\right)^{6}\right]$$

with ε and σ as the characteristic Lennard-Jones energy and length respectively. The Chapman-Enskog theory is used to calculate values for ε and σ, as presented in *Table A.1.1* in *Appendix A.1 (Poling et al., 2001).* Values for ε_{ij} and σ_{ij} are calculated as (k represents the Boltzman constant):

$$\frac{\varepsilon_{ij}}{k} = \left(\frac{\varepsilon_i}{k} \cdot \frac{\varepsilon_j}{k}\right)^{\frac{1}{2}}$$

and

$$\sigma_{ij} = \frac{\sigma_i + \sigma_j}{2}$$

Ω_D is calculated as a function of kT/ε for the Lennard-Jones 12-6 potential, calculations and values can be found in *Appendix A.1.*

5.4.3 KNUDSEN DIFFUSION

In order to take the Knudsen diffusion into account in the three mathematical models the following Knudsen diffusion coefficient $(D_{ij,k})$ for a multi-component gas mixture must be calculated from the free molecule flow theory (*Yuan et al., 2008; Bove et al., 2008)*:

$$D_{ij,k} = \frac{2}{3} r_e v_i = \frac{2r_e}{3}\left(\frac{8RT}{\pi M_{ij}}\right)^{1/2},$$

In which r_e is the effective radius, v_i the average molecular speed.

The Knudsen Number

The Knudsen number (Kn) is a dimensionless number that defines the ratio of the molecular mean free path to a physical length scale which in this case will be the pore diameter of the porous material. For Knudsen numbers greater than 10 collisions between molecules and the walls of the pores is of greater significance than the molecule-molecule collisions. Therefore the viscous flow and molecular diffusion are negligible and Knudsen diffusion dominates. Conversely, for Knudsen numbers below 0.1 viscous flow and molecular diffusion dominate the mass transport process. For intermediate values between 0.1 – 10 all three mass transfer mechanisms should be taken into account.

$$Kn = \frac{\lambda}{L'},$$

Where λ represents the mean free path and the physical length scale is represented by L'. In general SOFCs typically the pore size ranges from 0.05-2.6μm (*Bove, 2008; Krishna, 1996; Andersson et al., 2011*), and the mean free path for a typical working gas is 0.2μm (*Kong et al., 2011)*.

5.4.4 EFFECTIVE DIFFUSION COEFFICIENT

For diffusion in porous solids use is made of an effective diffusion coefficient which takes into account the microstructure of the material so the diffusion coefficients are corrected by porosity (ξ) and tortuosity (τ)(*Anderson et al., 2011; Yuan et al., 2008; Hewitt et al., 1997)*:

$$D_{ij,eff} = \frac{\xi}{\tau}\left(\frac{D_{ij,k} \cdot D_{ij,m}}{D_{ij,k} + D_{ij,m}}\right)$$

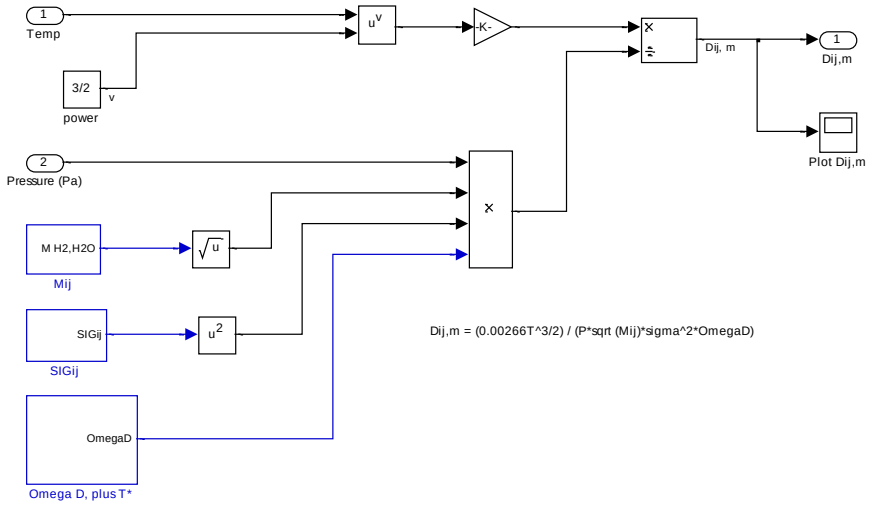

Figure 5-8: Simulink workspace illustrating equations required to determine the molecular diffusion coefficient.

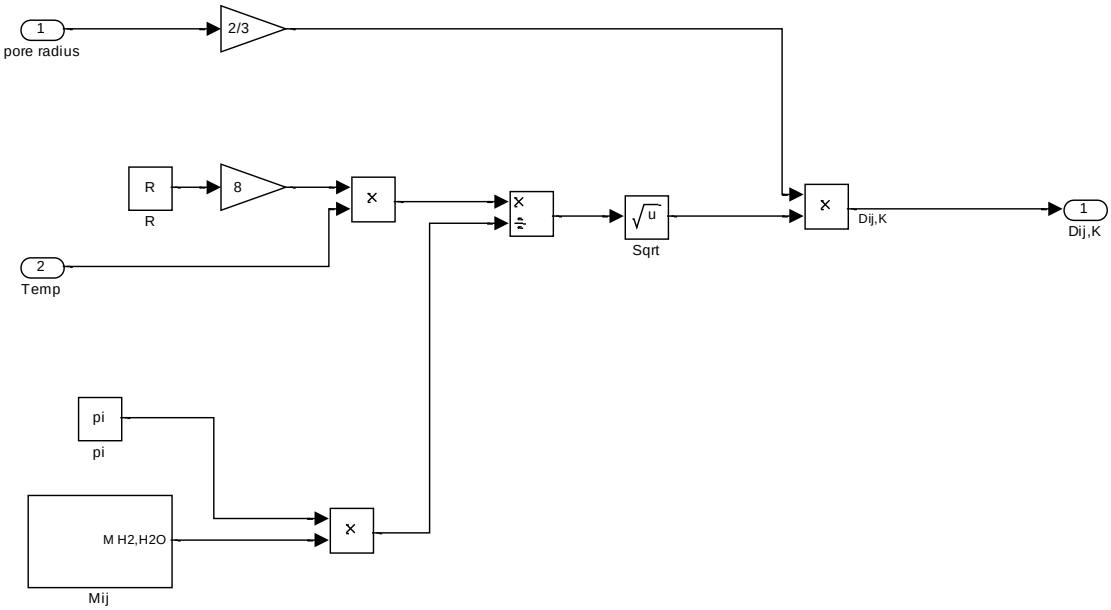

Figure 5-9: Knudsen diffusion coefficient calculations shown in Simulink.

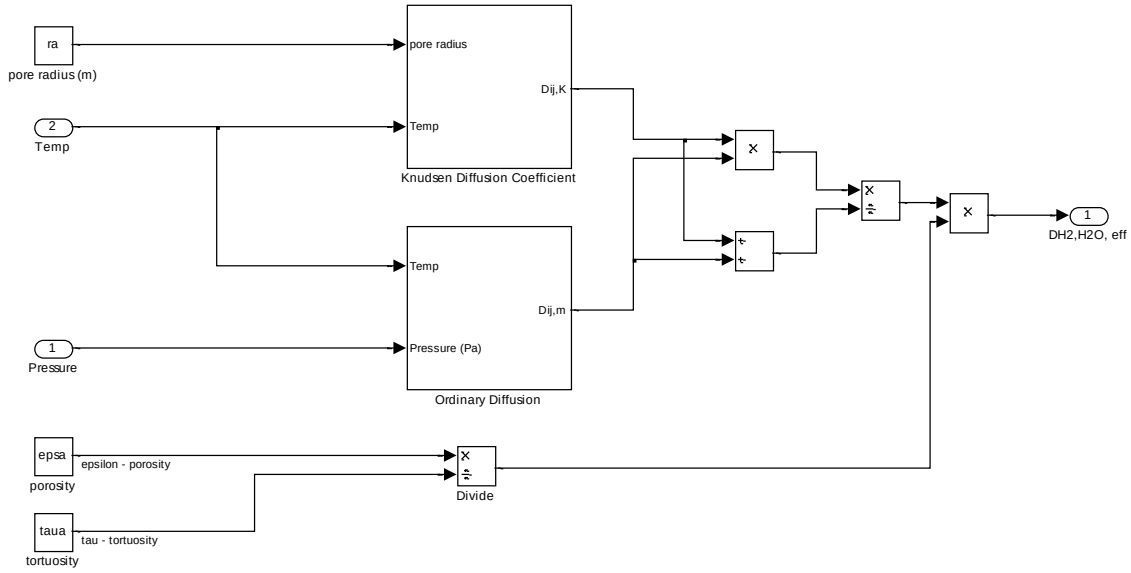

Figure 5-10: Effective diffusion calculations showing molecular and Knudsen subsystems, with corresponding results shown as a function of temperature.

5.4.5 FICK'S LAW

Fick's law is the simplest approach to gas diffusion (*Krishna et al., 1997; Bove et al., 2008; Andersson et al., 2011*), and the reason for the common application of this method is attributed to the fact that this approach will give an explicit analytical expression that can be directly applied in the mass conservation equation (*Kong et al., 2011*). The formula is described as:

$$\boldsymbol{N_i} = -D_i c_{gas} \nabla x_i,$$

D_i is the diffusion coefficient$\left(\frac{cm^2}{s}\right)$(or D_{ij}in the case of binary diffusion), c_{gas} is the total molar concentration of the gas mixture $\left(c_i = \frac{n_i}{V}\right)$, X_i is the mole fraction composition $\left(x_i = \frac{n_i}{n_{tot}}\right)$, and $\boldsymbol{N_i}$ is the diffusion flux $\left(\frac{mol}{cm^2.s}\right)$.

5.4.6 MAXWELL-STEFAN MODEL

The Maxwell-Stefan model is extensively used where ordinary molecular diffusion is experienced and is not limited to binary mixtures without electrostatic forces such as in Fick's law. Rather, in the Maxwell-Stefan expression the diffusion of each gas species is linked with the other species within the gas composition:

$$\sum_{j=1, j\neq i}^{n} \frac{x_j N_i - x_i N_j}{D_{ij}} = -c_{gas} \nabla x_i$$

Where n indicates the number of components in the gas mixture, and D_{ij} is the binary diffusion coefficient.

5.5 SOFC - PARTIAL PRESSURE AT THE REACTION ZONE

When the fuel cell is under load gradients of partial pressure for hydrogen, oxygen and water will be formed along the length of the electrodes and because of mass diffusion the partial pressure at the reaction site will be lower than those in the bulk flow. The Maxwell-Stefan approach will be used to determine the partial pressure of gases whilst the fuel cell is under load. The same theory can be used for other fuels such CO but there will be an opportunity to increase the hydrogen yield by shifting any CO to CO_2 whilst producing hydrogen during the syngas processing and filtration. As mentioned previous CO will also shift to CO_2 at the anode where Nickel (or similar catalyst is present):

$$\nabla x_i = \frac{RT}{P} \sum_{j=1, j\neq i}^{n} \frac{x_j N_i - x_i N_j}{D_{ij}}$$

The molar flux N can be defined by Faradays Law according to the following formulas for both the anode and cathode:

$$N_{H_2} = -N_{H_2O} = \frac{j}{2F}$$

$$N_{O_2} = \frac{j}{4F}\,, \qquad N_{N_2} = 0 \text{ (does not react)}$$

The molar concentrations are assumed to be known for flow rates entering the anode and cathode channels where $x_{H_2} + x_{H_2O} = 1$, and $x_{O_2} + x_{N_2} \approx 1$, and knowing that the molar concentration is directly proportional to the partial pressure ($p_i = x_i \times P$) the resulting Maxwell-Stefan equations looks like (*Nehrir et al., 2009*):

$$\frac{dp_{H_2}}{dx} = -\frac{RT}{D_{H_2,H_2O}} \frac{j}{2F};$$

$$\frac{dp_{H_2O}}{dx} = \frac{RT}{D_{H_2,H_2O}} \frac{j}{2F};$$

$$\frac{dx_{O_2}}{dx} = \frac{RT}{P_{ch,c} D_{O_2,N_2}} \frac{j}{4F} (x_{O_2} - 1)$$

Integrating these equations with respect to distance x from the channel surface to the reaction zone yields the following equations for the effective partial pressure at the reaction site:

$$p^*_{H_2} = p_{ch,H_2} - \frac{jRTt_a}{2FD_{H_2,H_2O}};$$

$$p^*_{H_2O} = p_{ch,H_2O} + \frac{jRTt_a}{2FD_{H_2,H_2O}};$$

$$p^*_{O_2} = P_{ch,c} - \left(P_{ch,c} - p_{ch,O_2}\right) \exp\left(\frac{jRTt_c}{4FP_{ch,c}D_{O_2,N_2}}\right)$$

These partial pressures will be used in the Nernst equation to find the fuel cell voltage. For modelling purposes it is assumed that the other gases present in syngas are not involved in the electrochemical so do not diffuse to the reaction zone. Partial pressures do take account of any other gases present at the anode.

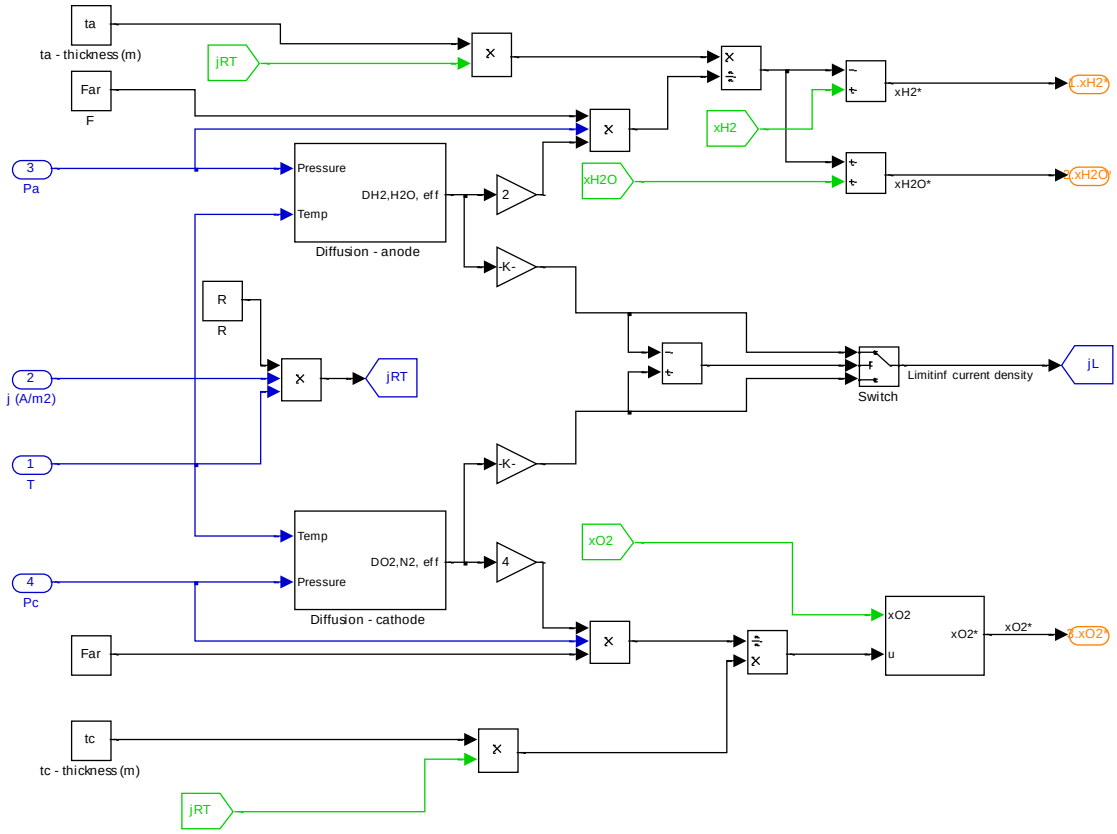

Figure 5-11: Molar concentration equations where results are used to evaluate the partial pressures at the reaction site. Calculations for the limiting current density are also done within this subsystem.

5.6 SOFC - ELECTROCHEMICAL REACTIONS

5.6.1 THE INTERPHASE REGION

The properties of a material vary between particles and forces acting at the boundaries and within the bulk of the material. Therefore the uniform properties of the electrolyte are perturbed in the interphase region by the presence of another phase. The particles present in the interphase region are arranged in response to the forces acting on the two phases and results in a compromise between the demands of both phases. This leads to an orientation of dipoles at the boundary of both phases thereby causing a breakdown of electroneutrality and a net charge to operate across the boundary, as illustrated in *Figure 5-10*. This is known as 'The Charge Double Layer' and describes a potential difference across the interface and although the potential difference is not large (~1V) because of the dimensions of the interphase region the gradient potential is enormous (~10^7V.cm^{-2}) (*Bockris et al., 2002*).

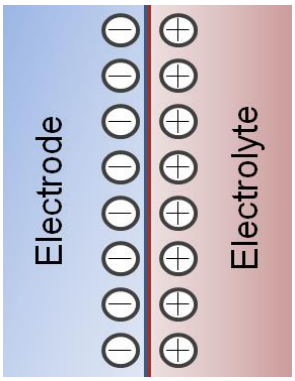

Figure 5-12: Schematic of the charge double layer effect occurring at the interphase region.

This layer of charge at the electrolyte/electrode interface causes this region to behave like an electrical capacitor causing a time delay to any change in current which influences the activation overvoltage.

The reaction rate is a process just like diffusion and as illustrated earlier the standard free energy of the system has to overcome an activation free energy $\Delta G_1^{\ddagger}$ in order for the reaction to proceed. The rate at which this process occurs can be given by:

$$J_1 = c_R^* f_1 e^{-\Delta G_1^{\ddagger}/RT}$$

Where J_1 represents the reaction rate in the forward direction, c_R^* is the surface concentration of the reactant (mol/cm^2), and $f_1$is the decay rate to product. The decay rate is often approximated to:

$$f = \frac{kT}{h}$$

Where k is the Boltzmann constant and h is the Planck constant.

When describing the reaction rate we must consider both the forward and reverse reactions where the net reaction will be a result of the difference between them:

$$J = J_1 - J_2$$

$$\therefore J = c_R^* f_1 e^{-\Delta G_1^{\ddagger}/RT} - c_P^* f_1 e^{-\Delta G_2^{\ddagger}/RT}$$

5.6.2 EXCHANGE CURRENT DENSITY

When modelling fuel cells we are most concerned with the current density j produced by the electrochemical reaction. The reaction rate is related to current density by $j = nFJ$, therefore following from the previous section the current density of the net reaction can be expressed as:

$$j = nFc_R^* f_1 e^{-\Delta G_1^{\ddagger}/RT} - nFc_P^* f_1 e^{-\Delta G_2^{\ddagger}/RT}$$

The exchange current density is defined at the point when both the forward and reverse reactions are in equilibrium i.e. no net reaction ($j = 0$). Therefore the exchange current density can be defined at the dynamic equilibrium where:

$$j_1 = j_2 = j_0$$

Based on the Arrhenius law (explained below) *Costamagna et al. (2003)* derived a set of equations which provide an expression for the anodic and cathodic exchange current densities as a function of the composition of the reacting gases:

$$j_{0,an} = \gamma_{an}\left(\frac{p_{H_2}}{P_{ref}}\right)\left(\frac{p_{H_2O}}{P_{ref}}\right)\exp\left(-\frac{E_{act,an}}{RT}\right)$$

$$j_{0,cat} = \gamma_{cat}\left(\frac{p_{O_2}}{P_{ref}}\right)^{0.25}\exp\left(-\frac{E_{act,cat}}{RT}\right)$$

Where γ is a pre-exponential factor and E_{act} is the activation energy required to allow the reaction to proceed.

- **ARRHENIUS'S LAW**

In order to fully understand the concept behind the Arrhenius equation it is better to first understand the reaction mechanisms involved during a chemical reaction. A chemical reaction can be described as a sequence of events where particles (reactants) experience a coming-together (collision) and a breaking-up of molecules (dissociation), into elementary or simpler units, and the final molecule that is created is the product of the reaction. Sometimes there may be intermediate species that are created and destroyed in subsequent steps before the final product is produced and as such does not appear in the net reaction equation.

During the collision phase the inter-atomic bonds are temporarily weakened, as bonds are distorted, leaving them susceptible to cleavage. This causes the bonds to expose their electron clouds with other reactants which might lead to the formation of new bonds and this then leads to the property known as activation energy (E_a). Neutral molecules will not react until they acquire the necessary energy needed to distort the prevailing bonds. This critical energy is the reaction's activation energy and is the energy required for the reacting system to proceed from reactants to products. *Figure 5-11* is a simple illustration of an exothermic reaction where after the initial activation energy of the forward reaction the product lies at a lower energy level than the initial reactant i.e. $\Delta H<0$ (for an endothermic reaction the energy level of the products would lie above the reactants but below the activation energy i.e. $\Delta H>0$)(*Lower, 2013*). It is important to remember that in the electrochemical

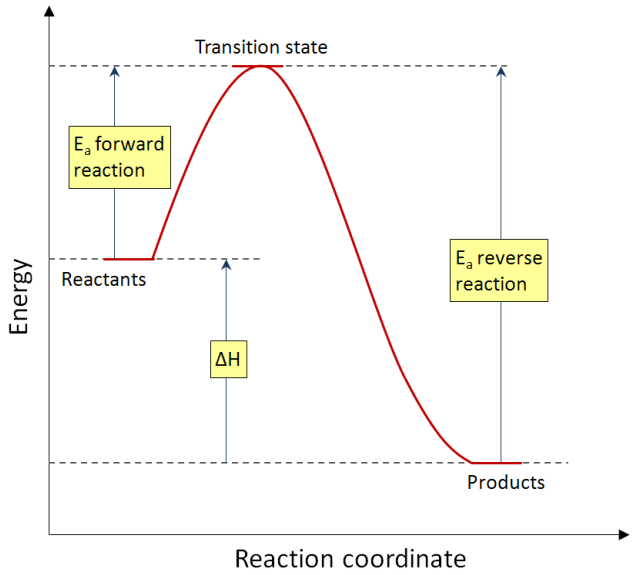

Figure 5-13: A conceptual illustration of the change in atomic coordinates during the energetic transition from reactant to product for an exothermic reaction where ΔH<0.

reactions being studied the reactants collide with electrodes and not with each other before combining.

Generally activation energy is supplied in the form of thermal energy and as the products are formed the activation energy is returned through kinetic vibration energy which is degraded to heat. Other sources of activation energy are; absorption of light (photoexcitation), and electrochemical activation (electrocatalysis) as the overpotential experienced between the electrodes provides the energy for activation.

A catalyst can be used to provide a lower activation energy pathway thereby speeding up the reaction without being consumed by it. The majority of industrial and biochemical process are facilitated by a catalyst (in biochemistry catalysts are made of protein enzymes). Catalysts do not however change the thermodynamic tendencies of the reaction they affect only the reaction kinetics so the ΔH for the equation does not change.

This led to the Arrhenius equation which looks to relate the rate of the chemical reaction as a function of temperature:

$$k = Ae^{-E_a/RT}$$

where A is a pre-exponential factor, R is the universal gas constant, T is temperature and k represents the reaction rate. Similarly the Tafel equation describes how the rate of the electrochemical reaction varies as a function of the potential:

$$j = j_0 e^{\alpha n F \eta_{act}/RT}$$

where j is current per unit area with units of ampere/m^2 (an ampere is a coulomb per second), j_0 is the exchange current density which is defined by the net reaction rate when the forward and reverse reactions are in equilibrium.

5.6.3 ACTIVATION LOSSES

Due to the activation energy required to overcome the charge double layer there are losses that affect the actual voltage output from the fuel cell. This activation voltage drop is generally calculated through the Butler-Volmer equation:

$$j = j_0 \left[exp\left(\frac{\alpha n_e F \eta_{act}}{RT}\right) - exp\left(-(1-\alpha)\frac{n_e F \eta_{act}}{RT}\right)\right]$$

Where α is the electron transfer coefficient (≈0.5 for SOFCs). Under conditions of high activation the first term of the Butler-Volmer equation is much larger and dominates over the second so under these conditions this formula can be simplified to:

$$\eta_{act} = \frac{RT}{\alpha n F} log\left(\frac{j}{j_0}\right)$$

Which represents the well known Tafel equation which was first observed in 1905 (*Larminie et al., 2003*). The relationship between the Butler-Volmer equation and the Tafel equation can be seen in *Figure 5-12*.

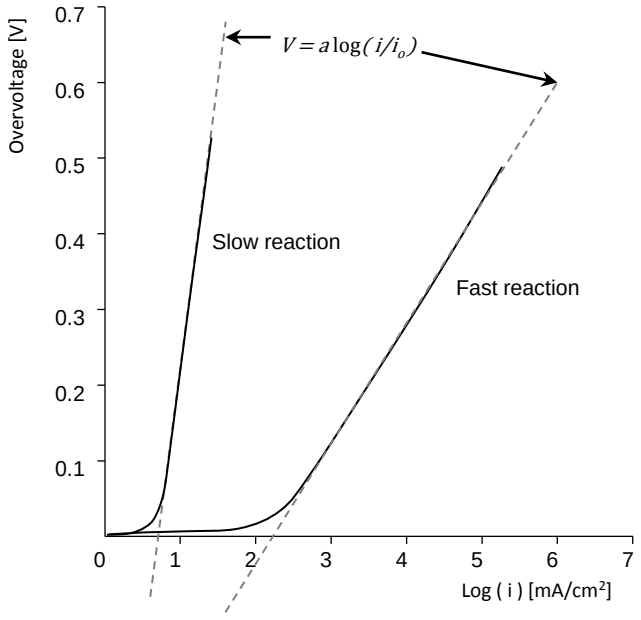

Figure 5-14: Tafel plots for slow and fast reactions with indicated formula for best fit.

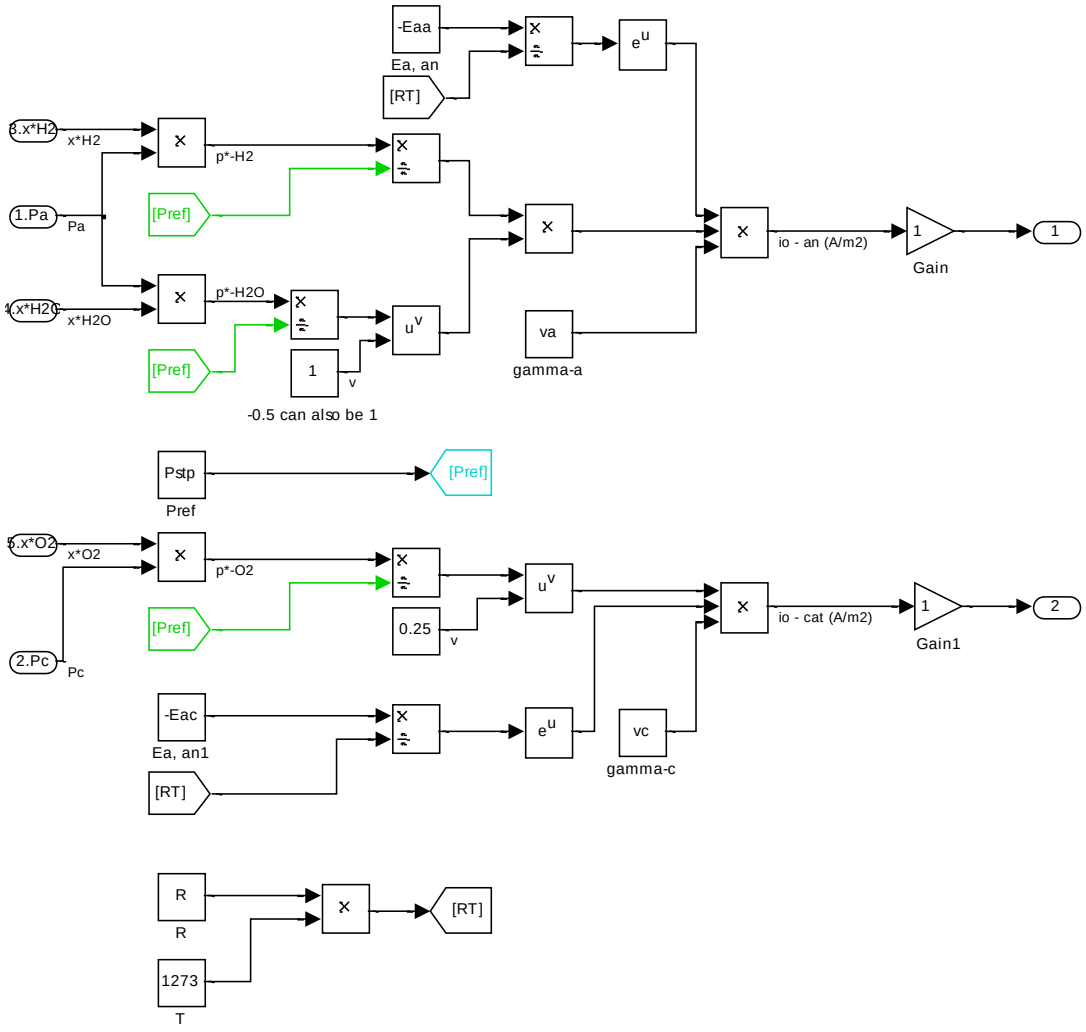

Figure 5-15: Calculations describing both anodic and cathodic exchange current densities.

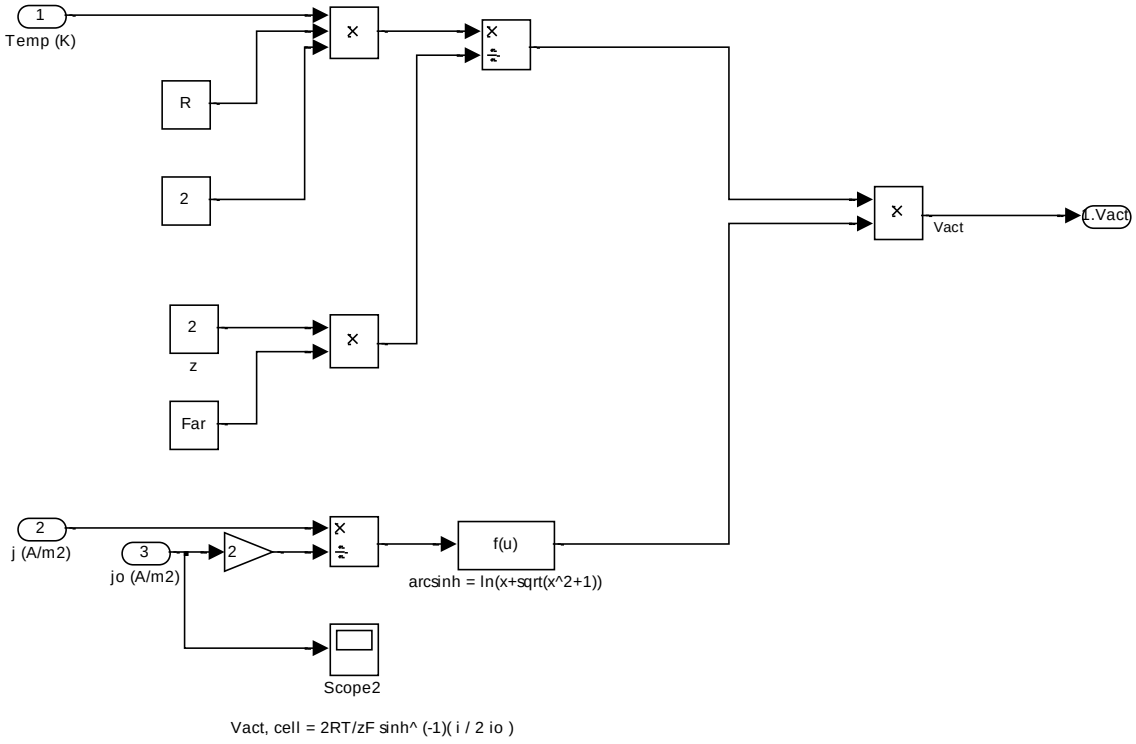

Figure 5-16: Using the values calculated for the exchange current density the losses attributed to activation.

5.6.4 CONCENTRATION LOSSES

At high current densities a situation occurs where reactants are restricted from transporting to the reaction site as a result of slow diffusion and the increase of H_2O partial pressure at the anode. This imbalance of partial pressure at the anode causes drop from actual internal voltage calculated by the Nernst equation and this difference in voltage is called the concentration voltage drop. Therefore we can determine at what current density value this phenomenon will reach maximum by assuming $c_R^* = 0$ in order to calculate the limiting current density (O'*Hayre et al., 2009*):

$$j = nFD_{ij,eff}\frac{c_R^* - c_R^0}{t};$$

$$\therefore j_L = nFD_{ij,eff}\frac{c_R^0}{t}$$

Then if we are to consider the drop in voltage caused by the concentration loss we come up with the following equation:

$$\eta_{conc} = E_{Nernst}^0 - E_{Nernst}^*$$

$$= \left(E^0 - \frac{RT}{nF}\ln\frac{1}{c_R^0}\right) - \left(E^0 - \frac{RT}{nF}\ln\frac{1}{c_R^*}\right)$$

$$= \frac{RT}{nF}\ln\frac{c_R^0}{c_R^*}$$

Which when combined with the limiting current density equation the result is:

$$\eta_{conc} = \frac{RT}{nF}\ln\frac{j_L}{j_L - j}$$

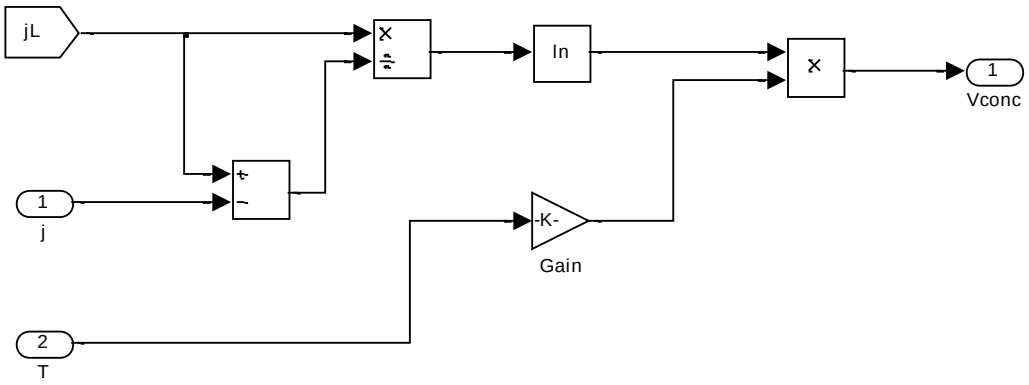

Figure 5-17: Concentration losses calculated according to the limiting current density.

5.6.5 OHMIC LOSSES

Whenever there is a transfer of charge we can expect to find losses due to resistance, as conductors are never perfect. In a fuel cell because there is a transfer of ions and electrons we must include losses which are associated to both:

$$\eta_{ohmic} = i(R_{elec} + R_{ohmic})$$

The resistance to conductivity is geometry dependent and scales proportionally to area and thickness which is why fuel cell resistance is often normalised per cm^2 and which is why electrolytes are made as thin as possible. Also resistance is additive so losses experienced in different layers can be added together in series. By relating current density with the normalised resistance, otherwise known as area-specific resistance (ASR), we can define the losses as:

$$\eta_{ohmic} = j(ASR_{ohmic})$$

and according to the thickness:

$$ASR = \frac{L}{\sigma}$$

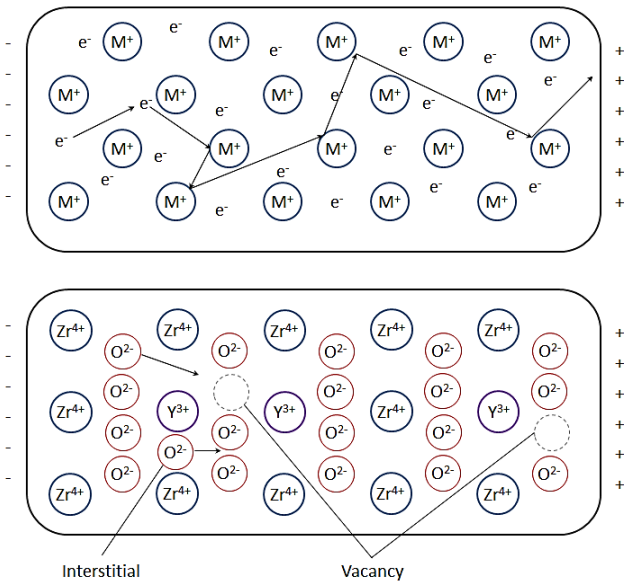

Figure 5-18: a) Illustration of electron transport in a metal where valence electrons move freely in response to potential difference.

b) Charge transport of mobile anions which 'hop' between defects such as vacancies and interstitial sites within the material.

Where σ refers to conductivity ($\Omega^{-1}cm^{-1}$). Therefore conductivity plays an important role in defining resistance and *Figure 5-16* illustrates the electron and ion transport mechanisms experienced. The expression for conductivity can be expressed using the Nernst-Einstein equation:

$$\sigma_i = \frac{c(zF)^2 D_i}{RT}$$

Where z is the valence of the diffusing ion. And the diffusivity equation for of ion through a crystal lattice is expressed as:

$$D_i = D_0 e^{-\Delta G_{act}/RT}$$

Where D_0 is a constant reflecting the attempt frequency of the hoping process, and ΔG_{act} is the energy barrier for the hopping process.

These two equations can be combined and usually simplified to form the following expression:

$$\sigma_0 = A_{SOFC} e^{-\Delta G_{act}/RT}$$

where

$$A_{SOFC} = \frac{c(zF)^2 D_0}{RT}$$

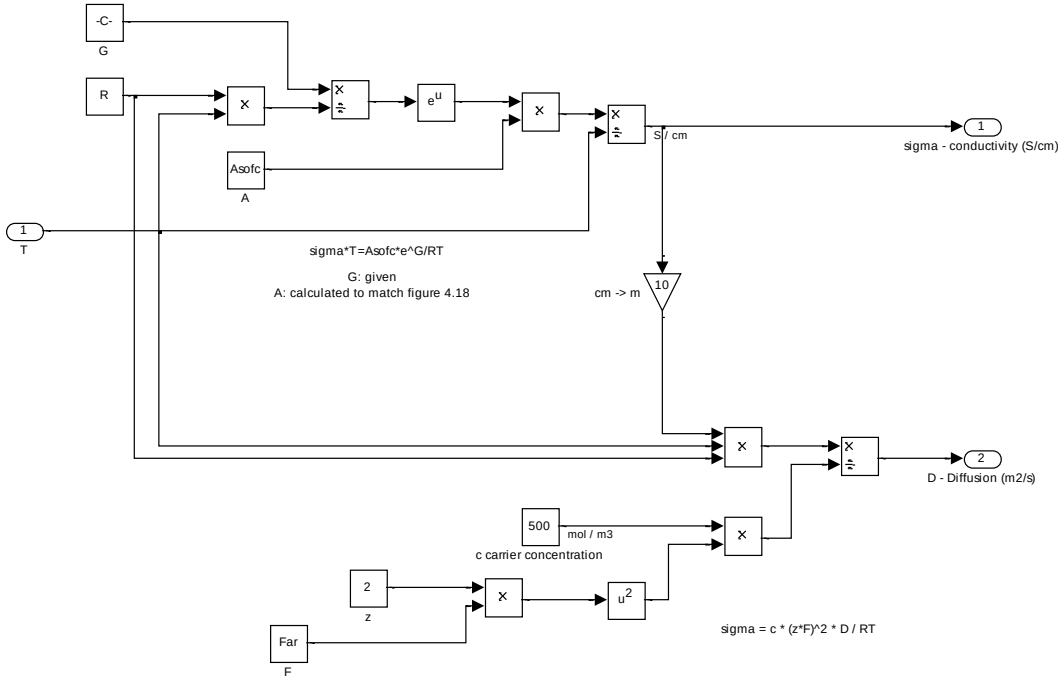

Figure 5-19: Simulink calculations of the ion conductivity of the electrolyte.

5.6.6 REVERSIBLE VOLTAGE AS A FUNCTION OF TEMPERATURE

According to the first law of thermodynamics the change in energy of a system can be expressed in terms of the heat entering the system and the amount of work being done by the system under constant volume as:

$$\mathrm{d}U = \mathrm{d}Q - \mathrm{d}W$$

And when the internal energy is expressed as a function of enthalpy under constant pressure:

$$\mathrm{d}H = \mathrm{d}Q - \mathrm{d}W$$

Then to introduce the second law of thermodynamics where:

$$\mathrm{d}S = \frac{\mathrm{d}Q}{T}$$

This then leads to the introduction of Gibbs energy which represents the maximum amount of electrical work that can be done by the system under constant temperature and pressure:

$$W_{elec} = -\Delta g_{rxn} = \Delta h_{rxn} - T\Delta s_{rxn}$$

In order to calculate the reversible voltage as a function of temperature manipulation of the above equations is required and when Δs is assumed to be independent of temperature the following approximation can be given (*O'Hayre et al., 2009*):

$$E_0 = \frac{\Delta \hat{g}^0_{rxn}}{nF}$$

$$E_T = E_0 + \frac{\Delta \hat{s}}{nF}(T - T_0)$$

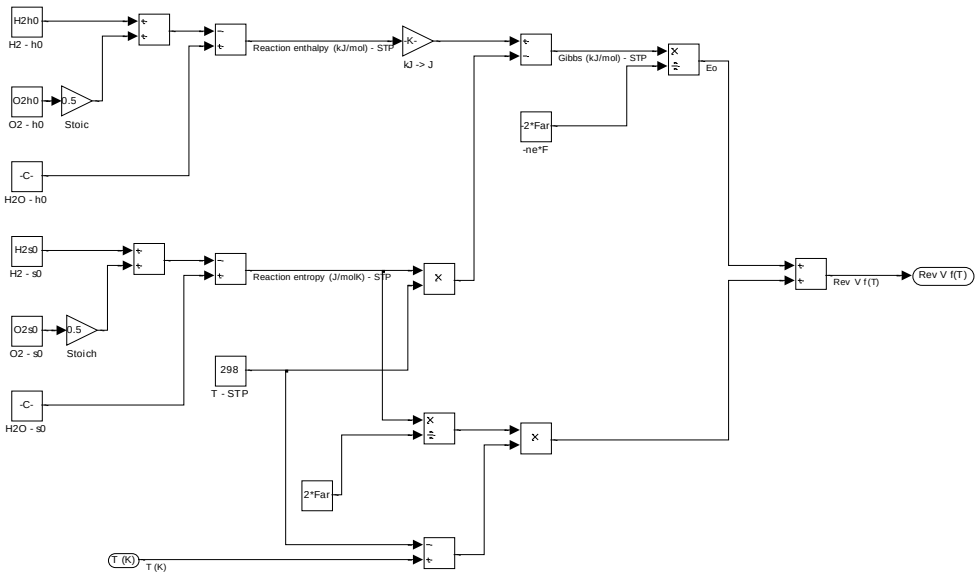

Figure 5-20: Equations calculating the maximum reversible voltage as a function of temperature.

5.7 THERMODYNAMIC ENERGY BALANCE

Heat transfer within the fuel cell is carried out by means of; convection, radiation and mass flow. The mechanisms of heat transfer are extremely complex and to elaborate completely is beyond the scope of this research. So the approach used will rely on a number of broad assumptions that look at the various mechanisms in a broad way and where possible component specific variables will brought together and represented using averages found in litereature. Where variables are not explicitly nominated please refer to *Appendix A.2*. The fuel cell is also assumed to behave adiabatically with the environment so only heat transfer within the cell is considered.

Based on the conservation of energy the heat is generated from the electrochemical reaction and can be defined as:

$$\dot{q}_{gen} = \dot{q}_{chem} - \dot{q}_{elec}$$

where

$$\dot{q}_{chem} = \dot{n}_{H_2,consumed}.\Delta H$$

and

$$\dot{q}_{elec} = V_{out}.i$$

The equations used to calculate heat transfer resulting from radiation and convection are:

$$\dot{q}_{rad} = \varepsilon\sigma A(T_{hot}^4 - T_{cold}^4)$$

$$\dot{q}_{conv} = hA(T_{hot} - T_{cold})$$

Where ε is the emissivity of the heat emitting surface, σ the Stefan-Boltzmann constant (5.6696×10^{-8} W(m^2K^4)), *A* is the surface area, and *h* is the heat transfer coefficient which can be calculated by (*Incropera, 2011*):

$$h = k\frac{Nu}{Dh}$$

Where *k* is the thermal conductivity (W/m.K), *Nu* is the Nusselt number and *Dh* is the hydraulic diameter. The Nusselt number is a function of the geometry ratio w/h (fuel channel width/height), and hydraulic diameter is defined as:

$$Dh = \frac{4A}{P}$$

Where *P* is the perimeter length.

In order to obtain suitable values of *k* and *Nu* at varying temperatures and geometry ratios reference values of *k* and *Nu* have been used to generate a trend line using fourth-order polynomials and is used to obtain more accurate results:

$$k, Nu = a + bT + cT^2 + dT^3 + eT^4$$

Values for *a, b, c, d* and *e* for *k* and *Nu* can be found in *Appendix A.1*.
Heat transfer from flow is simulated using:

$$\dot{q}_{flow} = \sum_i n_i\, C_{p,i} \left(\frac{dT}{dt}\right)$$

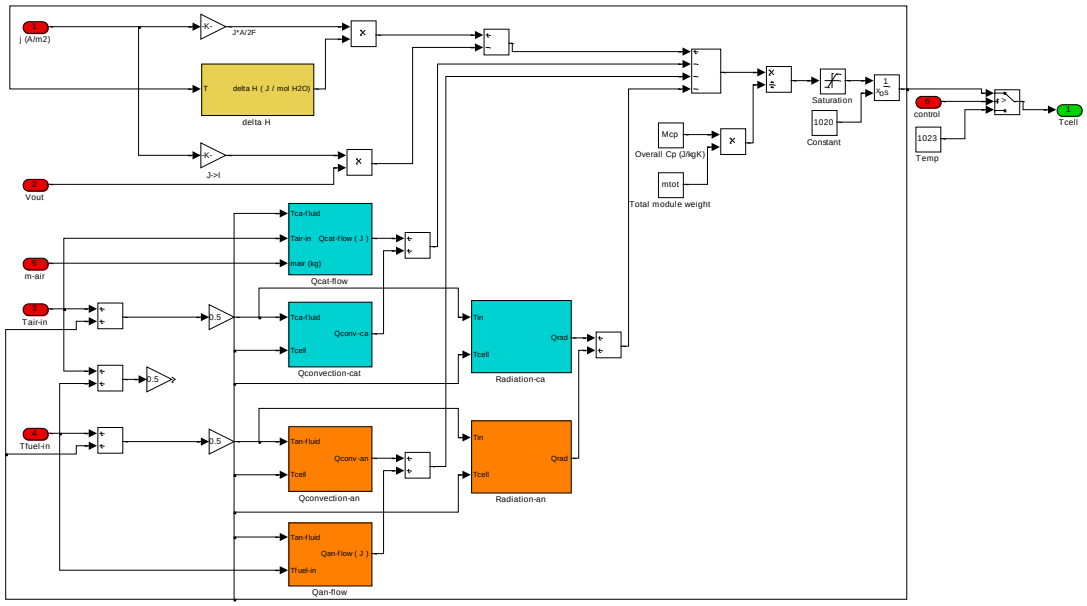

Figure 5-21: Simulink representation of the overall thermal calculations in order to calculate the fuel cell's operating temperature.

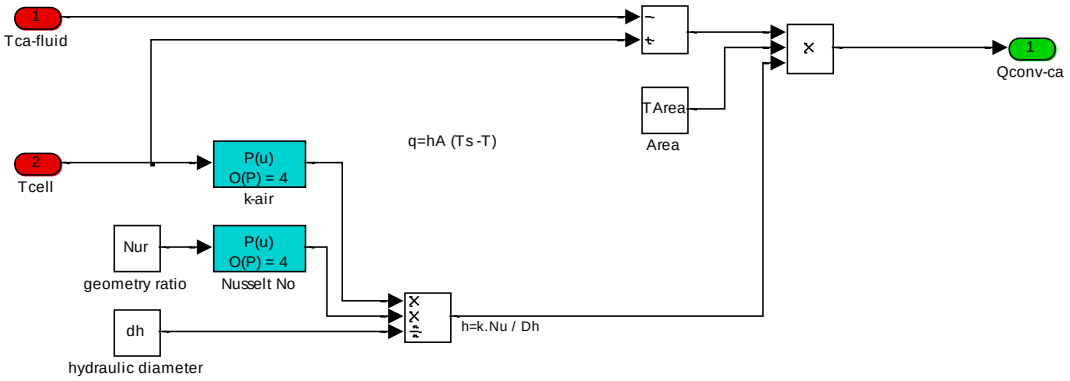

Figure 5-22: Heat transfer calculation for convection at the cathode.

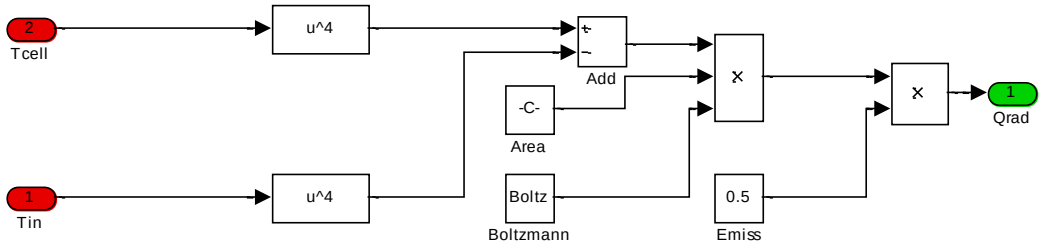

Figure 5-23: Heat transfer calculation for radiation at the cathode.

5.8 GASIFICATION

The four main reactions describing the gasification of a carbonaceous fuel are as follows (standard enthalpies of formation at 298K):

$\Delta H^0 = -111\ \text{kJ/kmol}$	$C + \frac{1}{2}O_2 \longrightarrow CO$	Equ. 4-7-1
$\Delta H^0 = -173\ \text{kJ/kmol}$	$C + CO_2 \leftrightarrow 2CO$ **(Boudouard)**	Equ. 4-7-2
$\Delta H^0 = +131\ \text{kJ/kmol}$	$C + H_2O \leftrightarrow CO + H_2$ **(Water gas)**	Equ. 4-7-3
$\Delta H^0 = -75\ \text{kJ/kmol}$	$C + 2H_2 \leftrightarrow CH_4$	Equ. 4-7-4

Most gasification processes are dominated by a balance between Equ. 4-7-1 and 4-7-3 so the overall reaction can be expressed as:

$$C_nH_m + \frac{n}{2}O_2 = nCO + \frac{m}{2}H_2 \qquad \text{Equ. 4-7-5}$$

5.8.1 THERMODYNAMIC EQUILIBRIUM

The double arrow in each of the above equations indicates that these reactions can proceed in forward and reverse directions, and generally reactions take place in both directions simultaneously but at different rates. Reaction rates are proportional to the quantity of reactants to drive the reaction in a particular direction. For example, considering the water gas shift reaction:

$$CO + H_2O \leftrightarrow CO_2 + H_2$$

The forward reaction rate r_f is proportional to the molar concentrations of CO and H_2O per unit volume:

$$r_f = k_f \cdot [CO] \cdot [H_2O]\,, \qquad \text{similarly for the reverse,} \qquad r_r = k_r \cdot [CO_2] \cdot [H_2]$$

Where k_f and k_r are the temperature dependant proportionality constant.

Over time these forward and reverse reaction will reach a state of equilibrium where both reaction rates tend to a common value. Equilibrium can be defined by a temperature dependant equilibrium constant:

$$K_p = \frac{k_r}{k_f} = \frac{[CO_2] \cdot [H_2]}{[CO] \cdot [H_2O]}$$

And assuming ideal gases:

$$K_p = \frac{P_{CO_2} \cdot P_{H_2}}{P_{CO} \cdot P_{H_2O}}$$

The temperature dependency of the equilibrium constant can be derived from fundamental data but are usually expressed as a correlation of (*Higman et al., 2003*):

$$\ln(K_{p,T}) = \ln\left(K_{p,T0}\right) + f(T)$$

For a generic reaction the overall equilibrium calculation runs as:

$$rR + sS \ldots = pP + qQ \ldots$$

$$K_e = \frac{a_P^p \cdot a_Q^q}{a_R^r \cdot a_S^s}$$

$$\ln K_e = A + \frac{B}{T}$$

Where

a:	Species activity (concentration for liquid phases, and partial pressures for vapour phases)
R, S:	Reactant species
P, Q:	Product species
p, q, r, s:	Exponent of species
T:	System temperature (K)
A, B:	Correlated parameters

Using ChemCAD to model gasification equilibrium reactions are calculated by Gibbs free energy minimisation using a GIBs UnitOp (*Figure 5-22*). The equation calculating the change in Gibbs free energy where the equilibrium constant is used is known as the van't Hoff isotherm:

$$\Delta G = -RT \ln K_e$$

ΔG is used to measure how far a given reaction is away from equilibrium. If ΔG is large and negative the reaction is spontaneous, and far from equilibrium. Therefore only when $\Delta G = 0$ will a position of equilibrium be found.

ChemCad derives the physical properties of liquids and gases using several methods eg. equation coefficients of the DIPPR (Design Institute for Physical Properties Research) equations. Equations of state models such as Soave-Redlich-Kwong are also available and thermodynamic models for predicting enthalpy and equilibrium values can be specified as a default the UNIFAC or NRTL methods are applied.

These reactors do not require stoichiometry to be defined but maintains an atom balance during the simulation. The following physical properties are required to perform these calculations:

1) Molecular formulas – to maintain atom balance
2) Ideal gas gibbs free energy of formation
3) Ideal gas heat capacity
4) Heat of vaporisation
5) Liquid heat capacity

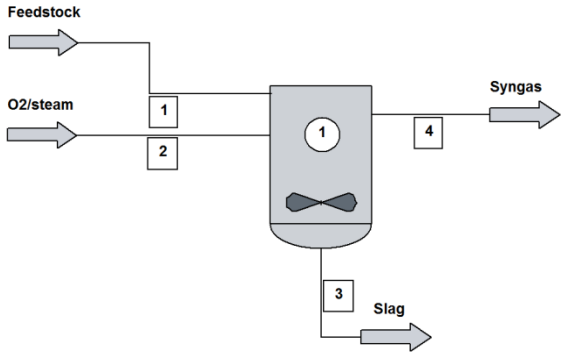

Figure 5-24: GIBs UnitOp showing inlets and outlets for gasification modelling.

Calculations for gasification are based on thermodynamics, mass and energy, operating conditions (temperature and pressure), and the addition or subtraction of indirect heat. Therefore the ultimate analysis of the feedstock is required. For MSW the following information has been found from literature (*Table 5-1 and Figure 5-23*):

Table 5-1: Ultimate analysis of various sources of MSW within the UK.

	MSW (*CIWM, 2003*)	**MSW** (*Ricketts et al., 2002*)	**RDF** (*Ricketts et al., 2002*)	**MSW** (*Optimat Ltd., 2001*)	**MSW** (*Ray et al., 2012*)	**RDF** (*Davidson R., 1999*)
Ultimate analysis, wt%						
C	24.0%	22.2%	54.5%	22.1%	43.0%	28.3%
H	3.2%	3.2%	7.6%	3.2%	5.6%	4.2%
O	15.9%	14.2%	20.5%	14.2%	26.6%	24.3%
N	0.7%	0.6%	0.7%	0.6%	0.6%	0.6%
S	0.1%	0.1%	0.2%	0.1%	0.3%	0.3%
Cl	0.7%	0.6%	0.8%	0.6%	0.3%	0.0%
Si (Ash)	24.2%	27.8%	11.7%	27.8%	12.1%	11.6%
Moisture	31.2%	31.4%	4.1%	31.4%	11.5%	30.7%
HHV/**LHV** (MJ/kg)	**10.6**	9.4	23.5	9.39	21.0 **(dry)**	11.17

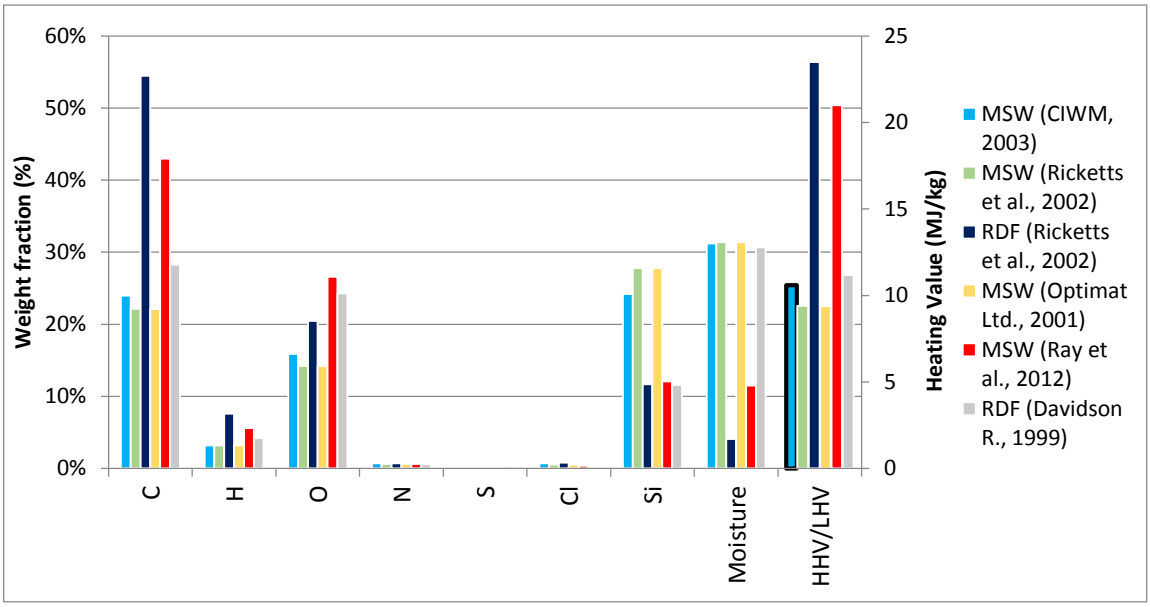

Figure 5-25: Graphical representation of changes in composition and heating values published from various authors.

5.8.2 GASIFICATION OPERATION

As mentioned previously, the gasifier has a number of variables to consider during operation all of which have an effect on the performance of the gasifier and the quality of the syngas produced. The most important aspects to look at are:

- **STOICHIOMETRIC OXYGEN RATIO (λ):**

$$\lambda = \frac{external\ O_2\ supply/fuel\ supply}{stoichiometric\ O_2\ requirement/unit\ of\ fuel\ input} \qquad \text{Equ. 4-7-6}$$

- **STEAM-TO-BIOMASS RATIO (SB):**

$$SB = \frac{steam\ mass\ flow}{fuel\ feed\ flow} \qquad \text{Equ. 4-7-7}$$

- **MODIFIED STEAM-TO-BIOMASS RATIO (SB*):**

$$SB^* = \frac{steam\ mass\ flow + fuel\ moisture\ mass\ flow}{dry, ash - free\ fuel\ feed\ flow} \qquad \text{Equ. 4-7-8}$$

- **ENERGY CONVERSION EFFICIENCY (ECE):**

$$ECE = \frac{net\ energy\ content\ of\ the\ syngas\ [MW]}{net\ energy\ content\ of\ the\ input\ fuel\ [MW]} \qquad \text{Equ. 4-7-9}$$

- **CARBON CONVERSION EFFICIENCY (CCE):**

$$CCE = \left(1 - \frac{carbon\ content\ of\ residue\ [kmol/h]}{carbon\ content\ of\ input\ fuel\ [kmol/h]}\right) \qquad \text{Equ. 4-7-10}$$

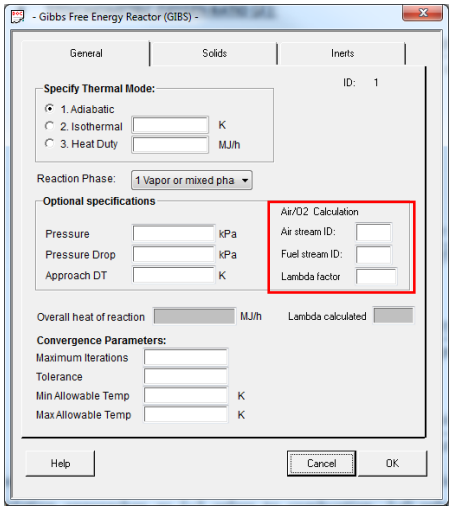

Figure 5-26: ChemCad GIBs UnitOp input screen indicating functions controlling lambda.

The stoichiometric oxygen ratio (also called equivalence ratio) is used to identify different oxidation approaches as λ=1 refers to combustion, λ=0 refers to pyrolysis, and 0 < λ < 1 represents gasification. Exothermic oxidation is also used to control the operating temperature of the reactor so whilst very low λ values will generate high yields of hydrogen and carbon monoxide greater levels of oxygen are required to sustain the gasification process by controlling the temperature.

ChemCad will automatically calculate the lambda value which makes modelling quicker and easier. Users can also set the lambda value to allow ChemCad to set the inlet airflow rate (*Figure 5-24*). Typical values used in fluidised bed gasification vary between 0.2 and 0.4 (*Siedlecki et al., 2011; Chapman et al., 2010*)

Although the most common fluidisation/moderator and oxidation medium used for gasification is air high levels of nitrogen within the product gas will significantly lower the heating value of the gas. Therefore it is more beneficial to use a combination of oxygen and steam as steam can contribute to the quality of the syngas, as it is a reactant in many of the reactions, but it can also be easily removed. This is why knowing the moisture content and using the modified steam-to-biomass ratio (SB*) is very important as the steam content influences the carbon conversion, energy conversion efficiency, and heating value of the syngas (*Siedlecki et al., 2011*).

Selected values for SB between 0.3 and 1.0 have shown to have a positive effect on carbon conversion, energy conversion efficiency, hydrogen yield, and tar reduction (*Siedlecki et al., 2011*). Whereas in Ray et al. (2012) the researchers prefer to control the steam quantity according to the designed oxygen flow using a steam to O_2 molar ratio between 1.15 to 2.5 and an O_2 to fuel weight ratio between 0.51 to 0.78.

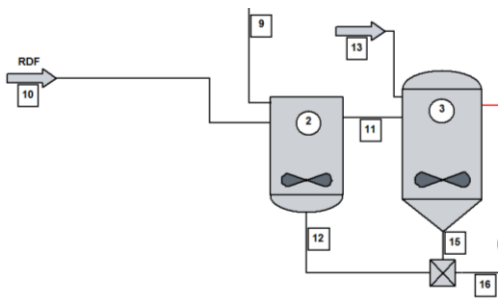

Figure 5-27: Modelling of two-stage fluidised bed plasma gasification unit.

In order to simulate the two-stage fluidised bed plasma gasification configuration a secondary GIBs UnitOp has been used using a set operating temperature for the unit that reflects published information, shown in *Figure 5-25*.

The plasma converter is modelled by assuming a fixed operating temperature which is required to breakdown the tar contaminants. In reality these reactors work with a combination of thermal energy coming from the thermal plasma and also from a secondary supply of oxygen, and the two are controlled to maximise the energy conversion efficiency whilst minimising the parasitic loss which affects overall efficiency.

Advanced Plasma Power have published information (*Materazzi et al., 2013b*) with these details so the electrical power required to maintain the thermal plasma reactor temperature will be derived from *Figure 5-26* and will be accounted for during the overall energy consumption calculation and will be reflected in the power available for export to the grid as well as the overall efficiency of the WHHE Energy Centre.

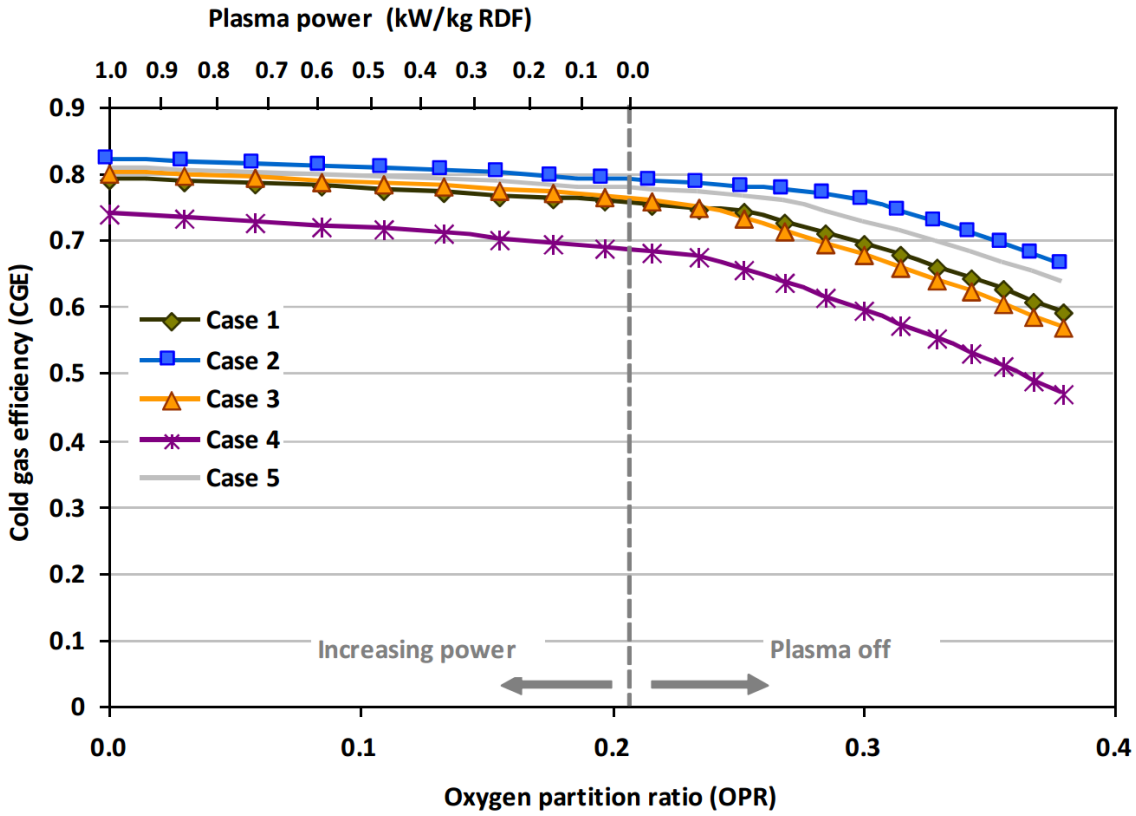

Figure 5-28: The effect of the oxygen partition ratio and plasma power on the cold gas efficiency. Case 1 to 5 represent experiments using varying O_2/fuel ratios, bed temperatures and waste compositions, published information can be found in *Materazzi et al., 2013b*. The waste composition used in Case 3 is representative of the waste composition used in this research.

5.9 GAS FILTERING AND PROCESSING

The modelling of the gas filtering and processing encompasses the ASU, ceramic hot gas filtering using sodium bicarbonate, high temperature and low temperature shift reaction, and desulphurisation using Selexol™.

5.9.1 AIR SEPARATION UNIT

Although the plant will benefit from a supply of pure oxygen from the electrolyser the ASU will have to be scaled to meet peak demand in order to cover periods where the electrolyser will not be operating. Because the proposed system is not sensitive to the inclusion of nitrogen, and because the size of the plant is relatively small oxygen purification has been modelled using PSA theory (as described in *Section 3.3.6*), shown in *Figure 5-27.* Here a compressor is used to compress the incoming air before being separated at a purity to match commercial units.

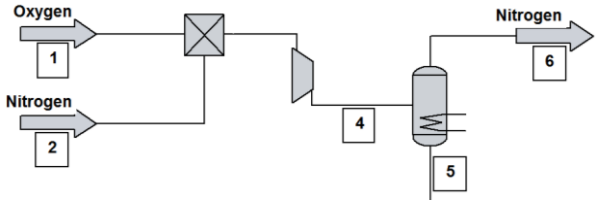

Figure 5-29: PSA modelling in ChemCad showing compression and component separation.

5.9.2 HOT GAS FILTERING

To simulate the influence of sodium bicarbonate in the ceramic gas filtering process an equilibrium reactor is used to support the following reactions:

$$NaHCO_3 + HCl \longrightarrow NaCl + H_2O + CO_2$$

$$2NaHCO_3 + SO_2 + \frac{1}{2}O_2 \longrightarrow Na_2SO_4 + 2CO_2 + H_2O$$

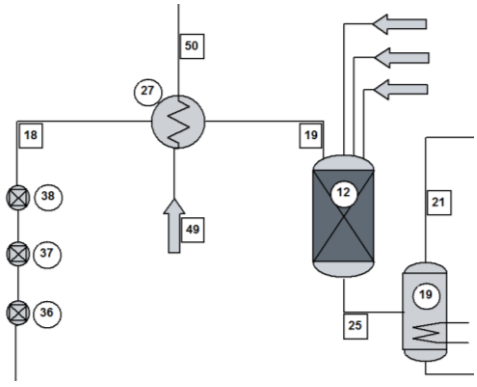

Figure 5-30: ChemCad representation of the hot gas ceramic filters.

The simulation setup shown in *Figure 5-28* shows the equilibrium reactor (unit number 12) with the syngas inlet (stream number 19) and three further inlets for the addition of the $NaHCO_3$ and O_2, as would be the case in reality. The controllers 36, 37 and 38 are used to control the molar balance of $NaHCO_3$ and O_2 according to the amount of HCl and SO_2 present in the syngas. The syngas from the gasifier must still be cooled before entering the hot gas filtration unit so a heat exchanger is used to control the inlet temperature using air, and this air will be used at the inlet to the fuel cell cathode. To simulate the removal of the solid build-up on the filters a solid separation unit is used to remove the salts formed.

5.9.3 HIGH AND LOW TEMPERATURE SHIFT REACTIONS

Simulation of the high and low temperature shift reactions is carried out using predefined shift equlibrium reactors where reactions are allowed to be carried out adiabatically (i.e. no heat loss), this option is preferred as the objective is to recover as much heat as possible to protect overall efficiencies. The purpose of using two reactors at high and low temperatures is to maximise the hydrogen yield by using various catalysts which are sensative to temperature (*Byun at al., 2011*). In *Figure 5-29* the cooling fluid used to recover and control the temperatures before and after the various reactors is shown at inlet number 55 and the fluid used is water. The first heat exhchanger (unit number 6) is used to lower the temperature of the gas, in preparation for desulphurisation after compression (unit number 29). After which the water collant is used to lower the gas temperature (unit number 15) coming from the high temperature reactor (unit number 13) in preparation for the low temperature reactor (unit number 16). Water is inlet to both shift reactors but in the case of the high temperature reactor a heat exchanger (unit number 14) is used as a steam generator for the incoming water which serves to control the reactor temperature. Conversely water is directly fed into the low temperature reactor in order to keep the reactor temperature down. Heating or cooling of the reactors is controlled by either decreasing or increasing the flow rate of water respectively.

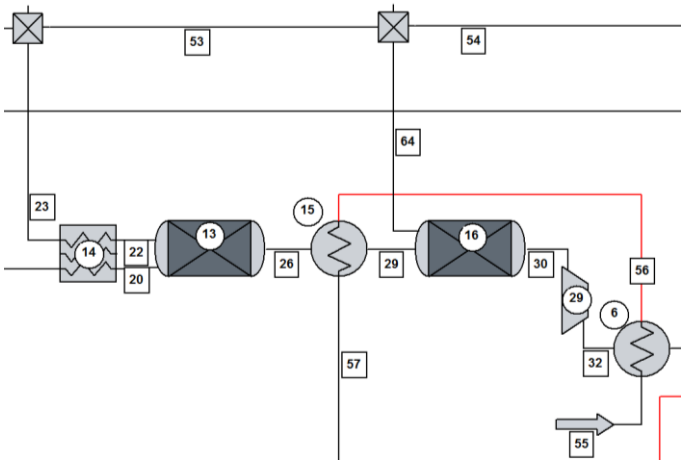

Figure 5-31: High temperature and low temperature shift reactors.

5.9.4 SELEXOL™ DESULPHURISATION

Simulation of the Selexol™ absorption (*Figure 5-30*) is carried out using a standard distillation column (unit number 7) operating at elevated pressures and near ambient temperatures. The syngas is compressed (unit number 29) and cooled (unit number 6) before entering the bottom of the adsorption tower. The filtered syngas then exits from the top of the column where the gas is flashed back to ambient temperature (unit number 10). The Selexol™, rich in H_2S, CO_2 and some COS, is pumped then flashed under pressure (unit number 34) coming from the adsorption column to a secondary column (unit number 8) for regeneration where contaminants desorb from the Selexol™. Regeneration is carried out at a lower pressure and higher temperature than adsorption.

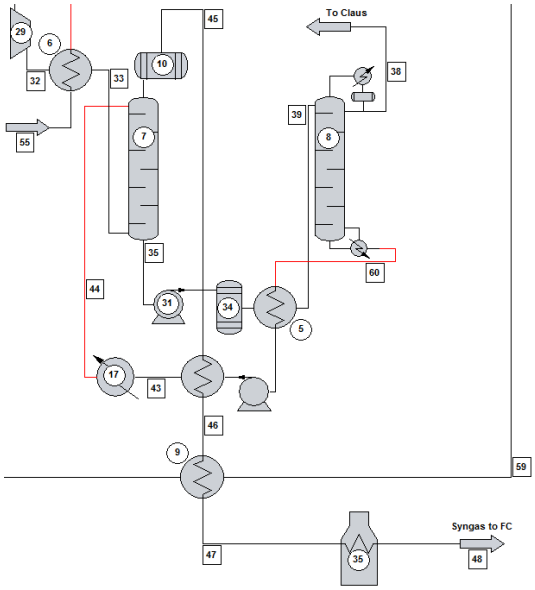

Figure 5-32: ChemCad illustration of the Selexol™ adsorption and regeneration cycle.

The recovered H_2S, CO_2 and COS is then sent to a Claus reactor to produce elemental sulphur from the contaminants.

The lean Selexol™ is then recycled from the bottom of the column where heat from the exothermic regeneration is used to increase the temperature of the rich Selexol™ stream which experiences a drop in temperature as a result of the sudden drop in pressure. The temperature of the lean Selexol™ stream is lowered further using the low temperatures of the lean syngas leaving the adsorption column. If these processes do not drop the lean Selexol™ to the required temperature a refrigeration step is used.

The syngas temperature is increased as much as possible from the heat coming from the water used to cool the earlier syngas entering the low temperature shift reactor.

Because of the large volumes of non-reactant gases entering the fuel cell the heat from electrochemical reaction may not be sufficient to maintain the required operating temperature therefore the incoming gases may need to be preheated before entering the fuel cell.

If preheating is required the detailed Simulink model will evaluate what the requirements will be for the given mass flow rates. Heating of the gases is carried out using a fuelled heater (unit number 35).

Figure 5-31 shows the complete ChemCad design showing the various process boundaries and fluid flows – full details of flow conditions at each stage are shown in Appendix A.3.

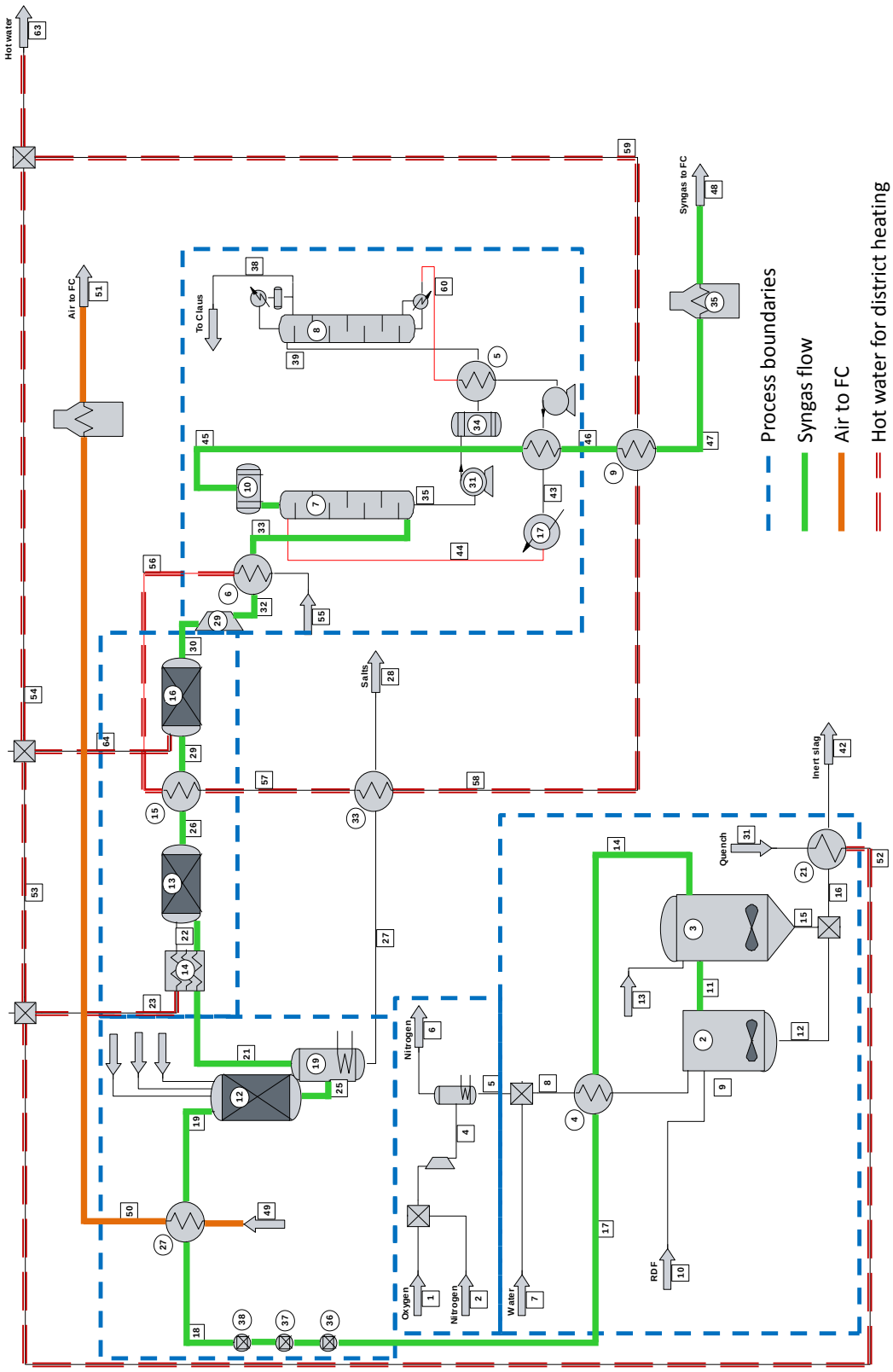

Figure 5-33: Illustration of the Chemcad user interface showing the various UnitOps. Various processes have been highlighted using boundary lines and the flows of syngas, hot air and hot water have been highlighted.

5.10 HEAT ENGINE (GT)

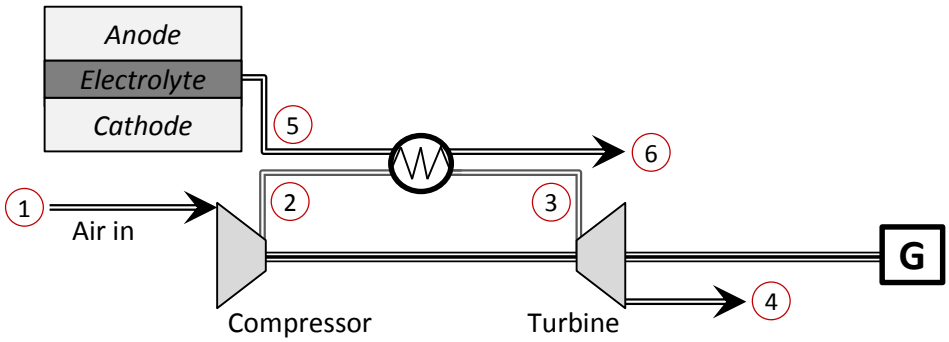

Figure 5-34: Unpressurised SOFC-GT hybrid configuration showing heat from the fuel cell transferred to the GT cycle via a heat exchanger.

Gas turbine (GT) theory and modelling is very mature so application into Simulink is straight forward. *Figure 5-32* illustrates how the GT is implemented making use of heat from the fuel cell to charge the compressed air coming from the compressor via a heat exchanger.

Isentropic expansion in gas turbines is not possible therefore to account for losses experienced in practical applications an expression for isentropic efficiency is used (practical values for isentropic efficiency has been found in literature [*Saravanamuttoo et al., 2001*]).

The thermodynamic expression for the change in temperature for a given pressure ratio and isentropic efficiency is given by:

$$T_{02} - T_{01} = \frac{T_{01}}{\eta_c}\left[\left(\frac{p_{02}}{p_{01}}\right)^{(\gamma-1)/\gamma} - 1\right]$$

Where γ is the ratio of specific heats for the fluid – in this case air.

Similarly for the turbine:

$$T_{03} - T_{04} = \eta_t T_{03}\left[1 - \left(\frac{1}{p_{03}/p_{04}}\right)^{(\gamma-1)/\gamma}\right]$$

When dealing with heat exchanges there is zero work involved and therefore reduces the Energy Equation to: $\cancel{\dot{W}} + \dot{Q} = \dot{m}c_p\Delta T$. The effectiveness for the intercooler can then be expressed by the ratio of the heat available to that which is absorbed:

$$effectiveness = \frac{\dot{m}_{FC-fluid}c_{p_{FC-fluid}}(T_{03} - T_{02})}{\dot{m}_{air}c_{p_{air}}(T_{05} - T_{02})}$$

The complexity in simulating the heat exchanger will be to accurately calculate the mass flow rate of the gases exiting the fuel cell along with their corresponding specific heats (c_p). This also means T_3 will also be affected by the mass flow of air coming from the compressor, see *Figure 5-33*.

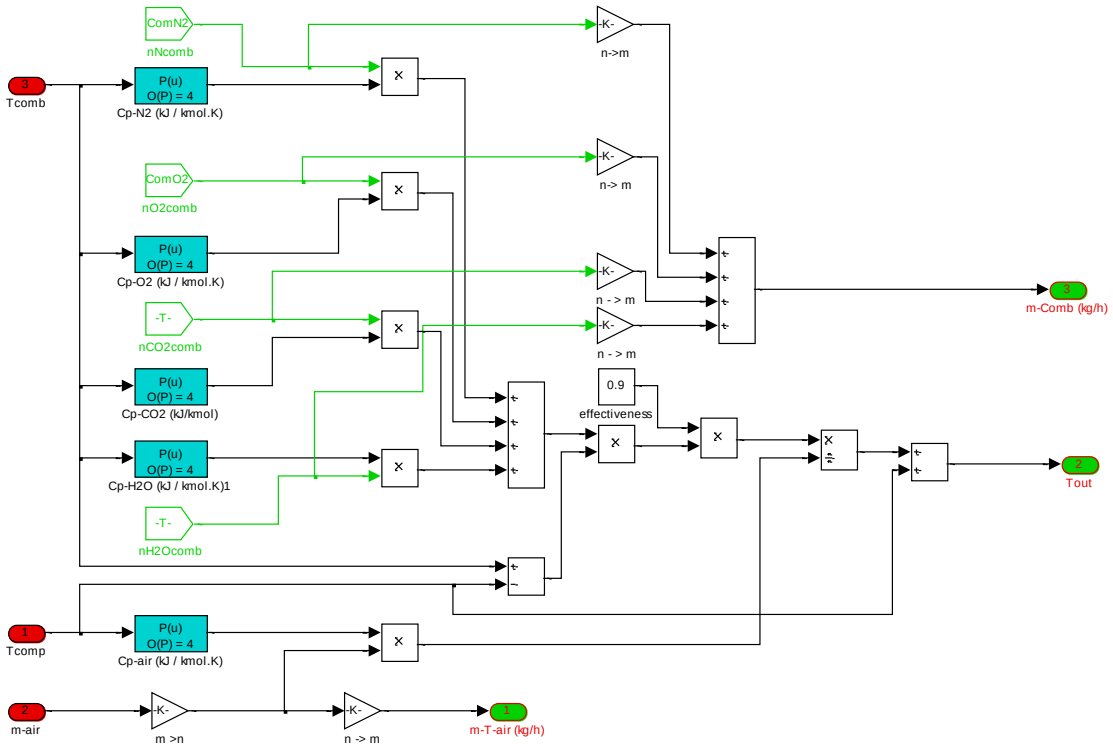

Figure 5-35: Heat exchanger between fuel cell and heat engine showing the mass flow and specific heat calculations for gases coming from the fuel cell and compressor.

The work generated by the turbine is used to drive the compressor which is located on a common shaft experiencing minimal mechanical losses. The work that is not used to drive the compressor is used to drive a synchronous generator to produce power. *Figure 5-34* shows the Brayton cycle as a function of temperature and entropy for the schematic shown in *Figure 5-32*.

The work output provided to the generator will be:

$$\therefore \dot{W}_{net} = \dot{W}_{tur} - \dot{W}_{com}$$

$$\Longrightarrow \dot{W} = \dot{m} c_p \Delta T$$

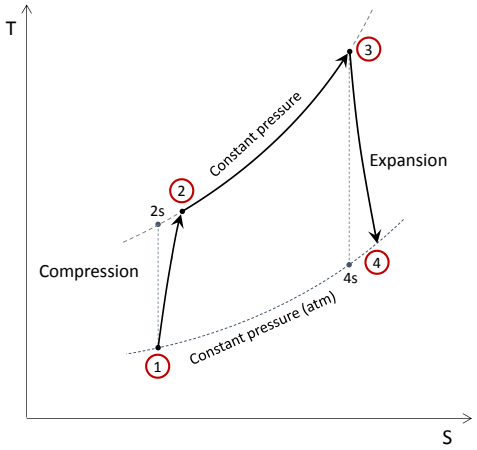

Figure 5-36: Brayton cycle expressed in terms of Temperature (T) and Entropy (S).

5.11 ELECTROLYSER

Electrolysis is the function of a fuel cell working in reverse. By passing a current between two electrodes separated by an electrolyte we are able to decompose water into its elementary components H_2 and O_2. The electrochemical reaction can be expressed as:

$$H_2O + electrical\ energy \longrightarrow H_2 + \frac{1}{2}O_2$$

According to Faraday's law the production of hydrogen is directly proportional to the amount of current provided (*Uzunoglu et al., 2009; Ural et al., 2013*):

$$\dot{n}_{H_2} = \eta_F \frac{i_e}{2F}$$

Where η_F is the Faraday efficiency which is the ratio between the theoretical and actual maximum amount of hydrogen produced by the electrolyser, and i_e is the electrolyser current (A). The Faraday efficiency (η_F) can be derived as (*Uzunoglu et al., 2009; Ural et al., 2013*):

$$\eta_F = \frac{j^2}{f_1 + j^2} f_2$$

Where j is the current density (A/m^2), and f_1 and f_2 are coefficients derived from experimental results and vary linearly with temperature as published by *Ulleberg* (*2003*).

Table 5-2: Faraday efficiency coefficients (Ulleberg, 2003).

T (°C)	40	60	80
$\boldsymbol{f_1}$	150	200	250
$\boldsymbol{f_2}$	0.990	0.985	0.980

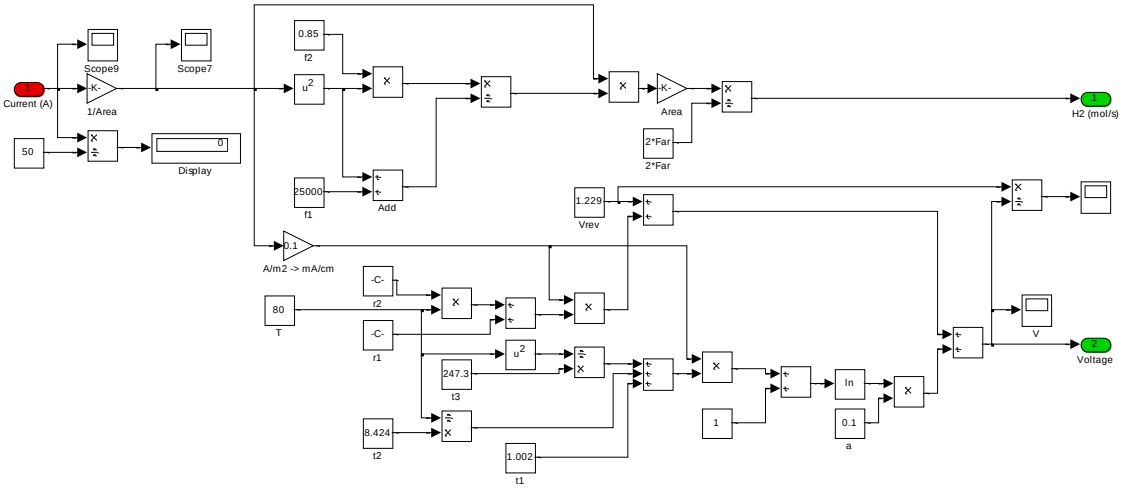

Figure 5-37: Electrolyser simulation as represented in Simulink.

5.12 HYDROGEN STORAGE

The potential to store hydrogen in solid state hydrogen storage containers using hydride materials often consisting of binary, ternary, or quaternary hydride compounds.

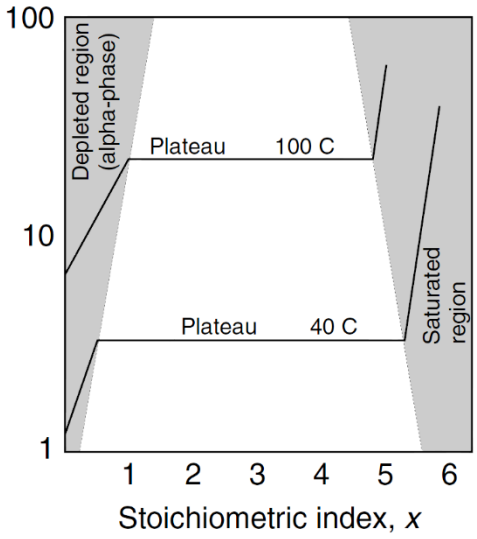

Figure 5-38: Idealised pressure-stoichiometry plot for hydrides (*Da Rosa, 2009*).

To explain the material characteristics an idealised pressure-stoichiometric plot is presented in *Figure 5-36*, where the shaded region illustrate the change from the initial metallic alloy in the alpha-phase, to the single hydride (beta-phase), with the mixed alpha-beta phase region in between. In the alpha-phase hydrogen may be stored by occupying the interstices between the material granules without altering the chemical composition of the hydride material. As the concentration increases a plateau region is reached where pressure is nearly independent of concentration. Here there is an equilibrium between the alpha and beta phases, and as the concentration increases the more of the beta phase exists until the material is completely hydrided (alpha-phase no longer exists). Different pressure plateaus correspond to different temperatures.

The reaction of hydrogen with these metallic compounds involves changes in enthalpy with absorption being exothermic and desorption endothermic. The change in free energy in a gas compressed isothermally can be expressed as:

$$\Delta G = RT \ln \frac{p}{p_0}$$

Where p_0 is the reference pressure. But

$$\Delta G = \Delta H - T\Delta S = RT \ln \frac{p}{p_0}$$

$$\therefore \ln \frac{p}{p_0} = -\frac{\Delta S}{R} + \frac{\Delta H}{RT}$$

This equation is another form of the van't Hoff equation. When considering the various materials available the materials used in current commercial applications are magnesium based (MgH_2), *Figure 5-37* shows the gravimetric and volumetric storage densities for various hydride materials (*McPhy, 2014*). MgH_2 presents advantages of high storage capacity by weight (7.6% H-wt% [*de Rango et al., 2007]*), and materials are abundant and cheap. However, disadvantages are that magnesium based materials have slow sorption kinetics and high thermodynamic stability ranges therefore requiring higher temperatures for desorption. Producing nanocrystalline particles have

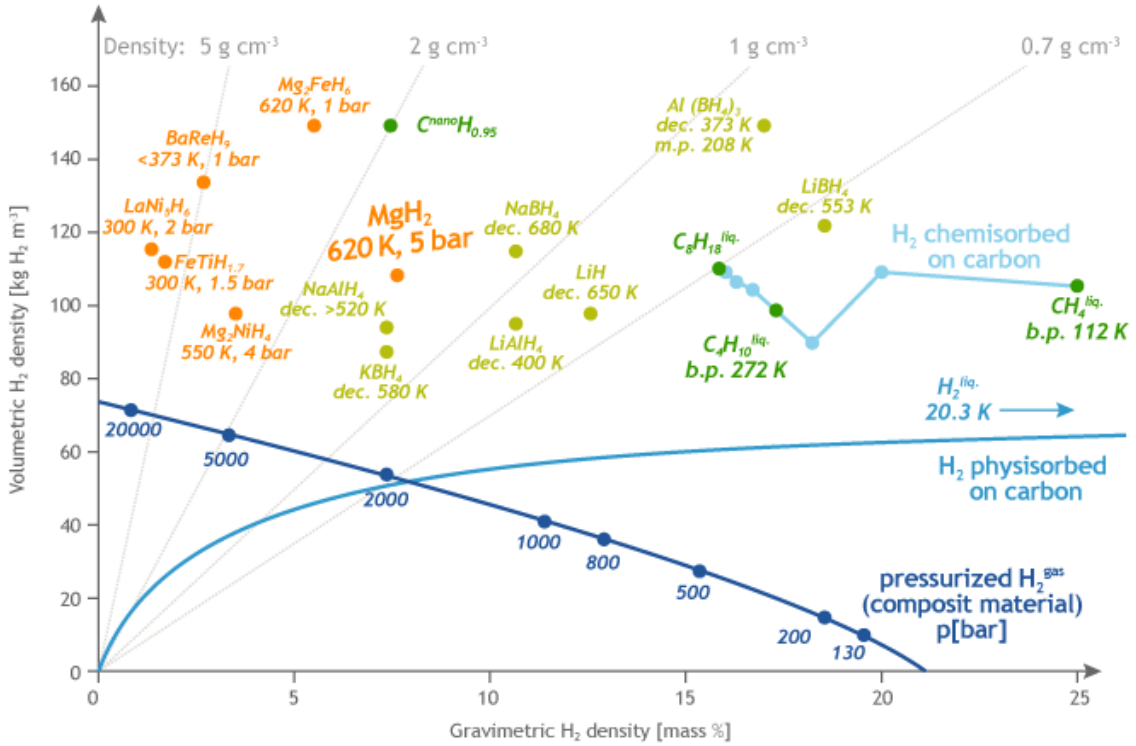

Figure 5-39: Volumetric and gravimetric comparison of various materials used for hydrogen storage (*McPhy, 2014*).

shown to improve kinetics, and the inclusion of catalyst materials has also enhanced reaction kinetics further. Values of ΔH and ΔS for magnesium hydrides is -75 kJ/mol and -135.6 kJ/K/kmol.

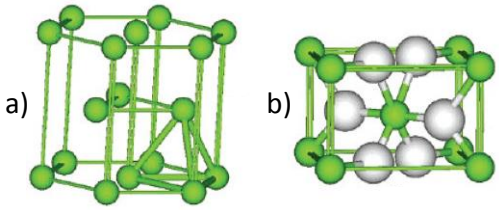

Figure 5-40: a) Mg crystal structure of alpha-phase bulk magnesium, b) MgH_2 beta-phase crystal structure.

Figure 5-38 illustrates the crystal structure of the bulk alpha-phase magnesium and the conversion to the beta-phase MgH_2 crystal structure during absorption.

The high temperatures required for desorption is not a major factor for this research as there is an abundant supply of high grade heat (>350°C) produced by both the GT and fuel cell. Therefore the application of magnesium based hydrogen storage is well suited. The storage capacity will be limited by the amount of heat available above the operating temperature for desorption, but must be large enough to cover scheduled maintenance of the gasifier. Absorption can be carried out at ambient conditions but because of the exothermic nature of the reaction energy for cooling will be required to maintain the absorption kinetics. Therefore in order to identify the amount of heat required to be removed and provided during absorption and desorption the enthalpy of formation is required. Typical values of the reaction enthalpy for MgH_2 is 37.5kJ/(kg H_2) (*Dornheim, 2011; Zhong et al., 2011*). Therefore, for simulation purposes a value of 37.5 MJ/(kg H_2) has been used to calculate the required heat transfer.

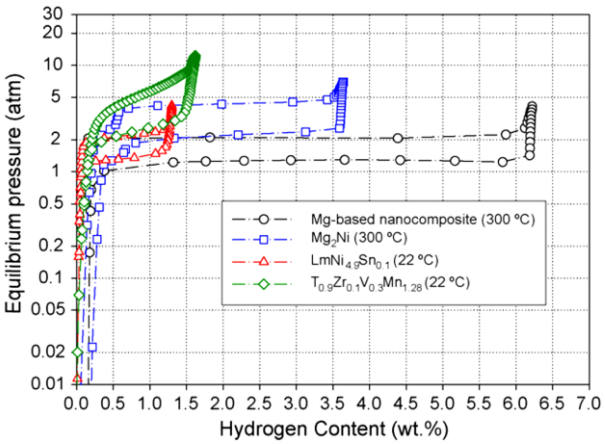

Figure 5-41: Pressure-composition isotherms of different types of metal hydrides showing Mg-based nanocomposites offer higher energy densities at lower pressures (*Dehouche et al., 2008*).

Absorption takes place at 2bar and 30°C and desorption will take place at atmospheric pressure and 320°C. *Figure 5-39* illustrates the absorption and desorption characteristics of Mg-based nanocomposite materials operating at 300°C and near atmospheric pressure. *Figure 5-39* also shows that magnesium based metal hydrides show favourable energy densities when compared to other metal hydrides (*Dehouche et al., 2008*).

From this information the heat transfer to and from the hydrogen unit can be calculated via:

$$Q = mC_p\Delta T$$

Isolating the required mass flow results in:

For cooling $$\dot{m}_{air} = \frac{\dot{m}_{H_2} 37.5\times10^3}{C_{p_{air}}(303-T_{amb})}$$

For heating $$\dot{m}_{hot} = \frac{\dot{m}_{H_2} 37.5\times10^3}{C_{p_{hot}}(T_{hot}-593)}$$

Where the subscript hot indicates fluid coming from either the turbine or the oxy combustor.

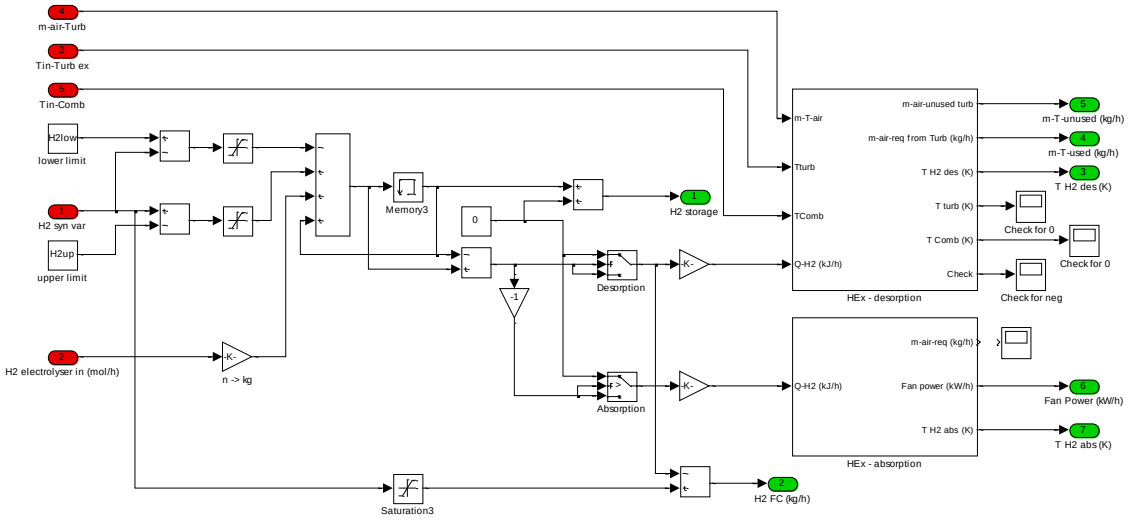

Figure 5-42: Simulink system controlling the supply and demand of hydrogen from the hydride storage.

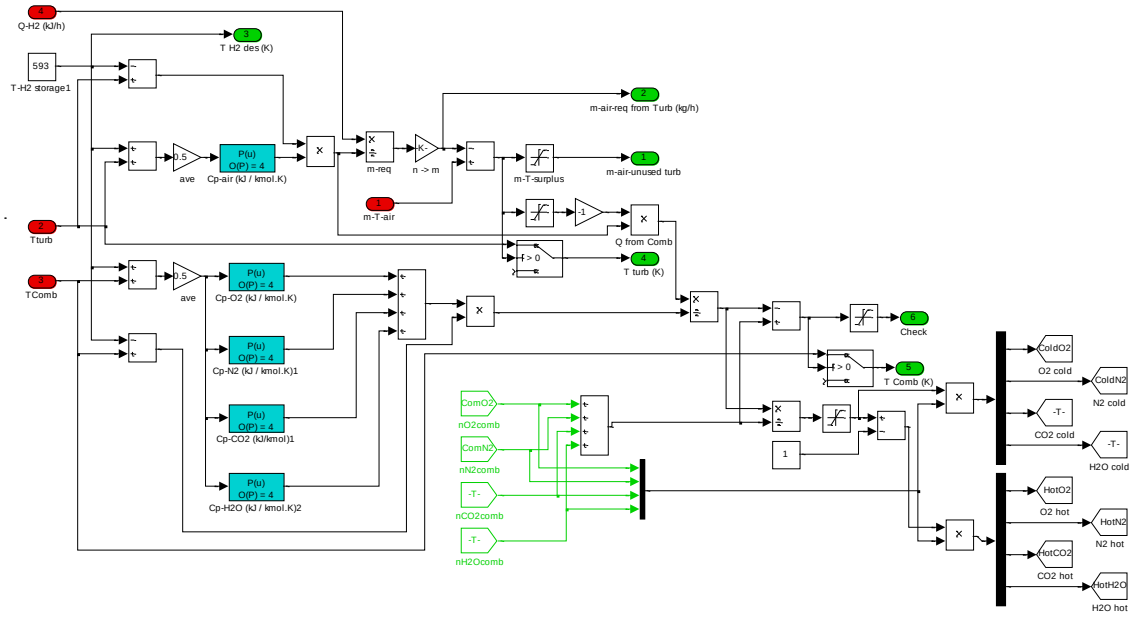

Figure 5-43: Thermal calculations required to maintain the temperature of the hydride materials during desorption.

5.13 OXY COMBUSTOR

The exhaust gas leaving the fuel cell will still contain unutilised fuel in the form of H_2 and CO. So in order to capture this remaining energy a combustion chamber is used to oxide the remaining to fuel thereby increasing the turbine inlet temperature.

In order to calculate the flame temperature it must be assumed that the process is adiabatic, in other words it is assumed that no heat is lost to the surroundings and all the heat is used to elevate the temperature of the products. Therefore from the SFEE our assumptions yield:

$$\sum H_{reactants} = \sum H_{products}$$

It must then also be assumed that the combustion is complete, therefore having a complete conversion of H_2 to H_2O, and CO to CO_2, enabling us to calculate the molar quantities after combustion. The simplest method of calculating the adiabatic flame temperature is to use a constant average C_p (*McAllister et al., 2011*)(In order to obtain satisfactory values for C_p an initial guess is required and refined until the value for C_p matches the average temperature achieved):

$$T_P \approx T_R + \frac{-Q^0_{rxn,p}}{\sum_i n_{i,P} C_{pi}}$$

where

$$-Q^0_{rxn,p} = \sum_i n_{i,R} \Delta\hat{h}^0_{i,R} - \sum_i n_{i,P} \Delta\hat{h}^0_{i,P}$$

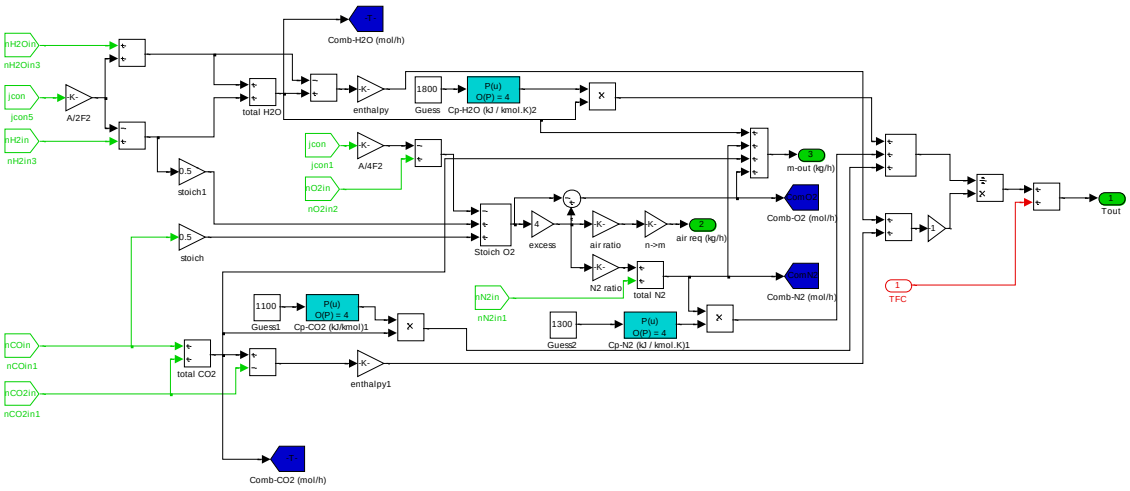

Figure 5-44: Simulink model of the combustor where the adiabatic flame temperature is calculated according to the flow of H_2 and CO in the fuel cell exhaust.

5.14 FUEL DYNAMICS

As mentioned in Section 3.1.2, the fluctuations in waste composition will have an effect on the element analysis. To take this into account the fuel inlet to Simulink model uses a Microsoft Excel file where variations have been added to the results obtained from ChemCad and was achieved using a simple "Random" excel function and based on the results published by *Chester et al. (2008)* and described in *Section 3.1.2*. For simplification variations are made every 24 hours and as seen in *Figure 5-43* the scheduled maintenance periods have been simulated using three 4 day breaks of no

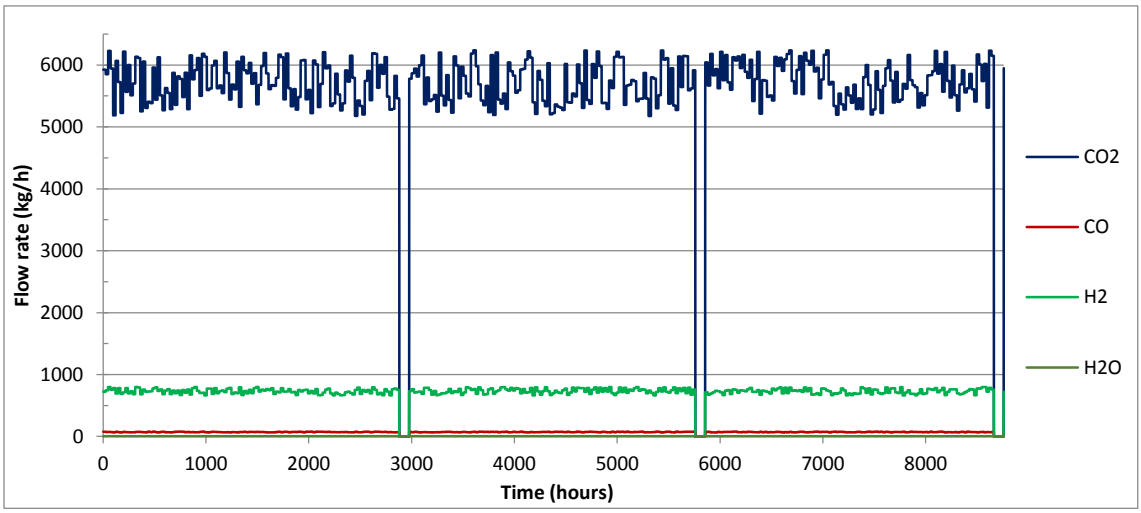

Figure 5-45: Variations in syngas composition including three 4 day maintenance periods.

fuel.

The operating strategy also calls for a reliable supply of hydrogen to the fuel cell meaning an upper and lower limit (shown in *Figure 5-44)* must be set for the amount of hydrogen sent to the fuel cell. The excess hydrogen must then be sent to the hydrogen storage and deficiencies must be buoyed by hydrogen from the hydrogen storage. This includes maintenance periods where the hydrogen storage must provide the minimum required amount of hydrogen to keep the fuel cell operational (i.e. to prevent the fuel cell from cooling).

The complete Simulink model is shown in *Figure 5-45*.

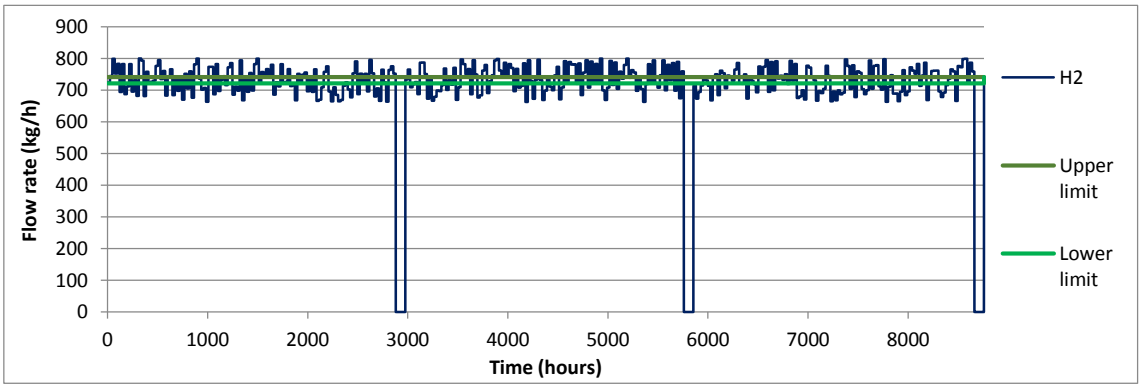

Figure 5-46: Upper and lower limit showing excesses and deficiencies coming from the variations in the syngas.

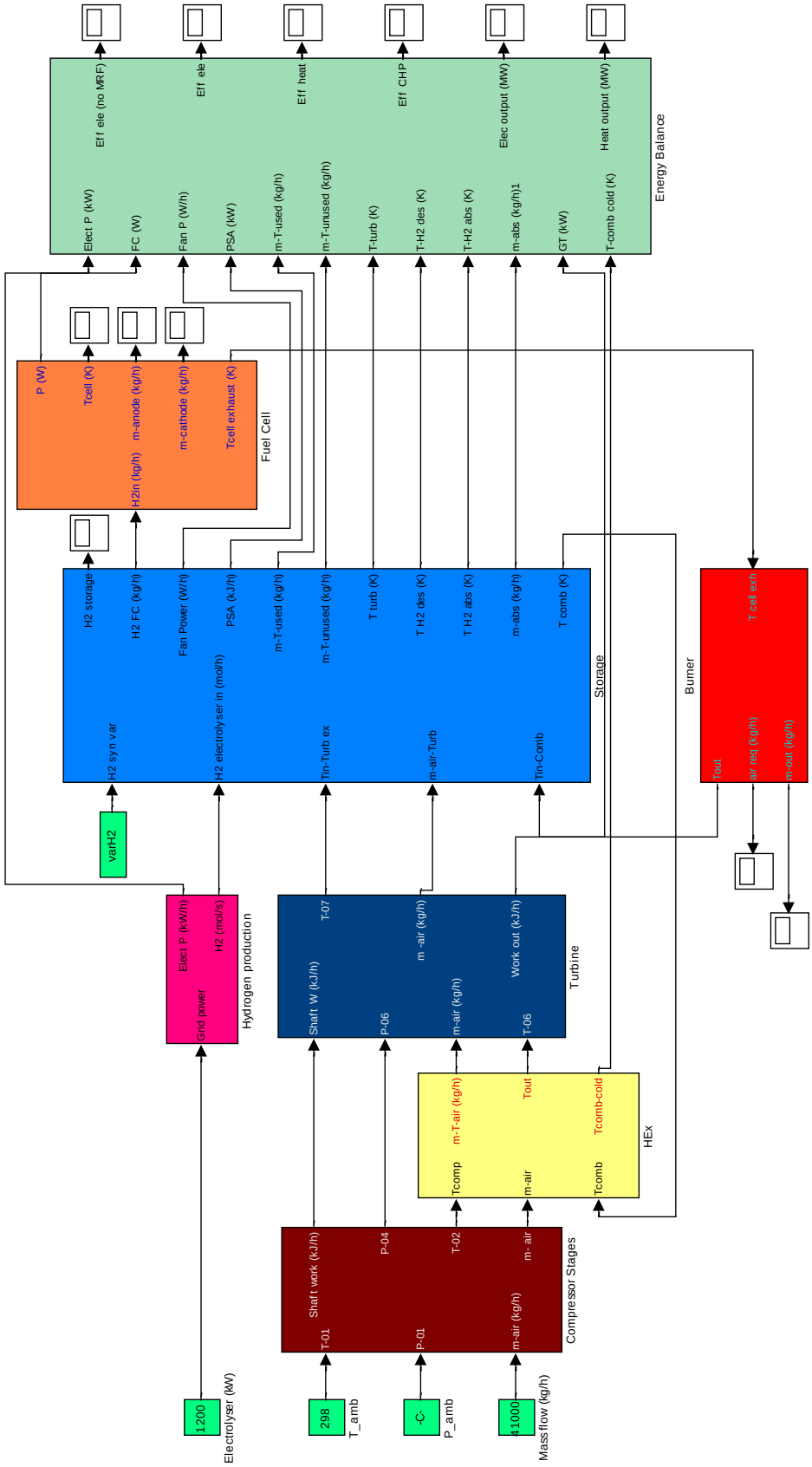

Figure 5-47: Complete Simulink model

5.15 MARKET DYNAMICS

The overall success of such innovative systems will be the economic strength justifying investment. The electricity market can be very lucrative especially with incentives such as Feed-in Tariffs (FIT), Renewable Heat Incentives (RHI) and renewable energy certificates for the organic proportion of the waste. Electricity demand is projected to grow at a steady pace: 1.5% per year in 2005-2030 (*EC, 2008*). Electricity is projected to cover almost 50% of total energy consumption of the services sector in 2030, up from 42% in 2005 and 31% in 1990.

However, it is the spot power volatility in Europe's wholesale electricity price which offers huge potential to help commercialise these energy systems. Price variation commonly ranges between 50 - 200% (*Rademaekers, 2008*). These dynamic daily variations can only be exploited by a system such as the WHHE Energy Centre which is capable of rapidly responding to the market. For instance 1 MWh is approximately equal to 115 litres of standard gasoline (31.1MJ/l) (*U.S. D.O.E., 2000*) which cost the consumer as much as £150, (assuming £1,30 per litre) compared to around £30 for hydrogen (*Guinea et al., 2010*). Therefore as an energy carrier stored for use in the transport sector, hydrogen can create a strong potential revenue stream when compared to the sale of standard gasoline even after losses from hydrogen production are accounted for, especially when considering the market for local hydrogen could be very large with 1-5million hydrogen powered vehicles predicted in the EU by 2020 (*HFP Europe, 2007*; *Pike Research, 2010*). This initiative also has the added benefit of helping to enable the EU to decouple from its dependency on imported oil which is >75% (*EC EUR, 2003*).

Table 5-3: Compensation paid to wind farms for not generating power (*REF, 2011*).

Wind Farm	*Rate Paid per MWh*	*Total paid in April 2011*	*Wind Farm Owner*
Whitelee	£180	£308,000	Scottish Power
Farr	£800	£265,000	RWE nPower
Hadyard Hill	£140	£140,000	SSE Renewables
Black Law	£180	£130,000	Scottish Power
Millennium	£300	£33,000	Falck Renewables
Beinn Tharsuin	£180	£11,500	Scottish Power

Energy storage solutions will enable further penetration of renewable technologies assist the 20-20-20 goals. These solutions can help eliminate the need for 'constraint payments' due to excess supply during which energy is lost due to inflexibility in the grid and lack of energy storage solutions. 'Constraint payments' are as much as twenty times the value of the electricity that would have otherwise been generated (*REF, 2011*), see *Table 5-3*.

The potential for district heating (and cooling) is also huge. By implementing district heating and cooling the EU could possibly save 404 million tonnes of CO_2 annually, whilst reducing the primary energy supply by 2.6% (*Euroheat & Power, 2011*).

A by-product of hydrogen produced via electrolysis is pure oxygen, this provides a further synergy benefit as oxygen is required as an input to the gasifier. Therefore having a reliable supply of oxygen will mitigate the demand placed on the air separation unit which in turn will improve the overall energy performance of the plant whilst at the same time reducing costs. Pure oxygen can also be used to burn any excess hydrogen leaving the fuel cell whilst ensuring the complete conversion of CO to CO_2 and also supplying further heat to the smart heat management system.

The social and environmental impacts of WHHE Energy Centres would be extremely positive. In terms of the potential for CO_2 reduction, if ten per cent of EU's landfill waste was diverted to WHHE Energy Centres it would offset 40million tCO_2/a (assuming the organic fraction of the waste in the EU is 40% [*Europa, 2010*]). WHHE Energy Centres will also allow the commercially driven introduction of hydrogen production into populated areas which will be critical in order to catalyse the transition to clean hydrogen fuelled vehicles predicted by the SET plan (*EC COM (2009) 519*). As local energy centres there would also be benefits in terms of job creation. Local energy security is an additional benefit and the energy storage capacity will facilitate high penetration of local renewable energy.

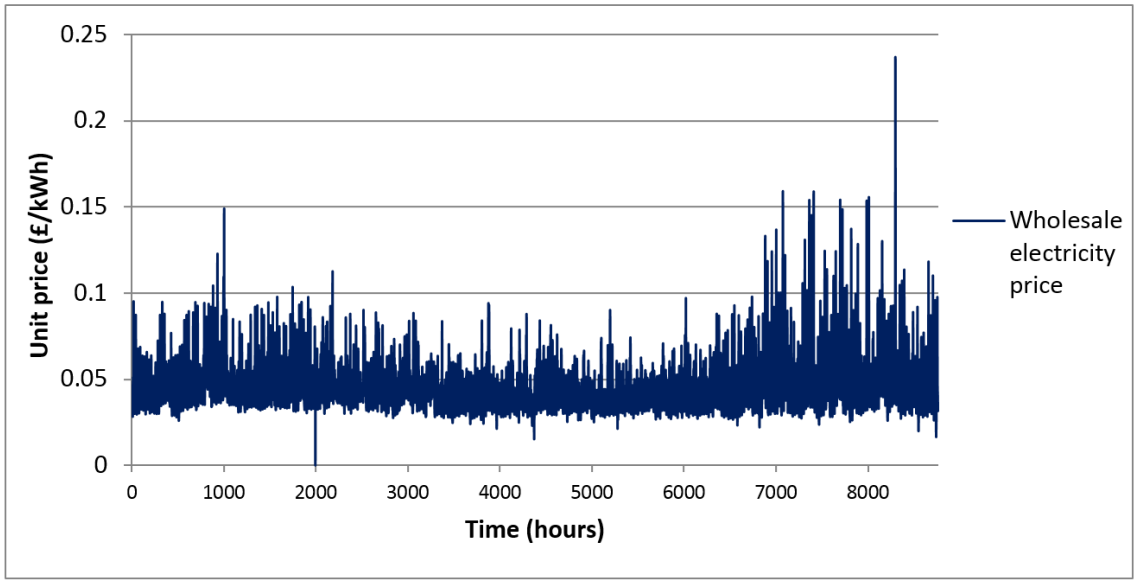

Figure 5-48: Fluctuating wholesale price of electricity in the UK in 2012 (*APX, 2012*).

This means when trading on in the wholesale electricity market in order for WHHE Energy Centres to maximise profits power should be exported when wholesale prices are profitable, and import and store power when wholesale prices are unprofitable. This requires an in depth look at the financial returns available for every kWh of electricity exported to the grid which in turn requires an understanding of the fluctuations in the price of wholesale electricity which is invariably dictated by demand, see *Figure 5-46*.

Readers Guide

Overview

1. Introduction

2. The WHHE Concept

3. Literature Digest

4. SOFCs

5. Modelling

6. Modelling Results

Gasification
- Syngas composition and flow rates

Filtering and Processing
- Composition and flow rates

Heat engine
- Annual output

Fuel cell
- I-V curves
- Thermal performance
- Annual output

Electrolysis
- Annual output

Hydrogen Storage
- Mass transfer
- Thermal performance

Overall WHHE Performance
- Annual outputs
- Sankey diagram

Economic and Environmental Performance
- Annual financial analysis
- CO_2 savings

7. Experimental Research

8. micro-CHP in the UK Market

9. Conclusions

References

Appendices

6. MODELLING RESULTS

The WHHE Energy Centre will be sized to handle 100,000 tonnes/year of MSW, of which 40% will be recycled with the remaining 60% converted to RDF. Outputs from the centre will be; electricity, hydrogen (hydrogen economy), inert slag (aggregate), NaCl (kitchen salt), Na_2SO_4 (sodium salt used as detergent filler), H_2S and COS (and finally elemental sulphur), CO_2 (available for sequestration), hot air (for the fuel cell), and hot water to be used in district heating.

The overall simulation of the WHHE Energy Centre has been carried out using ChemCad for the chemical processes prior to the hydrogen storage, and Simulink (Matlab) has been used for all remaining simulations and calculations. ChemCad produces a steady state solution for a fixed set of inputs allowing Matlab to provide more dynamic solutions using fluctuating input variables. Complete details of all models and simulation results are presented in *Appendix A.2* and *A.3*.

6.1 GASIFICATION

The ASU is assumed to operate at a reasonable 8 bar providing an oxygen purity of 95% (*Higman et al., 2003*).

In order to find the operating conditions where the amount of oxygen and steam provided to the gasifier is sufficient to maintain the required operating temperature, whilst at the same time maximising the energy conversion efficiency, a parametric study of λ (Equ. 5-8-6), SB* (Equ.5-8-8), CGE (Equ. 5-8-10), and operating temperature is required.

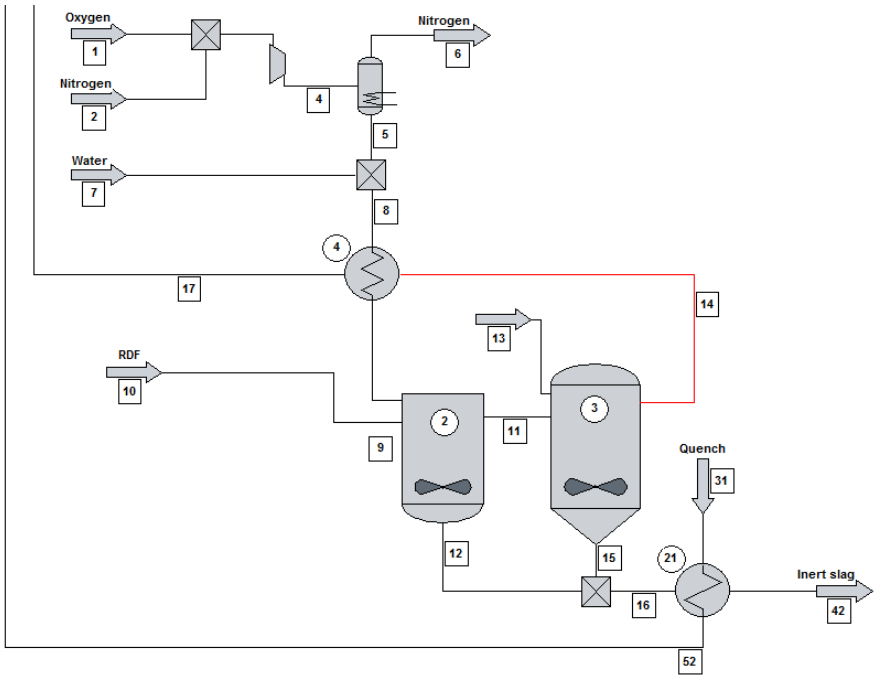

Figure 6-1: Chemcad image showing the ASU and fluidised bed/plasma gasification units along with associated UnitOp numbers and stream numbers.

Whilst at the same time it is interesting to note the change in the carbon conversion efficiency (Equ.5-8-10).

Studying *Figure 6-2*, for the given feedstock (MSW), we can see that temperature favours high values of λ and low amounts of SB* (steam). This is intuitive as oxidation reactions are exothermic and steam serves as a moderator. On the other hand *Figure 6-3* illustrates ECE is highest when both λ and SB* are low meaning the reactor is operating closer to pyrolysis.

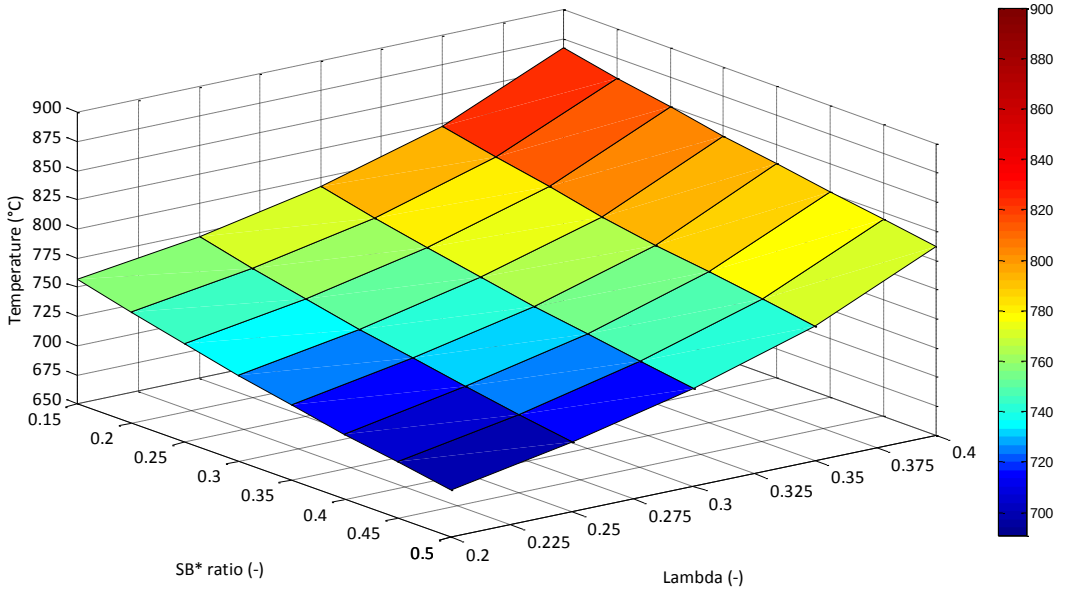

Figure 6-3: 3D surface plot showing the variation in temperature according to λ and SB*.

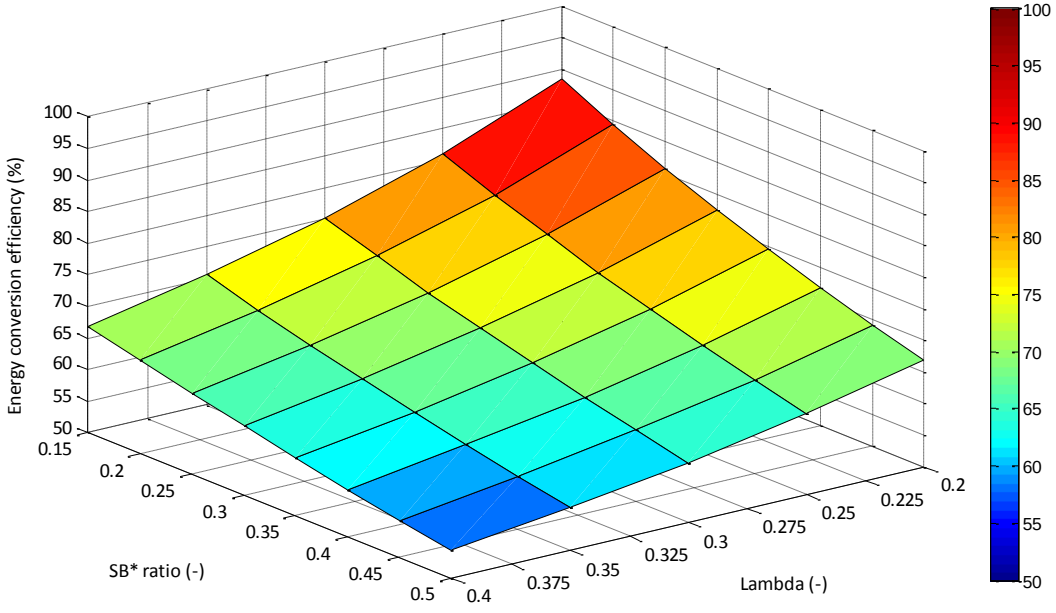

Figure 6-3: 3D surface plot showing the variation in ECE according to λ and SB*.

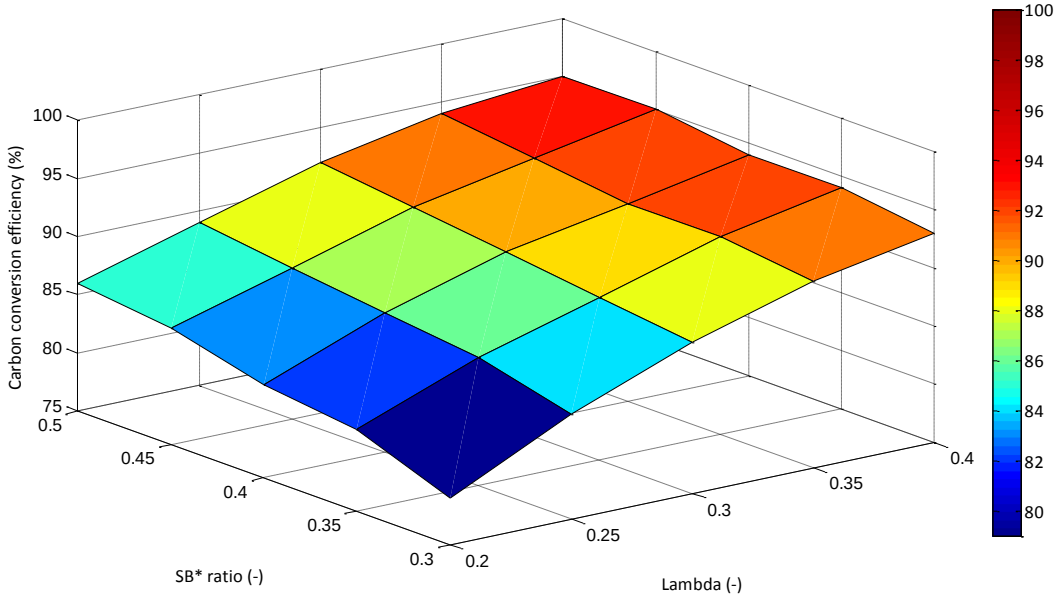

Figure 6-4: 3D surface plot showing the CCE according to λ and SB* when operating at 850°C.

Therefore the reactor should operate with the lowest values of λ and SB* whilst maintaining a suitable temperature.

As a result for the remaining simulations the values for λ and SB* will be 0.35 and 0.2 respectively producing the following syngas composition at 816°C:

Table 6-1: Molar concentration of syngas coming from gasifier at 816°C.

Stream No.	11
Name	Gasifier sy
- - Overall - -	
Molar flow kmol/h	191.8851
Heating values (60 F)	
Gross kJ/kg	1.098E+004
Net kJ/kg	9644.
Component mole %	
Hydrogen	38.833204
Methane	0.037993
Carbon Monoxide	31.395420
Carbon Dioxide	12.924461
Water	16.076790
Oxygen	0.000000
Nitrogen	0.325323
Benzene	0.000000
Toluene	0.000000
Hydrogen Chlorid	0.146969
Sulfur Dioxide	0.000000
Nitrogen Dioxide	0.000000
Hydrogen Sulfide	0.117369

The secondary plasma reactor is modelled with the same UnitOp except that the temperature of the reactor is assumed to be at a constant 1200°C consuming 0.6 kW/kg RDF (*Materazzi et al., 2013b*). Therefore at a scale of 60,000 tonnes per year the plasma torch will consume ca. 4.1MW_e. This correlates well with other information published in *E4Tech* (*2009*) that states an APP plant of the same scale operates with a parasitic load of ca. 4.5MW_e (including all other loads).

The inert slag being produced at a rate of 929kg/h is quenched in water where heat is captured through a heat exchanger and serves to supply the water demands of the high and low temperature shift reactors before being exported via the district heating network.

6.2 GAS FILTERING AND PROCESSING

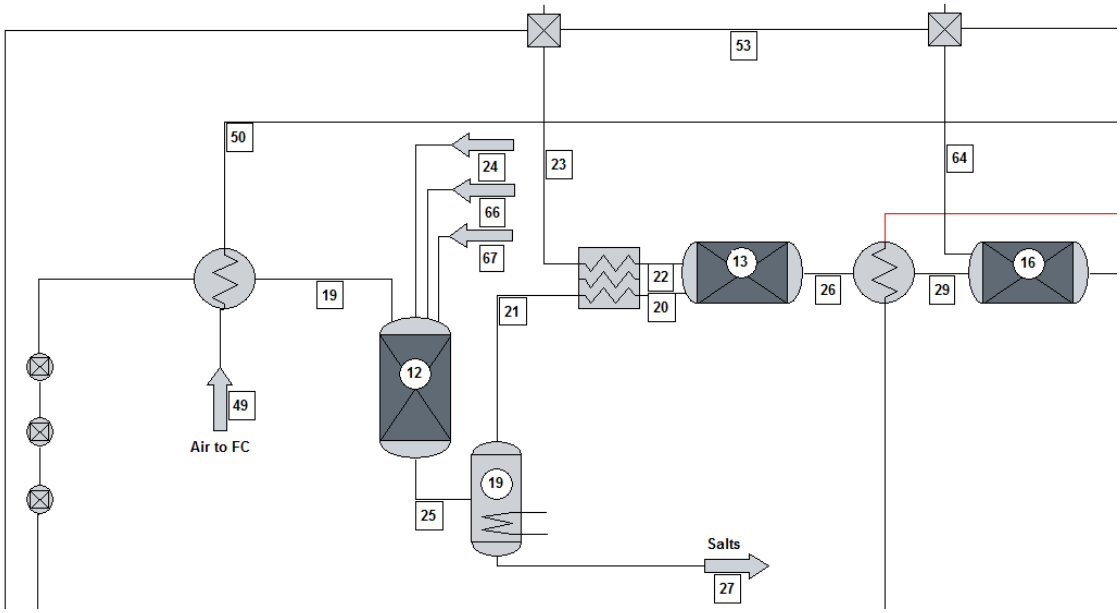

Figure 6-5: ChemCad representation of the hot gas filtration (12&19), high (13) and low (16) temperature shift reactors.

Before the syngas can be filtered through the ceramic hot gas filtration unit it must be cooled to ca. 450°C, and because of the high grade heat (>1100°C) available this is an excellent opportunity to preheat the air required by the fuel cell, as seen in *Figure 6-5.* At the ceramic filter the gas is injected with sodium bicarbonate which converts the HCl and SO_2 to valuable NaCl (table salt) and Na_2SO_4 (detergent filler material). The solid materials are removed from the gas where the salts can be extracted (stream 27) and sold. The expense and operation of the ceramic filter is assumed to be insignifanct as the the process is largely passive with most of the cost being offset from the sale of the salt products (which also has not been accounted for).

From here the gas is moved to the high temperature shift reactor where the temperature of the incoming gas is controlled by a heat exchanger to ensure the gas is not above 450°C and serves to heat any water required by the reactor. From here the gas is further cooled, using water, to a temperature of 140°C. These shift reactions are exothermic so it is important to use the additional water added to the reactor to maintain the temperature within the designed limits.

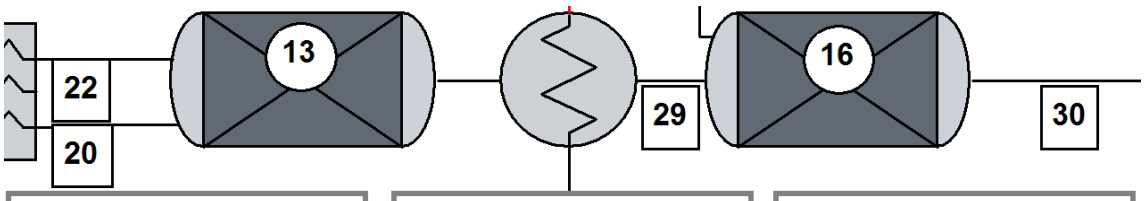

Stream No.	20
Name	
- - Overall - -	
Temp C	450.0001
Flow rates in kg/h	
Hydrogen	363.2477
Carbon Monoxide	5269.5161
Carbon Dioxide	1979.1642

Stream No.	29
Name	
- - Overall - -	
Temp C	140.0000
Flow rates in kg/h	
Hydrogen	473.4135
Carbon Monoxide	3738.7378
Carbon Dioxide	4384.3623

Stream No.	30
Name	
- - Overall - -	
Temp C	163.2917
Flow rates in kg/h	
Hydrogen	737.2159
Carbon Monoxide	73.1423
Carbon Dioxide	10143.8359

Figure 6-6: Stream compositions flowing entering and exiting the shift reactors showing CO conversion and H_2 production ratios.

From the flow compositions shown in *Figure 6-6* the change of CO, CO_2 and H_2 illustrate a 30% increase in H_2 as a result of the high temperature shift reactor, and a 55% increase from the low temperature shift giving a total increase of 103%.

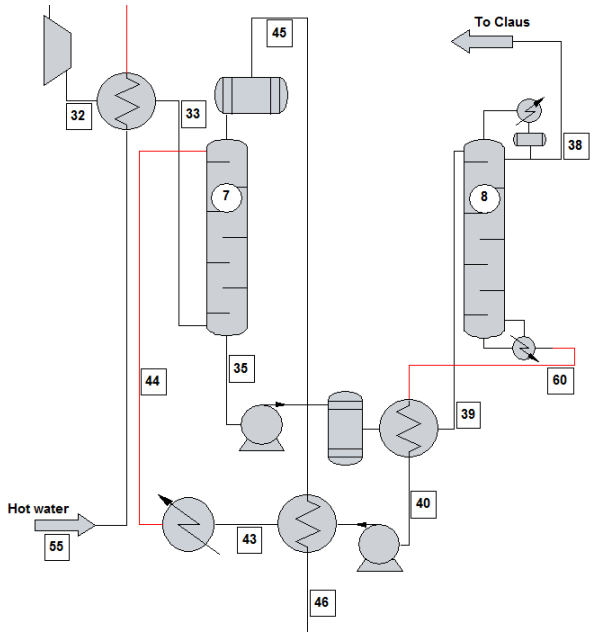

Figure 6-7: Illustration of the desulphurisation circuit showing distillation columns for Selexol™ adsorption and regeneration.

From the low temperature shift the gas is then compressed and cooled in preparation for desulphurisation, seen in *Figure 6-7*. The Selexol™ adsorbent then extracts H_2S, COS, CO_2, N_2 and a small amount of H_2 at high pressure (40bar) and near ambient temperature in a 20 stage distillation column. The rich Selexol™ is then pumped to a secondary 6 stage distillation column that includes a condenser and reboiler. Before entering the secondary column the pressure of the Selexol™ is dropped to 6.9bar and heated to 125°C. The column itself operates at ambient pressure and the distillate temperature for condensing is 100°C and the reboiler recycles the now lean Selexol™ from the bottom of the column at 150°C. Before being recycled back to the first column the Selexol™ must be cooled to -6°C. Much of this is done by heating the purified syngas as it leaves the first column as the gas experiences a drop in temperature when expanding from 40bar to ambient pressure. The remaining cooling is carried out through a refrigeration cycle which will add to the parasitic load.

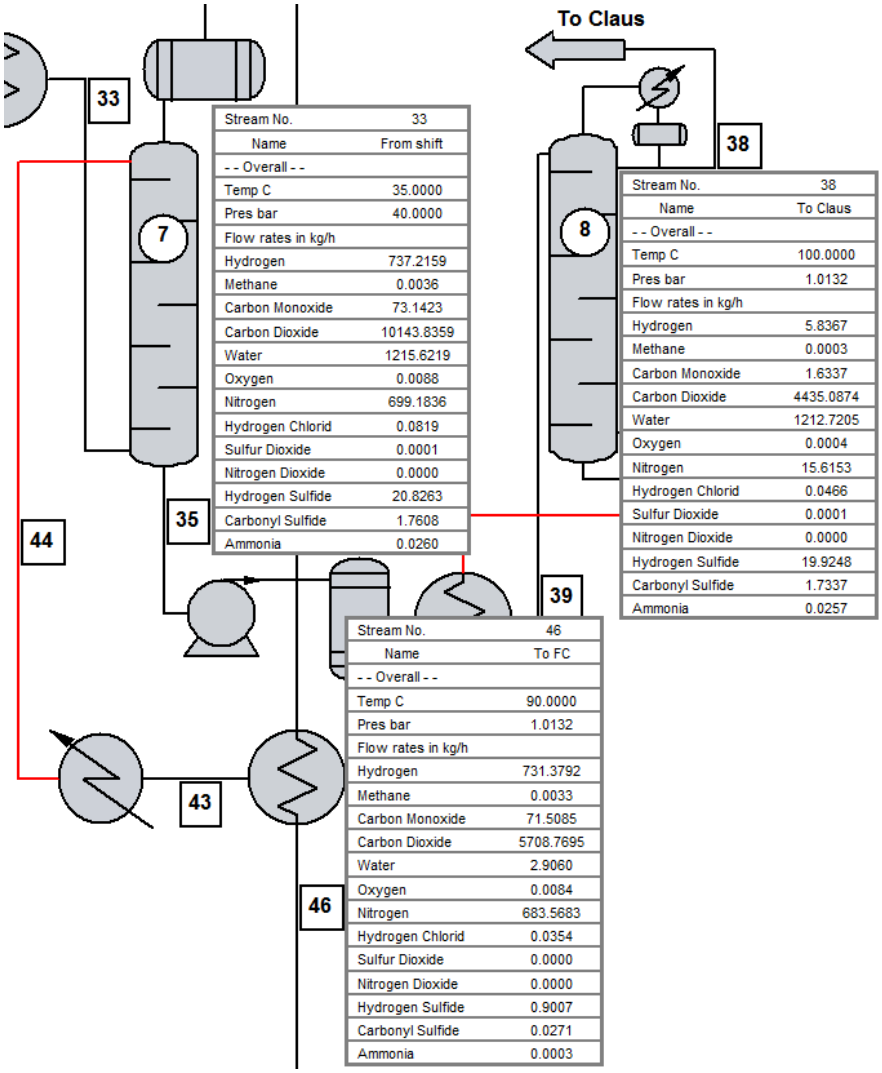

Figure 6-8: Stream compositions of gases entering and exiting the desulphurisation cycle illustrating purification efficiency.

Figure 6-8 shows the level of H_2S prior to adsorption at 20.826kg/h and 0.901kg/h after purification; this is a 97% reduction in H_2S. Similarly, COS reduces from 1.761 to 0.027kg/h a 99% reduction. The amount of CO_2 is also substantially reduced by 50.9% allowing for simple sequestration if required.

Table 6-2 provides a complete breakdown of contaminants and the level of purification achieved.

Table 6-2: Composition of the syngas entering and exiting the desulphurisation cycle showing the reduction in contaminants.

Compound	Stream 33 kg/h	Stream 46 kg/h	Reduction (%)
H_2	737.216	731.379	0.8%
CH_4	0.0036	0.0033	8.3%
CO	73.142	71.509	2.2%
CO_2	10143.836	5708.770	43.7%
H_2O	1215.622	2.906	99.8%
O_2	0.0088	0.0084	4.5%
N_2	699.184	683.568	2.2%
HCl	0.0819	0.0354	56.8%
H_2S	20.826	0.901	95.7%
COS	1.761	0.0271	98.5%
NH_3	0.026	0.000	100.0%

The syngas and air destined for the fuel cell may require heating prior to entry as the exothermic reaction in the fuel cell may not be sufficient to maintain the required operating temperature. To do this auxiliary heaters have been used in ChemCad and results from the Matlab simulation will be used to determine the temperatures required.

Table 6-3: ChemCad simulation results.

MSW feed-rate	6,849	kg/h
MSW LHV	15.7	MJ/kg
Lambda	0.35	(-)
SB*	0.2	(-)
Gasifier temperature	814	°C
ECE	61.4	%
CCE	76.9	%
Plasma temperature	1,200	°C
Hot gas filtering temperature	345	°C
Sodium bicarbonate flow rate	71.44	kg/h
Sodium chloride out flow rate	45.052	kg/h
Sodium sulfate out flow rate	0.155	kg/h
High temperature shift temperature	482	°C
Low temperature shift temperature	140	°C
Desulphurisation pressure	40	Bar
Desulphurisation temperature	14.7	°C
Regeneration pressure	1	Bar
Regeneration temperature	150	°C
CO_2 out	4,435.09	kg/h
H_2S out	19.92	kg/h
COS out	1.73	kg/h
H_2O out	1,212.72	kg/h
Heat recovery		
Water flow rate (@86°C)	7,320	kg/h
Air flow rate	24,000	kg/h
Purified Syngas Composition		
Total flow rate	6,976	kg/h
Gas composition	wt %	
H_2	10.16%	
CH_4	0.00%	
CO	0.99%	
CO_2	79.30%	
H_2O	0.04%	
O_2	0.00%	
N_2	9.50%	
C_6H_6	0.00%	
HCl	0.00%	
SO_2	0.00%	
NO_2	0.00%	
H_2S	0.01%	
NH_3	0.00%	

6.3 SOLID OXIDE FUEL CELL

Using the mathematical descriptors defined in *Chapter 4* the following j-V and j-P curves have been generated to describe the overall performance of the fuel cell (*Figure 6-9*), along with voltage and power outputs according to the annual fluctuations in the fuel supply (H_2, CO_2, CO and H_2O) and a hydrogen flow rate between 702 - 707kg/h (*Figure 6-10 and 6-11).* Due to the effort made to increase the hydrogen yield through shifting any CO to CO_2 and because of the neglible amount of CO available the potential for CO to fuel the SOFC is ignored (although the affect on partial pressures is accounted for):

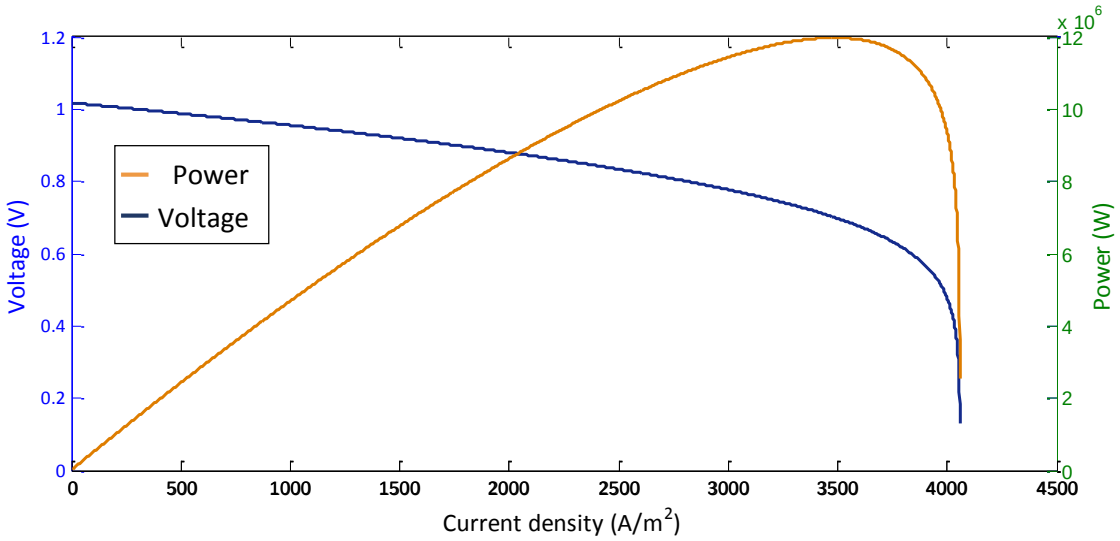

Figure 6-9: Simulink simulation of the solid oxide fuel cell showing voltage and power curves as a function of current density.

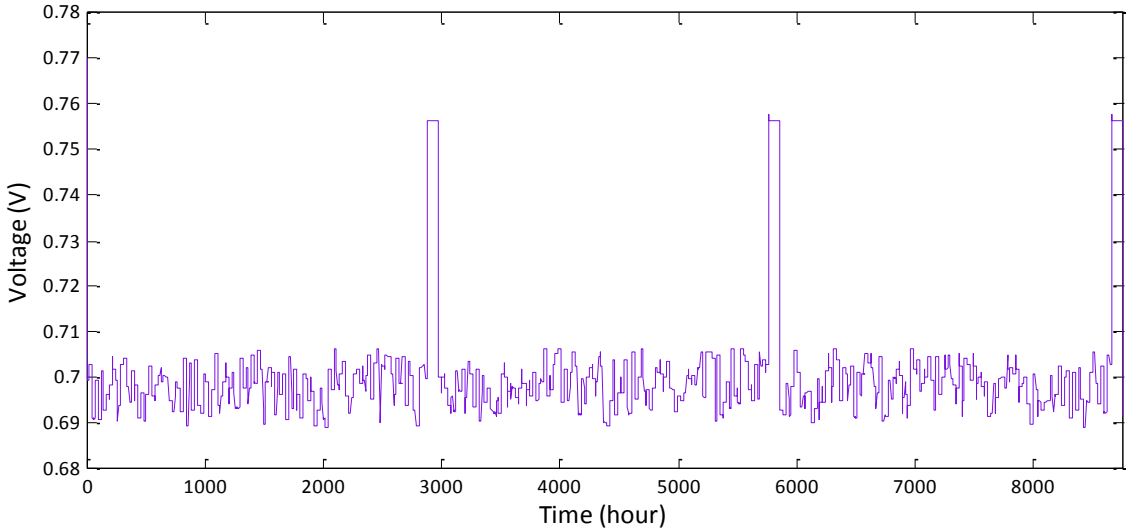

Figure 6-10: Variation in voltage according to variations in fuel supply. Increased voltage is seen during the maintenance periods as the supply of hydrogen is undiluted thereby providing higher partial pressures.

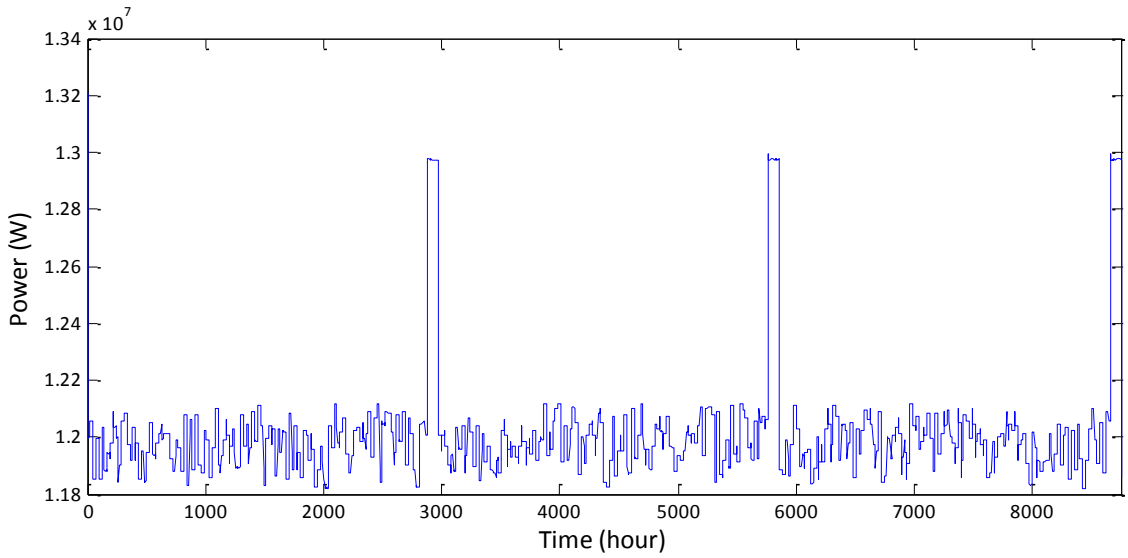

Figure 6-11: The annual power fluctuation is directly related to the voltage output therefore both voltage and power show the same trend in variation.

The variation in electrical efficiency fluctuates according the flow of hydrogen to the fuel cell and benefits when the fuel cell is supplied with pure hydrogen from the hydrogen storage over the maintenance periods and is illustrated by the three spikes above 55%.

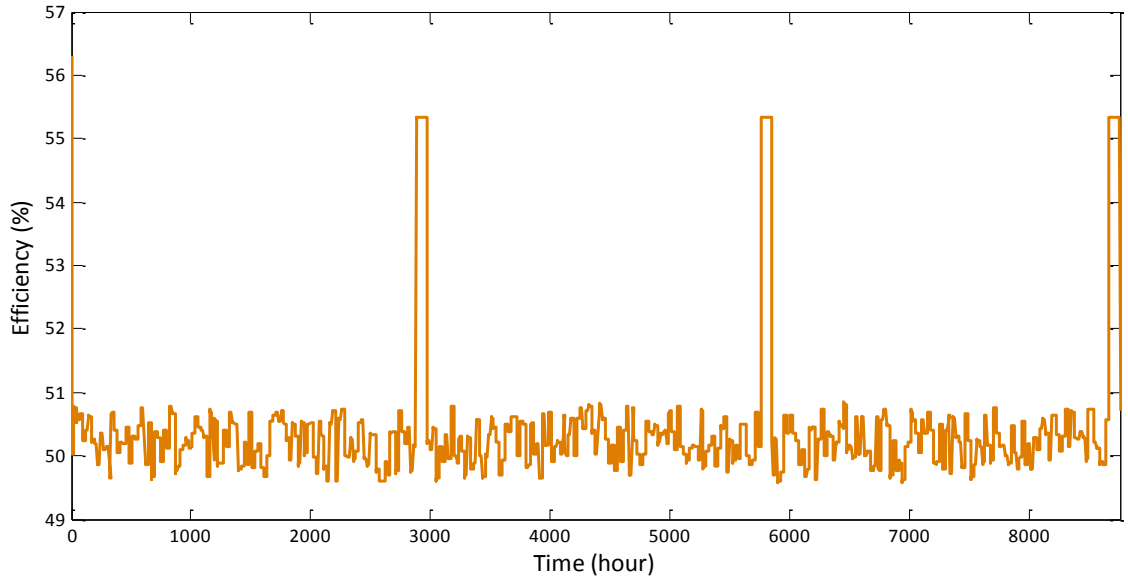

Figure 6-12: Annual fluctuation in electrical efficiency of the fuel cell.

The simulation has been scaled and calibrated using the following variables shown in *Table 6-4*:

Table 6-4: SOFC characteristics and variables. (Where references have not been provided values have been calculated or assumed)

Cell Geometry			
Layer thicknesses			
Anode	0.0005	m	
Electrolyte	0.00003	m	
Cathode	0.00003	m	
Planar dimensions			
Channel length	0.1	m	
Channel width	0.005	m	
Channel height	0.005	m	
Channels per cell	20		
Total no. of cells	1,764,177,570		
Nusselt geometry ratio	1		
Hydraulic diameter (*Hd*)	0.005		
Material properties			
Densities			
Anode	6,200	kg/m^3	[*Wang et al., 2009]*
Electrolyte	5,560	kg/m^3	[*Wang et al., 2009]*
Cathode	6,000	kg/m^3	[*Wang et al., 2009]*
Interconnects	7,700	kg/m^3	[*Wang et al., 2009]*
Specific heats (C_p)			
Anode	650	J/kg.K	[*Wang et al., 2009]*
Electrolyte	300	J/kg.K	[*Wang et al., 2009]*
Cathode	900	J/kg.K	[*Wang et al., 2009]*
Interconnects	800	J/kg.K	[*Wang et al., 2009]*
Electrolyte conductivity (σ)	0.65	1/ohm.cm	
Diffusion			
Porosity – anode (ξ)	0.35		
Porosity – cathode (ξ)	0.35		
Tortuosity – anode (τ)	4.5		[*Wang et al., 2009]*
Tortuosity – cathode (τ)	4.5		[*Wang et al., 2009]*
Pore radius – anode (r_e)	9.60E-07	m	
Pore radius – cathode (r_e)	9.60E-07	m	
Exchange current density			
Pre-exponential factor – anode (γ)	5.50E+08	A/m^2	[*Costamagna et al., 2003]*
Pre-exponential factor – cathode (γ)	7.00E+08		[*Costamagna et al., 2003]*
Activation energy – anode (E_{act})	100,000	J/mol	[*Costamagna et al., 2003]*
Activation energy – cathode (E_{act})	120,000	J/mol	[*Costamagna et al., 2003]*
Electron transfer coefficient – anode (α)	0.5		[Larminie et al., 2003]
Electron transfer coefficient – cathode (α)	0.5		[Larminie et al., 2003]

To understand the thermal performance of the fuel cell the operating temperature has been simulated using the thermodynamic energy balance taking into account the heat provided by the chemical reaction and heat lost through convection, radiation and mass transport. The results shown if *Figure 6-13* illustrate the equilibrium achieved for various inlet temperatures and also the effect of recovering heat from the exhaust gas to preheat the incoming air and fuel. This shows that supplying air and fuel at ambient temperature, and at these given flow rates and compositions, the fuel cell is unable to reach the required operating temperature. So the gases coming from the gasification plant will have to be heated to a temperature of 760K before being passed on to the fuel cell. This heat can be recovered from the syngas during cooling prior to filtration, from heat captured at systems requiring cooling or via an auxiliary burner. In this simulation the air stream is heated from the syngas prior to filtration and the fuel is heated from systems requiring water cooling (i.e. WGS).

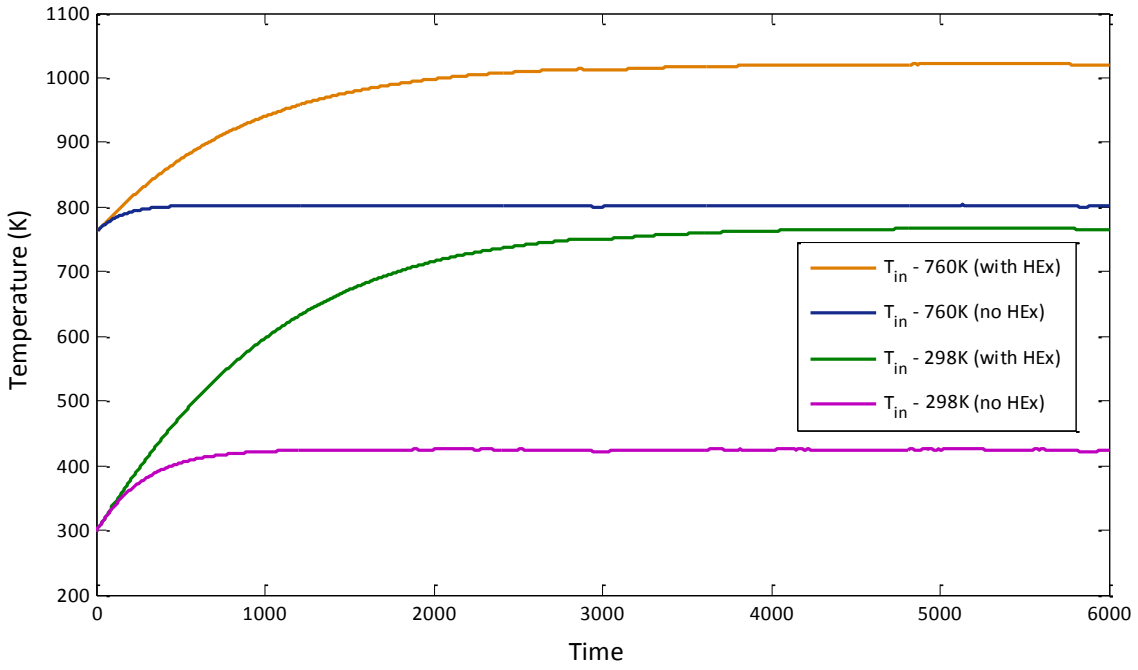

Figure 6-13: Simulation of the fuel cell's operating temperature as a function of inlet temperature and heat recovery option.

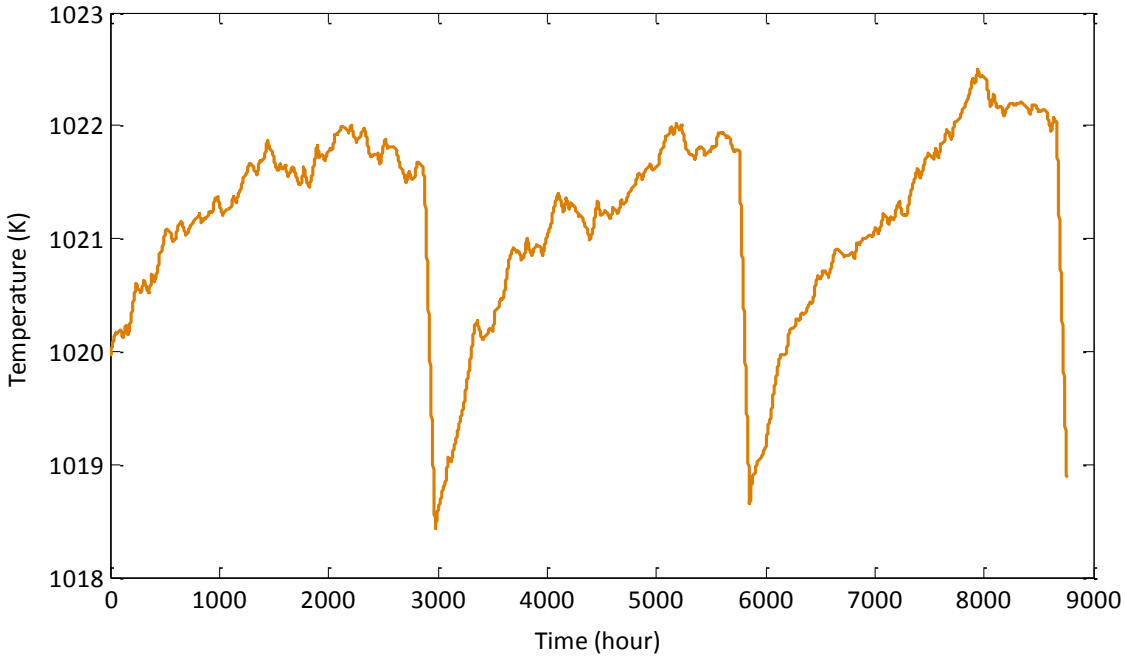

Figure 6-14: Cell temperature as a function of the annual syngas fluctuations whilst using an inlet temperature of 760°C.

Figure 6-14 shows that by applying an inlet temperature of 760K and by using the annual variation of the syngas composition the fuel cell will continue to operate close to its designated 850°C. *Figure 6-14* also shows sharp drops in temperature as the fuel composition changes during the scheduled maintenance periods (syngas is replaced with pure hydrogen). Further investigation shows these drops are mainly caused by the overall thermal conductivity (*k*) that increases over these periods causing greater heat transfer and hence greater heat removal.

6.4 HYDROGEN PRODUCTION AND STORAGE

There are important aspects to consider when implementing hydrogen storage especially when scaled to cover the maintenance period of such a large system. Hydrogen is collected from excess coming from fluctuations in the syngas and from an electrolyser whose operation is controlled by the feasibility of the wholesale electricity price. This means the accumulation of hydrogen is determined by; the upper and lower hydrogen tolerance limits, feasibility threshold, and size of electrolyser. *Figure 6-15* shows the upper and lower hydrogen limits against the incoming hydrogen variation, and *Figure 6-16* shows the accumulation of hydrogen when relying purely on hydrogen from the syngas. *Figure 6-17* shows the hourly flow rate of hydrogen coming from the electrolyser sized at 1.2MW. In this scenario it is important to keep the feasibility ratio as low as possible as the hydrogen produced by the electrolyser includes losses from the fuel cell, electrolyser and eventually the hydrogen storage unit when considering the initial hydrogen coming from the syngas. This will become less of an issue as more renewable energy comes on line and the spot price of electricity comes down during periods where grid flexibility is required. This could be made easier by directly connecting these renewables to WHHE Energy Centres.

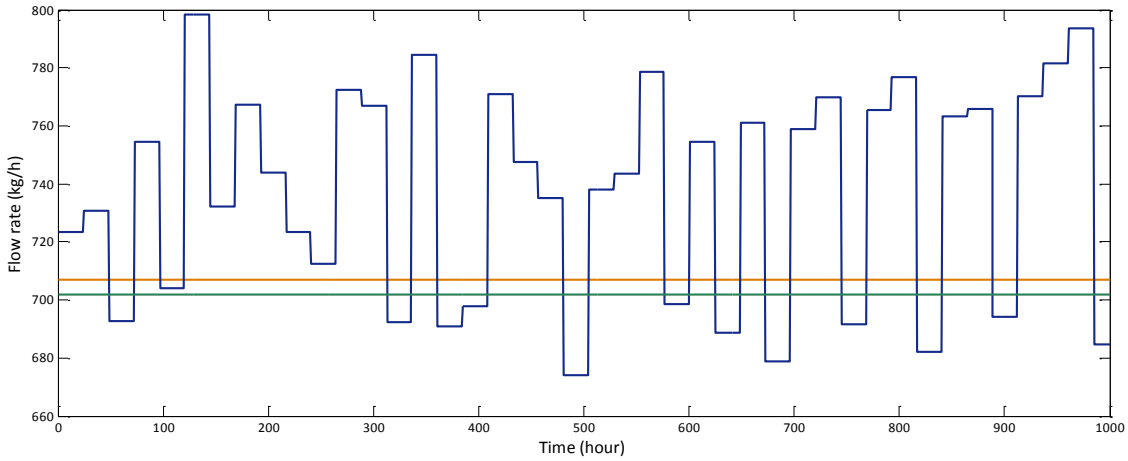

Figure 6-15: The upper and lower hydrogen limits shown against the variation in hydrogen for the first 1000 hours.

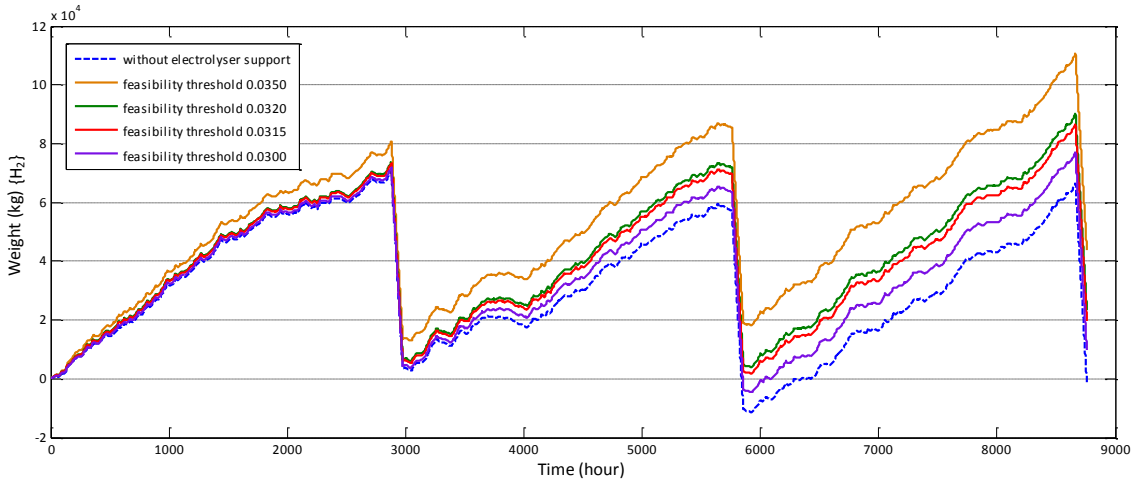

Figure 6-16: Meeting annual hydrogen demand by changes to feasibility threshold showing for the given upper and lower hydrogen limits a feasibility threshold of 0.0315 £/kWh.

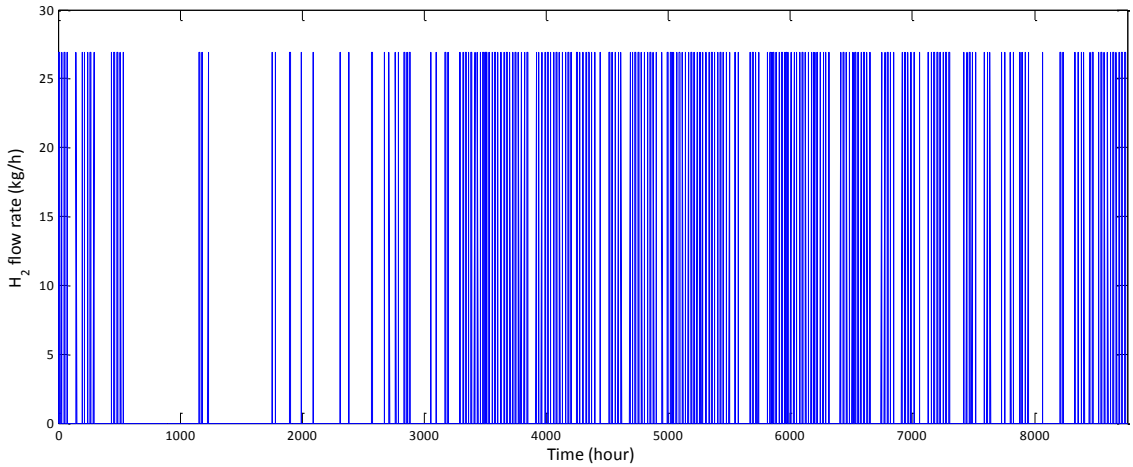

Figure 6-17: Hydrogen flow rate from the electrolyser when feasibility threshold is at 0.0315 £/kWh.

6.5 HEAT ENGINE (GAS TURBINE)

The gas turbine operates with an assumed pressure of 10 bar (*Bove et al. 2008*) with heat coming from the fuel cell and oxy combustor (*Bove et al., 2008*). The compressor and expander have simulated with isentropic efficiencies of 85% and 86% respectively (*Saravanamuttoo et al., 2001*). During the scheduled maintenance periods the priority is to ensure the fuel cell remains operational meaning the heat required by the hydrogen storage becomes of greater importance. This means during these periods heat from the burner could be diverted to the hydrogen storage before entering the GT heat exchanger thereby affecting performance as shown in *Figure 6-18*.

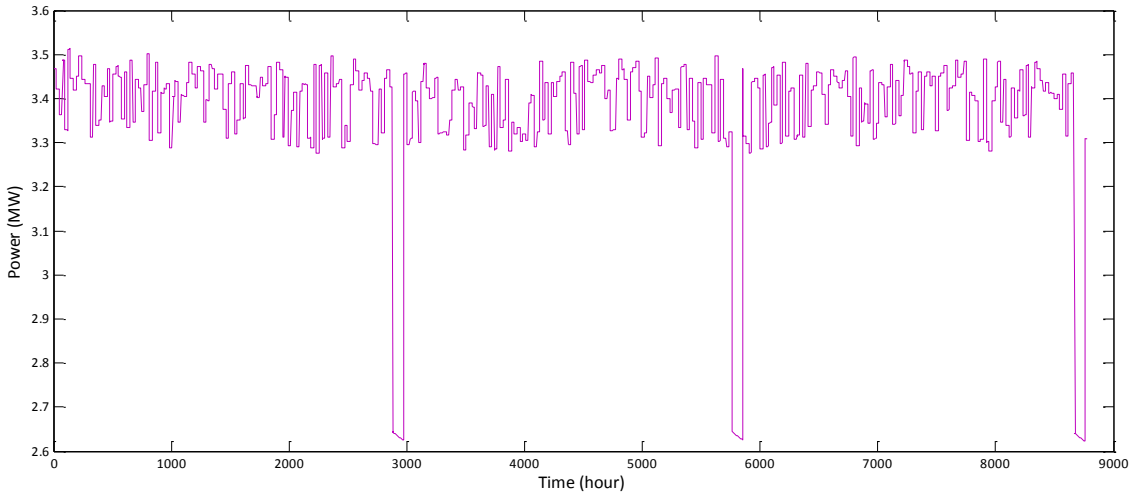

Figure 6-18: Power fluctuations according to changes in fuel composition to the burner and heat used to drive the hydrogen storage during scheduled maintenance.

Heat from the turbine is used to supply the heat demand of the hydrogen storage and only when this heat is insufficient will heat from the combustor be used as identified in *Figure 6-19*.

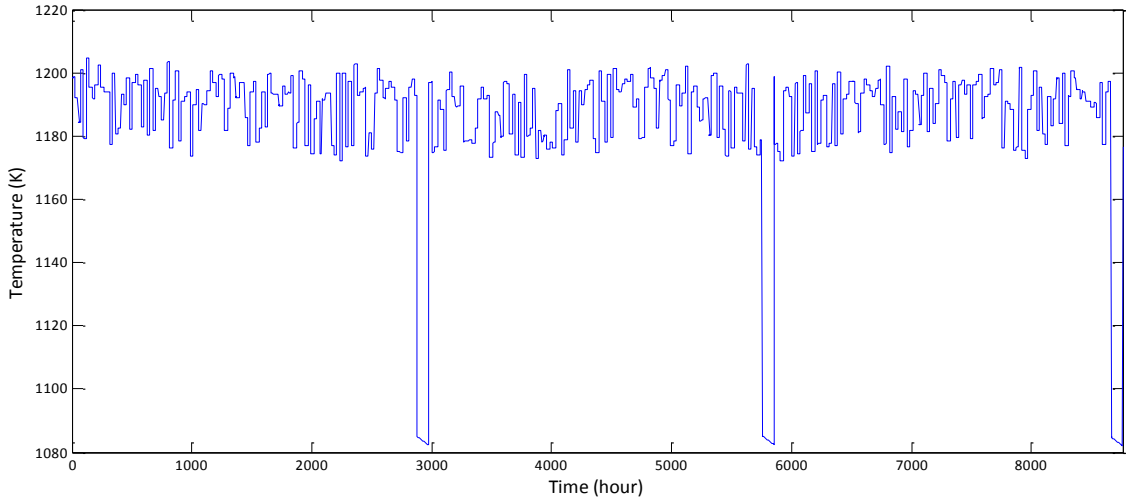

Figure 6-19: Turbine inlet temperature variation.

6.6 Overall WHHE Energy Performance

The parasitic load for the WHHE Energy Centre include; material recovery facility, air separation unit, plasma torch, the desulphurisation circuit (compressor, pumps, refrigeration), hot water pumps, hydrogen storage cooling fans, and the electrolyser. The material recovery facility is assumed to consume 20kWh/tonne (*DECCW NSW, 2010; RMCT, 2003*). The average annual output and demand of the various components are shown in *Table 6-5.*

Table 6-5: Overall average outputs.

Parasitic load	**MW**
MRF	0.137
ASU	1.47
PSA	0.0025
Plasma torch	3.311
Desulphurisation cycle	1.055
Hot water pumps	0.00022
H_2 storage fan	0.024
Electrolyser	0.106
Outputs	
Heat output (thermal)	11.02
Electrical output (FC)	11.56
Electrical output (GT)	3.38
Net electrical output	**8.83**
Overall efficiencies	
Electrical efficiency	29.5%
Heat efficiency	36.9%
CHP efficiency	66.4%

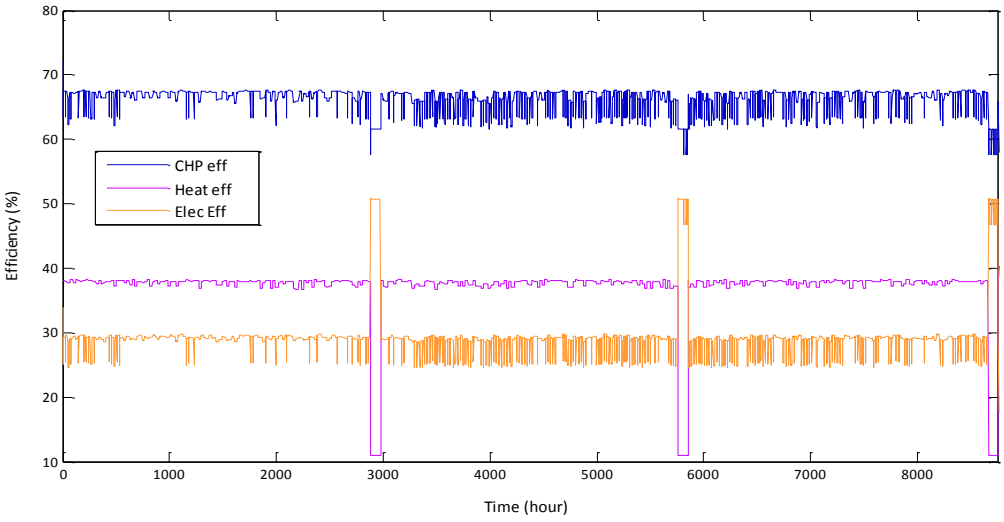

Figure 6-20: Annual Electrical, heat and CHP efficiencies.

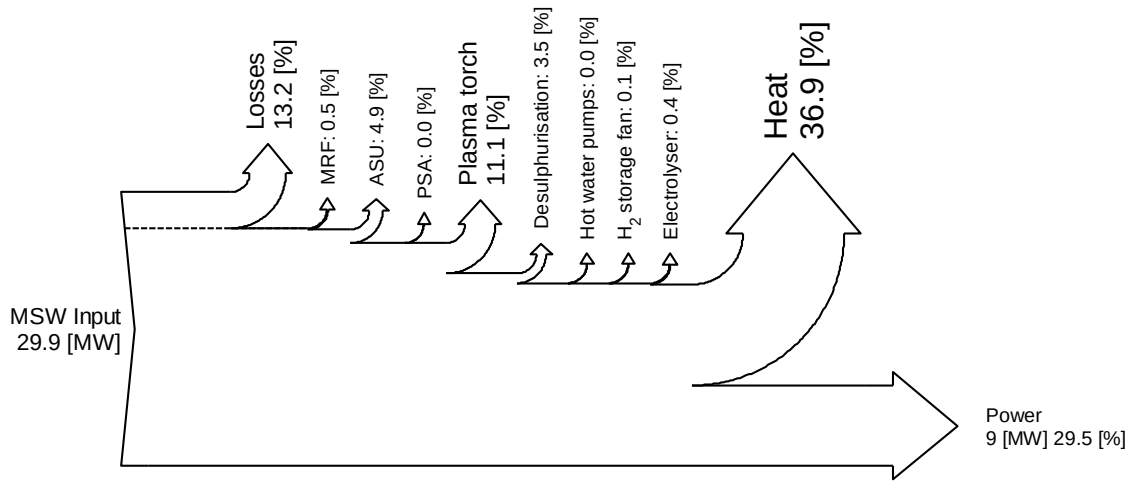

Figure 6-21: Sankey diagram illustrating the losses and parasitic loads taken away from the initial energy input.

6.7 INCOME AND EXPENSES

6.7.1 INCOME

Aside from the obvious revenue streams relating to income from electricity production (£/kWe) and thermal heating energy supply (£/kWth), additional commercial gain can be derived from accepting MSW, sales of Plasmarok® waste aggregate to the construction industry and hydrogen for vehicles.

Typically, the solid by-products from waste-to-energy have to be paid to be disposed of and are usually sent to land fill at substantial cost. However, vitrified slag (Plasmarok®) from plasma gasification can be sold as an aggregate in the construction industry. Average aggregate costs €7-8 per tonne, with an annual demand of 3 billion tonnes in the EU. In 2008 only 6.1% of the aggregate used in the EU was recycled (*Tiess et al., 2011*). Gate fees for 2012/13 in the UK for energy from waste and MRFs are £111 and -£7 per tonne (*WRAP, 2013*). The negative gate fee for MRFs is a result of the lucrative sale of recyclate which for comingled recyclables is estimated at £44 per tonne (*FOE, 2009*).

Renewables Obligation is the mechanism for supporting the renewable electricity projects in the UK. Renewable Obligation Certificates are certificates issued to accredited renewable electricity producers for the eligible renewable energy they produce. The number of ROCs issued is determined according to the type of technology used and the amount generated. Each type of technology falls under a banding level that indicates the number of ROCs issued for each MWh generated. A WHHE Energy Centre is categorised as an advanced gasification/pyrolysis system and is eligible for 2 ROCs per MWh (*Gov.uk, 2013*).

Table 6-6: Income categories and rates.

Income	Price	Unit
Gate fee - WtE	111	£/tonne
Gate fee - MRF	-7	£/tonne
Recyclate	44	£/tonne
Aggregate	6	£/tonne
Ave. ROC price	45.53	£/MWh
ROC banding level	2	ROC/MWh
RHI	4.1	p/kWh
Wholesale elec. price	var	£/kWh

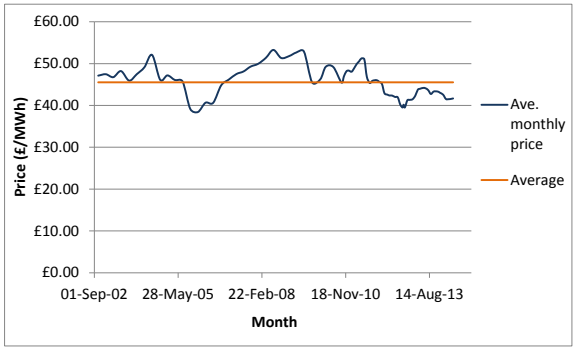

Figure 6-22: Average monthly ROC price from Oct 2002 – May 2014 (*e-roc, 2014*).

The non-domestic renewable heat incentive is another mechanism for supporting renewables in the UK. The government provides subsidises for eligible non-domestic renewable heat generators for a period of 20 years and the tariff available for WHHE Energy Centres is 4.1 p/kWh under the category for solid biomass CHP systems. As explained before the eligible fraction considered to be renewable is 40% for MSW. A summary of the available income rates and categories used in this research is summarised in *Table 6-6* (actual wholesale electricity prices for 2012 will be used).

6.7.2 EXPENSES

Advanced Plasma Power have stated that the capital cost for a facility that includes the MRF, gasification and plasma units, and fuel filtering and processing would be approximately £50 million for a capacity of 100,000 tonnes per year (60,000 RDF/40,000 recyclate). The stated operating costs would be approximately £4.8 million per year (*E4Tech, 2009*), these figures do not include the cost of the fuel cell, GT, hydrogen storage or electrolyser.

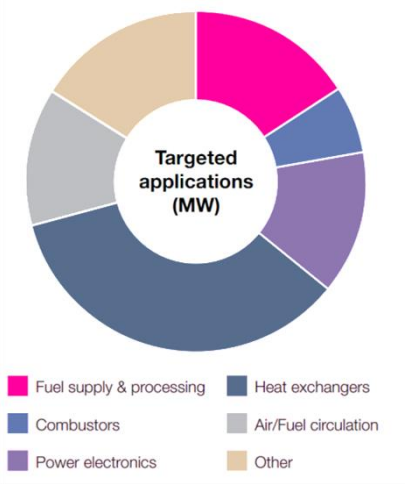

Figure 6-23: Breakdown of costs of principal components and sub-systems for SOFCs (*IEA, 2010*).

Specific targets for SOFC systems fuelled by biomass as set by the International Energy Agency (IEA), which are widely accepted by many nations, is by 2020 to develop a CHP fuel system (100kW-3MW) with 90% CHP efficiency and durability of 60,000 hours at a cost of 2,100 USD/kW {1,365 £/kW @ 0.65 £/$}(*IEA, 2012b*). Where the stack represents 30% of the overall fuel cell system costs (*IEA, 2010*).

For large scale low temperature electrolysers the U.S. D.O.E. use an uninstalled cost of 408 USD/kW {265 £/kW @ 0.65 £/$}(*Sauer et al., 2011*). The annual maintenance cost is expected to be 5% of the capital cost (*ITM, 2012*)

Targets for material based hydrogen storage systems as set by the U.S. D.O.E. for 2017 are 67 USD/kg H_2 {43.5 £/kg H_2 @ 0.65 £/$}(*U.S. D.O.E., 2012*).

Gas turbines in the 3-4 MW range can cost between 480-560 USD/kW {312-364 £/kW @ 0.65 £/$}(*www.gas-turbines.com, 2014*). Gas fired gas turbines have an approximate annual operational and maintenance cost of £34 per kW (*RA Eng, 2004*).

Table 6-7 provides a summary of the capital expenditure (capex) and operational expenditure (opex) for the various components at their respective scales.

Table 6-7: Scale of components along with associated costs.

Scale		
Gasification plant (plus MRF and ancillaries)	60,000	tpa
Fuel cell	13	MW_e
Gas Turbine	3.6	MW_e
Electrolyser	1.2	MW_e
Hydrogen storage	86.7	Tonne (H_2)
Capex		
Gasification plant (plus MRF and ancillaries)	50,000,000	£
Fuel cell	17,745,000	£
Gas turbine	1,216,800	£
Electrolyser	318,000	£
Hydrogen storage	5,808,900	£
Opex		
Gasification plant (plus MRF and ancillaries)	4,800,000	£
Fuel cell (stack replacement)	777,153	£
GT	122,400	£
Electrolyser	15,900	£

The simple payback period for the WHHE Energy Centre under the current operating conditions can be calculated via:

$$SPB = \frac{Equipment\ capex}{Net\ annual\ operational\ income\ (savings)}$$

Table 6-8 shows a breakdown of the amounts used in the SPB calculations.

Table 6-8: Simple payback period figures

Annual Income		
Gate fee - WtE	6,660,000	£
Recyclate	1,760,000	£
Aggregate	133,713	£
ROC	2,816,285	£
RHI	1,583,065	£
Wholesale electricity	3,474,597	£
Annual Expense		
Gate fee - MRF	280,000	£
Gasification plant (plus MRF and ancillaries)	4,800,000	£
Fuel cell (stack replacement)	777,153	£
GT	122,400	£
Electrolyser	15,900	£
Net Operational Income/Cost	10,432,206	£
Simple Payback Period	**7.20**	years

6.7.3 CO_2 SAVINGS

Conventional CO_2 emission factors were obtained from *Pout (2011)*.

Table 6-9: CO_2 savings compared to conventional grid sourced heat and power.

Conventional CO_2 factors		
Gas (when used to provide heat)	0.212	kg CO_2/kWh
Grid supplied electricity	0.522	kg CO_2/kWh
Combined CO_2 factor	0.350	kg CO_2/kWh
CO_2 produced (Conventional grid supply)		
Heating	20,464,020	kg
Electricity	40,360,780	kg
Total	60,824,800	kg
WHHE total CO_2 emissions (fossil based)	53,046,592	kg
WHHE combined CO_2 factor	0.305	kg CO_2/kWh
CO_2 savings	**13%**	

Table 6-9 illustrates that the WHHE Energy Centre has the potential to reduce CO_2 emissions in the UK energy sector by 13% which could mean an overall saving of 5% (*DECC, 2013b*) of UK emissions if these systems were adopted throughout. These savings could be further improved by increasing the bio-fraction above the 40% already assumed in this research, and can be done by biomass enrichment. These savings also do not include offset emissions coming from landfill sites in the form of landfill gas which is rich in methane and has a carbon dioxide equivalent factor of 25. A large amount of CO_2 is also isolated during the desulphurisation process which lends well to future carbon sequestration techniques to be applied without major alteration to the existing facility.

6.8 SIMULATION WITHOUT ELECTROLYSER

To test whether the electrolyser is economically feasible using the current WHHE design and market conditions the centre is modelled without the electrolyser. This means all electricity produced from the WHHE Centre is exported and sold. The knock-on effect does mean the scale of the hydrogen storage and fuel cell will need to change because in order for the hydrogen storage to accumulate enough hydrogen from the incoming syngas the upper and lower hydrogen limits to fuel cell must be lowered (as shown in *Figure 6-24* with reference to *Figure 6-25*).

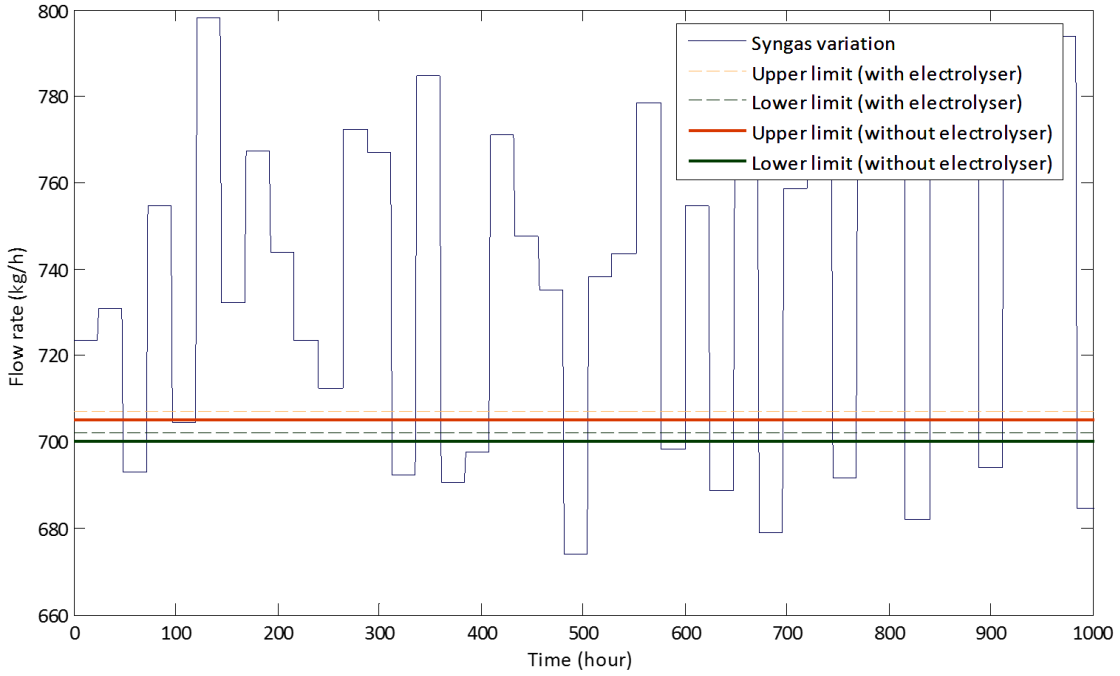

Figure 6-25: Upper and lower limits of the simulations with and without the electrolyser shown against the incoming syngas variation for the first 1000hours.

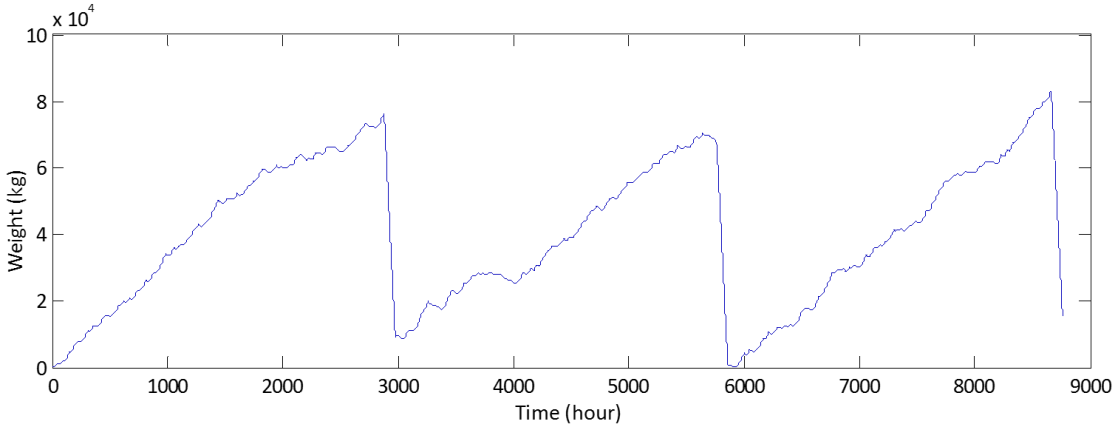

Figure 6-25: Hydrogen storage accumulation without electrolyser using the new upper and lower hydrogen limits to meet the annual demand.

6.8.1 OVERALL ENERGY PERFORMANCE

The overall energy performance benefits from exporting more electricity shown in the "Net electrical output" (in *Table 6-10*) which therefore slightly improves the electrical efficiency. The amount of heat available for export decreases slightly as there is less hydrogen going to the fuel cell and subsequent gas turbine. However, this increase in electrical efficiency and decrease in heat efficiency provides a net 0.1% increase in CHP efficiency, as shown in *Table 6-10* below.

Table 6-10: Overall average output comparison

	with electrolyser	without electrolyser
Parasitic load	**MW**	**MW**
MRF	0.137	0.137
ASU	1.47	1.47
PSA	0.0025	0.0025
Plasma torch	3.311	3.311
Desulphurisation cycle	1.055	1.055
Hot water pumps	0.00022	0.00022
H_2 storage fan	0.024	0.024
Electrolyser	0.106	0
Outputs		
Heat output	11.02	10.99
Electrical output (FC)	11.56	11.54
Electrical output (GT)	3.38	3.33
Net electrical output	**8.83**	**8.87**
Overall efficiencies		
Electrical efficiency	29.5%	29.7%
Heat efficiency	36.9%	36.8%
CHP efficiency	66.4%	66.5%

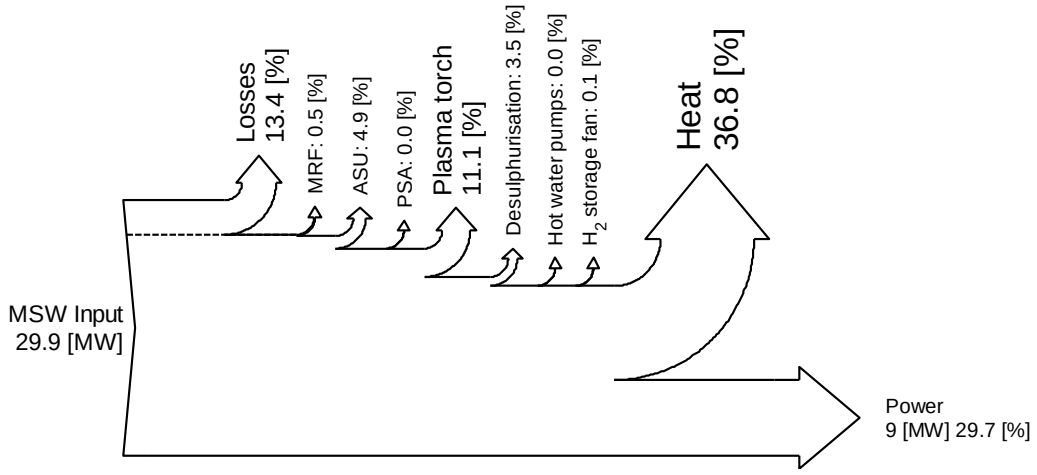

Figure 6-26: Sankey diagram illustrating losses and parasitic loads.

6.8.2 INCOME AND EXPENSES

Using the same income and expense rates as previously the Centre without the electrolyser is compared with the original centre with the electrolyser. The increased electrical export will see an increase in revenue, and because there is a reduction in the amount of hydrogen needed to be stored there are savings to be made on the capital cost of the hydrogen storage module. The size of the fuel cell unit is also slightly smaller as the amount of hydrogen going to the system is less.

Table 6-11: Comparison of scale of components along with associated costs.

	with electrolyser	without electrolyser	
Scale			
Gasification plant (plus MRF and ancillaries)	60,000	60,000	tpa
Fuel cell	13	12.8	MW_e
Gas Turbine	3.6	3.6	WM_e
Electrolyser	1.2	0	MW_e
Hydrogen storage (H2)	86.7	83.1	Tonne (H_2)
Capex			
Gasification plant (plus MRF and ancillaries)	50,000,000	50,000,000	£
Fuel cell	17,745,000	17,472,000	£
Gas turbine	1,216,800	1,216,800	£
Electrolyser	318,000	-	£
Hydrogen storage	5,808,900	5,567,700	£
Opex			£
Gasification plant (plus MRF and ancillaries)	4,800,000	4,800,000	£
Fuel cell opex (stack replacement)	777,153	765,197	£
GT opex	122,400	122,400	£
Electrolyser	15,900	-	£

Again, using the same methodology as previously the figures for the SPB are presented in *Table 6-12*. Due to savings from the smaller hydrogen storage module and fuel cell plus the increased revenue from the sale of more electricity the payback period is brought closer to 7.13 years.

Table 6-12: Comparison of simple payback periods.

	with electrolyser	without electrolyser	
Annual Income			
Gate fee - WtE	6,660,000	6,660,000	£
Recyclate	1,760,000	1,760,000	£
Aggregate	133,713	133,713	£
Ave. ROC price	2,816,285	2,831,409	£
RHI	1,583,065	1,579,315	£
Wholesale elec. Price	3,474,597	3,506,003	£
Annual Expense			
Gate fee - MRF	280,000	280,000	£
Gasification plant (plus MRF and ancillaries)	4,800,000	4,800,000	£
Fuel cell opex (stack replacement)	777,153	777,153	£
GT opex	122,400	122,400	£
Electrolyser	15,900	-	£
Net Operational Income/Cost	10,432,206	10,490,886	£
Simple Payback Period	**7.20**	**7.13**	years

Readers Guide

- Overview
- 1. Introduction
- 2. The WHHE Concept
- 3. Literature Digest
- 4. SOFCs
- 5. Modelling
- 6. Modelling Results
- 7. Experimental Research
  - Introduction
    - Carbon formation pathways
  - Experimental
    - Experimental Set-up
    - Operating conditions
    - Methodology
  - Results and Discussion
    - OCV
    - EIS
    - Exhaust gas analysis
  - Conclusion
- 8. micro-CHP in the UK Market
- 9. Conclusions
- References
- Appendices

7. EXPERIMENTAL RESEARCH

7.1 ABSTRACT

The integration of solid oxide fuel cells (SOFCs) with gasification systems have theoretically been shown to have a great potential to provide highly efficient distributed generation energy systems that can be fuelled by biomass including municipal solid waste. The syngas produced from the gasification of carbonaceous material is rich in hydrogen, carbon monoxide and methane that can fuel SOFCs. However, other constituents such as tar can cause catalyst deactivation, and blockage of the diffusion pathways. This work examines the impact of increasing concentrations of toluene as a model tar in a typical syngas composition fed to a NiO-GDC/TZ3Y/8YSZ/LSM-LSM SOFC membrane electrode assembly operating at 850°C and atmospheric pressure. Results suggest that up to 20 g/Nm^3 of toluene and a low fuel utilisation factor (ca. 17%) does not negatively impact cell performance and rather acts to increase the available hydrogen by undergoing reformation. At these conditions carbon deposition does occur, detected through EDS analysis, but serves to decrease the ASR rather than degrade the cell.

Alternatively, the cell operating with 32 g/Nm^3 toluene and with a fuel utilisation of 66.7% is dramatically affected through increased ASR which is assumed to be caused by increased carbon deposition. In order to test for the presence of tar products at the anode exhaust samples have been captured using an absorbing filter with results from HS-GC/MS analysis showing the presence of toluene only.

Keywords: SOFC, syngas, model tar, carbon deposition

7.2 INTRODUCTION

The driving need to diversify and improve the global energy market is obvious and extensively discussed, and within this change fuel cell technology is widely regarded to have the potential to meet many of the demands of a sustainable future. High temperature SOFCs, which operate up to temperatures of 1000°C, are electrochemical engines with distinct advantages as well as challenges. Whilst these high temperatures are required to maximise the ion conductivity of the electrolyte they also provide advantages of fuel flexibility and the availability of high grade heat that can be used in combined heat and power (CHP) systems. Already there are commercial small scale residential systems operating on the existing natural gas infrastructure which have an electrical efficiency of 60% and a total CHP efficiency of 85% (*CFCL, 2009*). In these systems methane (CH_4) is steam reformed into hydrogen (H_2) and carbon monoxide (CO)(*Equ. 7-2-1*) which can be further converted to carbon dioxide (CO_2) and more H_2 through a water gas shift (WGS)(Eq. 3) or can be used as a fuel itself (Eq. 9). In order to initiate these reactions steam which is produced at the anode is recirculated from the exhaust to the incoming fuel and the exothermic reactions (*Equ. 7-2-5* and *7-2-7*) at the electrode is used to supply the endothermic reforming reaction.

$\Delta H^0 = 206\ \text{kJ.mol}^{-1}$ $CH_4 + H_2O \leftrightarrow CO + 3H_2$ Eq. 1

$\Delta H^0 = 869\ \text{kJ.mol}^{-1}$ $C_7H_8 + 7H_2O \leftrightarrow 7CO + 11H_2$ Eq. 2

$\Delta H^0 = -41\ \text{kJ.mol}^{-1}$ $CO + H_2O \leftrightarrow CO_2 + H_2$ **(WGS)** Eq. 3

$C_nH_m + nH_2O \leftrightarrow nCO + \left(n + \frac{m}{2}\right)H_2$ Eq. 4

$\Delta H^0 = -242\ \text{kJ.mol}^{-1}$ $H_2 + O^{2-} \rightarrow H_2O + 2e^-$ Eq. 5

$\Delta H^0 = -111\ \text{kJ.mol}^{-1}$ $C + O^{2-} \leftrightarrow CO + 2e^-$ Eq. 6

$\Delta H^0 = -283\ \text{kJ.mol}^{-1}$ $CO + O^{2-} \leftrightarrow CO_2 + 2e^-$ Eq. 7

$\Delta H^0 = -3772\ \text{kJ.mol}^{-1}$ $C_7H_8 + 9O^{2-} \leftrightarrow 7CO_2 + 4H_2O + 18e^-$ Eq. 8

$C_xH_y + \left(\frac{y}{2} + 2x\right)O^{2-} \leftrightarrow \frac{y}{2}H_2O + xCO_2 + (y + 4x)e^-$ Eq. 9

Another source of hydrogen that has the potential to fuel a SOFC is synthesis gas or syngas derived from the gasification of carbonaceous material, often coal but also biomass and municipal solid waste (MSW). Syngas comprises mainly of CO, CO_2, and H_2 along with smaller concentrations of CH_4, steam (H_2O), nitrogen (N_2)(if air is used for gasification), and trace amounts of tar, volatile alkali metals, nitrogen compounds, sulphur compounds, chlorine compounds and particulates (*Coll et al., 2001; Higman and van der Burgt, 2003; Lorente, 2013*). The tolerance of SOFCs against many of these impurities is uncertain and remains a topic for continued research. This is further complicated as the concentration of these impurities can vary widely even between the same gasifier type and depends on factors such as; feedstock, feedstock size, moisture content, temperature, pressure, gasification agent, residence time and the presence of bed catalysts (E4Tech, 2009).

In terms of gasifier categories and the amount of tar products formed the general agreement is that updraft systems are the worst producing ca.100g/Nm^3, fluidised bed systems are intermediate at ca.10g/Nm^3, and the downdraft the best producing ca.1g/Nm^3 (*Milne et al., 1998*). The formation of tar is a function of temperature, time, feedstock size, the gasification agent (O_2, steam), geometry, and mixing in the chamber which can cause a large disparity between the type of the system and the amounts mentioned. Also, methods for extraction and analysis of the tar products can cause misleading results as capturing the full array of tars with their various boiling points is a difficult task.

The general definition of a tar is reported in *Milne et al* (1998) as: “The organics, produced under thermal or partial-oxidation regimes (gasification) of any organic material, are called “tars” and are generally assumed to be largely aromatic.”

The typical tar composition for a biomass gasifier is presented in *Table 7-1* (*Milne et al., 1998; Col et al., 2001; Singh et al., 2005, and Mermelstein et al., 2009*).

Table 7-1: Typical tar composition from biomass gasification

Compound	Composition (wt %)
Benzene	37.9
Toluene	14.3
Other one-ring aromatic hydrocarbons	13.9
Naphthalene	9.6
Other two-ring aromatic hydrocarbons	7.8
Three-ring aromatic compounds	3.6
Four-ring aromatic compounds	0.8
Phenolic compounds	4.6
Heterocyclic compounds	6.5
Others	1.0

In order to test the performance of a SOFC running on tar-laden syngas a synthetic composition using a model tar can be used, as reported by *Mermelstein et al. (2010 and 2011)* using benzene, *Namioka et al. (2011)* and *Liu et al. (2013)* using toluene, and *Mermelstein (2009)* using both benzene and toluene. Other studies using naphthalene have been reported by *Aravind (2008)* and *Hauth (2011)*. Limited studies using real syngas having been carried out and reported in *Hofmann (2007, 2008, 2009)* which were undertaken within the EU project BioCellUS (Biomass fuel Cell Utility System), and real tar from a coal gasifier have also been presented by *Lorente et al. (2012, 2013)*. In *Lorente (2012)* real tar from a coal gasifier was compared against toluene, as a real tar versus a model tar assessment, and results illustrated that carbon deposition arising from toluene were greater than that of the real tar. Therefore the results derived from using toluene as a model tar could be regarded as an overestimation of the effects of the total carbon deposition.

The influence of anode material can also have a substantial effect on the tolerance of the fuel cell to contaminants (*Finnerty et al., 2000; Zhu et al., 2003; Aravind et al., 2008; Lorente et al., 2013*). In *Lorente et al. (2013)* test conducted using model and real tars on Ni/YSZ and Ni/GDC anode materials illustrated that the Ni/GDC material performed better than the conventional Ni/YSZ anode material and supports the argument that Ceria-based materials are more effective in suppressing carbon formation (*Zhu et al., 2003*). This resistance to carbon formation can also be explained by the influence of Ceria on the Nickel catalyst. Ceria serves to reduce the NiO crystallite size whilst increasing the metal dispersion which results in higher oxygen mobility and improved reducibility (*Koo et al., 2014; Yong-zhao et al., 2013; Daza et al., 2009*). For this reason a cell purchased from *H.C.Starck Ceramics GmbH* comprising of NiO-GDC/TZ3Y/8YSZ/LSM-LSM anode/electrolyte/cathode (double layer) has been used for these experiments.

The purpose of this research is to identify the conditions that would lead to carbon formation from the hydrocarbon species present in the syngas and how carbon deposition impacts the electrical performance of the SOFC. Further analysis of the exhaust gas will be used to provide insight into the reaction pathway of the tar and the level of reformation occurring.

Previous studies have concluded that carbon deposition caused by the presence of tar at the anode can cause deactivation of the nickel catalyst whilst also restricting the diffusion pathways (*Liu et al., 2013; Lorente et al., 2012; Lee et al., 2012, Mermelstein et al., 2011*). Thereby impacting the electrical performance and can also cause irreversible damage to the cell. If allowed to condense these tar compounds can also build up inside pipework and foul the gas flow (*Mermelstein, 2011*). Testing of the exhaust gas for the presence of volatile organic compounds (VOCs) will provide further understanding of the reaction pathway of the model tar, as there is a concern that the decomposition of the tar may lead to the growth of higher hydrocarbon molecules (*Mermelstein, 2011*).

7.2.1 CARBON FORMATION PATHWAYS

Carbon forming reactions:

$\Delta H^0 = 75\ \mathrm{kJ.mol^{-1}}$ $CH_4 \leftrightarrow C + 2H_2$ Eq. 10

$\Delta H^0 = 50\ \mathrm{kJ.mol^{-1}}$ $C_7H_8 \leftrightarrow 7C + 4H_2$ Eq. 11

$\Delta H^0 = -173\ \mathrm{kJ.mol^{-1}}$ $2CO \leftrightarrow C + CO_2$ **(Boudouard)** Eq. 12

$\Delta H^0 = -131\ \mathrm{kJ.mol^{-1}}$ $CO + H_2 \leftrightarrow C + H_2O$ Eq. 13

The formation of carbon at the anode is directly related to the operating conditions of the cell and can be suppressed by employing a sufficiently high oxygen-to-carbon ratio which can be done by increasing the steam content at the inlet (this will promote steam reformation of the hydrocarbons, *Equ. 7-2-1, 7-2-2* and *7-2-3*), and/or by operating at sufficiently high current densities to ensure a large amount of oxygen ions are available to oxidise the carbon species (*Equ. 7-2-5, 7-2-6, 7-2-7* and *7-2-8*).

Temperature also plays an important role in carbon formation and there are a number of studies that use thermodynamic modelling to predict the potential for carbon formation, but as illustrated in *Mermelsein (2011)* and *Lorente (2013)* thermodynamic modelling should only be used as a guide as carbon has shown to form beyond predicted limits.

7.3 EXPERIMENTAL

7.3.1 EXPERIMENTAL SET-UP

A square single cell SOFC test station has been modified to include the addition of a model tar by diverting nitrogen through a temperature controlled tar evaporator. The test station is equipped to supply the cell with a mixture of H_2, O_2, N_2, CO_2, CO, and CH_4 which are controlled using Bronkhorst Mass flow Controllers, and H_2O is supplied either through a Bronkhorst Controlled Evaporator Mixer (CEM) or a temperature controlled evaporator. Pipe work leading to the cell from the tar evaporator is trace heated to prevent condensation and the exit pipe coming from the anode is also trace heated to ensure none of the gases are able to condense prior to the first gas sampling point. After this sampling point the anode off-gas is bubbled through a condenser before passing through an

absorber to eliminate any remaining moisture before a second gas sampling point which is connected to an Agilent Technologies 490 Micro GC. The ceramic cell housing is made from Al_2O_3 and is designed to provide a gas tight seal by using weights to apply pressure to an appropriate gasket seal, in this case gaskets were cut from Termiculite® 866 mica. A platinum mesh spot welded to platinum wires is used to transfer current to the cathode and similarly a nickel mesh spot welded to platinum wires is used as a current collector at the anode. This housing is located in a furnace made up of ceramic insulating bricks. Further details of this setup can be found in *Liu et al. (2013)*. In order to protect the cell from damage caused by excessive current, and also to avoid the risk of nickel oxidation, the experiments limit drawing current that pushes the voltage below 0.65V.

Table 7-2: Cell materials, characteristics and dimensions of the electrodes and electrolyte.

Cell material and geometry

Layer	Material description	Area dimensions (mm)	Thickness (µm)
Anode	Porous NiO/GDC	90 x 90	40 ± 10
Electrolyte	Dense TZ3Y	108 x 108	95 ± 15
Cathode	Porous 8YSZ/LSM-LSM double layer	90 x 90	40 ± 10

A current is drawn from the cell using an electrical load (PLZ603W Kikusui Electronics Corp.) with an additional compensation load (SM30-100D Delta Elektronika), which are connected in series with the cell. Electrochemical Impedance Spectroscopy (EIS) measurements and potential measurements are recorded using a Gamry Instruments FC350™ Fuel Cell Tester (FCI4™ interface) and works with the electrical load operated via a PC using Gamry Echem Analyst™ software. Thermocouples are placed throughout the test station measuring oven, cell, inlet and outlet tracing temperatures as well as the fluid temperatures in both the tar and water evaporators.

In order to control the amount of tar being added to the gas composition an evaporator using N_2 as a carrier gas was used. By controlling the flow rate of the carrier gas and the temperature of the evaporator the vapour pressure of a substance can be predicted using the Antoine equation.

$$\log_{10} P_{C_7H_8} = A - \frac{B}{T + C - 273.15} \qquad \text{Equ. 7-3-1.}$$

$$P_{C_7H_8} = x_{C_7H_8}.P_{evaporator} \qquad \text{Equ. 7-3-2.}$$

Here $P_{C_7H_8}$ and $P_{evaporator}$ represent the vapour pressure of the toluene and overall pressure inside the evaporator respectively, A, B, and C are the Antoine coefficients specific to toluene and T is the evaporator temperature, and $x_{C_7H_8}$ is the molar fraction of toluene.

Sampling of the untreated anode off-gas was taken using a 100ml syringe fitted with an absorbing filter to capture and test for any hydrocarbons that may be present at the exhaust. Filters were immediately frozen to preserve the contents before being tested for the presence of VOCs, tests were carried out by a commercial laboratory using Headspace Gas Chromatography/Mass Spectrometry (HS-GC/MS).

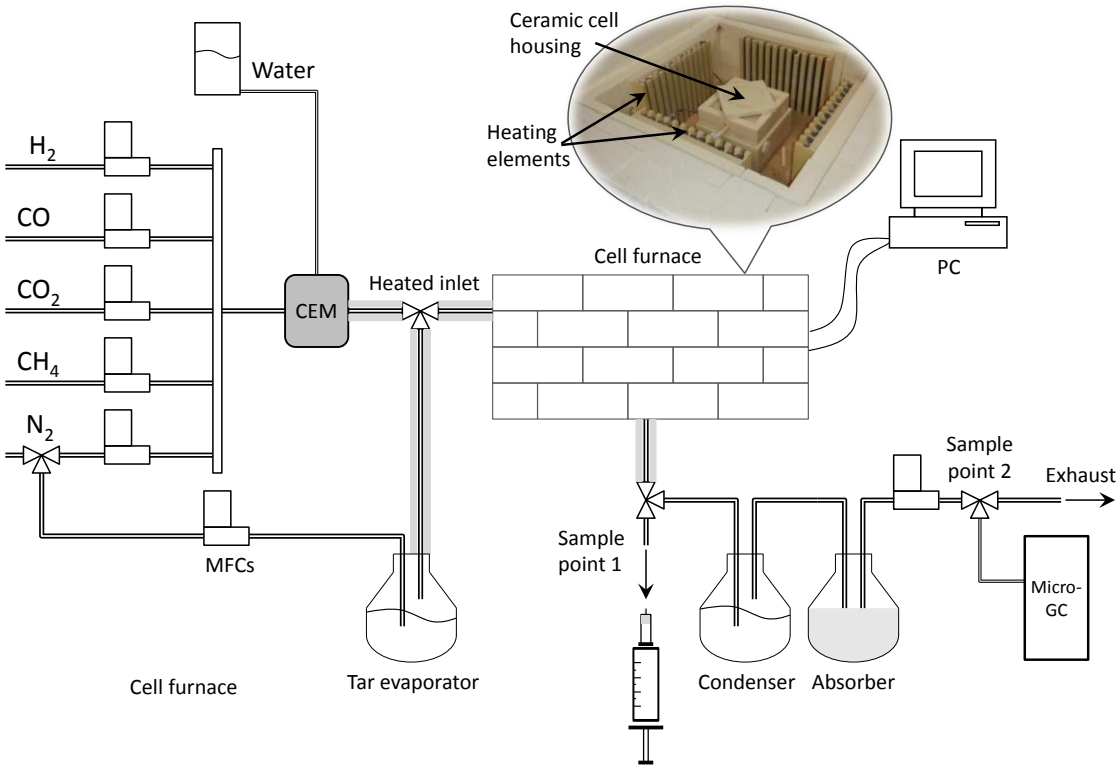

Figure 7-1: A schematic representation of the experimental setup.

7.3.2 OPERATING CONDITIONS

After the NiO at the anode was reduced Ni, using a mixture of H_2 and N_2, the cell was operated at a constant temperature of 850°C and at atmospheric pressure. The study included five variations in gas composition with the first four operating with a low fuel utilisation factor (U_f)(*Equ. 7-3-3*) and changes in the composition were specific to the tar, H_2O and N_2 concentrations. The variations in H_2O were to ensure the experiments were conducted with an oxygen-to-carbon ratio (O/C) of ca. 1.8 which would protect the test station from carbon deposition in the pipework thereby preventing the need for costly repairs. The variation in N_2 was needed to ensure consistency in the volume fraction of the remaining gases. The fifth experiment aimed to substantially increase the fuel utilisation factor whilst also increasing the tar concentration. The cathode was supplied with a mixture that represents a typical air composition of 320Nml/min O_2 and 1180 Nml/min N_2.

$$U_f = \frac{\mathrm{I}}{2F\dot{n}(x_{H_2} + x_{CO} + 4x_{CH_4} + 18x_{C_7H_8})} \qquad \text{Equ. 7-3-3.}$$

Where I is current (A), F is the Faraday constant (C/mol), $\dot{n}$ is the total anode molar flow rate (mol/s), and x_i is the input molar fraction of the gas.

Table 7-3: Operating conditions of the five experiments undertaken indicating syngas composition and utilisation factor at 200 mA/cm^2 for each.

Experiment	**1**		**2**		**3**		**4**		**5**	
	Nml/min	vol %	Nml/min	vol %	Nml/min	vol %	Nml/min	vol %	Nml/min	vol %
H_2	306	28.2	306	27.9	306	27.9	306	27.9	77	29.0
CO_2	144	13.3	144	13.1	144	13.1	144	13.1	36	13.6
CO	286	26.3	286	26.1	286	26.1	286	26.1	72	27.1
N_2	119	11.0	115	10.5	97	8.9	60	5.4	13.9	5.2
CH_4	7.7	0.7	7.7	0.7	7.7	0.7	7.7	0.7	1.8	0.7
H_2O	10.8	g/hr	11.5	g/hr	12.3	g/hr	14	g/hr	3	g/hr
Toluene	0	g/Nm^3	5	g/Nm^3	10	g/Nm^3	20	g/Nm^3	32	g/Nm^3
U_f (@200 mA/cm^2)	18.1%		17.4%		16.8%		15.7%		66.7%	
O/C ratio	1.8		1.8		1.8		1.8		1.64	

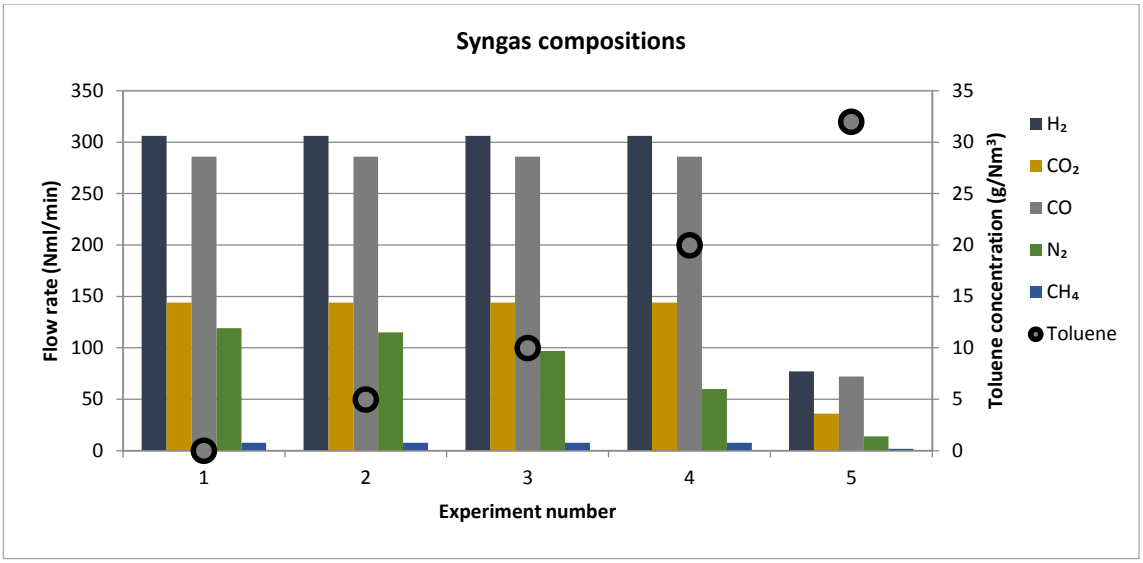

Figure 7-2: Graphical representation of gas composition indicating increasing levels of toluene concentration from 0 – 32 g/Nm³.

7.3.3 METHODOLOGY

In order to measure the performance drop caused by the inclusion of the syngas reference measurements were taken prior to the introduction of any carbon species to the cell. For this purpose an I-V curve and EIS measurements were taken whilst supplying the cell with 400 Nml/min of H_2 and 800 Nml/min of N_2. EIS measurements were also taken after the completion of each experiment to record any changes to the cell's characteristics as a result of possible carbon deposition. For each experiment the gas composition at the exhaust was measured at open circuit voltage (OCV), 100 mA/cm^2 and again at 200 mA/cm^2 in order to track the changes to the CO and CO_2 flow rates which would indicate the level of reformation of the two hydrocarbon species and will give insight into the reaction pathways of the model tar. This was further assisted by capturing samples, at the first sampling point, using absorbing filters which have been tested for the presence of any tar products which would elucidate on the possibility of the initial hydrocarbons to break and reform into other hydrocarbon species. Also, to visualise and quantify the change in performance caused by the inclusion and removal of the model tar OCV readings were recorded for 10min before the inclusion of the tar, then a further 30min with the tar added, and until the voltage stabilised after the tar was removed.

7.4 RESULTS AND DISCUSSION

7.4.1 OCV

The OCV, illustrated in *Figure 7-3*, of the reference experiment using just H_2 and N_2 at the anode is higher than that of the syngas experiments which is owed to the slightly higher partial pressure of H_2 and also due to the lack H_2O at the anode. Given the relatively consistent amounts of H_2 and H_2O the OCV of the syngas experiments are very similar and the fact that experiment 5 shows a slightly elevated OCV indicates that the high concentration of tar is undergoing reformation to increase the flow of H_2 (and hence the partial pressure). A localised drop in temperature caused by the endothermic reformation could also contribute to the increased voltage as temperature directly influences the Gibbs free enthalpy. Interestingly the gradient, which is an indication of the cells area specific resistance (ASR), is improved for experiments 1-4 illustrating improved cell performance under these conditions, even when compared to the carbon-free reference experiment. We can therefore postulate that small levels of carbon deposition can positively influence the electrical conductivity of the cell, but whether this can be maintained over a longer period remains to be answered. Experiment 5 demonstrates a visible increase in ASR which in this case could be a result of an over accumulation of carbon, which was confirmed by the EDS, at the anode.

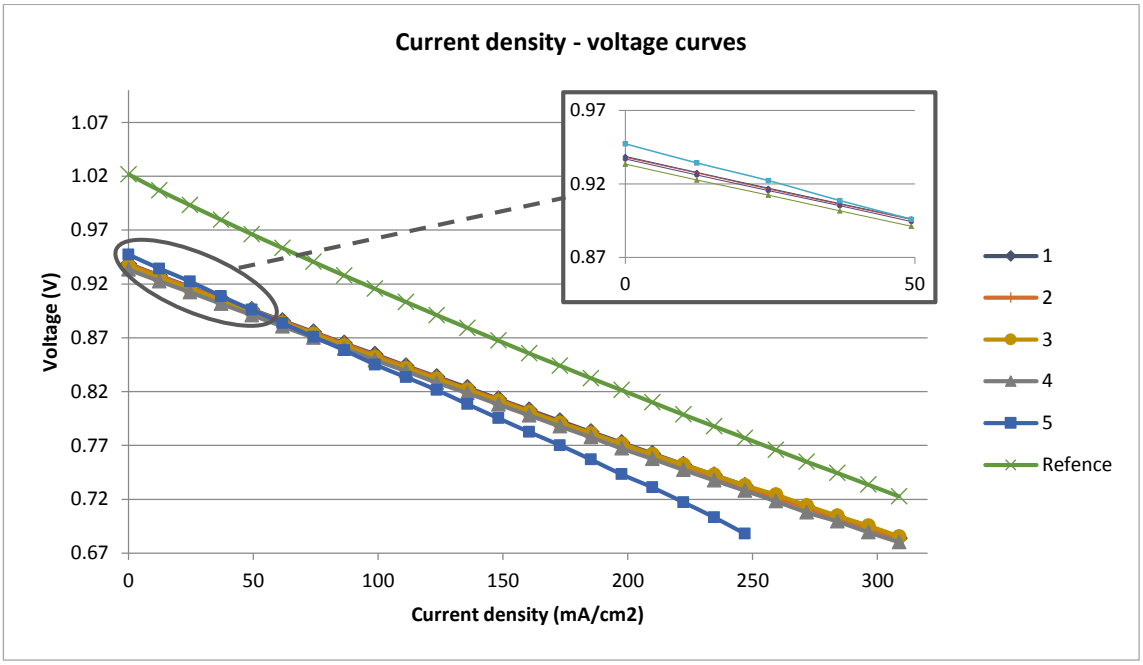

Figure 7-3: V-J curves for the five experiments undertaken along with a preliminary reference measurement taken for H_2/N_2 fuel mix with a similar H_2 partial pressure to the syngas experiments.

Results from monitoring the OCV at the inclusion, operation, and removal of the model, *Figure 7-4*, shows that at the inclusion of the tar the OCV increases (demonstrating more clearly that the tar is contributing to the amount of hydrogen available at the anode as a result of reformation) and remains constant for the 30min period. As mentioned above, the endothermic reforming of the tar may also cause a localised drop in temperature which would contribute to the identified increase in

OCV. This is explained by an increase in the Gibbs free enthalpy which varies with temperature and a drop in temperature would result in a slightly increased OCV. Once the tar is removed we can see that the OCV recovers to its original level indicating no damage is caused from the introduction of tar to the fuel. These results were measured during experiment 4 (tar flow - 20 g/Nm^3).

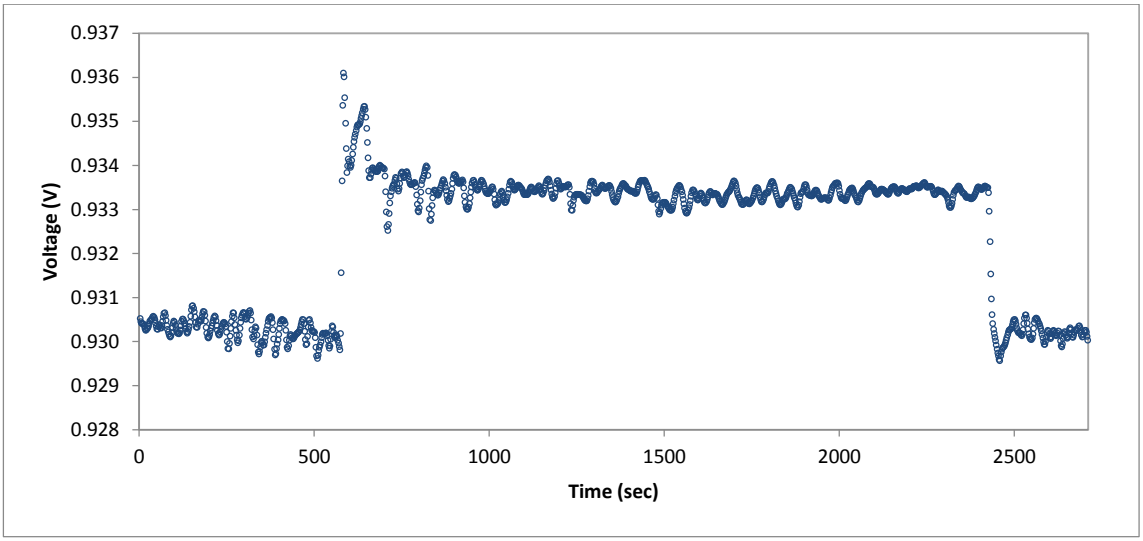

Figure 7-4: OCV measurements taken over time showing changes caused by the inclusion and removal of the tar species, taken during experiment 4.

7.4.2 EIS

Figure 7-5 presents the Nyquist plots of impedance and illustrates an ohmic resistance (defined by the *x* intercept in the high frequency region) of ca. 0.7 Ω cm^2 for all experiments with a small increase in resistance for syngas experiments 1-5. The overall impedance for the cell in the reference experiment is ca. 1.5 Ω cm^2, 1.4 Ω cm^2 for experiment 5, and ca. 1.1 Ω cm^2 for experiments 1-4 which reflects the change in slope identified in *Figure 7-3*. The overall polarization (the difference between the ohmic resistance and overall impedance) for the reference experiment is ca. 0.79 Ω cm^2, ca. 0.64 Ω cm^2 for experiment 5, and ca. 0.4 for experiments 1-4. It can be seen that for experiments 1-4 the impedance characteristics are not dissimilar even though the levels of tar are steadily increased and demonstrates no identifiable change to the structure of the material resulting from any possible carbon deposition. Experiment 5 is clearly adversely affected by the high tar concentration and the increased utilisation factor, which will influence the gas concentration along the surface of the anode thereby affecting the gas diffusion process, combined with the carbon deposition identified through SEM analysis we can conclude that these conditions are not suitable for this cell. The localised drop in temperature caused by the endothermic reforming of the hydrocarbon species in experiment 5 could further explain the increased overall impedance. An argument for decreased overall impedance for experiments 1-4 compared to the reference H_2/N_2 can be attributed to the participation of C and CO (*Equ. 7-2-6 and 7-2-7*) thereby reducing the polarization resistance by combining with the O^{2-} ions at the triple phase boundary. It is reasonable to conclude that if any carbon is being formed at the anode in experiments 1-4 there are little signs to show significant degradation. Results from energy dispersive spectrometer (EDS) presented in ***Figure 7-7*** **illustrate**

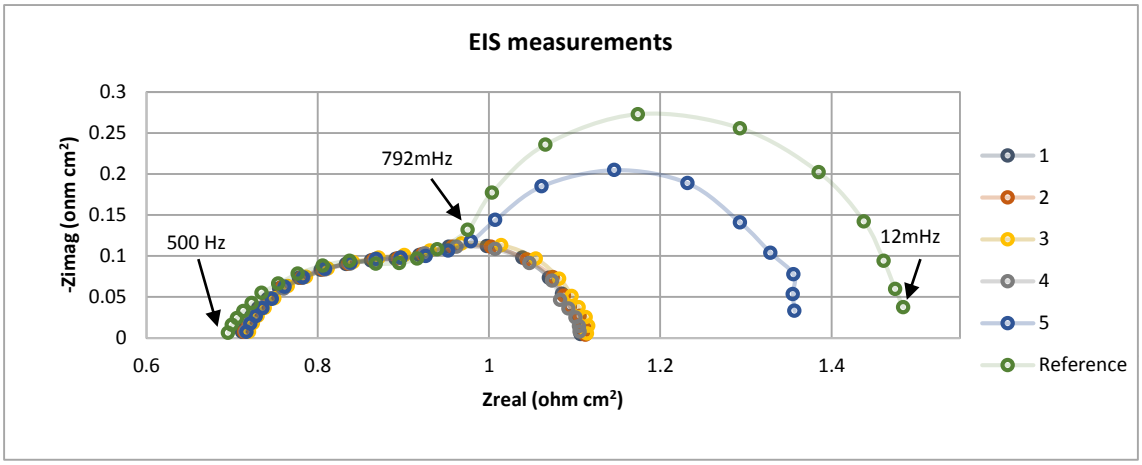

the presence of carbon as a result of these experiments and with the evidence provided we can assume the conditions present in experiment 5 are most likely responsible.

7.4.3 EXHAUST GAS ANALYSIS

By studying the trends in CO and CO_2 at the exhaust we can see that the amount of CO_2 is substantially increased compared to the inlet which would be expected owing to the steam reforming of the CH_4 and C_7H_8 (toluene)(*Equ. 7-2-1 and 7-2-3*) to CO and the shifting of CO to CO_2 through the WGS (*Eq. 2*). Hydrocarbon species can also undergo reformation straight to CO_2 without the WGS resulting in the same molar balance. The considerable amount of CO at the exhaust indicates the majority of the increase in CO_2 must result from the reformation of the hydrocarbon species. The gradual decrease in CO and CO_2 as the current density increases is an indication that there is either a fall in hydrocarbon reformation or, more likely, the production of solid carbon at the anode. Interestingly this trend increases even though the flux of oxygen ions at anode increases. As indicated and noted from the EIS measurements (*Figure 7-5*) the CO and CO_2 trends for experiment 5 indicate further carbon deposition which accounts for the substantial increase in the overall impedance and the drop in CO and CO_2 concentrations.

Results from the samples captured at the anode exhaust via the absorbing filters, shown in *Table 7-4*, show that the toluene model tar is still present at the exhaust and is the only tar product detected from the VOCs tested (the compounds tested and the limits of their detection are presented in *Table 7-4*). Even though the large array of hydrocarbon species tested is not exhaustive, these results begin to show that the reaction pathway of the toluene is to reform (*Equ. 7-2-4*) and not to combine into other hydrocarbon species. Whilst reformation is taking place results show that the tar is not completely reformed thereby leaving scope to optimise the conditions further to maximise the potential of the tar to fuel the SOFC. The trends for the VOC testing are not always consistent and may be a result of a number of factors that include; condensation at the sampling point, inconsistent drawing of the syringe, or insufficient protection of the filters during transportation.

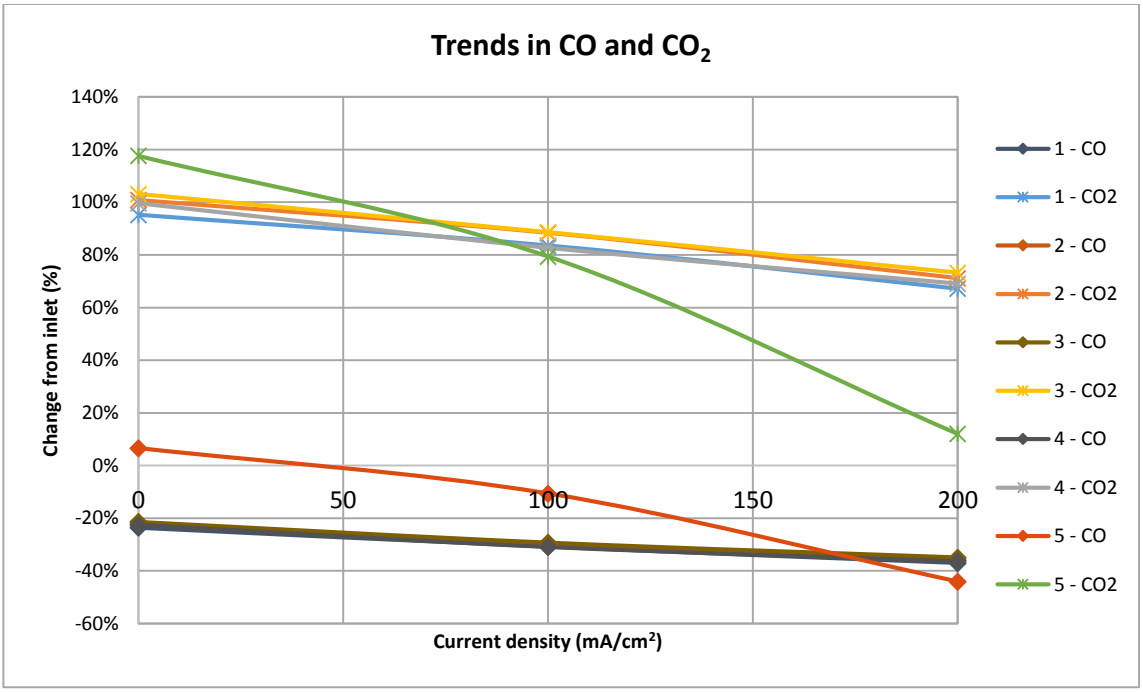

Figure 7-6: Graphical representation of the change in CO and CO_2 at the exhaust compared to the amount CO and CO_2 at the inlet measured at increasing current density.

Table 7-4: Third party HS-GC/MS analysis of samples captured via absorption filters at the anode exhaust. Tests were performed to detect the presence of VOCs and the list of compounds tested and the corresponding detection limits are shown. The only positive results came from the presence of toluene, all other compounds were not detected above the given detection limits.

Experiment			2			3			4			5		
Current density at time of extraction (mA/cm²)			0	100	200	0	100	200	0	100	200	0	100	200
Compound	**Unit**	**Limit of detection**												
Toluene	µg/kg	1	3.4	6.2	1.1	5.6	3.7	2.5	5.1	2.2	2.8	< 1.0	< 1.0	7.6

Other compounds tested with [Limit of detection in µg/kg]:
Chloromethane [4], Chloroethane [2], Bromomethane [6], Vinyl Chloride [24], Vinyl Chloride [24], Trichlorofluoromethane [5], 1,1-dichloroethene [7], 1,1,2-Trichloro 1,2,2-Trifluoroethane [7], Cis-1,2-dichloroethene [7], MTBE (Methyl Tertiary Butyl Ether) [1], 1,1-dichloroethane [6], 2,2-Dichloropropane [6], Trichloromethane [7], 1,1,1-Trichloroethane [7], 1,2-dichloroethane [4], 1,1-Dichloropropene [7], Trans-1,2-dichloroethene [7], Benzene [1], Tetrachloromethane [7], 1,2-dichloropropane [6], Trichloroethene [6], Dibromomethane [7], Bromodichloromethane [7], Cis-1,3-dichloropropene [7], Trans-1,3-dichloropropene [8], 1,1,2-Trichloroethane [5], 1,3-Dichloropropane [8], Dibromochloromethane [2], Tetrachloroethene [8], 1,2-Dibromoethane [3], Chlorobenzene [7], 1,1,1,2-Tetrachloroethane [4], Ethylbenzene [1], p & m-xylene [1], Styrene [5], Tribromomethane [7], o-xylene [1], 1,1,2,2-Tetrachloroethane [5], Isopropylbenzene [7], Bromobenzene [11], N-Propylbenzene [5], 2-Chlorotoluene [11], 4-Chlorotoluene [11], 1,3,5-Trimethylbenzene [4]. Tert-Butylbenzene [4], 1,2,4-Trimethylbenzene [5], Sec-Butylbenzene [5], 1,3-dichlorobenzene [7], P-Isopropyltoluene [16], 1,2-dichlorobenzene [5], 1,4-dichlorobenzene [8], Butylbenzene [4], 1,2-Dibromo-3-chloropropane [7], 1,2,4-Trichlorobenzene [9], Hexachlorobutadiene [7], 1,2,3-Trichlorobenzene [10].

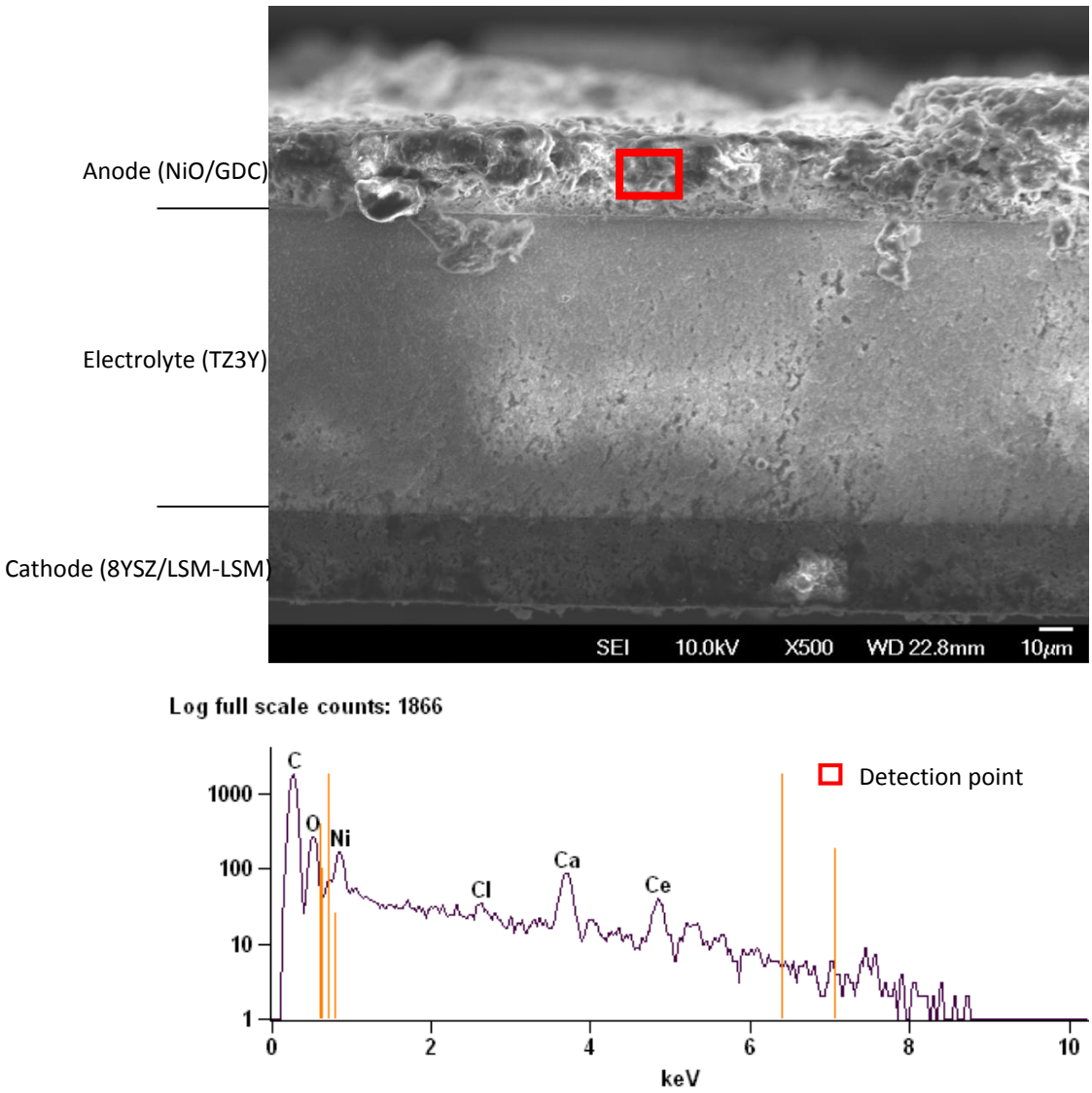

Figure 7-7: SEM image of a cross section of the cell illustrating the anode, electrolyte and cathode layers accompanied by an EDS analysis at the indicated region at the anode showing the presence of carbon.

7.5 CONCLUSIONS

From the experiments carried out we can conclude that the inclusion of toluene as a model tar, at concentrations that one would expect from a fluidised bed gasifier, have no immediate negative impact on the SOFC when using GDC as the anode material. Reasons contributing to this tolerance may include the low utilisation factor employed, the anode material used, as well as the controlled O/C ratio which was kept at ca.1.8. Increasing the utilisation factor along with the tar concentration did however have a large impact on performance which from the results presented can be attributed to high levels of carbon formation and deposition at the anode. This is also supported by post experimental tests using scanning electron microscope (SEM) images and EDS analysis which show substantial levels of carbon deposition at the anode. Interesting that the EDS indicates the presence of Ca and Cl whilst neither of these elements were present in the experiments but the lack of

evidence showing Gd may suggest that these elements have misidentified. As a recommendation to progress this research it would be beneficial to run these experiments with higher utilisation factors in order to identify the cell's sensitivity. Another important conclusion is shown by the VOC analysis at the exhaust that suggests whilst the model tar does undergo reformation that contributes to hydrogen production there is no evidence to suggest the formation of any other hydrocarbon species. The exhaust gas analysis shows that a certain amount of toluene is still present, even under favourable SOFC conditions for the steam reforming, indicating that the conditions are yet to be optimized for better electrical performance.

7.6 ACKNOWLEDGEMENTS

The authors would like to thank the personnel at TU Delft for contributing with support and advice from the initial setup to analysing the final results. This research was funded in part by BRISK, a European Commission Capacities Project in the 7th Framework Programme, along with the Engineering and Physical Sciences Research Council in the UK.

Readers Guide

Overview

1. Introduction

2. The WHHE Concept

3. Literature Digest

4. SOFCs

5. Modelling

6. Modelling Results

7. Experimental Research

8. micro-CHP in the UK Market

- Introduction
- Methodology
- Results and Discussion
  - Whispergen
  - ecoPOWER
  - Bluegen
- Conclusion

9. Conclusions

References

Appendices

8. MICRO-CHP IN THE UK MARKET

NOTE: This chapter is not directly related to the main body of work presented in this thesis but is a result of research carried out for BDSP (the EngD industry sponsor), and as such relates to building services. There are two threads than can be associated with the overall research undertaken which include; the commercial application of SOFCs which will be required to create consumer demand that will drive economies of scale that will reduce manufacturing costs, and also cogeneration of heat and power to provide environmental carbon redustions.

8.1 ABSTRACT

Widespread uptake of decentralized energy production has the potential to reduce carbon emissions whilst making the energy market more affordable, sustainable and robust. The application of micro-CHP systems in the domestic market has the potential to alleviate pressure on the national grid by displacing electrical and heating demands, and also through the export of excess electricity. Initial market support for this has been shown by the UK's Feed-in-tariff scheme which is currently incentivizing efficient micro-CHP systems (<2kW) by providing a financial return for every unit of electrical energy produced and further reward for every unit (kWh) exported to the grid. It is the aim of this research to attempt to identify those m-CHP systems available on the market and to quantify the expected benefits in terms of cost, CO_2 savings and overall energy efficiency when feeding a typical domestic property in the UK. In an attempt to maximize financial income from the FIT scheme an operating strategy of constant supply, at the maximum rated output, is compared against the conventional heat led approach most often used in CHP applications. Overall results indicate that the heat-to-power ratio for a given m-CHP has a direct impact on all of the performance factors being measured and also determines the preferred operating strategy that should be followed.

8.2 INTRODUCTION

Combined heat and power (CHP) systems are designed to utilize the useful heat and electrical energy produced from a single source, and near the point of use. Environmental and economical benefits are a result of reduced fuel consumption and emissions whilst increasing overall energy efficiency. Considering existing centralized energy plants lose two thirds of their energy to the atmosphere, in the form of heat, along with further losses caused by distribution. The advantages of distributed power generation in small decentralized units are becoming ever more apparent. The implementation of CHP systems is actively being promoted in Europe through the Cogeneration Directive 2004/08/EC where the initial objectives were to deliver primary energy savings but has grown in importance as the climate agenda has become more of a concern. By reducing the scale of these systems (~2kWe) these micro-CHP devices can be installed at the point of use within a domestic environment and can be fuelled by conventional natural gas supplies. Producing onsite electricity means centrally generated electricity is displaced and by utilizing the heat produced to

supply domestic hot water and space heating demands further savings in overall gas consumption can be made.

In order for us to fully understand the benefits of such systems it is important to explore the environmental and economic factors that will decide their commercial success. In recognition of the potential to reduce carbon emissions attributed to the households, the UK government is supporting the uptake of m-CHP (<2kW) through the national feed-in-tariff (FIT) scheme which has increased from 11p/kWh to 13.45p/kWh (*DECC, 2012a; EST, 2015*) (at time when all other tariffs have been reduced and the renewable heat incentive (RHI) is taking off). The common technologies used in the category of m-CHP are; internal combustion engines (ICE), Stirling engines, organic Rankine cycle and fuel cells. *Table 8-1* illustrates the various products currently available in the sub-2kW m-CHP market.

Table 8-1: Market summary of available m-CHP systems with their respective performance values.

Brand	Product	Technology	Electrical output kW(eff)	Thermal output kW(eff)	Overall efficiency	Heat-to-power ratio	Fuel
Whisper Tech Limited	WhisperGen	Stirling engine	1.2(12%)	7.8(78%)	90%	6.5	NG
Stirling systems	SEM	Stirling engine	1.2(18%)	5(72%)	90%	4.17	NG
Baxi	Ecogen	Stirling engine	1.1(9%)	10.1(83%)	92%	9.22	NG
Baxi	Innotech	PEMFC	1(32%)	1.8(59%)	91%	1.8	NG
Otag	Lion-powerblock	Rankine engine	2(12%)	16(73%)	85%	8	NG
Energetix Genlec	Kingston	Rankine engine	1(12%)	6.8(78%)	90%	6.8	NG, LPG
Climate Energy	freewatt (Honda)	ICE	1.2(26%)	2.7(59%)	85%	2.25	NG, LPG
Valliant	EcoPOWER (Honda)	ICE	1(26%)	2.5(66%)	92%	2.5	NG, LPG
CFCL	Bluegen	SOFC	1.5(60%)	0.54(25%)	85%	0.36	NG

Natural Gas (NG), Liquid Petroleum Gas (LPG)

Due to their high electrical efficiencies, low noise and gas emissions fuel cells are a very attractive option as residential m-CHP systems. There is now a high temperature fuel cell unit that is commercially available and is accredited under the UK's Micro Generation Scheme (MCS) making this product eligible for the UK feed-in-tariff. This elevates the status of this technology out of the stage of research and development and now faces the challenges associated with new technologies entering into the market.

8.3 METHODOLOGY

This paper will look to evaluate the performance of the products specified in *Table 8-1* whilst supplying a load which is representative of a typical home found in the UK. Electrical and domestic hot water (DHW) loads were obtained from a study carried out by the International Energy Agency Energy Conservation in Buildings and Community Systems (ECBCS) under the title COGEN-SIM and published results are presented in Annex 42 (*IEA, 2012*). The electrical demand profile from the study was obtained from actual readings of a 65m^2 home in Newcastle. The DHW profile represents a 200 l/day consumption rate where values have been obtained from probability functions with the assumption that the temperature of the water is increased by 35°C relative to the inlet feed temperature. Space heating demands have been generated through thermal modelling using TAS software developed by Environmental Design Solutions Limited (*EDSL, 2012*). In order to represent a building similar to that of the property monitored in Newcastle u-values representing pre-1980 domestic constructions were obtained from the National Calculation Method (NCM) as defined by the Department for Communities and Local Government which provides a database of constructions and services for evaluating the performance of a building's energy consumption. Building layouts were obtained using information published by the Energy Savings Trust (EST, 2010a; EST, 2010b) and a floor plan of a typical semi-detached house was used. See *Table 8-2* for a summary of the constructions used for the various building elements and the subsequent thermal properties calculated by the software.

Table 8-2: Description of construction layers and materials applied to various building elements for thermal modelling.

Building Element	Construction layers and materials	u-value (W/m^2.°C)
Ground floor	50mm flooring screed, 10mm insulation, 100mm concrete, 25mm brick slips, underfloor clay	0.849
External wall	102mm brick, 50mm air layer, 100mm brick, 13mm dense plaster	1.287
Internal wall	100mm concrete block, 25mm air layer, 60mm insulation, 13mm plasterboard	0.821
Pitched roof	9.5mm plasterboard, 200mm insulation, 1m loft space, 10mm concrete tiles	0.178
Suspended floor	30mm plywood, 20mm insulation, 35mm air layer, 100mm concrete	0.532
PVC double glazing	PVC frame with two hollow chambers, 4mm clear glass, 6mm air layer, 4mm clear glass	3.297
External door	9mm plywood, 25mm insulation, 9mm plywood	0.755

Figure 8-1 illustrates the annual heating and electrical demand profile for a typical domestic property in the UK. The annual electrical consumption stands at 3,028kWh and the heating demand, divided into DHW and space heating stands at 2,980kWh and 13,425kWh respectively, and in terms of the property the annual contribution from each is 69% towards space heating and 16% and 15% for electrical and DHW respectively. These values are consistent with UK's gas and electricity regulator Ofgem who use typical medium consumption figures of 3,300kWh and 16,500kWh for electricity and gas respectively (*Ofgem, 2011*).

The main objective of this study is to compare the energy, financial and environmental performance of a home with and without the application of a m-CHP system and how incentives such as the UK's FIT scheme can contribute to their widespread uptake.

To do this successfully the performance of this typical home must be identified according to the standard grid efficiency, unit price per kWh for electricity and gas and CO_2 emission factors associated with the consumption of both electricity and gas. For a summary of these values please refer to *Table 8-3*. According to information published by the UK's Department of Energy and Climate Change (DECC) the total primary energy (including renewables) used for the production of electricity in 2012 for the UK was 901.3TWh and the total amount of electricity delivered to the consumer was 320.5TWh (*MacLeay et al., 2012*). This amounts to an overall efficiency of 35.6% for the electricity supplied from the grid.

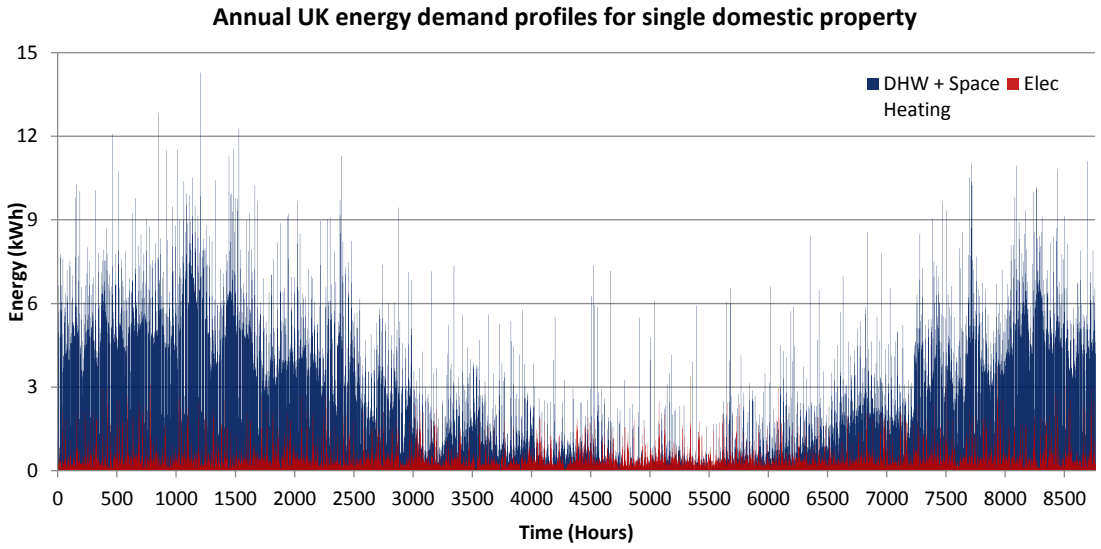

Figure 8-1: The graph represents the annual fluctuations in the heating demand, comprising of the DHW and space heating requirements, as well as the electrical demand for an average domestic property in the UK with a total annual heating demand of 16,406kWh and electrical demand of 3028kWh.

Table 8-3: Information describing the cost and performance of the UK nation grid.

UK Grid		
Electrical Efficiency (%)	35.6	
Average boiler efficiency (%)	79	(*EST, 2012; Hogg, 2012*)
Unit cost for electricity (p/kWh)	14.04	(*DECC, 2015b*)
Unit cost for gas (p/kWh)	4.41	(*DECC, 2015b*)
CO_2 factor for electricity ($kgCO_2/kWh$)	0.5246	(*Carbon Trust, 2011*)
CO_2 factor for gas ($kgCO_2/kWh$)	0.1836	(*Carbon Trust, 2011*)
Gross calorific value for natural gas (MJ/m^3)	39.4	(DECC, 2011)
UK Feed-in-tariff scheme for m-CHP (<2kW)		
Generation (p/kWh)	13.45	(EST, 2015)
Export (p/kWh)	4.85	(EST, 2015)

8.4 RESULTS & DISCUSSION

With this hourly energy information for the building we can begin to analyse the performance of the building and we shall begin by applying the variables set out in *Table 8-3* to describe the financial, environmental and energy performance for the given loads. In comparison we must understand how the m-CHP systems described in *Table 8-1* will influence the values expressed in *Table 8-4*. For this comparison we assume all excess electricity is exported to the grid and excess heat is stored in a hot water storage tank which incurs a heat loss of 10% per hour. The m-CHP system will be installed along with the existing boiler that will be used to cope with any demand that cannot be met by the m-CHP and hot water storage tank, and similarly electricity will be imported to make up for any shortfall in electrical supply. Also, to be considered is the operating strategy of the m-CHP unit as conventional CHP systems are heat led but systems such as the high temperature fuel cell are required to run at a constant supply. So for the purpose of this analysis one representative technology from the above systems will be operated at constant supply and as a comparison will also operate as conventional heat led systems which will give us an opportunity to evaluate the best strategy to adopt in terms of financial payback using the FIT scheme, environmental CO_2 emissions and overall system efficiency.

Table 8-4: Resulting energy bill, CO_2 emissions and system efficiency for a typical UK home.

	Energy bill	Total CO_2 emissions	System Efficiency
Electricity	£ 425	1,589 kg	35.6%
Gas	£ 916	3,012 kg	79.0%
Overall	£1,341	4,601 kg	72.2%

WHISPERGENIt is clear to see that the m-CHP systems with high heat-to-power ratios such as the Stirling engine based Whispergen are far better off operating under the heat led strategy. In terms of meeting the demand and efficiency, illustrated in *Figure 8-2* a) and b), the heat led strategy

enables the unit to meet 99% of the building's heat demand but only 44% of the electrical and allows the unit to maintain a high level of efficiency with the total household efficiency, including imported backup electricity and gas, standing at 85%, as seen in *Table 8-5*. This is supported by the financial analysis, shown in *Figure 8-2* c) and d) which shows that when the Whipsergen is heat led the total grid cost is constantly below the cost expected without the m-CHP unit which will provide an annual financial saving of 42% and an overall CO_2 saving of 16%. During constant supply the unit generates a large amount of heat that cannot be utilized by the building and therefore has a detrimental effect on the system efficiency and operating cost of the unit.

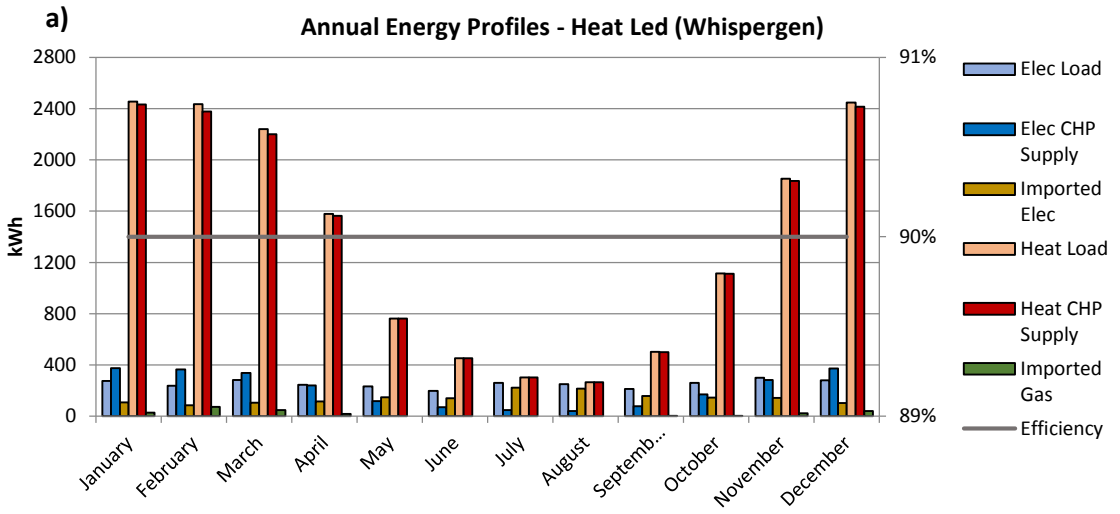

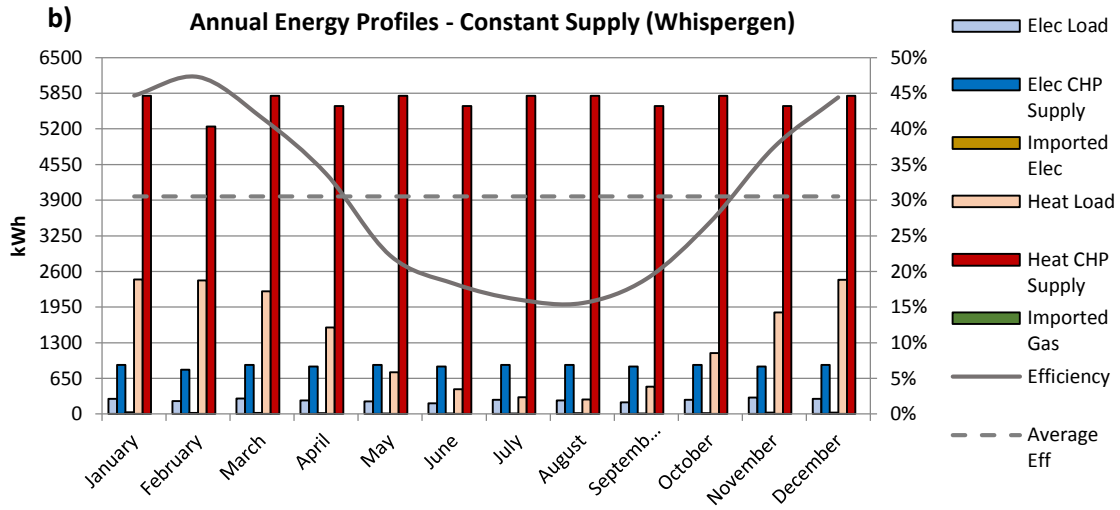

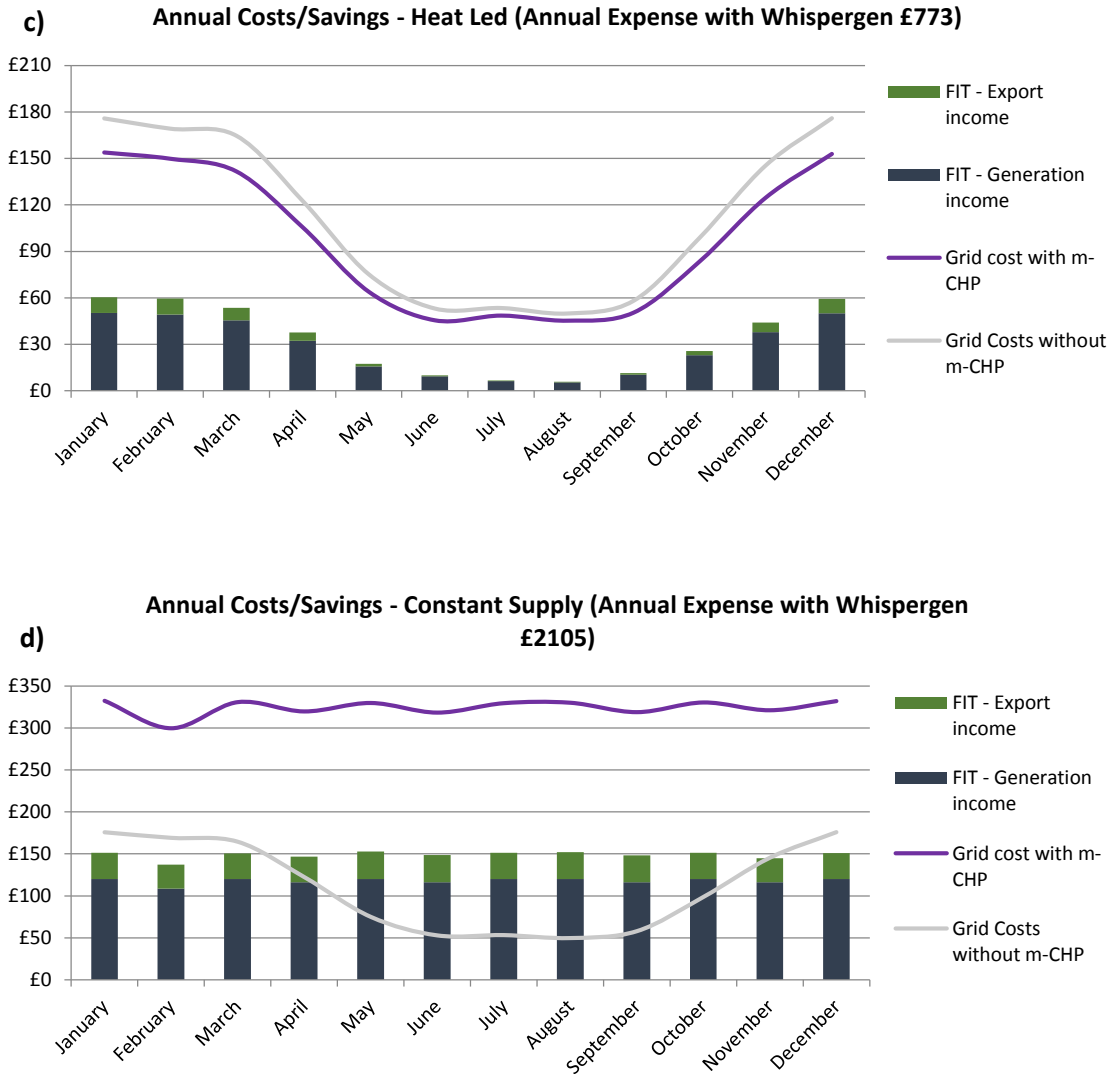

Figure 8-2: Graphs a) and b) illustrate the monthly quantities of demand and supply of the home and Whispergen as well excess energy imported to meet peak demands outside of the m-CHP's rated capacity, the overall monthly system efficiency is also plotted. Graphs c) and d) represent the financial incomes and expenses according to the unit cost of gas and electricity and the UK's FIT scheme with and without the m-CHP.

i) EcoPOWER

The reduced heat-to-power ratio of the ICE EcoPower unit shows a smaller performance gap between heat led and constant operation strategy, seen in *Figure 8-3* a) and b), and the decision on which strategy is most suitable is not clear as the heat led strategy meets only 63% and 60% of the heating and electrical load whilst the constant supply strategy supplies 79% and 91% of the heating and electrical requirements. Also, operating at constant supply the unit indicates a greater financial saving of 81% compared to 60% for the heat led, and the CO_2 savings marginally favour the heat led strategy with a 21% saving compared to 15% for the constant supply. So environmentally the heat led strategy is best but if cost is the main driver the constant supply would be favoured, it is important to mention that these financial benefits are due to the FIT and that without the FIT the heat led strategy would be the best strategy to adopt, as illustrated in *Figure 8-3* c) and d).

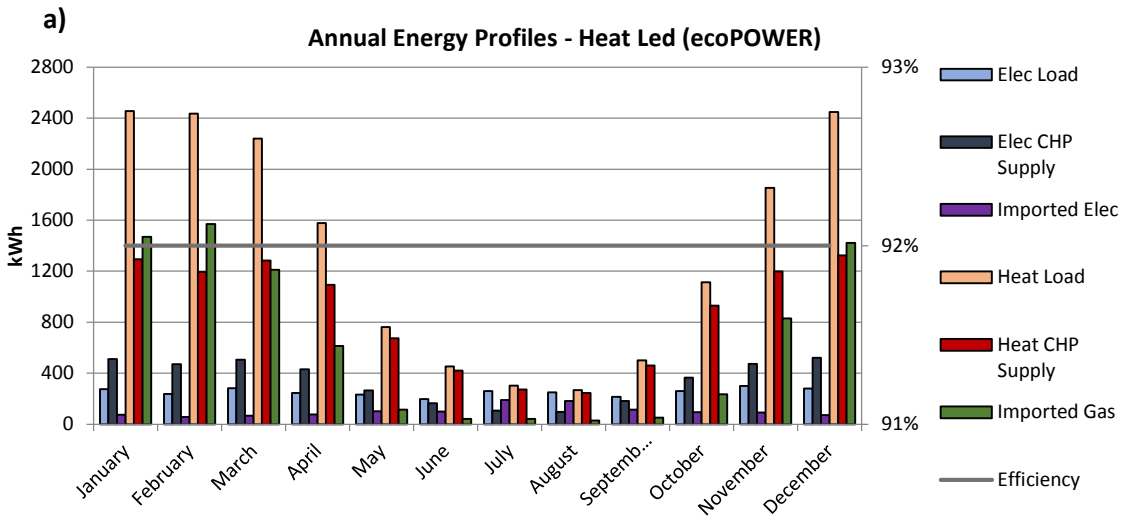

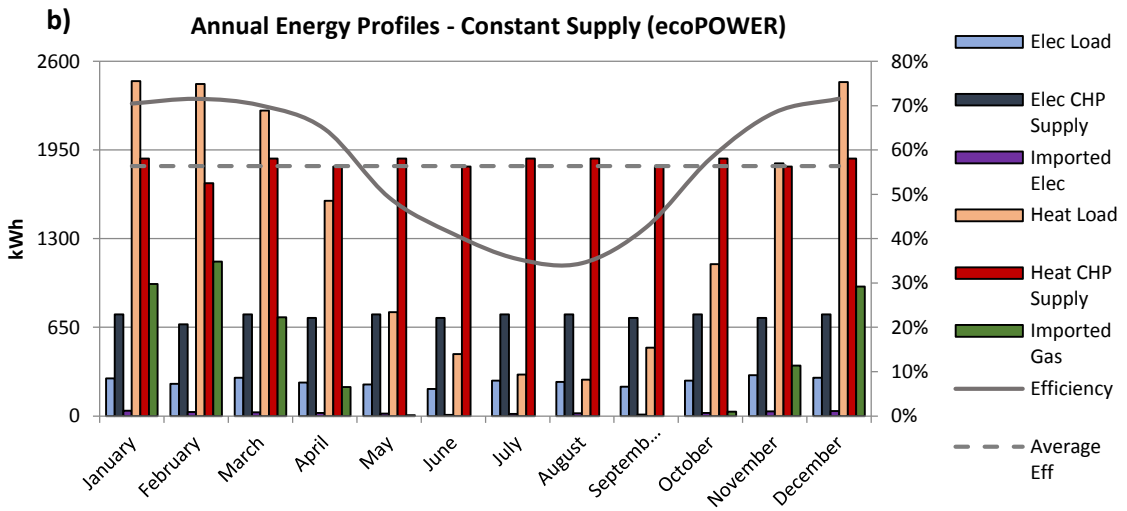

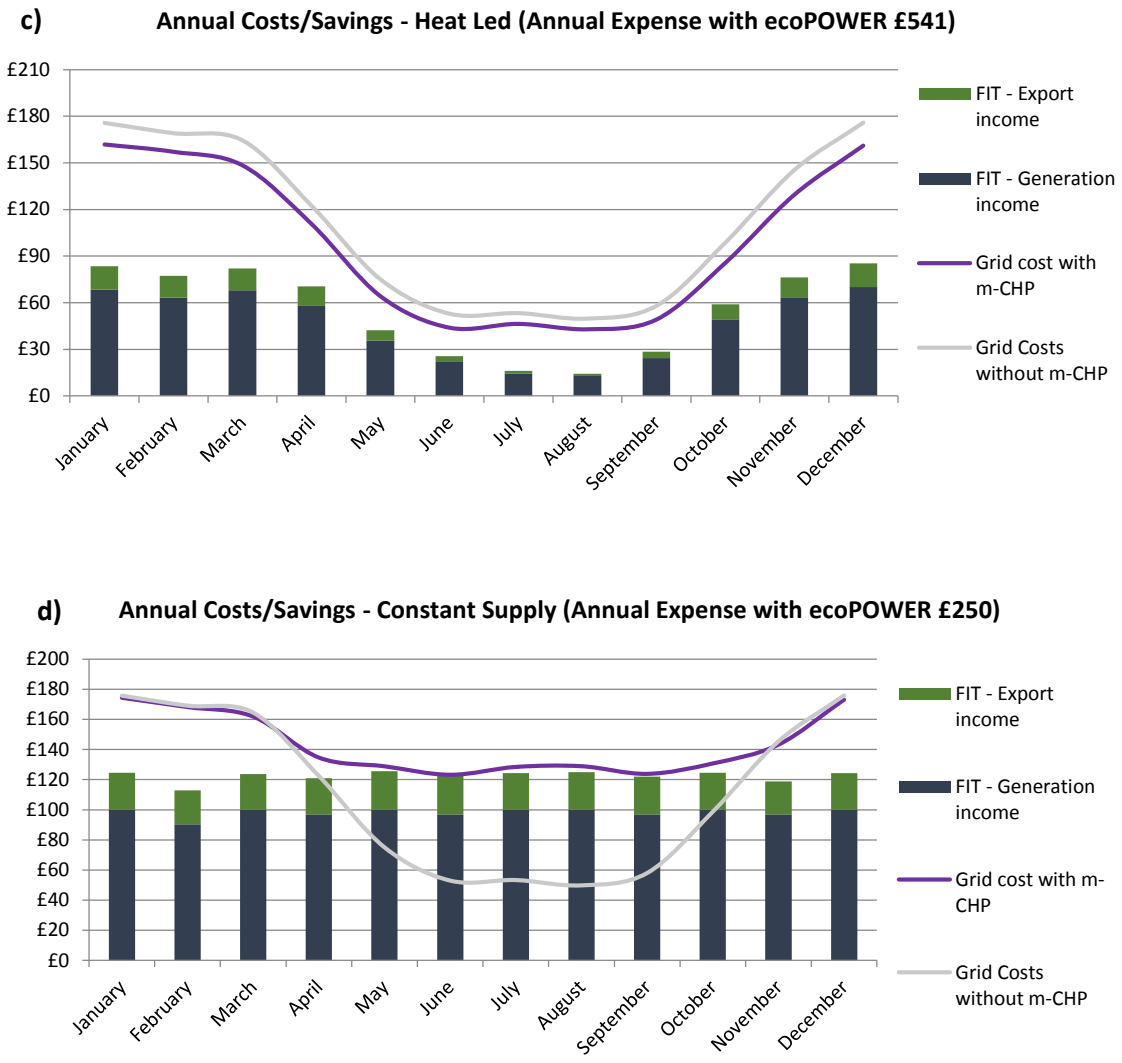

Figure 8-3: Similar to the Whispergen graphs of the EcoPOWER unit displays higher operating efficiency during both heat led and constant supply operating strategy seen in a) and b). This benefit also influences the financial cost of the unit as seen in c) and d) both values are lower than the Whispergen with the constant supply being the most cost effective, although not without the support of the FIT.

ii) BLUEGEN

The high temperature fuel cell Bluegen unit offers the lowest heat-to-power ratio of all the technologies tested and the results in *Figure 8-4* a) indicate a very high level of efficiency throughout the year with an expected drop in the summer where there is insufficient demand for the heat produced. The constant supply of heat only satisfies 28% of the heating demand, which is why an installation of this kind would require a secondary gas boiler or an electric immersion heater providing further heating to the hot water storage tank whilst utilizing the m-CHP's constant electrical output. The unit satisfies 97% of the annual electrical demand and benefits greatly from the FIT scheme as the unit will provide an annual income of £623 which equates to a financial saving of 146%, again this is solely due to the FIT and if we study the grid cost lines in *Figure 8-4* b) it can be seen that without the FIT the unit would cost more to run compared to the existing grid connection. Therefore for this system to be commercially competitive a long term tariff will be

required for the power produced and/or there will need to be an increase in the grid price for electricity. Along with the substantial financial savings Bluegen unit will also provide a CO_2 saving of 36% and an overall household efficiency of 78%.

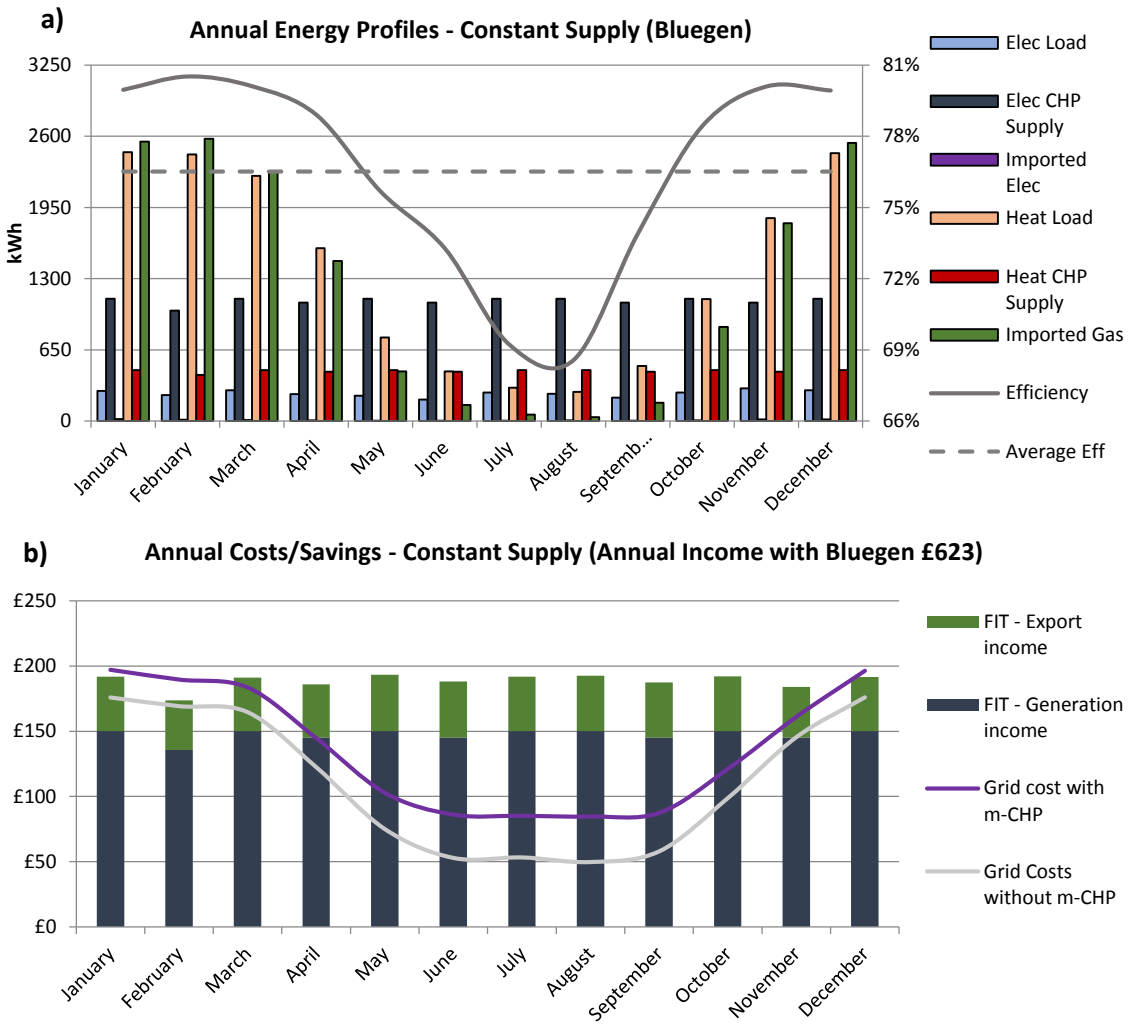

Figure 8-4: The high temperature fuel cell is only measured under constant supply as this is the standard operating procedure used in order to protect the lifespan of the unit. The surplus heat generated over the summer months clearly has an effect on the operating efficiencies and is clearly illustrated in a). In b) we can see the benefit of the increased electrical capacity which results in a financial income owing to the UK's FIT.

Table 8-5: Resulting energy bill, CO_2 savings and efficiency for a typical UK home.

	WHISPERGEN		ECOPOWER		BLUEGEN
	Heat led	Constant	Heat led	Constant	Constant
Gas cost (m-CHP)	£ 918	£3,865	£ 694	£1,486	£ 966
FIT - generation	£ 336	£1,414	£ 550	£1,178	£1,767
FIT - export	£ 56	£ 372	£ 111	£ 291	£ 495
Grid import (Gas&Elec)	£ 248	£ 27	£ 508	£ 233	£ 673
Total cost/income	£ 773	£2,105	£ 541	£ 250	£ 623
CO_2 savings	16%	-74%	21%	15%	36%
Overall household efficiency	85%	31%	83%	61%	78%

Underlined values indicate income rather than expense. Constant indicates the unit operates continually at the maximum rated output.

8.5 CONCLUSIONS

The factors influencing the feasibility of the m-CHP system studied have shown to be the heat-to-power ratio as this has a direct influence on the optimal operating strategy. It can be seen that those m-CHP units with high heat-to-power ratios (identify heat to power ratios in tables) benefit from being heat led as operating costs are reduced, even before accounting for the financial income generated through the FIT, and CO_2 savings are far greater compared to being run at constant supply. Reducing the heat-to-power ratio has shown to have similar cost savings when run as heat led but when including savings generated through the FIT, because more electricity is being produced, overall costs are further reduced. The high temperature fuel cell with its much lower heat-to-power ratio is the only unit which sees a positive income for the year and because of the reduced amount of heat produced can successfully be run at a constant supply resulting in the unit constantly generating income. It is also interesting to note that the percentage of CO_2 savings steadily increases with reduced heat-to-power ratio (explain further). This can be attributed to the difference in grid supplied electrical efficiency and heat supplied by a supplement boiler which in this study operates with a 79% efficiency. By minimizing the heat generated over the summer period with a low heat-to-power ratio losses can be reduced whilst allowing the m-CHP unit to operate at constant supply.

Readers Guide

9. CONCLUSIONS

The aim of this research was to produce a dynamic simulation to test the integration of a SOFC into a gasification cycle to produce an advanced IGFCC that could improve the performance of existing WtE plants, whilst enabling these systems to be located closer to the consumer. The main challenge came from the need to design a bespoke numerical model to simulate the operation of a SOFC running on syngas. As a requirement the numerical model needed to take into account the; mass transport, electrochemical and thermal characteristics of the fuel cell. This was achieved through an extensive literature review of published research as well as understanding of the fundamental principles behind fuel cells and their operation. In line with the ambition to integrate fuel cells in such a way it was decided that further synergies existed with metal hydride hydrogen storage systems and electrolysis and by further integration of these systems an ambitious distributed energy system could be designed. Dubbed the "WHHE Energy Centre" it will be able to; generate hydrogen through gasification and electrolysis to run the fuel cell; store hydrogen (energy) using metal hydrides to enrich the syngas, cover maintenance and allow dynamic following of energy demands; provide heat (from the gasifier and fuel cell) to generate further electricity using a heat engine, supply the demands of the hydrogen storage material, and export to consumers; and the oxygen produced from the electrolyser can be used to feed the demands of the gasifier. Waste by-products such as inert slag and elemental sulphur also have a commercial value and can be used to strengthen the commercial strength of these systems.

Further elaboration into the SOFC led to a review of fuel cell materials and their construction. From understanding how particular materials are brought together to engineer improved performance practical experiments were carried out on a single cell SOFC using a synthesized tar laden syngas. Results from this research culminated in a journal publication providing insight into the performance of a GDC SOFC in a tar rich environment and the reaction pathway of toluene (representative tar).

To better understand the commercial and environmental potential of SOFCs in CHP applications a spreadsheet tool was created to test and compare the performance of varying commercial mCHP systems.

Conclusions from this thesis can be divided into the following sections:

9.1 THE FUTURE OF WASTE-TO-ENERGY

The results presented show that the WHHE Energy Centre can offer considerable advancement of WtE systems by offering:

- Improved overall electrical efficiency of 29.5% which surpasses the industry target of 25% (including MRF energy demands).
- Controlled emissions and plant designs that preclude the need for tall ventilation stacks would make these systems better suited for more central locations where intelligent heat networks can be utilised.
- The ability to export heat as a CHP plant would increase the combined efficiency to 66.4%.

- After extensive recycling (removal of paper and plastic rich in hydrogen) a RDF with reasonable heating value can be produced.
- Employing high temperature plasma ensures a high quality syngas with fewer tars is produced and also means the WHHE Energy Centre can handle almost any waste grade.
- WHHE Energy Centres will not only serve to reduce the need for landfill but can also be used to mine landfill sites containing extremely large amounts of stored waste. Allowing land to be reclaimed and protected against future deposits.
- An onsite hydrogen refuelling station would facilitate the much needed decarbonizing of the transport sector.
- Hydrogen production through electrolysis does not offer an immediate benefit using historical wholesale electricity prices but if connected directly with renewables or when renewables begin to have a bigger impact on wholesale prices the inclusion of an electrolyser will support both the financial and energy storage targets. The inclusion of the electrolyser represents 0.4% of the capital cost and 0.3% of the annual operating costs.

9.2 THE ROLE OF SOFCS IN WTE

The aim of the research and experiments was to better understand the practical limitations of a SOFC operating with a tar laden syngas. Tar products which are commonly produced through gasification have proven to be a major obstacle in the success of gasification systems as the accumulation of tar can lead to sudden stoppages with expensive maintenance routines.

- Experimental results suggest that a SOFC using GDC material at the anode has good resistance to short term tar loading showing favourable operation with syngas with low fuel utilisation factors.
- Important future work should be made to test the cell's sensitivity to fuel utilisation.
- The heat recovered from the gasification process is sufficient to maintain the SOFCs operating temperature.
- The ability for SOFCs to use CO as a fuel source means there can be less requirements to convert CO to CO_2.

9.3 COMBINED HEAT AND POWER

The ability to place energy system closer to the consumer will eneable more effective building-to-building connectivity with distributed energy systems. This will enable low carbon technologies such as the WtE system being researched to be fully exploited enabling strong financial returns on investments. The difficulty when applying such CHP systems is matching supply and demand ratios and because electricity is easily transported (using existing infrastructure) and heat generated through modern boilers can be done very efficiently (ca. 90%) maximising electrical output through low heatto-power ratios proves most beneficial.

- Comparing various CHP units against a common heat and electrical demand show that smaller heat-to-power ratios resulting from improved electrical efficiency have a highly beneficial impact on overall performance and financial returns.
- By reducing the thermal output and installing hot water storage cylinders CHP units can be sized larger thereby improving environmental benefits.
- SOFCs with the improved electrical efficiencies compared to conventional combustion engines have great potential to contribute to the domestic CHP market.
- SOFCs offer great potential for cost effective energy and lower CO_2 emissions when applied as residential m-CHP systems in line with the UK's FIT incentive scheme.

From the understanding that society's reliance on fossil fuel has escalated dramatically over the past century and that our ever increasing demand for energy continues we will soon have to find alternative and more sustainable sources of energy. Whilst at the same time the global population is becoming more urbanised and strives to become more affluent the waste we produce and dispose of increases too. Therefore answering these questions with a single approach as discussed in this thesis becomes more obvious.

The WHHE Energy Centre investigated in this thesis does have many challenges to overcome if it is to contribute to the future energy mix as existing WtE systems using successful incineration methods do exist and are widely used. With results showing the potential to provide healthy financial returns along with reduced GHG emission the WHHE Energy Centre must be a contender for a place in the future energy landscape and the challenges that are expected (i.e. balancing grid demand and supply dynamics). Promoting hydrogen energy systems will also help the ongoing struggle to decarbonise the transport sector by providing a feasible and environmentally friendly supply of hydrogen for upcoming fuel cell electric vehicles.

9.4 RECOMMENDATIONS

Moving forward there are number aspects of this research that would benefit from progressing the views expressed in this thesis with further scope to discover new knowledge. Some easily identifiable topics may include:

- Gasifications solutions that are designed to produce tar-free syngas which would be suitable for fuel cell integration. Gasification using microwave plasma technology has shown good potential in this area.
- With an isolated supply of carbon dioxide there would be many environmental benefits to investigating the potential to sequestrate this carbon dioxide by either processing the gas to produce a usable byproduct or by putting the gas into the ground for storage. May other solutions may also provide viable alternatives.
- There is great scope to increase our understanding the performance of SOFCs running on syngas as the affect of the numerous contaminants is not fully understood.

- The integration of SOFCs with gas turbines is of great interest and offers many benefits and further research is required to optimise the integration.
- As with all low carbon energy systems it is important to understand not only their financial return on investments but also their energy and carbon payback periods. This in itself would require a substantial amount of research.
- Solid state hydrogen technology and the various materials being used are sensitive to their environments and if they are to used in energy systems as described in this research more work must be done to understand their longterm stability and their sensitivity to contaminants.

This research in itself would benefit from a more in depth analysis of some of the energy systems where assumptions have been made to simplify the amount of work required over the four year period.

The next major contribution to knowledge will come from building and testing the hypotheses that have been proposed in this thesis from which more questions can be answered.

REFERENCES

Akiba E., 2010. *Research and Development of hydrogen storage materials in Japan – From fundamentals to applications*. AIST. Sourced online at: http://www.cosy-net.eu/Downloads/NESSHY-COSY-Final_10-10-05-06_Akiba.pdf

Andersson M., Yuan J., Sunden B., 2011. *SOFC modelling considering electrochemical reactions at the active three phase boundary*, International Journal of Heat and Mass Transfer 55 773-788 (2012).

APP, 2012. *Advanced Plasma Power, Process Overview*. Sourced online at: [www. http://advancedplasmapower.com].

APX, 2012. *UKPX Auction Historical Date*. Sourced online at: [http://www.apxendex.com/].

Aravind P.V., Ouweltjes J.P., Woudstra N., Rietveld G., 2008. *Impact of biomass derived contaminants on SOFCs with Ni/Gadolinia-doped ceria anodes*. Electrochemical and Solid State Letters 11, B24-B28.

Aravind P.V., Woudstra T., Woudstra N., Spliethoff H., 2008. *Thermodynamic evaluation of small-scale systems with biomass gasifiers, solid oxide fuel cells with Ni/GDC anodes and gas turbines*. Journal of Power Sources 190 (2), 461-475, (2009).

Asadullah M., Miyazawa T., ichi Ito S., Kunimori K., Yamada M., Tomishige K., 2004. *Gasification of different biomasses in a dual-bed gasifier system combined with novel catalysts with high energy efficiency*. Applied Catalysis A: General 267, 95 – 102.

Badwal S., Ciacchi F., Milosevic D., 2000. *Scandia-zirconia electrolytes for intermediate temperature solid oxide fuel cell operation*. Solid State Ionics 136-137, 91-99.

Bakas I., Sieck M., Hermann T., Andersen F., Larsen H., 2011. *Projection of Municipal Waste Management and Greenhouse Gases*. European Environment Agency ETC/SCP 2011.

Bang-Moller C., Rokni M., Elmegaard B., 2011. Exergy analysis and optimisation of a biomass gasification, solid oxide fuel cell and micro gas turbine hybrid system. Energy 36, 4740-4752.

Bhavanam A. and Sastry R.C., 2011. *Biomass Gasification Processes in Downdraft Fixed Bed Reactors: A Review*. International Journal of Chemical Engineering and Applications 2, 425-433

Bockris J. O'M., Reddy A. K. N., Gamboa-Aldeco M., 2002. Modern Electrochemistry – Volume 2A, 2nd edition, Fundamentals of Electrodics. Kluwer Academic Publishers, ISBN: 0-306-46166-8.

Bove R. (Ed), Ubertini S. (Ed), 2008. *Modeling Solid Oxide Fuel Cells*, Springer 2008.

Bram M., Reckers S., Drinovac P., Monch J., Steinbrech R. W., Buchkremer, H. P., Stover D., 2004. *Deformation behavior and leakage tests of alternate sealing materials for SOFC stacks.* Journal of Power Sources 138, 111-119.

Brinkman N., Wang M., Weber T., Darlington T., 2005. *Well-to-Wheels Analysis of Advanced Fuel/Vehicle Systems — A North American Study of Energy Use, Greenhouse Gas Emissions, and Criteria Pollutant Emissions*. Office of Energy Efficiency and Renewable Energy. Sourced online at: http://www1.eere.energy.gov/bioenergy/pdfs/well_to_wheels_analysis.pdf.

Burr B., Lyddon L., 2014. *A comparison of physical solvents for acid gas removal*. Bryan Research and Engineering, Inc., USA. Sourced online at: [http://www.bre.com/portals/0/technicalarticles/a%20comparison%20of%20physical%20solvesol%20for%20acid%20gas%20removal%20revised.pdf].

Byun Y., Cho M., Chung J. W., Namkung W., Lee H. D., Jang S. D., Kim Y.-S., Lee J.-H., Lee C.-R., Hwang, S.-M., 2011. *Hydrogen recovery from the thermal plasma gasification of solid waste*. Journal of Hazardous Materials 190, 317 – 323.

Carbon Trust, 2011. *Conversion factors – Energy and carbon conversions 2011 update*. Sourced online at: [http://www.carbontrust.com/resources/guides/carbon-footprinting-and-reporting/conversion-factors].

CFCL, 2009. CFCL generator achieves 60% efficiency, Fuel Cells Bulletin, Volume 2009, Issue 4, ISSN 1464-2859.

Chapman C., Taylor R., Ray R., 2010. *The Gasplasma™ process: its application in Enhanced Landfill Mining*. 1st International Symposium on Enhanced Landfill Mining, Houthalen-Helchteren, 4-6 October 2010.

Chemstation, 2014. Chemcad, version 6.5. Available at: [http://www.chemstations.com/Downloads/].

Chester, M., Stupples, D. and Lees, M., 2008. *A comparison of the physical and chemical composition of UK waste streams based on hypothetical compound structure.* 13th European Biosolids and Organic Resources Conference, 10-12 November, Manchester.

Chiba, R., Takeshi K., Himeko O., Hiroaki T., Kazuhiko N., Hajime A., 2008. *An SOFC Cathode Composed of $LaNi_{0.6}Fe_{0.4}O_3$ and Ce(Ln)O2 (Ln= Sm, Gd, Pr)*. Journal of the Korean Ceramic Society 45, 12, 766-771.

CIWM, 2003. *Energy from Waste: A good practice guide*. IWM Business Service Ltd., The Chartered Institution of Wastes Management.

Coll R., Salvado J., Farriol X., Montane D., 2001. *Steam reforming model compounds of biomass gasification tars: conversion at different operating conditions and tendency towards coke formation*. Fuel Processing Technology 74 (2001) 19-31.

Core Technology Venture Services: *2010 Report on the European Transport H2 Refuelling Infrastructure.* Sourced online at: [www.coretecventures.com/press/] accessed Nov 2011.

Costamagna P., Selimovic A., Del Borghi M., Agnew G., 2003. *Electrochemical model of the integrated planar solid oxide fuel cell (IP-SOFC)*. Chemical Engineering Journal 102 61-69 (2004).

Council of Europe, 2007. *Report: Management of municipal solid waste in Europe*. Committee on the Environment, Agriculture and Local and Regional Affairs, Doc. 11173.

Coutelieris F.A., Douvartzides S., Tsiakaras P., 2003. *The importance of the fuel choice on the efficiency of a solid oxide fuel cell system*. Journal of Power Sources 123 (2), 200-205.

CRES, 2011. *CRES wind-hydrogen experimental plant*. Sourced online at: [http://www.creswindfarm.gr/site1/H2_prod_en.htm].

Da Rosa A.V., 2009. *Fundamentals of Renewable Energy Processes*, second edition. Academic Press, Elsevier, USA.

Davidson R., 1999. *Experience of cofiring waste with coal*. IEA Coal Research 1999, ISBN 92-9029-322-5.

Daza C.E., Kiennemann A., Moreno S., Molina R., 2009. *Dry reforming of methane using Ni–Ce catalysts supported on a modified mineral clay*. Applied Catalysis A: General 364, 65-74.

de Rango P., Chaise A., Charbonnier J., Fruchart D., Jehan M., Marty Ph., Miraglia S., Rivoirard S., Skryabina N., 2007. *Nanostructured magnesium hydride for pilot tank development*. Journal of Alloys and Compounds 446-447, 52-57.

DECC, 2011. *Carbon Emission Factors and Calorific Values from the UK Greenhouse Gas Inventory (AEA, 2011) to Support the EU ETS*. https://www.gov.uk/government/uploads/system/uploads/attachment_data/file/41785/5642-carbon-emission-factors-cvs-2011.xls

DECC, 2012a. *Providing certainty for Feed-in Tariffs and the Renewable Heat Incentive*. Department of Energy and Climate Change. Sourced online at: http://www.decc.gov.uk/en/content/cms/news/pn12_085/pn12_085.aspx].

DECC, 2012b. A National Statistics Publication - Quarterly energy prices. Department of Energy and Climate Change. Sourced online at:

[https://www.gov.uk/government/uploads/system/uploads/attachment_data/file/65940/7341-quarterly-energy-prices-december-2012.pdf].

DECC, 2013. *UK Greenhouse Gas Emissions: Performance against emissions reduction targets*. DECC, UK Greenhouse Gas Statistics & Inventory Team. Sourced online via: [https://www.gov.uk/government/uploads/system/uploads/attachment_data/file/211907/Progress_towards_targets_2012_provisional_figures.pdf].

DECC, 2013b. *2013 UK Greenhouse Gas Emission, Provisional Figures and 2012 UK Greenhouse Gas Emissions, Final Figures by Fuel Type and End-User*. Department of Energy and Climate Change. Sourced online at: [https://www.gov.uk/government/uploads/system/uploads/attachment_data/file/295968/20140327_2013_UK_Greenhouse_Gas_Emissions_Provisional_Figures.pdf].

DECC, 2015a. *UK progress towards GHG emissions reduction targets*. Department for Energy and Climate Change. Sourced online at: [https://www.gov.uk/government/uploads/system/uploads/attachment_data/file/414241/20150319_Progress_to_emissions_reductions_targets_final.pdf].

DECC, 2015b. *Annual domestic energy bills. Department of Energy and Climate Change*. Sourced online at: [https://www.gov.uk/government/statistical-data-sets/annual-domestic-energy-price-statistics].

DECCW NSW, 2010. *Appendix 7 – Assumption, Collection, treatment, material recovery and energy assumptions, Environment benefits of recycling*. Department of Environment, Climate Change and Water NSW, Sydney.

DEFRA, 2013. *Energy from Waste: A guide to the debate*. Sourced online at: https://www.gov.uk/government/uploads/system/uploads/attachment_data/file/221042/pb13892-energy-from-waste.pdf.

DEFRA, 2013. *Forecasting 2020 Waste Arisings and Treatment Capacity*. Sourced online at: https://www.gov.uk/government/uploads/system/uploads/attachment_data/file/251567/pb13883-forecasting-2020-waste-arisings-131017.pdf.

Dehouche Z., Grimard N., 2006. *Nanocomposite materials for hydrogen storage*. Chapter on New Nanotechnology Research, Nova Science Publishers.

Dehouche Z., Lafi L., Grimard N., Goyette J., Chahine R., 2005. *The catalytic effect of single-wall carbon nanotubes on the hydrogen sorption properties of sodium alanates*. Nanotechnology 16 (4) : 402- 409.

Dehouche Z., Peretti H.A., Hamoudi S., Yoo Y., Belkacemi K., 2008. *Effect of activated alloys on hydrogen discharge kinetics of MgH_2 nanocrystals*. Journal of Alloys and Compounds 455 (1-2): 432- 439.

Dehouche, Z., Peretti, H.A., Yoo, Y., Belkacemi, K. and Goyette, J., 2009. *Catalyzed light hydride nanomaterials embedded in a micro channels hydrogen storage container*. Recent Patents on Nanotechnology 3 (2) : 116- 134.

Dehouche, Z., Savard, M., Laurencelle, F. and Goyette, J., 2005. *Ti-V-Mn based alloys for hydrogen compression system*. Journal of Alloys and Compounds 400 (1-2) : 276- 280.

DHC+ Technology Platform, 2009. District Heating & Cooling: A vision towards 2020-2030-2050.

Dohogne J., 2014. *Inventory of good practices regarding (bio)-waste minimization in Europe*. Miniwaste.eu. Sourced online at: [http://www.miniwaste.eu/mediastore/fckEditor/file/Miniwaste_good_practices_inventory.pdf].

Dornheim M., 2011. *Thermodynamics of Metal Hydrides: Tailoring Reaction Enthalpies of Hydrogen Storage Materials, Thermodynamics - Interaction Studies - Solids, Liquids and Gases*, Dr. Juan Carlos Moreno Pirajan (Ed.), ISBN: 978-953-307-563-1, InTech, DOI: 10.5772/21662. Available from: http://www.intechopen.com/books/thermodynamics-interaction-studies-solids-liquids-and-gases/thermodynamics-of-metal-hydrides-tailoring-reaction-enthalpies-of-hydrogen-storage-materials.

Douvartzides S.L., Coutelieris F.A., Demin A.K., Tsiakaras P.E., 2003. *Fuel options for solid oxide fuel cells: a thermodynamic analysis*. AIChE J. 49 (1), 2003, 248–257.

E4Tech, 2009. *Review of Technologies for Gasification of Biomass and Wastes: Final Report*. NNFC Project 09/008.

EB Nationwide, 2004. *Variation in the composition of Household Collected Waste*. EB Nationwide (shanks first fund).

EC, 2004. *European Hydrogen and Fuel Cell Projects*. European Commission: Community research, European Communities. ISBN: 92-894-8003-3.

EC COM 109, 2011. *Energy Efficiency Plan 2011*. EC Communication COM(2011) 109 final.

EC COM 519, 2009. *Investing in the Development of Low Carbon Technologies (SET-Plan)*. EC Communication COM (2009) 519 final.

EC COM 571, 2011. *Roadmap to a Resource Efficient Europe*. EC Communication COM(2011) 571 final.

EC COM 639, 2010. *Energy 2020: A strategy for competitive, sustainable and secure energy*. EC Communication COM (2010) 639

EC COM 677, 2010. *Energy infrastructure priorities for 2020 and beyond – A Blueprint for an integrated European energy network*. EC Communication COM(2010) 677 final.

EC Environment, 2012. *EC Environment: Waste*. Sourced online at: http://ec.europa.eu/environment/waste/index.htm

EC EUR, 2003. *Hydrogen Energy and Fuel Cells: A vision of our future*. EC Directorate General for Research, document EUR 20719 EN.

EC, 2008. *European Energy and Transport: Trends to 2030 – Update 2007*. Directorate-General for Energy and Transport.

EDSL, 2012. Tas (version 9.2.1). *Environmental Design Solution*. Sourced online at: [http://www.edsl.net].

Eguchi K., Kojo H., Takeguchi T., Kikuchi R., Sasaki K., 2002. *Fuel flexibility in power generation by solid oxide fuel cells*. Solid State Ionics 152–153.

EIA, 2013. *U.S. Energy Information Administration*. Sourced online at: [http://www.eia.gov].

El-Emam R.S., Dincer I., Naterer G.F., 2011. *Energy and exergy analysis of an integrated SOFC and coal gasification system*. International Journal of Hydrogen Energy 37 1689-1697.

ENV18, 2013. *Local authority collected waste: annual results tables*. Sourced online at: [https://www.gov.uk/government/publications/local-authority-collected-waste-management-annual-results].

EPRI, 2010. *Electric Energy Storage Technology Options: A White Paper Primer on Applications, Costs, and Benefits*. EPRI, Palo Alto, CA.

e-roc, 2014. *Track Record*. Home website: www.e-roc.co.uk. Sourced online via: [http://www.e-roc.co.uk/trackrecord.htm].

ESA, 2014. *Pumped Hydroelectric Storage*. Energy Storage Association. Sourced online via: [http://energystorage.org/energy-storage/technologies/pumped-hydroelectric-storage].

EST, 2010a. *EST House types comparison complete set*. Energy Saving Trust. Sourced online at: [http://www.energysavingtrust.org.uk/].

EST, 2010b. *Fabric first - Focus on fabric and services performance to increase energy performance in new homes*. Energy Saving Trust. Sourced online at: [http://www.energysavingtrust.org.uk/].

EST, 2012. *Saving assumptions for the Free lunch project*. Energy Saving Trust. Sourced online at: [http://www.energysavingtrust.org.uk/].

EST, 2015. *Feed-in Tariff Scheme*. Energy Saving Trust. Sourced online at: [http://www.energysavingtrust.org.uk/].

Euroheat & Power, 2009. *District Heating and Cooling – 2009 Statistics*. DHC & Statistics, Euorheat & Power. Sourced online via: [http://www.euroheat.org/DHC---Statistics-4.aspx].

Euroheat & Power, 2011. *District Heating in Buildings*. Euroheat & Power, Brussels, Belgium.

Europa, 2010. *Brochure – Being wise with waste: the EU's approach to waste management*. European Union, Luxembourg, 2010. Sourced online at: [http://ec.europa.eu/environment/waste/pdf/WASTE%20BROCHURE.pdf].

Europa, 2011: *Waste management – Packaging and packaging waste*. Last update 08/09/2011. Sourced online at: [http://europa.eu/legislation_summaries/environment/waste_management/l21207_en.htm, May 2014].

Eurostat, 2009. *Municipal waste generation and treatment, by type of treatment method*. Sourced online via: [http://epp.eurostat.ec.europa.eu/portal/page/portal/waste/key_waste_streams/municipal_waste].

Eurostat, 2010. *Municipal waste management in the EU*. Sourced online via: [http://epp.eurostat.ec.europa.eu/portal/page/portal/waste/key_waste_streams/municipal_waste].

Eurostat, 2012. *Treatment of waste*. Sourced online via: [http://appsso.eurostat.ec.europa.eu/nui/show.do].

Fagbemi L., Khezami L., Capart R., 2001. *Pyrolysis products from different biomasses: application to the thermal cracking of tar*. Applied Energy 69, 293-306.

Fergus J.W., 2004. *Lanthanum chromite-based materials for solid oxide fuel cell interconnects*. Solid State Ionics 171, 1-15.

Fergus J.W., 2005. *Metallic interconnects for solid oxide fuel cells*. Materials Science and Engineering: A, 397, 271-283.

Fichtner Consulting Engineers, 2004. *The Viability of Advanced Thermal Treatment of MSW in the UK, ETSET Report*. ETSET, 2004. Sourced online via: [http://www.esauk.org/reports_press_releases/esa_reports/thermal_treatment_report.pdf].

Finnerty C.M., Ormerod R.M., 2000. I*nternal reforming over nickel/zirconia anodes in SOFCs operating on methane: influence of anode formulation, pre-treatment and operating conditions.* Journal of Power Sources 86, 390-394.

Florez-Escobar W.F., Brebbia C.A., Chejne F., Mondragon F., 2015. *Energy and Sustainability VI*. WIT Press, ISBN: 978-1-84564-944-9.

FOE, 2009. *Briefing: Recycling collections – source separated or comingled*? Friends of the Earth. Sourced online via: [http://www.foe.co.uk/sites/default/files/downloads/recycling_collections.pdf].

Fuel Cells Bulletin, 2011. *Waste-to-energy plant in Korea using Ballard fuel cells to power grid*. Fuel Cells Bulletin, Volume 2011, Issue 11, November 2011.

Galeno G., Minutillo M., Perna A., 2011. *From waste to electricity through integrated plasma gasification/fuel cell (IPGFC) system*. International Journal of Hydrogen Energy 36, 1692-1701.

Glosfume, 2013. *Brochure – Hot Gas Filtration*. Sourced online at: http://www.glosfumebrochures.co.uk/oct13_hgf/01.html#1

Gov.uk, 2013. *Calculating Renewable Obligation Certificates, RO banding*. Sourced online via: [https://www.gov.uk/government/uploads/system/uploads/attachment_data/file/211292/ro_banding_levels_2013_17.pdf].

Grol E., 2009. *Technical Assessment of an Integrated Gasification Fuel Cell Combined Cycle with Carbon Capture*. Energy Procedia 1 4307-4313.

Guinea D.M., Martὶn D., Garcὶa-Alegre M.C., Guinea D., Agila W.E., 2010. *Extensive Analysis of Hydrogen Costs*. Proceedings of the 18th World Hydrogen Energy Conference 2010 - WHEC 2010, ISBN: 978-3-89336-655-2.

H2Mobility, 2011. *H2Mobility.Org: Hydrogen Vehicles Worldwide*. Sourced online at: [www.netinform.net/H2/H2Mobility/Default.aspx].

Haga K., Adachi S., Shiratori Y., Itoh K., Sasaki K., 2008. *Poisoning of SOFC anodes by various fuel impurities*. Solid State Ionics 179, 1427-1431.

Han J., Kim H., 2008. *The reduction and control technology of tar during biomass gasification/pyrolysis: An overview*. Renewable and Sustainable Energy Reviews 12, 397-416.

Harper CA. (2001). *Handbook of Ceramics*, Glasses and Diamonds. McGraw-Hill.

Hasler P., Nussbaumer Th., 1999. *Gas cleaning for IC engine applications from fixed bed biomass gasification*. Biomass and Bioenergy 16, 385-395.

Hauth M., Lerch W., Konig K., Karl J., 2011. *Impact of naphthalene on the performance of SOFCs during operation with synthetic wood gas.* Journal of Power Sources 196, 7144-7151.

He M., Liu S., Guo X., Luo S., Xu Z., Feng Y., Hu Z., 2008. *Hydrogen-rich gas from catalytic steam gasification of municipal solid waste (MSW): Influence of steam to MSW ratios and weight hourly space velocity on gas production and composition*. International Journal of Hydrogen Energy 34 2174-2183 (2009).

Heung L.K., 2003. *Report: Using metal hydrides to store hydrogen*. Savannah River Technology Center, USDOE Contract Number DE-AC09-09SR18500.

Hewitt G., Shires G., Polezhaev I.(eds), 1997. *International encyclopaedia of heat and mass transfer*. CRC Press, 1997.

HFP Europe, 2007. *Implementation plan – Status 2006*. European Hydrogen & Fuel Cell Technology Platform. Sourced online via: [http://ec.europa.eu/research/fch/pdf/hfp_ip06_final_20apr2007.pdf].

Higman C., van der Burgt M., 2003. *Gasification*. Burlington, Elsevier Science.

Hofmann P., Panapoulos K.D, Fryda L., Schweiger A., Ouweltjes J.P., Karl J., 2007. *Integrating biomass gasification with solid oxide fuel cells: Effect of real product gas tars, fluctuations and particulates on Ni-GDC anode*. International Journal of Hydrogen Energy 33, 2834-2844.

Hofmann P., Schweiger A., Fryda L.E., Panopoulos K.D., Hohenwarter U., Bentzen J.D., Ouweltjes J.P., Ahrenfeldt J., Henriksen U., Kakaras E., 2007. *High temperature electrolyte supported Ni-GDC/YSZ/LSM SOFC operation on two-stage Viking gasifier product gas*. Journal of Power Sources 173, 357-366.

Hofmann Ph., Panapoulos K.D, Aravind P.V., Siedlecki M., Schweiger A., Karl J., Ouweltjes J.P., Kakaras E., 2009. *Operation of solid oxide fuel on biomass product gas with tar levels > 10 h* Nm^{-3}. International Journal of Hydrogen Energy 34, 9203-9212.

Hogg E., 2012. T*echnical Document - MAC Curves for the Domestic and Non-Domestic Building Sectors*. Committee on Climate Change.

Huang S., Feng S., Wang H., Li Y., Wang C., 2011. $LaNi_{0.6}Fe_{0.4}O_3$-$Ce_{0.8}Sm_{0.2}O_{1.9}$*-Ag composite cathode for intermediate temperature solid oxide fuel cells.* International Journal of Hydrogen Energy 36, 10968-10974.

HyWays, 2013. *The HyWays project*. Sourced online via: [www.hyways.de].

IEA, 2010. *International Energy Agency Advanced Fuel Cells, Implementing Agreement – Annual Report*. IEA Advanced Fuel Cells Executive Committee. Sourced online via: [http://www.ieafuelcell.com/documents/AnnualReport2010_v4.pdf].

IEA, 2012. *The ECBCS Research Programme*. IEA Energy Conservation in Buildings & Community Systems. Sourced online at: [http://www.ecbcs.org/annexes/index.htm].

IEA, 2012b. *International Energy Agency Advanced Fuel Cells, Implementing Agreement – Annual Report*. IEA Advanced Fuel Cells Executive Committee. Sourced online via: [http://www.ieafuelcell.com/documents/AnnualReport2012.pdf].

IIASA, 2012. *The Global Energy Assessment: Toward a Sustainable Energy Future*. Sourced online via: [http://www.iiasa.ac.at/web/home/about/achievments/scientificachievementsandpolicyimpact/Sustainable.en.html].

Ikebe T., Muroyama H., Matsui T., Eguchi K., 2010. *Fabrication of Redox Tolerant Anode with an Electronic Conductive Oxide of Y-Doped $SrTiO_3$*. Journal of Electrochemical Society, 157, B970-B974.

Incropera F., 2011. *Fundamentals of Heat and Mass Transfer*. John Wiley & Sons, ISBN 0470501979.

ITM, 2012. *Update on Hydrogen Cost Structure*. Sourced online via: [http://www.itm-power.com/news-item/update-on-hydrogen-cost-structure/].

Jaya A., 2013. *Air separation units – Engineering design guide*. KLM Technology Group. Sourced online via: [http://kolmetz.com/pdf/EDG/ENGINEERING_DESIGN_GUIDELINE_Air_Separation_Units_Rev01web.pdf].

Jeangros Q., Hansen T., Wagner J., Damsgaard C., Dunin-Borkowski R., Hebert C., Van herle J., Hessler-Wyser A., 2013. *Reduction of nickel oxide particles by hydrogen studied in an environmental TEM*. Journal of Materials Science, Springer US, 48, 2893-2907.

Jepsen J., Bellosta von Colbe J.M., Klassen T., Dornheim M., 2012. *Economic potential of complex hydrides compared to conventional hydrogen storage systems*. International Journal of Hydrogen Energy 37, 4204-4214.

Jiang S.P., 2008. *Development of lanthanum strontium manganite perovskite cathode materials of solid oxide fuel cells: a review*. Journal of Material Science 43, 6799-6833.

Jiang S.P., Chan S.H., 2004. *A review of anode materials development in solid oxide fuel cells*. Journal of Material Science 39, 4405-4439.

Jones A., Nesaratnam S., Porteous A., 2008. *The Open University Household Waste Study: Key findings from 2008*. Defra, August 2008.

Khartchenko N.V., Kharchenko V.M., 2013. *Advanced Energy Systems, Second Edition*. CRC Press, ISBN: 9781482216882.

Kharton V.V., Marques F.M.B., Atkinson A., 2004. *Transport properties of solid oxide electrolyte ceramics: a brief review*. Solid State Ionics 174, 135-149.

Kim S., Yoon S., Nam S., Hyun S., Hong S., 2002. *Fabrication and characterization of a YSZ/YDC composite electrolyte by a sol-gel coating method*. Journal of Power Sources 110, 222-228.

Kojima Y., Kawai Y., Haga T, 2006. *Magnesium-based nano-composite materials for hydrogen storage*. Journal of Alloys and Compounds 424, 294-298.

Komatsu T., Yoshida Y., Watanabe K., Chiba R., Taguchi H., Orui, H., Arai H., 2010b. D*egradation behavior of anode-supported solid oxide fuel cell using LNF cathode as function of current load*. Journal of Power Sources 195, 5601 - 5605.

Komatsu Y., Kimijima S., Szmyd J.S., 2010. *Performance analysis for the part-load operation of a solid oxide fuel cell-micro gas turbine hybrid system*. Energy 35, 982-988.

Kong W., Zhu H., Fei Z., Lin Z., 2011. *A modified dusty gas model in the form of a Fick's model for the prediction of multicomponent mass transport in a solid oxide fuel cell anode*. Journal of Power Sources 206, 171-178 (2012).

Koo K.Y., Lee S., Jung U.H., Roh H., Yoon W.L., 2014. *Syngas production via combined steam and carbon dioxide reforming of methane over Ni–Ce/$MgAl_2O_4$ catalysts with enhanced coke resistance*. Fuel Processing Technology 119, 115-157.

Krishna R., Wasselingh J.A., 1996. *The Maxwell-Stefan approach to mass transfer*, Chemical Engineering Science 52 861-911 (1997).

Kurokawa H., Yang L., Jacobson C.P., De Jonghe L.C., S.J. Visco S.J., 2007. *Y-doped $SrTiO_3$ based sulphur tolerant anode for solid oxide fuel cells*. Journal of Power Sources 164, 510-518.

Lacey R. Pramanick A. Lee J. C. Jung, J., Jiang B., Edwards D.D., Naum R., Misture S.T., 2010. *Evaluation of Co and perovskite Cr-blocking thin films on SOFC interconnects*. Solid State Ionics 181, 1294-1302.

Larminie J., Dicks A., 2003. *Fuel Cell Systems Explained*. John Wiley & Sons Ltd, 2003.

Lee W.Y., Hanna J., Ghoniem A.F., 2012. *On the Predictions of Carbon Deposition on the Nickel Anode of a SOFC and Its Impact on Open-Circuit Conditions*. Journal of the Electrochemical Society 160 (2), F94-F105.

Lessing P., 2007. *A review of sealing technologies applicable to solid oxide electrolysis cells*. Journal of Materials Science 42, 3465-3476.

LGA, 2013. *District Heating*. Local Government Association. Sourced online via: [www.idea.gov.uk/idk/core/page.do?pageId=25065716].

Li X.T., Grace J.R., Lim C.J., Watkinson A.P., Chen H.P., Kim J.R., 2004. *Biomass gasification in a circulating fluidized bed*. Biomass and Bioenergy 26, 171-193.

Liang J., Paul Kung W.C., 2005. *Confinement of Mg–MgH_2 Systems into Carbon Nanotubes Changes Hydrogen Sorption Energetics*. The Journal of Physical Chemistry B 2005 109 (38), 17837-17841.

Liu, K.; Cui, Z. & Fletcher, T. H., 2009. *Chapter 4: Coal Gasification, Hydrogen and Syngas Production and Purification Technologies*. John Wiley & Sons, Inc., 156-218. ISBN: 978-0-471-71975-5.

Liu M., van der Kleij A., Verkooijen A.H.M., Aravind P.V., 2013. *An experimental study of the interaction between tar and SOFCs with Ni/GDC anodes*. Applied Energy 108, 149-157.

Lohner T., D'Aveni A., Dehouche Z., Johnson P., 2013. *Integration of large-scale hydrogen storages in a low-carbon electricity generation system*. International Journal of Hydrogen Energy, Volume 38, Issue 34.

Lohner T., Dehouche Z., Johnson P., 2012. *Integration of large-scale Hydrogen Storages in a low-carbon Electricity Generation System*. Submitted to the World Hydrogen Energy Conference 2012 International Conference and Exhibition, June 3 – 7, 2012, Toronto Centre Sheraton, Toronto, ON, Canada.

Lorente E., Berrueco C., Millan M., Brandon N.P., 2013. *Effects of tar fractions from coal gasification on nickel-yttria stabilized zirconia and nickel-gadolinium doped ceria solid oxide fuel cell anode materials*. Journal of Power Sources 242, 824-831.

Lorente E., Millan M., Brandon N.P., 2012. *Use of gasification syngas in SOFC: Impact of real tar on anode materials*. International Journal of Hydrogen Technology 37, 7271-7278.

Lovins A.B., 2011. *Reinventing Fire*, Rocky Mountains Institute, Chelsea Green Publishing Company, Vermont.

Lower S., 2013. *General Chemistry Virtual Textbook, Chemical Kinetics and Dynamics - Collision and activation*. Sourced online via: [www.chem1.com].

Lucero C., Escudero M.T., Mesa V., 2011. *Integration of an alkaline electrolyser with a hydrogen storage system based on metal hydride technology and a fuel cell system for electricity*. Poster presented at Gordon Research Conference "Hydrogen-Metal systems".

MacLeay I., Harris K., Annut A., 2012. *Digest of United Kingdom Energy Statistics 2012.* Department of Energy and Climate Change. National Statistics.

Marsano F., Magistri L., Bozzolo M., Tarnowski O., 2004. *Influence of fuel composition on Solid Oxide Fuel Cell hybrid system layout and performance*. ASME Turbo Expo GT2004-53853, Vienna, Austria.

Marsh R, 2008. *Closing the energy gap – Summary paper*. WWF-UK. Sourced online via: [http://www.wwf.org.uk/filelibrary/pdf/energy_gap_summary.pdf].

Materazzi M., Lettieri P., Mazzei, L., Taylor R., Chapman C., 2013. Thermodynamic modelling and evaluation of a two-stage thermal process for waste gasification. Fuel 108, 356 - 369.

Materazzi M., Lettieri P., Mazzei, L., Taylor R., Chapman C., 2013b. *Technical Aspects and Thermodynamic Evaluation of a Two Stage Fluid Bed-Plasma Process for Solid Waste Gasification*. Refereed conference proceedings: The 14th Internation Conference on Fluidization – From Fundamentals to Products, Eds, ECI Symposium Series, Volume (2013). [http://dc.engconfintl.org/fluidization_xiv/13].

Matsuzaki Y., Yasuda I., 2000. *The poisoning effect of sulphur-containing impurity gas on a SOFC anode: Part I. Dependence on temperature, time, and impurity concentration*. Solid State Ionics 132, 261-269.

McAllister S., Chen J., Fernandez-Pello A.C., 2011. *Fundamentals of Combustion Processes, Chapter 2*. Springer, ISBN 978-1-4419-7942-1.

McKay G., 2002. Dioxin characterisation, formation and minimisation during municipal solid waste (MSW) incineration: review. Chemical Engineering Journal 86, 343-368.

McPhy, 2014. *Hydrogen Energy*. McPhy Energy S.A., company website. Sourced online via: [http://www.mcphy.com/en/markets/hydrogen-energy/].

Meerman J., Ramirez A., Turkenburg W.C., Faaij A.P.C., 2010. *Performance of simulated flexible integrated gasification polygeneration facilities. Part A: A technical-energetic assessment*. Renewable and Sustainable Energy Reviews 15 2563-2587 (2011).

Menzler M.H., Tietz F., Uhlenbruck S., Buckremer H.P., Stover D., 2010. *Materials and manufacturing technologies for solid oxide fuel cells*. Journal of Material Science 45 3109-3135.

Mermelstein J., Millan M., Brandon N., 2010. *The impact of steam and current density on carbon formation from biomass gasification tar on Ni/YSZ, and Ni/CGO solid oxide fuel cell anodes*. Journal of Power Sources 195, 1657-1666.

Mermelstein J., Millan M., Brandon N.P., 2009. *The impact of carbon formation on Ni-YSZ anodes from biomass gasification model tars operating in dry conditions*. Chemical Engineering Science 64, 492-500.

Mermelstein J., Millan M., Brandon N.P., 2011. *The interaction of biomass gasification syngas components with tar in a solid oxide fuel cell and operational conditions to mitigate carbon deposition on nickel-gadolinium doped ceria anodes*. Journal of Power Sources 196, 5027-5034.

Milne T. A.; Evans R. J.; Abatzoglou N., 1998. *Biomass gasifier "tars": Their nature, formation, and conversion*. Report NREL/TP-570-25357.

Minutello M., Perna A., Di Bona D., 2009. *Modelling and performance of an integrated plasma gasification combined cycle (IPGCC) power plant*. Energy Conversion and Management 50 2837-2842.

Mitsubishi, 2013. *Mitsubishi Heavy sees 4000 h pressurised SOFC-MGT operation*. Fuel Cells Bulletin 2013, pg4.

Mitsuyasu H., Nonaka Y., Eguchi K., 1998. *Analysis of solid state reaction at the interface of yttria-doped ceria/yttria-stabilized zircon*ia. Solid State Ionics 113-115, 279-284.

Mogensen M., Sammes N.M., G. Tompsett G.A., 2000. *Physical, chemical and electrochemical properties of pure and doped ceria*. Solid State Ionics 129, 63-94.

Molenda J., Swierczek K., Wajac W., 2007. *Functional Materials for the IT-SOFC*. Journal of Power Sources 173, 657-670 (2007).

Mondal P., Klein A., Jaegermann W., Hahn H., 1998. *Enhanced specific grain boundary conductivity in nanocrystalline Y2O3-stabilized zirconia*. Solid State Ionics 118, 331-119 (1999).

Mori H., ju Wen C., Otomo J., Eguchi K., Takahashi H., 2003. *Investigation of the interaction between NiO and yttria-stabilized zirconia (YSZ) in the NiO/YSZ composite by temperature-programmed reduction technique*. Applied Catalysis A: General 245, 79-85.

Morrin S., Lettieri P., Chapman C., Mazzei L., 2011. *Two stage fluid bed-plasma gasification process for solid waste valorisation: Technical review and preliminary thermodynamic modelling of sulphur emissions.* Journal of Waste Management 32 (2012) 676-684.

Mueller F., Gaynor R., Auld A.E., Brouwer J., Jabbari F., Samuelsen G. S., 2008. *Synergistic integration of a gas turbine and solid oxide fuel cell for improved transient capability*. Journal of Power Sources 176, 229-239.

Murzin D., Salmi T., 2005. *Catalytic Kinetics*. Elsevier.

Nagel F.P., Schildhauer T.J., Biollaz S.M.A., 2009a. *Biomass-integrated gasification fuel cell systems – Part 1: Definition of systems and technical analysis*. International Journal of Hydrogen Energy 34 6809-6825.

Nagel F.P., Schildhauer T.J., Sfeir J., Schuler A., Biollaz S.M.A., 2009b. *The impact of sulphur on the performance of a solid oxide fuel cell (SOFC) system operated with hydrocarboneous fuel gas*. Journal of Power Sources 189, 1127-1131.

Namioka T., Naruse T., Yomane R., 2011. *Behaviour and mechanisms of Ni/ScSZ cermet anode deterioration by trace tar in wood gas in a solid oxide fuel cell*. International Journal of Hydrogen Energy 36, 5581-5588.

NASA, 2013. *Global Climate Change*. NASA website. Sourced online via: [http://climate.nasa.gov].

Narváez I., Orío A., Aznar M.P., Corella J., 1996. *Biomass Gasification with Air in an Atmospheric Bubbling Fluidized Bed. Effect of Six Operational Variables on the Quality of the Produced Raw Gas*. Industrial & Engineering Chemistry Research 1996 35 (7), 2110-2120.

Nehrir M.H., Wang C., 2009. *Modeling and Control of Fuel Cells: Distributed Generation Applications*. Wiley-IEEE Press, 2009.

NETL, 2000. *Fuel Cell Handbook*. NETL, U.S. Department of Energy, 2000.

Nishi M., Yokokawa H., Kishimoto H., Yamaji K., Horita T., 2014. *Oxygen isotope labeling method and oxygen reduction reaction mechanism of an SOFC cathode*. Solid State Ionics 262, 392-397.

Novatlantis, 2005. *Smarter living - Generating a new understanding for natural resources as the key to sustainable development - the 2000-watt society*. Novatlantis, Dübendorf, Switzerland.

NWRWMG, 2010. *Household Waste Composition Analysis*. NWRWMG Residual Waste Project, IBR0108/Reports.

O'Hayre R., Cha S., Colella W., F.Prinz F.B., 2009. *Fuel Cell Fundamentals*, second edition. John Wiley & Sons, 2009.

Ofgem, 2011. *Typical domestic energy consumption figures – Factsheet 96*. Sourced online at: [https://www.ofgem.gov.uk/ofgem-publications/64026/domestic-energy-consump-fig-fs.pdf].

Ofgem, 2012. *Feed-in Tariff scheme: Tariff Table 1 December 2012 - 31 March 2013 Non-PV Only*. Sourced online at: [https://www.ofgem.gov.uk/environmental-programmes/feed-tariff-fit-scheme/tariff-tables].

Optimat Ltd., 2001. *Co-utilisation of coal and municipal wastes*. Report No. COAL R212 DTI/Pub URN 01/1302.

Oudhuis A.B.J., Bos A., Ouweltjes J.P., Rietveld G., van der Giesen A.B., 2004. *High Efficiency Electricity and Products from Biomass and Waste; Experimental Results and Proof of Principle of Staged Gasification and Fuel Cells*. Presented at "The 2nd World Conference and Technology Exhibition on Biomass for Energy, Industry and Climate Protection", Rome, Italy, 2004.

Panopoulos K.D., Fryda L.E., Karl J., Poulou S., Kakaras E., 2005. *High temperature solid oxide fuel cell integrated with novel allothermal biomass gasification Part I: Modelling and feasibility study*. Journal of Power Sources 159 570-585.

Park E., Taniguchi S., Daio T., Chou J.-T., Sasaki K., 2014. *Influence of cathode polarization on the chromium deposition near the cathode/electrolyte interface of SOFC*. International Journal of Hydrogen Energy 39, 1463 – 1475.

Payne R., Love J., Kah M., 2009. *Generating Electricity at 60% Electrical Efficiency from 1-2 kWe SOFC Products*. ECS Transactions, 25 (2) 231-239.

Peng R., Xia C., Liu X., Peng D., Meng G., 2002. *Intermediate-temperature SOFC's with thin Ce0.8Y0.2O1.9 films prepared by screen printing*. Solid State Ionics 152-153, 561-565.

Pihlatie M., Kaiser A., Mogensen M., 2009. *Redox stability of SOFC: Thermal analysis of Ni-YSZ composites*. Solid State Ionics 189, 1100-1112.

Pike Research, 2010. *Report: Fuel Cell Vehicles: Light Vehicles, Medium/Heavy-Duty Trucks, Transit Buses, and Hydrogen Refueling Infrastructure*. Pike Research. Sourced online via: [http://www.navigantresearch.com/research/fuel-cell-vehicles].

Poling B., Prausnitz J., O'Connell J., 2001. *The Properties of Gases and Liquids*, 5th Edition. McGraw Hill.

Pout C., 2011. *Proposed Carbon Emission Factors and Primary Energy Factors for SAP 2012*. Building Research Establishment, Watford, UK.

RA Eng, 2004. *The costs of generating electricity*. The Royal Academy of Engineering, ISBN: 1-903496-11-X.

Rademaekers K., Slingenberg A., Morsy S., 2008. *Final Report: Review and analysis of EU wholesale energy markets*. ECORYS Netherlands B.V. (EC DG TREN).

Ray R., Taylor R., Chapman C., 2012. *The deployment of an advanced gasification technology in the treatment of household and other waste streams*. Process safety and environmental Protection 90, 213-220.

Reddy G.K. and Smirniotis P.G., 2015. *Water Gas Shift Reaction: Research Development and Applications*. Elsevier, ISBN: 978-0124201545.

REF, 2011. *Information Note: High Rewards for Wind Farms Discarding Electricity 5-6th April 2011*. Renewable Energy Foundation. Sourced online via: [http://www.ref.org.uk/attachments/article/231/ref%20info%20note%2001%2005%2011.pdf].

Restmac, 2008. Brochure: *Cogeneration at Small Scale: Simultaneous Production of Electricity and Heat*. European Biomass Industry Association, EC FP6 TREN/05/FP6EN/S07.58365/020185.

Ricketts B., Hotchkiss R., Livingston B., Hall M., 2002. *Technology Status Review of Waste/Biomass Co-Gasification with Coal*. IChemE Fifth European Gasification Conference, Noordwijk, The Netherlands.

Rietveld B., Dekker N., Ouwltjes J.P., 2009. *Influence of Bio-Syngas Contaminants on SOFC: BioCellus & Green Fuel Cell*. ECN Fuel Quality Workshop, 2009.

RMCT, 2003. *Material Recovery Facility: Handbook*. Recycling marketing cooperative for Tennessee. Sourced online via: [http://ctasgis02.psur.utk.edu/Environment/solid%20waste%20documents/recycling/material%20recovery%20facility%20handbook.pdf].

Rokni M., 2013. *Thermodynamic analysis of SOFC (solid oxide fuel cell)-Stirling hybrid plants using alternative fuels*. Energy 61, 87-97.

Rokni M., 2014. *Biomass gasification integrated with a solid oxide fuel cell and Stirling engine*. [Article in press] Energy xxx, 1-13.

Sadhukan J., Zhao Y., Shah N., Brandon N.P., 2009. *Performance analysis of integrated biomass gasification fuel cell (BCFC) and biomass gasifcation combined cycle (BGCC) systems*. Chemical Engineering Science 65 1942-1954 (2010).

Sakai, N., Kishimoto H., Yamaji K., Horita T., Brito M., Yokokawa H., 2007. *Interface Stability of Perovskite Cathodes and Rare-Earth Doped Ceria Interlayer in SOFCs*. Journal of The Electrochemical Society 154 (12), B1331-B1337.

Sammes N., Tompsett G., Nafe H., Aldinger F., 1998. *Bismuth Based Oxide Electrolytes – Structure and Ionic Conductivity*. Journal of the European Ceramic Society 19, 1801-1826 (1999).

Saravanamuttoo H.I.H., Rogers G.F.C., Cohen H., 2001. Gas Turbine Theory. Prentice Hall, ISBN: 9780130158475.

Sauer G., Ainscough C., 2011. *Technical Report - U.S. Geographic Analysis of the Cost of Hydrogen from Electrolysis*. NREL, U.S. D.O.E., Office of Energy Efficiency & Renewable Energy.

Schimanke D., Mai B., Strohbach T., Lawrence J., 2010. *Integrated Stack Module with increased power*. Proceedings of the 9th European SOFC Forum, Lucerne, 2010.

Schuler J. A., Wuillemin Z., Hessler-Wyser A., Comminges C., Steiner N. Y., herle null J. V., 2012. *Cr-poisoning in (La,Sr)(Co,Fe)O3 cathodes after 10,000 h SOFC stack testing*. Journal of Power Sources 211, 177-183.

Setis, 2012. *Electricity Storage in the Power Sector*. Sourced online via: [http://setis.ec.europa.eu].

Shafiee S., Topal E., 2009. *When will fossil fuel reserves be diminished?* Energy Policy 37, 181-189.

Shaigan N., Qu W., Ivey D.G., Chen W., 2010. *A review of recent progress in coatings, surface modifications and alloy developments for solid oxide fuel cell ferritic stainless steel interconnects*. Journal of Power Sources 195, 1529-1542.

Shih S., Shargi-Moshtaghin R., De Guire M., Goettler R., Xing Z., Liu Z., Heuer A., 2011. *Mn Valence Determination for Lanthanum Strontium Manganite Solid Oxide Fuel Cell Cathodes*. Journal of The Electrochemical Society 158, B1276-B1280.

Siedlecki M., de Jong W., Verkooijen A., 2011. *Fluidized Bed Gasification as a Mature and Reliable Technology for the Production of Bio-Syngas and Applied in the Production of Liquid Transportation Fuels—A Review*. Energies 4, 389-434.

Simner S., Bonnett J., Canfield N., Meinhardt, K., Shelton, J. Sprenkle, V., Stevenson, J., 2003. *Development of lanthanum ferrite SOFC cathodes*. Journal of Power Sources 113, 1-10.

Simner S.P., Stevenson J.W., 2001. *Compressive mica seals for SOFC applications*. Journal of Power Sources 102, 310-316.

Sinden G., 2005. *Wind power and the UK wind resource*. Environmental Change Institute, University of Oxford, 2005.

Singh D., Hernandez-Pacheco E., Hutton P.N., Patel N., Mann M.D., 2004. *Carbon deposition in an SOFC fueled by tar-laden biomass gas: a thermodynamic analysis*. Journal of Power Sources 142, 194-199.

Singhal S.C., 2000. *Advances in solid oxide fuel cell technology*. Solid State Ionics 135, 2000.

Singhal S.C., Kendall K. (Eds), 2003. *High temperature solid oxide fuel cells: fundamentals, design and applications*. Elsevier Ltd, 2003.

Smith A.R., Klosek J., 2001. *A review of air separation technologies and their integration with energy conversion processes*. Fuel Processing Technology 70, 115-134.

Somiya S., Aldinger F., Claussen N., Spriggs R.M., Uchino K., Koumoto K., Kaneno M. (Eds.), 2003. *Handbook of Advanced Ceramics Volume II: Processing and their Applications*. Academic Press, Elsevier Ltd.

Song C., Ma X., 2009. *Chapter 5: Desulfurization Technologies, Hydrogen and Syngas Production and Purification Technologies*. John Wiley & Sons Inc., 219-310. ISBN: 978-0-471-71975-5.

Steele B., 1996. *Survey of Materials Selection for Ceramic Fuel Cells II*. Cathodes and Anodes. Solid State Ionics 86-88, 1223-1234.

Steele B., 2000. *Appraisal of $Ce_{1-y}Gd_yO_{2-y/2}$ electrolytes for IT-SOFC operation at 500°C*. Solid State Ionics 129, 95-110.

Steele B., Heinzel A., 2001. *Materials for fuel-cell technologies*. Nature 414, 345-352.

Strath.ac.uk, 2014. Dynamic performance of PEM fuel cell. University of Strathclyde, source online via: [http://www.esru.strath.ac.uk/EandE/Web_sites/12-13/PEM_fuel_cell/fc.html]

Sulzer, 2014. *Separation Technology - Distillation and Absorption*. Sulzer website. Sourced online via: [http://www.sulzer.com/mr/Products-and-Services/Separation-Technology/Distillation-and-Absorption/Distillation].

Sun C., Hui R., Roller J., 2010. *Cathode materials for solid oxide fuel cells: a review*. Journal of Solid State Electrochemistry, Springer-Verlag 14, 1125-1144.

Suwanwarankul R., Croiset E., Fowler M.W., Douglas P.L., Entchev E., Douglas M.A., 2002. *Performance comparison of Fick's, dusty-gas and Stefan-Maxwell models to predict the concentration overpotential of a SOFC anode*. Journal of Power Sources 122, 9-18 (2003).

Taguchi H., Chiba R., Komatsu T., Orui H., Watanabe, K., Hayashi, K., 2013. *LNF SOFC cathodes with active layer using Pr_6O_{11} or Pr-doped CeO_2.* Journal of Power Sources 241, 768-775.

Taroco H.A., Santos J.A.F., Domingues R.Z., Matencio T., 2011. *Ceramic Materials for Solid Oxide Fuel Cells, Advances in Ceramics - Synthesis and Characterization, Processing and Specific Applications*. Prof. Costas Sikalidis (Ed.), ISBN: 978-953-307-505-1, InTech, DOI: 10.5772/18297. Available from: [http://www.intechopen.com/books/advances-in-ceramics-synthesis-and-characterization-processing-and-specific-applications/ceramic-materials-for-solid-oxide-fuel-cells].

Thompson J.J., 1967. *An introduction to chemical energetics*. Longmans, Green and Co Ltd., London and Harlow.

Tiess G., Kriz A., 2011. *Aggregates Resources Policies in Europe*. International Journal of Environmental Protection 1, 54-61.

Tietz F., Buchkremer H.-P., Stover D., 2002. *Components manufacturing for solid oxide fuel cells*. Solid State Ionics 152-153, 373-381.

Torkelson J., Ye N., Li Z., Coutinho D., Fokema M., 2008. Robust low-cost water-gas shift membrane reactor for high purity hydrogen production from coal-derived syngas: Final technical report. Aspen Products Group, DOE Award # DE-FC26-05NT42452, August 2008.

U.S. D.O.E., 2000. *Hydrogen Program 2000 Annual Review: Overview of Storage Development DOE Hydrogen Program*. Sourced online via: [https://www1.eere.energy.gov/hydrogenandfuelcells/pdfs/storage.pdf].

U.S. D.O.E., 2012. *Gasification Technology R&D*. Sourced online at [www.fossil.energy.gov]. Accessed June 2012.

U.S. D.O.E., 2012b. *Executive Summaries for the Hydrogen Storage Materials Centers for Excellence, Period of performance: 5005-2010*. Fuel Cell Technologies Program, Office of Energy Efficiency and Renewable Energy. Sourced online via: [http://www.energy.gov/sites/prod/files/2014/03/f11/executive_summaries_h2_storage_coes.pdf].

Ulleberg Ø., 2003. *Modeling of advanced alkaline electrolyzers: a system simulation approach*. International Journal of Hydrogen Energy 28, 21-33.

UNDP, 2000. World Energy Assessment: Energy and the challenge of sustainability. United Nations Development Progamme (2000). ISBN: 92 1 126126 0.

University of Cambridge, 2012. *Solid oxide fuel cells*. Sourced online at: http://www.doitpoms.ac.uk/tlplib/fuel-cells/high_temp_sofc.php.

Ural Z., Gencoglu M.T., 2013. *Design and simulation of a solar-hydrogen system for different situations*. International Journal of Hydrogen Energy 39, 8833-8840 (2014).

Uzunoglu M., Onar O.C., Alam M.S., 2009. *Modeling, control and simulation of A PV/FC/UC based hybrid power generation system for stand-alone applications*. Renewable Energy 34, 509-520.

Vasileiadis S., Ziaka-Vasileiadou Z., 2004. *Biomass reforming process for integrated solid oxide-fuel cell power generation*. Chemical Engineering Science 59, 22-23.

Vijaya Lakshmi V., Bauri R., Gandhi A.S., Paul S., 2010. *Synthesis and characterization of nanocrystalline ScSZ electrolytes for SOFCs*. International Journal of Hydrogen Energy (2011).

Waldbillig D., Wood A., Ivey D.G., 2009. *Thermal analysis of the cyclic reduction and oxidation behaviour of SOFC anodes*. Solid State Ionics 176, 847-859.

Wang J., Ebner A.D., Ritter J.A., 2006. *Kinetic Behavior of Ti-Doped Sodium Aluminum Hydride when Co-Catalyzed with Carbon Nanostructures*. Journal of Physical Chemistry B, 110, 17353-17358.

Wang Q., Li L., Wang C., 2009. *Numerical study of thermoelectric characteristics of a planar solid oxide fuel cell with direct internal reforming of methane*. Journal of Power Sources, 186 (2), 399-407.

Wang Y., Li F., Cheng H., Fan L., Zhao Y., 2013. *A comparative study on the catalytic properties of high Ni-loading Ni/SiO_2 and low Ni-loading Ni-Ce/SiO_2 for CO methanation*. Journal of Fuel Chemistry and Technology 41 (8), 972-977.

Watson D., 2013. *Municipal waste management in the United Kingdom*. ETC/SCP, European Environment Agency. Sourced online via: [http://www.eea.europa.eu/publications/managing-municipal-solid-waste/united-kingdom-municipal-waste-management].

WEC, 2013. *2013 World Energy Issues Monitor*. World Energy Council, ISBN: 978 0 946121 20 5. Sourced online via: [http://www.worldenergy.org/publications/].

WEC, 2013b. World Energy Resource: Waste to Energy. World Energy Council, ISBN: 978 0 946121 29 8. Sourced online via: [http://www.worldenergy.org/wp-content/uploads/2013/10/WER_2013_7b_Waste_to_Energy.pdf].

WRAP, 2013. *Comparing the cost of alternative waste treatment options*. WRAP statistics. Sourced online via: [http://www.wrap.org.uk/sites/files/wrap/Gate_Fees_Report_2013_h%20(2).pdf].

Wu J., Liu X., 2010. *Recent Development of SOFC Metallic Interconnect*. Journal of Materials Science & Technology 26, 293-305.

www.gas-turbines.com, 2014. *Gas turbine prices by output*. Sourced online via: [http://www.gas-turbines.com/trader/outprice.htm].

Yakabe H., Hishinuma M., Uratani M., Matsuzaki Y., Yasuda I, 1999. *Evaluation and modelling of performance of anode-supported solid oxide fuel cell*, Journal of Power Sources 86 423-431 (2000).

Yi Y., Rao A.D., Brouwer J., Samuelsen G.S., 2005. *Fuel flexibility study of an integrated 25kW SOFC reformer system*. Journal of Power Sources 144, 67-76.

Yuan J., Huang Y., Sunden B., Wang W.G., 2008. *Analysis of parameter effects on chemical reaction coupled transport phenomena in SOFC anodes*. Heat Mass Transfer 45, 471-484 (2009).

Zhang X., Chan S.H., Li H.K., 2009. *A review of integration strategies for solid oxide fuel cells*. Journal of Power Sources 195, 685-702.

Zhen Y., Tok A., Jiang S., Boey F., 2007. *La(Ni,Fe)O_3 as a cathode material with high tolerance to chromium poisoning for solid oxide fuel cells*. Journal of Power Sources 170, 61-66.

Zhong H.C., Wang H., Liu J.W., Sun D.L., Zhu M., 2011. *Altered desorption enthalpy of MgH2 by the reversible formation of Mg(In) solid solution*. Scripta Materialia 65, 285-287.

Zhu W.Z., Deevi S.C., 2003. *A review on the status of anode materials for solid oxide fuel cells*. Materials Science and Engineering A362, 228-239.

Zuttel A., 2003. *Materials for Hydrogen Storage*. Materials Today, Elsevier, ISSN: 1369 7021.

APPENDIX A.1

A.1.1 Ordinary Diffusion Coefficient Calculations

$$\Omega_D = \frac{A}{(T^*)^B} + \frac{C}{\exp(DT^*)} + \frac{E}{\exp(FT^*)} + \frac{G}{\exp(HT^*)},$$

where

$$T^* = \frac{kT}{\varepsilon_{ij}},$$

$$A = 1.06036, \quad B = 0.1560, \quad C = 0.19300, \quad D = 0.47635,$$

$$E = 1.03587, \quad F = 1.52996, \quad G = 1.76474, \quad H = 3.89411$$

Table A.1.1: Lennard-Jones Potentials

Substance	σ, Å	ε/k, K
H_2	2.827	59.7
O_2	3.467	106.7
H_2O	2.641	809.1
CO	3.690	91.7
CO_2	3.942	195.2
N_2	3.798	71.4

APPENDIX A.2

In order to obtain suitable values of c_p at varying temperatures published values of c_p have been used to generate trend lines using fourth-order polynomials and provide more accurate results for ΔG and ΔH for the various gases:

$$c_p = a + bT + cT^2 + dT^3 + eT^4$$

Values for *a, b, c, d* and *e* for the various gases can be found below.

A.2.1 MatLab m-Code

```
% This m-code will be used to identify model variables for a sofc
% To load variables from this m-file ensure file is called under
% Model Properties -> Callbacks -> PreLoadFcn: {paste the following}
% set_param('modelname{.mdl using the var's}','PreloadFcn',
'EngD_mcode_development010614')
%-------------------------------------------
%Constants
% R(universal gas constant) = 8.314 J/molK
R=8.314;
% F (Faraday constant) = 96485 C/mol
Far=96485;
%Molar Mass (kg/kmol)
MH2=2;
MO2=32;
MH2O=18;
MCO=28;
MCO2=44;
MN2=28;
Mair=29;
% Stefan-Boltzmann constant = 5.670373e-08 J/(m2sK4)
Boltz=5.670373e-08;

%HHV of H2
LHVH2=120; %MJ/kg
HHVH2=141.88; % MJ/kg


%% FC inlet conditons

H2up=707; % kg/h upper limit
H2low=702; % kg/h lower limit

% Price threshold for importing elec

Pthresh=0.0315;

% BOUNDARY CONDITIONS
% Initial values
% Molar fraction at inlet
xH2=0.9;
xO2=0.21;
xH2O=0.1;

% STP conditions
Pstp=101325; %Pa
```

```
Tstp=298; %K


%% Material Properties
%
% Cell geometry
% Layer thicknesses (m)
ta=0.0005;
te=0.00003;
tc=0.00003;
% Channel
chh=0.005;
chw=0.005;
chl=0.1;
chA=chl*chw; %electrolyte
chV=chA*chh;
InArea=chA*4; %Assuming square channel
% Cell: assuming 10 channels per plate
Nchan=20;
cA=Nchan*chA; % m2
cV=Nchan*chV; % m3
% Total Area ie. total no. of cells
Ncells=1764177570;

TArea=cA*Ncells; %m2
TVol=cV*Ncells; %m3
TInArea=InArea*Ncells; % channel area exposed at each electrode
% Module geometry
Pl=0.12; % plate length
Pw=0.1; % plate width
Ph=0.005; % plate height
Th=Ph*Ncells; % Total height
% External surfaces and channel surface areas for thermal calculations
MSA=Th*Pl*2+Th*Pw*2; % Module Surface Area
CSA=chh*chl*2*10*Ncells+chw*chl*2*10*Ncells; % Channel Surface Area
% Hydraulic diameter Dh=4A/P where A is the cross sectional area and P is
% the perimeter %% ref- Heat transfer: A practical approach, Y. Cengel pg
% 379
dh=(4*chh*chw)/(2*(chh+chw));
% width/height ratio for Nusselt number
Nur=chw/chh;
% Module mass calculations
% Reference material properties obtained from Q. Wang et al. Numerical
% study of thermoelectric characteristics of a planar sofc with direct
% internal reforming. Journal of power sources 186 (2009) 399-407.
% Densities (kg/m3)
dan=6200;
dca=6000;
del=5560;
din=7700;
man=Pl*Pw*ta*dan*Ncells;
mca=Pl*Pw*tc*dca*Ncells;
mel=Pl*Pw*te*del*Ncells;
min=(Pl*Pw*Ph*Ncells-TVol)*din;
mtot=man+mca+mel+min;
% Specific heat (J/kg.K)
cpan=650;
cpca=900;
cpel=300;
```

```
cpin=800;
% Overall specific heat;
Mcp=(man*cpan+mca*cpca+mel*cpel+min*cpin)/mtot;

%% Calculating Area-specific Resistance ASR
%
% Electrolyte conductivity (1/ohm.cm)
conde=0.65;
% Electrolyte Resistance (ohm)
Rese=te/(cA*conde);
% Electrolyte ASR (ohm.cm2)->ohm.m2
ASRe=Rese*cA;

%% Diffusion
%
% Porosity (epsilon) - dimensionless [anode/cathode]
epsa=0.35;
epsc=0.35;
%Tortuosity (tau) - dimensionless [anode/cathode]
taua=4.5;
tauc=4.5;
% Pore radius (r) - m [anode/cathode]
ra=9.6e-07;
rc=9.6e-07;
% Lennard-Jones energy and length variables - (The Properties of Gases
and
% Liquids, Fifth ed)
% sigma
sigH2=2.2827;
sigO2=3.467;
sigH2O=2.641;
sigCO=3.690;
sigCO2=3.942;
sigN2=3.798;
% epsilon/k
ekH2=59.7;
ekO2=106.7;
ekH2O=809.1;
ekCO=91.7;
ekCO2=195.2;
ekN2=71.4;
% Collision integral constants to calculate omega
A=1.06036;
B=0.1560;
C=0.19300;
D=0.47635;
E=1.03587;
F=1.52996;
G=1.76474;
H=3.89411;
%
%_____________________________________________
% Electrolyte conductivity
%sigma*T=Asofc*e^(-deltaG/RT)
%A: calculated from excel plot comparison G: ref Fuel Cell Fundamentals
pg144
%see excel sheet conductivity_electrolyte.xlsx
Asofc=500000;
Gacte=89000;
```

```
%% Thermodynamic Properties
%First we will identify the polynomial constants that will produce
specific
%heat Cp values as a function of temperatures where:
% Cp = A + BT + CT^2 + DT^3 + ET^4 + FT^5  {kJ/mol.K}
%From Text Book For H2: A=+22.737, B=+37.693x10^3, C=-85.085x10^6,
D=+89.807x10^9,
%E=-42.908x10^12, F=+7.6821x10^15
% Calculated and verified values:
AH=26.4;
BH=0.01278;
CH=-2.342e-05;
DH=1.928e-08;
EH=-5.112e-12;
%From Text Book For O2: A=+30.737, B=-19.954x10^3, C=+72.554x10^6, D=-
80.005x10^9,
%E=+38.443x10^12, F=-6.8611x10^15
AO=28.02;
BO=-0.0006362;
CO=2.277e-05;
DO=-2.093e-08;
EO=5.706e-12;
%From Text Book For H2O: A=+32.262, B=+1.2532x10^3, C=+11.285x10^6, D=-
3.7103x10^9
AW=32.55;
BW=-0.001263;
CW=1.687e-05;
DW=-8.228e-09;
EW=1.205e-12;
% For air assuming M=28.97 g/mol
AA=31.05;
BA=-0.01561;
CA=3.877e-05;
DA=-2.83e-08;
EA=7.142e-12;
% For CO assuming M=28
ACO=30.04;
BCO=-0.005038;
CCO=1.846e-06;
DCO=2.37e-08;
ECO=-1.811e-11;
% For CO2 assumign M=44
ACO2=20.18;
BCO2=0.07086;
CCO2=-4.376e-05;
DCO2=-6.012e-09;
ECO2=1.395e-11;
% For N2
AN=42.27;
BN=-0.08905;
CN=0.0002003;
DN=-1.718e-07;
EN=5.136e-11;


% Thermal conductivity k (W/m.K) used in the calculation of conduction
and
% convection
```

```
% For air
kAA=-0.009920;
kBA=0.0001541;
kCA=-1.36e-07;
kDA=6.66e-11;
kEA=-8.29e-15;
% For H2
kAH=0.01705;
kBH=0.0006641;
kCH=-4.563e-07;
kDH=2.784e-10;
kEH=-5.358e-14;
% For H2O
kAW=0.01604;
kBW=-6.055e-05;
kCW=3.266e-07;
kDW=-3.331e-10;
kEW=1.298e-13;
% For CO
kACO=-0.006403;
kBCO=0.0001519;
kCCO=-2.218e-07;
kDCO=2.432e-10;
kECO=-1.03e-13;
% For CO2
kACO2=0.005228;
kBCO2=-1.434e-05;
kCCO2=2.416e-07;
kDCO2=-2.496e-10;
kECO2=8.423e-14;

% Nusselt number calculations according to table 8.1 -Fundamentals of
Heat
% and Mass Transfer (Incropera, De Witt) pg 496
ANu=3.265;
BNu=-0.8502;
CNu=0.6831;
DNu=-0.131;
ENu=0.007938;
%------------------------------------------------------------
%          Thermodynamic Calculations
%------------------------------------------------------------
%Specific Enthalpy and Entropy values as stated in literature
%
%                  h0{kJ/mol}        s0{J/mol.K}
% H2                  0                  130.67  [Fuel Cell
Thermodynamics]
% O2                  0                  205.14  [Fuel Cell
Thermodynamics]
% H2O              -241.84               188.82  [Fuel Cell
Thermodynamics]
% CO               -110.53               197.67
% CO2              -393.51               213.74
% N2                  0                  191.61
%
H2h0=0;
O2h0=0;
H2Oh0=-241.84;
COh0=-110.53;
```

```
CO2h0=-393.51;
N2h0=0;
H2s0=130.67;
O2s0=205.14;
H2Os0=188.82;

%% Prexponential constants
% Arrhenius Law
% io,c = vc*(pO2/pref)^0.25 * exp(-Ea,c/RT)
% io,a = va*(pH2/pref)(pH2O/pref)^(-0.5) * exp(-Ea,a/RT) {Costamagna
'98,'04}
vc=7e08; % (A/m^2)
va=5.5e08;
Eac=120000; %J/mol
Eaa=100000; %J/mol

%% Charge transfer coefficients
% Using the Tafel equation to calculate the activation losses
% Fuel Cell Systems Explained pg 48

alphaa=0.5; % Hydrogen electrode values vary between 0-1
alphac=0.5; % Oxygen electrode values vary between 0.1-0.5

%% Electrolyser variable
%Area m2
ElecA=6667; %m2
%% Calling syngas flow rate and composition

%Total molar flow rate kmol/h

%nsyn=100000;

%time=xlsread('syngasfluct','H2','A2:A8761')
varH2=xlsread('syngasfluct','H2','A2:B8761');% two-dimensional array
including timestep for From Workspace block
varCO=xlsread('syngasfluct','CO','A2:B8761');
varCO2=xlsread('syngasfluct','CO2','A2:B8761');
varH2O=xlsread('syngasfluct','H2O','A2:B8761');
%Varsyn=xlsread('syngasfluct')
%tsH2=timeseries(varH2,time)
%Var3.time=Var.hour;
%Var3.signal=Var.H2;
%Var3.dimension=1
%stor=xlsread('storage','A1:B35')
%varH2.time=Var.hour;
%varH2.signal=Var.H2;
%varH2.dimension=100;
varWelec=xlsread('Wholelec','A2:B8761');
test=xlsread('storage','A2:B35');

%% Hydrogen storage Fan

% SFP W/L/s

SFP=0.9; %
```

APPENDIX A.3

A.3.1 ChemCad Stream Compositions

CHEMCAD 6.5.2 Page 1

Simulation: Results Final Date: 01/25/2015
FLOW SUMMARIES:

Stream No.	1	2	3	4
Stream Name	Oxygen	Nitrogen		
Temp C	25.0000*	25.0000*	25	337.296
Pres bar	1.0132*	1.0132*	1.0132	8
Enth MJ/h	-1.0282	-2.9198	-3.9444	5469.5
Vapor mole frac.	1	1	1	1
Total kmol/h	123.6914	465	588.6913	588.6913
Total kg/h	3958	13026.5098	16984.5098	16984.5098
Total std L m3/h	3.5104	16.1199	19.6304	19.6304
Total std V m3/h	2772.37	10422.35	13194.72	13194.72
Flow rates in kg/h				
Hydrogen	0	0	0	0
Methane	0	0	0	0
Carbon Monoxide	0	0	0	0
Carbon Dioxide	0	0	0	0
Water	0	0	0	0
Oxygen	3958	0	3958	3958
Nitrogen	0	13026.5098	13026.5098	13026.5098
Benzene	0	0	0	0
Toluene	0	0	0	0
Hydrogen Chlorid	0	0	0	0
Sulfur Dioxide	0	0	0	0
Nitrogen Dioxide	0	0	0	0
Hydrogen Sulfide	0	0	0	0
Silicon Dioxide	0	0	0	0
Carbon	0	0	0	0
Carbonyl Sulfide	0	0	0	0
Sodium Chloride	0	0	0	0
APP MSW C	0	0	0	0
Air	0	0	0	0
Selexol (TM)	0	0	0	0
Ammonia	0	0	0	0
Sodium Bicarbona	0	0	0	0
Sodium Sulfate	0	0	0	0

CHEMCAD 6.5.2 Page 2

Simulation: Results Final Date: 01/25/2015
FLOW SUMMARIES:

Stream No.	5	6	7	8
Stream Name		Nitrogen	Water	*
Temp C	24.85	24.85	10	8.8761 *
Pres bar	1.01	1.01	1.0132	1.0100
Enth MJ/h	-1.8169	-4.6981	-21519	-21520
Vapor mole frac.	1	1	0	0.66985
Total kmol/h	146.9414	441.75	74.9376	221.8789
Total kg/h	4609.3262	12375.1846	1350	5959.3257
Total std L m3/h	4.3164	15.3139	1.35	5.6664
Total std V m3/h	3293.49	9901.23	1679.62	4973.12
Flow rates in kg/h				
Hydrogen	0	0	0	0
Methane	0	0	0	0
Carbon Monoxide	0	0	0	0
Carbon Dioxide	0	0	0	0
Water	0	0	1350	1350
Oxygen	3958	0	0	3958
Nitrogen	651.3259	12375.1846	0	651.3259
Benzene	0	0	0	0
Toluene	0	0	0	0
Hydrogen Chlorid	0	0	0	0
Sulfur Dioxide	0	0	0	0
Nitrogen Dioxide	0	0	0	0
Hydrogen Sulfide	0	0	0	0
Silicon Dioxide	0	0	0	0
Carbon	0	0	0	0
Carbonyl Sulfide	0	0	0	0
Sodium Chloride	0	0	0	0
APP MSW C	0	0	0	0
Air	0	0	0	0
Selexol (TM)	0	0	0	0
Ammonia	0	0	0	0
Sodium Bicarbona	0	0	0	0
Sodium Sulfate	0	0	0	0

CHEMCAD 6.5.2 Page 3

Simulation: Results Final Date: 01/25/2015
FLOW SUMMARIES:

Stream No.	9	10	11	12
Stream Name		RDF	Syngas Gas.	
Temp C	350	25.0000*	814.7201	814.7201
Pres bar	1.01	1.0132*	1	1
Enth MJ/h	-15831	-57116	-50835	-7781.7
Vapor mole frac.	1	0	1	1
Total kmol/h	221.8789	68.49	546.9755	77.5081
Total kg/h	5959.3257	6849	10277.7207	2537.3237
Total std L m3/h	5.6664	1.2221	17.6735	0.9947
Total std V m3/h	4973.12	1535.11	12259.72	1737.24
Flow rates in kg/h				
Hydrogen	0	0	409.9897	0.0522
Methane	0	0	3.0662	0.0004
Carbon Monoxide	0	0	4597.8154	0.3908
Carbon Dioxide	0	0	2992.0361	0.3923
Water	1350	0	1516.4641	0.0064
Oxygen	3958	0	0	0
Nitrogen	651.3259	0	699.0927	0.0651
Benzene	0	0	0	0
Toluene	0	0	0	0
Hydrogen Chlorid	0	0	28.1698	0.0048
Sulfur Dioxide	0	0	0	0
Nitrogen Dioxide	0	0	0	0
Hydrogen Sulfide	0	0	21.0257	0.0044
Silicon Dioxide	0	0	0	2007.3557
Carbon	0	0	8.4984	529.0514
Carbonyl Sulfide	0	0	1.4259	0.0003
Sodium Chloride	0	0	0	0
APP MSW C	0	6849	0	0
Air	0	0	0	0
Selexol (TM)	0	0	0	0
Ammonia	0	0	0.1363	0
Sodium Bicarbona	0	0	0	0
Sodium Sulfate	0	0	0	0

CHEMCAD 6.5.2 Page 4

Simulation: Results Final Date: 01/25/2015
FLOW SUMMARIES:

Stream No.	13	14	15	16
Stream Name				
Temp C	25.0000*	1200	1200	736.6972
Pres bar	1.0000*	1.0132	1.0132	1

Enth MJ/h	0	-45151	13.707	-8089.5
Vapor mole frac.	1	1	1	1
Total kmol/h	0	546.7578	0.6067	78.2064
Total kg/h	0	10470.4131	7.2869	2545.71
Total std L m3/h	0	16.9861	0.0032	0.9984
Total std V m3/h	0	12254.84	13.6	1752.89
Flow rates in kg/h				
Hydrogen	0	347.0594	0	0.0522
Methane	0	0.0028	0	0.0004
Carbon Monoxide	0	5149.4639	0	0.3908
Carbon Dioxide	0	2137.8433	0	0.3923
Water	0	2086.0417	0	0.0065
Oxygen	0	0	0	0
Nitrogen	0	699.1848	0	0.0651
Benzene	0	0	0	0
Toluene	0	0	0	0
Hydrogen Chlorid	0	28.1695	0	0.0048
Sulfur Dioxide	0	0.0239	0	0
Nitrogen Dioxide	0	0	0	0
Hydrogen Sulfide	0	20.8016	0	0.0044
Silicon Dioxide	0	0	0	2007.3557
Carbon	0	0	7.2869	537.4376
Carbonyl Sulfide	0	1.7988	0	0.0003
Sodium Chloride	0	0	0	0
APP MSW C	0	0	0	0
Air	0	0	0	0
Selexol (TM)	0	0	0	0
Ammonia	0	0.0243	0	0
Sodium Bicarbona	0	0	0	0
Sodium Sulfate	0	0	0	0

CHEMCAD 6.5.2 Page 5

Simulation: Results Final Date: 01/25/2015
FLOW SUMMARIES:

Stream No.	17	18	19	20
Stream Name				
Temp C	923.2656	923.2656	400	450.0001
Pres bar	1.0132	1.0132	1.0132	1.0132
Enth MJ/h	-47839	-47839	-57837	-57331
Vapor mole frac.	1	1	1	1
Total kmol/h	546.666	546.666	546.666	547.438
Total kg/h	10269.3154	10269.3154	10269.3154	10289.0576
Total std L m3/h	16.9897	16.9897	16.9897	17.0115

Total std V m3/h	12252.78	12252.78	12252.78	12270.08
Flow rates in kg/h				
Hydrogen	363.2477	363.2477	363.2477	363.2477
Methane	0.0036	0.0036	0.0036	0.0036
Carbon Monoxide	5269.5161	5269.5161	5269.5161	5269.5161
Carbon Dioxide	1945.2131	1945.2131	1945.2131	1979.1642
Water	1941.3514	1941.3514	1941.3514	1955.2391
Oxygen	0	0	0	0.0088
Nitrogen	699.1835	699.1835	699.1835	699.1836
Benzene	0	0	0	0
Toluene	0	0	0	0
Hydrogen Chlorid	28.1695	28.1695	28.1695	0.0819
Sulfur Dioxide	0.0181	0.0181	0.0181	0.0001
Nitrogen Dioxide	0	0	0	0
Hydrogen Sulfide	20.8263	20.8263	20.8263	20.8263
Silicon Dioxide	0	0	0	0
Carbon	0	0	0	0
Carbonyl Sulfide	1.7608	1.7608	1.7608	1.7608
Sodium Chloride	0	0	0	0
APP MSW C	0	0	0	0
Air	0	0	0	0
Selexol (TM)	0	0	0	0
Ammonia	0.026	0.026	0.026	0.026
Sodium Bicarbona	0	0	0	0
Sodium Sulfate	0	0	0	0

CHEMCAD 6.5.2 Page 6

Simulation: Results Final Date: 01/25/2015
FLOW SUMMARIES:

Stream No.	21	22	23	24
Stream Name				
Temp C	450	200	99.9983	25.0000*
Pres bar	1.0132	1.0132	1.0132	1.0132*
Enth MJ/h	-57331	-0.00013644	-0.000162	-807.89
Vapor mole frac.	1	1	0	0
Total kmol/h	547.438	0	0	0.8499
Total kg/h	10289.0576	0	0	71.3936
Total std L m3/h	17.0115	0	0	0.0322
Total std V m3/h	12270.08	0	0	19.05
Flow rates in kg/h				
Hydrogen	363.2477	0	0	0
Methane	0.0036	0	0	0

Carbon Monoxide	5269.5161	0	0	0
Carbon Dioxide	1979.1642	0	0	0
Water	1955.2391	0	0	0
Oxygen	0.0088	0	0	0
Nitrogen	699.1836	0	0	0
Benzene	0	0	0	0
Toluene	0	0	0	0
Hydrogen Chlorid	0.0819	0	0	0
Sulfur Dioxide	0.0001	0	0	0
Nitrogen Dioxide	0	0	0	0
Hydrogen Sulfide	20.8263	0	0	0
Silicon Dioxide	0	0	0	0
Carbon	0	0	0	0
Carbonyl Sulfide	1.7608	0	0	0
Sodium Chloride	0	0	0	0
APP MSW C	0	0	0	0
Air	0	0	0	0
Selexol (TM)	0	0	0	0
Ammonia	0.026	0	0	0
Sodium Bicarbona	0	0	0	71.3936
Sodium Sulfate	0	0	0	0

CHEMCAD 6.5.2 Page 7

Simulation: Results Final Date: 01/25/2015
FLOW SUMMARIES:

Stream No.	25	26	27	28
Stream Name			Salts	
Temp C	450	556.9481	450	543.2336
Pres bar	1.0132	1.0132	1.0132	1.0132
Enth MJ/h	-57702	-57331	-370.96	-1.09E+05
Vapor mole frac.	1	1	0	1
Total kmol/h	548.2889	547.4379	0.8509	486.65
Total kg/h	10340.8984	10289.1016	51.842	8767
Total std L m3/h	17.0353	18.5975	0.0239	8.767
Total std V m3/h	12289.15	12270.08	19.07	10907.6
Flow rates in kg/h				
Hydrogen	363.2477	473.4135	0	0
Methane	0.0036	0.0036	0	0
Carbon Monoxide	5269.5161	3738.7378	0	0
Carbon Dioxide	1979.1642	4384.3623	0	0
Water	1955.2391	970.6978	0	8767
Oxygen	0.0088	0.0088	0	0
Nitrogen	699.1836	699.1836	0	0

Benzene	0	0	0	0
Toluene	0	0	0	0
Hydrogen Chlorid	0.0819	0.0819	0	0
Sulfur Dioxide	0.0001	0.0001	0	0
Nitrogen Dioxide	0	0	0	0
Hydrogen Sulfide	20.8263	20.8263	0	0
Silicon Dioxide	0	0	0	0
Carbon	0	0	0	0
Carbonyl Sulfide	1.7608	1.7608	0	0
Sodium Chloride	45.0521	0	45.0521	0
APP MSW C	0	0	0	0
Air	0	0	0	0
Selexol (TM)	0	0	0	0
Ammonia	0.026	0.026	0	0
Sodium Bicarbona	6.6346	0	6.6346	0
Sodium Sulfate	0.1553	0	0.1553	0

CHEMCAD 6.5.2 Page 8

Simulation: Results Final Date: 01/25/2015
FLOW SUMMARIES:

Stream No.	29	30	31	32
Stream Name			Quench	
Temp C	140	163.2917	10	828.3630 *
Pres bar	1.0132	1.0132	1.0132	40.0000 *
Enth MJ/h	-65029.	-1.04E+05	-1.66E+05	-86902
Vapor mole frac.	1	1	0	1
Total kmol/h	547.4379	691.9009	577.8518	691.9009
Total kg/h	10289.1016	12891.7061	10410	12891.7061
Total std L m3/h	18.5975	24.9979	10.41	24.9979
Total std V m3/h	12270.08	15508.02	12951.77	15508.02
Flow rates in kg/h				
Hydrogen	473.4135	737.2159	0	737.2159
Methane	0.0036	0.0036	0	0.0036
Carbon Monoxide	3738.7378	73.1423	0	73.1423
Carbon Dioxide	4384.3623	10143.8359	0	10143.8359
Water	970.6978	1215.6219	10410	1215.6219
Oxygen	0.0088	0.0088	0	0.0088
Nitrogen	699.1836	699.1836	0	699.1836
Benzene	0	0	0	0
Toluene	0	0	0	0
Hydrogen Chlorid	0.0819	0.0819	0	0.0819

Sulfur Dioxide	0.0001	0.0001	0	0.0001
Nitrogen Dioxide	0	0	0	0
Hydrogen Sulfide	20.8263	20.8263	0	20.8263
Silicon Dioxide	0	0	0	0
Carbon	0	0	0	0
Carbonyl Sulfide	1.7608	1.7608	0	1.7608
Sodium Chloride	0	0	0	0
APP MSW C	0	0	0	0
Air	0	0	0	0
Selexol (TM)	0	0	0	0
Ammonia	0.026	0.026	0	0.026
Sodium Bicarbona	0	0	0	0
Sodium Sulfate	0	0	0	0

CHEMCAD 6.5.2 Page 9

Simulation: Results Final Date: 01/25/2015
FLOW SUMMARIES:

Stream No.	33	34	35	36
Stream Name	From shift			
Temp C	35	2.2781	14.6999	14.7254
Pres bar	40	40	40	41
Enth MJ/h	-1.10E+05	-51837	-83998	-83989
Vapor mole frac.	0.90393	0.99994	1.44E-05	0
Total kmol/h	691.9009	519.6821	395.0513	395.0513
Total kg/h	12891.7061	7199.1069	64508.3125	64508.3125
Total std L m3/h	24.9979	18.2906	63.8181	63.8181
Total std V m3/h	15508.02	11647.97	8854.54	8854.54
Flow rates in kg/h				
Hydrogen	737.2159	731.3792	5.8367	5.8367
Methane	0.0036	0.0033	0.0003	0.0003
Carbon Monoxide	73.1423	71.5085	1.6338	1.6338
Carbon Dioxide	10143.8359	5708.7695	4466.251	4466.251
Water	1215.6219	2.906	1239.0225	1239.0225
Oxygen	0.0088	0.0084	0.0004	0.0004
Nitrogen	699.1836	683.5683	15.6153	15.6153
Benzene	0	0	0	0
Toluene	0	0	0	0
Hydrogen Chlorid	0.0819	0.0354	0.047	0.047
Sulfur Dioxide	0.0001	0	0.0001	0.0001
Nitrogen Dioxide	0	0	0	0
Hydrogen Sulfide	20.8263	0.9007	20.3333	20.3333
Silicon Dioxide	0	0	0.1343	0.1343
Carbon	0	0	0.3653	0.3653

Carbonyl Sulfide	1.7608	0.0271	1.785	1.785
Sodium Chloride	0	0	0	0
APP MSW C	0	0	0	0
Air	0	0	0	0
Selexol (TM)	0	0.0005	58757.2578	58757.2578
Ammonia	0.026	0.0003	0.0264	0.0264
Sodium Bicarbona	0	0	0	0
Sodium Sulfate	0	0	0	0

CHEMCAD 6.5.2 P age 10

Simulation: Results Final Date: 01/25/2015
FLOW SUMMARIES:

Stream No.	37	38	39	40
Stream Name		To Claus		
Temp C	92	100	125	102.677
Pres bar	6.9	1.0132	6.9	1.0132
Enth MJ/h	-73398	-55503	-67564	-14169
Vapor mole frac.	0.26425	1	0.37528	0
Total kmol/h	395.0513	172.3185	395.0513	222.7328
Total kg/h	64508.3125	5719.0112	64508.3125	58789.3008
Total std L m3/h	63.8181	6.7329	63.8181	57.0851
Total std V m3/h	8854.54	3862.29	8854.54	4992.26
Flow rates in kg/h				
Hydrogen	5.8367	5.8367	5.8367	0
Methane	0.0003	0.0003	0.0003	0
Carbon Monoxide	1.6338	1.6337	1.6338	0
Carbon Dioxide	4466.251	4435.0874	4466.251	31.1636
Water	1239.0225	1212.7205	1239.0225	26.3019
Oxygen	0.0004	0.0004	0.0004	0
Nitrogen	15.6154	15.6153	15.6154	0.0001
Benzene	0	0	0	0
Toluene	0	0	0	0
Hydrogen Chlorid	0.047	0.0466	0.047	0.0005
Sulfur Dioxide	0.0001	0.0001	0.0001	0
Nitrogen Dioxide	0	0	0	0
Hydrogen Sulfide	20.3333	19.9248	20.3333	0.4084
Silicon Dioxide	0.1343	0	0.1343	0.1343
Carbon	0.3653	0	0.3653	0.3653
Carbonyl Sulfide	1.785	1.7337	1.785	0.0513
Sodium Chloride	0	0	0	0
APP MSW C	0	0	0	0
Air	0	0	0	0
Selexol (TM)	58757.2578	26.3863	58757.2578	58730.8711

Ammonia	0.0264	0.0257	0.0264	0.0007
Sodium Bicarbona	0	0	0	0
Sodium Sulfate	0	0	0	0

CHEMCAD 6.5.2 P age 11

Simulation: Results Final Date: 01/25/2015
FLOW SUMMARIES:

Stream No.	41	42	43	44
Stream Name		Inert slag		
Temp C	103.4435	80	90.4328	-6.0000*
Pres bar	40	1	40	40.0000*
Enth MJ/h	-13883	-10099	-15411	-25626
Vapor mole frac.	0	1	0	0
Total kmol/h	222.7328	78.2064	222.7328	222.7328
Total kg/h	58789.3008	2545.71	58789.3008	58789.3008
Total std L m3/h	57.0851	0.9984	57.0851	57.0851
Total std V m3/h	4992.26	1752.89	4992.26	4992.26
Flow rates in kg/h				
Hydrogen	0	0.0522	0	0
Methane	0	0.0004	0	0
Carbon Monoxide	0	0.3908	0	0
Carbon Dioxide	31.1636	0.3923	31.1636	31.1636
Water	26.3019	0.0065	26.3019	26.3019
Oxygen	0	0	0	0
Nitrogen	0.0001	0.0651	0.0001	0.0001
Benzene	0	0	0	0
Toluene	0	0	0	0
Hydrogen Chlorid	0.0005	0.0048	0.0005	0.0005
Sulfur Dioxide	0	0	0	0
Nitrogen Dioxide	0	0	0	0
Hydrogen Sulfide	0.4084	0.0044	0.4084	0.4084
Silicon Dioxide	0.1343	2007.3557	0.1343	0.1343
Carbon	0.3653	537.4376	0.3653	0.3653
Carbonyl Sulfide	0.0513	0.0003	0.0513	0.0513
Sodium Chloride	0	0	0	0
APP MSW C	0	0	0	0
Air	0	0	0	0
Selexol (TM)	58730.8711	0	58730.8711	58730.8711
Ammonia	0.0007	0	0.0007	0.0007
Sodium Bicarbona	0	0	0	0
Sodium Sulfate	0	0	0	0

CHEMCAD 6.5.2 P age 12

Simulation: Results Final Date: 01/25/2015
FLOW SUMMARIES:

Stream No.	45	46	47	48
Stream Name		To FC		
Temp C	-4.2053	90	475	650
Pres bar	1.0132	1.0132	1.0132	1.0132
Enth MJ/h	-51836	-50307	-43607	-40398
Vapor mole frac.	1	1	1	1
Total kmol/h	519.6821	519.6821	519.6821	519.6821
Total kg/h	7199.1069	7199.1069	7199.1069	7199.1069
Total std L m3/h	18.2906	18.2906	18.2906	18.2906
Total std V m3/h	11647.97	11647.97	11647.97	11647.97
Flow rates in kg/h				
Hydrogen	731.3792	731.3792	731.3792	731.3792
Methane	0.0033	0.0033	0.0033	0.0033
Carbon Monoxide	71.5085	71.5085	71.5085	71.5085
Carbon Dioxide	5708.7695	5708.7695	5708.7695	5708.7695
Water	2.906	2.906	2.906	2.906
Oxygen	0.0084	0.0084	0.0084	0.0084
Nitrogen	683.5683	683.5683	683.5683	683.5683
Benzene	0	0	0	0
Toluene	0	0	0	0
Hydrogen Chlorid	0.0354	0.0354	0.0354	0.0354
Sulfur Dioxide	0	0	0	0
Nitrogen Dioxide	0	0	0	0
Hydrogen Sulfide	0.9007	0.9007	0.9007	0.9007
Silicon Dioxide	0	0	0	0
Carbon	0	0	0	0
Carbonyl Sulfide	0.0271	0.0271	0.0271	0.0271
Sodium Chloride	0	0	0	0
APP MSW C	0	0	0	0
Air	0	0	0	0
Selexol (TM)	0.0005	0.0005	0.0005	0.0005
Ammonia	0.0003	0.0003	0.0003	0.0003
Sodium Bicarbona	0	0	0	0
Sodium Sulfate	0	0	0	0

CHEMCAD 6.5.2 P age 13

Simulation: Results Final Date: 01/25/2015
FLOW SUMMARIES:

Stream No.	49	50	51	52

Stream Name	Air to FC		Air to FC	
Temp C	25.0000*	482.8367	650	99.9983
Pres bar	1.0132*	1.0132	1.0132	1.0132
Enth MJ/h	-5.1297	9992.3	13882	-1.62E+05
Vapor mole frac.	1	1	1	0
Total kmol/h	728.6795	728.6795	728.6795	577.8518
Total kg/h	21096	21096	21096	10410
Total std L m3/h	24.4734	24.4734	24.4734	10.41
Total std V m3/h	16332.36	16332.36	16332.36	12951.77
Flow rates in kg/h				
Hydrogen	0	0	0	0
Methane	0	0	0	0
Carbon Monoxide	0	0	0	0
Carbon Dioxide	0	0	0	0
Water	0	0	0	10410
Oxygen	0	0	0	0
Nitrogen	0	0	0	0
Benzene	0	0	0	0
Toluene	0	0	0	0
Hydrogen Chlorid	0	0	0	0
Sulfur Dioxide	0	0	0	0
Nitrogen Dioxide	0	0	0	0
Hydrogen Sulfide	0	0	0	0
Silicon Dioxide	0	0	0	0
Carbon	0	0	0	0
Carbonyl Sulfide	0	0	0	0
Sodium Chloride	0	0	0	0
APP MSW C	0	0	0	0
Air	21096	21096	21096	0
Selexol (TM)	0	0	0	0
Ammonia	0	0	0	0
Sodium Bicarbona	0	0	0	0
Sodium Sulfate	0	0	0	0

Simulation: Results Final Date: 01/25/2015
FLOW SUMMARIES:

Stream No.	53	54	55	56
Stream Name			Hot water	
Temp C	99.9983	99.9983	10	111.5619 *
Pres bar	1.0132	1.0132	1.0132	1.0132 *

	-1.6200E+005			
Enth MJ/h	-	1.22E+05	-1.40E+05	-1.16E+05
Vapor mole frac.	0	0	0	1
Total kmol/h	577.8518	433.3889	486.65	486.65
Total kg/h	10410	7807.5005	8767	8767
Total std L m3/h	10.41	7.8075	8.767	8.767
Total std V m3/h	12951.77	9713.82	10907.6	10907.6
Flow rates in kg/h				
Hydrogen	0	0	0	0
Methane	0	0	0	0
Carbon Monoxide	0	0	0	0
Carbon Dioxide	0	0	0	0
Water	10410	7807.5005	8767	8767
Oxygen	0	0	0	0
Nitrogen	0	0	0	0
Benzene	0	0	0	0
Toluene	0	0	0	0
Hydrogen Chlorid	0	0	0	0
Sulfur Dioxide	0	0	0	0
Nitrogen Dioxide	0	0	0	0
Hydrogen Sulfide	0	0	0	0
Silicon Dioxide	0	0	0	0
Carbon	0	0	0	0
Carbonyl Sulfide	0	0	0	0
Sodium Chloride	0	0	0	0
APP MSW C	0	0	0	0
Air	0	0	0	0
Selexol (TM)	0	0	0	0
Ammonia	0	0	0	0
Sodium Bicarbona	0	0	0	0
Sodium Sulfate	0	0	0	0

CHEMCAD 6.5.2 P age 15

Simulation: Results Final Date: 01/25/2015
FLOW SUMMARIES:

Stream No.	59	60	63	64
Stream Name			Hot Water	
Temp C	168.627	150	99.9983	99.9983
Pres bar	1.0132	1.0132	1.0132	1.0132
Enth MJ/h	-1.15E+05	-8333.9	-2.58E+05	-40500
Vapor mole frac.	1	0	0	0
Total kmol/h	486.65	222.7328	920.0388	144.463

Total kg/h	8767	58789.3008	16574.5	2602.5
Total std L m3/h	8.767	57.0851	16.5745	2.6025
Total std V m3/h	10907.6	4992.26	20621.43	3237.94
Flow rates in kg/h				
Hydrogen	0	0	0	0
Methane	0	0	0	0
Carbon Monoxide	0	0	0	0
Carbon Dioxide	0	31.1636	0	0
Water	8767	26.3019	16574.5	2602.5
Oxygen	0	0	0	0
Nitrogen	0	0.0001	0	0
Benzene	0	0	0	0
Toluene	0	0	0	0
Hydrogen Chlorid	0	0.0005	0	0
Sulfur Dioxide	0	0	0	0
Nitrogen Dioxide	0	0	0	0
Hydrogen Sulfide	0	0.4084	0	0
Silicon Dioxide	0	0.1343	0	0
Carbon	0	0.3653	0	0
Carbonyl Sulfide	0	0.0513	0	0
Sodium Chloride	0	0	0	0
APP MSW C	0	0	0	0
Air	0	0	0	0
Selexol (TM)	0	58730.8711	0	0
Ammonia	0	0.0007	0	0
Sodium Bicarbona	0	0	0	0
Sodium Sulfate	0	0	0	0

CHEMCAD 6.5.2 P age 16

Simulation: Results Final Date: 01/25/2015
FLOW SUMMARIES:

Stream No.	65	66	67	68
Stream Name				
Temp C	923.2656	25.0000*	25	923.2656 *
Pres bar	1.0132	1.0132*	1.0132	1.0132
Enth MJ/h	-47839	-0.53622	-1.17E-06	-47839
Vapor mole frac.	1	0	1	1
Total kmol/h	546.666	0.0006	0.0001	546.666
Total kg/h	10269.3154	0.0474	0.0045	10269.3154
Total std L m3/h	16.9897	0	0	16.9897
Total std V m3/h	12252.78	0.01	0	12252.78

Flow rates in kg/h				
Hydrogen	363.2477	0	0	363.2477
Methane	0.0036	0	0	0.0036
Carbon Monoxide	5269.5161	0	0	5269.5161
Carbon Dioxide	1945.2131	0	0	1945.2131
Water	1941.3514	0	0	1941.3514
Oxygen	0	0	0.0045	0
Nitrogen	699.1835	0	0	699.1835
Benzene	0	0	0	0
Toluene	0	0	0	0
Hydrogen Chlorid	28.1695	0	0	28.1695
Sulfur Dioxide	0.0181	0	0	0.0181
Nitrogen Dioxide	0	0	0	0
Hydrogen Sulfide	20.8263	0	0	20.8263
Silicon Dioxide	0	0	0	0
Carbon	0	0	0	0
Carbonyl Sulfide	1.7608	0	0	1.7608
Sodium Chloride	0	0	0	0
APP MSW C	0	0	0	0
Air	0	0	0	0
Selexol (TM)	0	0	0	0
Ammonia	0.026	0	0	0.026
Sodium Bicarbona	0	0.0474	0	0
Sodium Sulfate	0	0	0	0

A.3.2 ChemCad Stream Properties

CHEMCAD 6.5.2 Page 1

Simulation: Results Final Date: 01/25/2015
STREAM PROPERTIES

Stream No.	1	2	3	4
Name	Oxygen	Nitrogen		
- - Overall - -				
Molar flow kmol/h	123.6914	465	588.6913	588.6913
Mass flow kg/h	3958	13026.5098	16984.5098	16984.5098
Temp C	25	25	25	337.296
Pres bar	1.0132	1.0132	1.0132	8
Vapor mole fraction	1	1	1	1
Enth MJ/h	-1.0282	-2.9198	-3.9444	5469.5
Tc C	-118.57	-146.95	-141.8253	-141.8253
Pc bar	50.7638	33.9388	36.0471	36.0471
Std. sp gr. wtr = 1	1.128	0.808	0.865	0.865
Std. sp gr. air = 1	1.105	0.967	0.996	0.996
Degree API	-6.0011	43.6021	32.0428	32.0428
Average mol wt	31.999	28.014	28.8513	28.8513
Actual dens kg/m3	1.3089	1.1453	1.1796	4.5325
Actual vol m3/h	3023.9729	11374.3232	14398.3506	3747.3096
Std liq m3/h	3.5104	16.1199	19.6304	19.6304
Std vap 0 C m3/h	2772.3745	10422.3467	13194.7207	13194.7207
- - Vapor only - -				
Molar flow kmol/h	123.6914	465	588.6913	588.6913
Mass flow kg/h	3958	13026.5098	16984.5098	16984.5098
Average mol wt	31.999	28.014	28.8513	28.8513
Actual dens kg/m3	1.3089	1.1453	1.1796	4.5325
Actual vol m3/h	3023.9729	11374.3232	14398.3506	3747.3096
Std liq m3/h	3.5104	16.1199	19.6304	19.6304
Std vap 0 C m3/h	2772.3745	10422.3467	13194.7207	13194.7207
Cp kJ/kg-K	0.9189	1.0416	1.013	1.0631
Z factor	0.9994	1	0.9999	1.0035
Visc N-s/m2	2.04E-05	1.78E-05	1.83E-05	3.09E-05
Th cond W/m-K	0.0262	0.0253	0.0255	0.0465
- - Liquid only - -				
Molar flow kmol/h				
Mass flow kg/h				
Average mol wt				
Actual dens kg/m3				
Actual vol m3/h				
Std liq m3/h				

Std vap 0 C m3/h
Cp kJ/kg-K
Z factor
Visc N-s/m2
Th cond W/m-K
Surf. tens. N/m

CHEMCAD 6.5.2 Page 2

Simulation: Results Final Date: 01/25/2015
STREAM PROPERTIES

Stream No.	5	6	7	8
Name		Nitrogen	Water	
- - Overall - -				
Molar flow kmol/h	146.9414	441.75	74.9376	221.8789
Mass flow kg/h	4609.3262	12375.1846	1350	5959.3257
Temp C	24.85	24.85	10	8.8761
Pres bar	1.01	1.01	1.0132	1.01
Vapor mole fraction	1	1	0	0.6699
Enth MJ/h	-1.8169	-4.6981	-21519	-21520
Tc C	-123.8184	-146.95	374.2	25.2422
Pc bar	46.6632	33.9388	221.1823	64.0241
Std. sp gr. wtr = 1	1.068	0.808	1	1.052
Std. sp gr. air = 1	1.083	0.967	0.622	0.927
Degree API	1.0081	43.6021	10	3.0451
Average mol wt	31.3685	28.014	18.015	26.8585
Actual dens kg/m3	1.2795	1.1422	999.3663	1.728
Actual vol m3/h	3602.4473	10834.9111	1.3509	3448.7773
Std liq m3/h	4.3164	15.3139	1.35	5.6664
Std vap 0 C m3/h	3293.4922	9901.2285	1679.6239	4973.1162
- - Vapor only - -				
Molar flow kmol/h	146.9414	441.75		148.6262
Mass flow kg/h	4609.3262	12375.1846		4639.6772
Average mol wt	31.3685	28.014		31.2171
Actual dens kg/m3	1.2795	1.1422		1.3458
Actual vol m3/h	3602.4473	10834.9111		3447.457
Std liq m3/h	4.3164	15.3139		4.3468
Std vap 0 C m3/h	3293.4922	9901.2285		3331.2542
Cp kJ/kg-K	0.9362	1.0416		0.9408
Z factor	0.9995	1		0.9992
Visc N-s/m2	2.00E-05	1.78E-05		1.90E-05
Th cond W/m-K	0.0261	0.0253		0.0247
- - Liquid only - -				
Molar flow kmol/h			74.9376	73.2528
Mass flow kg/h			1350	1319.6487

Average mol wt			18.015	18.015
Actual dens kg/m3			999.3663	999.4711
Actual vol m3/h			1.3509	1.3203
Std liq m3/h			1.35	1.3197
Std vap 0 C m3/h			1679.6239	1641.8618
Cp kJ/kg-K			4.187	4.187
Z factor			0.001	0.001
Visc N-s/m2			0.001318	0.001356
Th cond W/m-K			0.5837	0.5819
Surf. tens. N/m			0.0747	0.0749
CHEMCAD 6.5.2			Page	3

Simulation: Results Final Date: 01/25/2015
STREAM PROPERTIES

Stream No.	9	10	11	12
Name		RDF	Syngas Gas.	
- - Overall - -				
Molar flow kmol/h	221.8789	68.49	546.9755	77.5081
Mass flow kg/h	5959.3257	6849	10277.7207	2537.3237
Temp C	350	25	814.7201	814.7201
Pres bar	1.01	1.0132	1	1
Vapor mole fraction	1	0	1	1
Enth MJ/h	-15831	-57116	-50835	-7781.7
Tc C	25.2422	0	-80.7795	-142.7607
Pc bar	64.0241	0	52.5006	52.9105
Std. sp gr. wtr = 1	1.052	5.604	0.582	2.551
Std. sp gr. air = 1	0.927	3.453	0.649	1.13
Degree API	3.0451	-106.2513	111.8221	-76.0309
Average mol wt	26.8585	100	18.7901	32.7362
Actual dens kg/m3	0.5237	5604.2324	0.208	445.4283
Actual vol m3/h	11379.4229	1.2221	49415.1719	5.6964
Std liq m3/h	5.6664	1.2221	17.6735	0.9947
Std vap 0 C m3/h	4973.1162	1535.1107	12259.7168	1737.2402
- - Vapor only - -				
Molar flow kmol/h	221.8789		546.2679	0.0517
Mass flow kg/h	5959.3257		10269.2227	0.9167
Average mol wt	26.8585		18.7989	17.716
Actual dens kg/m3	0.5237		0.2078	0.1958
Actual vol m3/h	11379.4229		49415.168	4.6805
Std liq m3/h	5.6664		17.6697	0.0018
Std vap 0 C m3/h	4973.1162		12243.8574	1.1597
Cp kJ/kg-K	1.2472		1.9419	2.027
Z factor	0.9999		1.0002	1.0003
Visc N-s/m2	3.09E-05		4.19E-05	4.16E-05

Th cond W/m-K	0.0502		0.1645	0.1906
- - Liquid only - -				
Molar flow kmol/h				
Mass flow kg/h				
Average mol wt				
Actual dens kg/m3				
Actual vol m3/h				
Std liq m3/h				
Std vap 0 C m3/h				
Cp kJ/kg-K				
Z factor				
Visc N-s/m2				
Th cond W/m-K				
Surf. tens. N/m				

CHEMCAD 6.5.2 Page 4

Simulation: Results Final Date: 01/25/2015
STREAM PROPERTIES

Stream No.	13	14	15	16
Name				
- - Overall - -				
Molar flow kmol/h	0	546.7578	0.6067	78.2064
Mass flow kg/h	0	10470.4131	7.2869	2545.71
Temp C	0	1200	1200	736.6972
Pres bar	0	1.0132	1.0132	1
Vapor mole fraction	0	1	1	1
Enth MJ/h	0	-45151	13.707	-8089.5
Tc C	0	-59.0035	374.2	-142.7556
Pc bar	0	48.3737	221.1823	52.9111
Std. sp gr. wtr = 1	0	0.616	2.25	2.55
Std. sp gr. air = 1	0	0.661	0.415	1.124
Degree API	0	98.0544	-68.6116	-76.0064
Average mol wt	0	19.15	12.011	32.5512
Actual dens kg/m3	0	0.1584	2201.3794	474.7487
Actual vol m3/h	0	66096.7344	0.0033	5.3622
Std liq m3/h	0	16.9861	0.0032	0.9984
Std vap 0 C m3/h	0	12254.8359	13.5981	1752.8895
- - Vapor only - -				
Molar flow kmol/h		546.7578	0	0.0517
Mass flow kg/h		10470.4131	0	0.9167
Average mol wt		19.15	18.015	17.716
Actual dens kg/m3		0.1584	0.149	0.211
Actual vol m3/h		66096.7344	0.0001	4.345
Std liq m3/h		16.9861	0	0.0018

Std vap 0 C m3/h	12254.8359	0	1.1597
Cp kJ/kg-K	2.0268	2.6182	2.0015
Z factor	1.0002	1.0001	1.0003
Visc N-s/m2	5.20E-05	5.53E-05	3.96E-05
Th cond W/m-K	0.1952	0.1692	0.1807
- - Liquid only - -			
Molar flow kmol/h			
Mass flow kg/h			
Average mol wt			
Actual dens kg/m3			
Actual vol m3/h			
Std liq m3/h			
Std vap 0 C m3/h			
Cp kJ/kg-K			
Z factor			
Visc N-s/m2			
Th cond W/m-K			
Surf. tens. N/m			

CHEMCAD 6.5.2 Page 5

Simulation: Results Final Date: 01/25/2015
STREAM PROPERTIES

Stream No.	17	18	19	20
Name				
- - Overall - -				
Molar flow kmol/h	546.666	546.666	546.666	547.438
Mass flow kg/h	10269.3154	10269.3154	10269.3154	10289.0576
Temp C	923.2656	923.2656	400	450.0001
Pres bar	1.0132	1.0132	1.0132	1.0132
Vapor mole fraction	1	1	1	1
Enth MJ/h	-47839	-47839	-57837	-57331
Tc C	-68.044	-68.044	-68.044	-67.5442
Pc bar	47.7551	47.7551	47.7551	47.7918
Std. sp gr. wtr = 1	0.604	0.604	0.604	0.605
Std. sp gr. air = 1	0.649	0.649	0.649	0.649
Degree API	102.5986	102.5986	102.5986	102.4493
Average mol wt	18.7854	18.7854	18.7854	18.7949
Actual dens kg/m3	0.1913	0.1913	0.3401	0.3167
Actual vol m3/h	53673.332	53673.332	30199.2344	32488.6328
Std liq m3/h	16.9897	16.9897	16.9897	17.0115
Std vap 0 C m3/h	12252.7783	12252.7783	12252.7783	12270.082
- - Vapor only - -				
Molar flow kmol/h	546.666	546.666	546.666	547.438
Mass flow kg/h	10269.3154	10269.3154	10269.3154	10289.0576

Average mol wt	18.7854	18.7854	18.7854	18.7949
Actual dens kg/m3	0.1913	0.1913	0.3401	0.3167
Actual vol m3/h	53673.332	53673.332	30199.2344	32488.6328
Std liq m3/h	16.9897	16.9897	16.9897	17.0115
Std vap 0 C m3/h	12252.7783	12252.7783	12252.7783	12270.082
Cp kJ/kg-K	1.9573	1.9573	1.7602	1.7801
Z factor	1.0002	1.0002	1.0002	1.0003
Visc N-s/m2	4.49E-05	4.49E-05	2.93E-05	3.09E-05
Th cond W/m-K	0.1683	0.1683	0.105	0.1114
- - Liquid only - -				
Molar flow kmol/h				
Mass flow kg/h				
Average mol wt				
Actual dens kg/m3				
Actual vol m3/h				
Std liq m3/h				
Std vap 0 C m3/h				
Cp kJ/kg-K				
Z factor				
Visc N-s/m2				
Th cond W/m-K				
Surf. tens. N/m				

Simulation: Results Final Date: 01/25/2015
STREAM PROPERTIES

Stream No.	21	22	23	24
Name				
- - Overall - -				
Molar flow kmol/h	547.438	0	0	0.8499
Mass flow kg/h	10289.0576	0	0	71.3936
Temp C	450	200	99.9983	25
Pres bar	1.0132	1.0132	1.0132	1.0132
Vapor mole fraction	1	1	0	0
Enth MJ/h	-57331	0.00013644	-0.000162	-807.89
Tc C	-67.5442	374.2	374.2	0
Pc bar	47.7918	221.1823	221.1823	0
Std. sp gr. wtr = 1	0.605	1	1	2.217
Std. sp gr. air = 1	0.649	0.622	0.622	2.901
Degree API	102.4493	10	10	-67.6758
Average mol wt	18.7949	18.015	18.015	84.007
Actual dens kg/m3	0.3167	0.4661	957.8149	2217.0259
Actual vol m3/h	32488.627	0	0	0.0322

Std liq m3/h	17.0115	0	0	0.0322
Std vap 0 C m3/h	12270.082	0	0	19.0483
- - Vapor only - -				
Molar flow kmol/h	547.438	0		
Mass flow kg/h	10289.0576	0		
Average mol wt	18.7949	18.015		
Actual dens kg/m3	0.3167	0.4661		
Actual vol m3/h	32488.627	0		
Std liq m3/h	17.0115	0		
Std vap 0 C m3/h	12270.082	0		
Cp kJ/kg-K	1.7805	1.9682		
Z factor	1.0003	0.9957		
Visc N-s/m2	3.09E-05	1.62E-05		
Th cond W/m-K	0.1114	0.0335		
- - Liquid only - -				
Molar flow kmol/h			0	
Mass flow kg/h			0	
Average mol wt			18.015	
Actual dens kg/m3			957.8149	
Actual vol m3/h			0	
Std liq m3/h			0	
Std vap 0 C m3/h			0	
Cp kJ/kg-K			4.2251	
Z factor			0.0008	
Visc N-s/m2			0.0002806	
Th cond W/m-K			0.676	
Surf. tens. N/m			0.0586	

CHEMCAD 6.5.2 Page 7

Simulation: Results Final Date: 01/25/2015
STREAM PROPERTIES

Stream No.	25	26	27	28
Name			Salts	
- - Overall - -				
Molar flow kmol/h	548.2889	547.4379	0.8509	486.65
Mass flow kg/h	10340.8984	10289.1016	51.842	8767
Temp C	450	556.9481	450	543.2336
Pres bar	1.0132	1.0132	1.0132	1.0132
Vapor mole fraction	1	1	0	1
Enth MJ/h	-57702	-57331	-370.96	-1.09E+05
Tc C	-67.5442	-97.4457	0	374.2
Pc bar	47.7918	57.4296	0	221.1823
Std. sp gr. wtr = 1	0.607	0.553	2.171	1
Std. sp gr. air = 1	0.651	0.649	2.104	0.622

Degree API	101.6033	124.2601	-66.3183	10
Average mol wt	18.8603	18.795	60.923	18.015
Actual dens kg/m3	0.3183	0.2759	2070.365	0.2691
Actual vol m3/h	32488.6504	37294.5898	0.025	32575.4941
Std liq m3/h	17.0353	18.5975	0.0239	8.767
Std vap 0 C m3/h	12289.1543	12270.0811	19.0727	10907.6016
- - Vapor only - -				
Molar flow kmol/h	547.438	547.4379		486.65
Mass flow kg/h	10289.0576	10289.1016		8767
Average mol wt	18.7949	18.795		18.015
Actual dens kg/m3	0.3167	0.2759		0.2691
Actual vol m3/h	32488.627	37294.5898		32575.4941
Std liq m3/h	17.0115	18.5975		8.767
Std vap 0 C m3/h	12270.082	12270.0811		10907.6016
Cp kJ/kg-K	1.7805	1.8771		2.1516
Z factor	1.0003	1.0003		0.9994
Visc N-s/m2	3.09E-05	3.46E-05		3.03E-05
Th cond W/m-K	0.1114	0.1429		0.0724
- - Liquid only - -				
Molar flow kmol/h				
Mass flow kg/h				
Average mol wt				
Actual dens kg/m3				
Actual vol m3/h				
Std liq m3/h				
Std vap 0 C m3/h				
Cp kJ/kg-K				
Z factor				
Visc N-s/m2				
Th cond W/m-K				
Surf. tens. N/m				

CHEMCAD 6.5.2 Page 8

Simulation: Results Final Date: 01/25/2015
STREAM PROPERTIES

Stream No.	29	30	31	32
Name			Quench	
- - Overall - -				
Molar flow kmol/h	547.4379	691.9009	577.8518	691.9009
Mass flow kg/h	10289.1016	12891.707	10410	12891.707
Temp C	140	163.2917	10	828.363
Pres bar	1.0132	1.0132	1.0132	40
Vapor mole fraction	1	1	0	1
Enth MJ/h	-65029	-1.04E+05	-1.66E+05	-86902

Tc C	-97.4457	-72.8589	374.2	-72.8589
Pc bar	57.4296	76.0388	221.1823	76.0388
Std. sp gr. wtr = 1	0.553	0.516	1	0.516
Std. sp gr. air = 1	0.649	0.643	0.622	0.643
Degree API	124.2601	142.8779	10	142.8779
Average mol wt	18.795	18.6323	18.015	18.6323
Actual dens kg/m3	0.5545	0.5204	999.3663	8.0647
Actual vol m3/h	18556.3887	24772.791	10.4166	1598.5393
Std liq m3/h	18.5975	24.9979	10.41	24.9979
Std vap 0 C m3/h	12270.0811	15508.0234	12951.7666	15508.0234
- - Vapor only - -				
Molar flow kmol/h	547.4379	691.9009		691.9009
Mass flow kg/h	10289.1016	12891.7061		12891.7061
Average mol wt	18.795	18.6323		18.6323
Actual dens kg/m3	0.5545	0.5204		8.0647
Actual vol m3/h	18556.3887	24772.791		1598.5393
Std liq m3/h	18.5975	24.9979		24.9979
Std vap 0 C m3/h	12270.0811	15508.0234		15508.0234
Cp kJ/kg-K	1.7109	1.8438		2.1588
Z factor	1	0.9999		1.0092
Visc N-s/m2	2.01E-05	2.03E-05		4.19E-05
Th cond W/m-K	0.081	0.0971		0.2067
- - Liquid only - -				
Molar flow kmol/h			577.8518	
Mass flow kg/h			10410	
Average mol wt			18.015	
Actual dens kg/m3			999.3663	
Actual vol m3/h			10.4166	
Std liq m3/h			10.41	
Std vap 0 C m3/h			12951.7666	
Cp kJ/kg-K			4.187	
Z factor			0.001	
Visc N-s/m2			0.001318	
Th cond W/m-K			0.5837	
Surf. tens. N/m			0.0747	
CHEMCAD 6.5.2			Page	9

Simulation: Results	Final	Date:	01/25/2015	
STREAM PROPERTIES				
Stream No.	33	34	35	36
Name	From shift			
- - Overall - -				
Molar flow kmol/h	691.9009	519.6821	395.0513	395.0513
Mass flow kg/h	12891.707	7199.1069	64508.3125	64508.3125

Temp C	35	2.2781	14.6999	14.7254
Pres bar	40	40	40	41
Vapor mole fraction	0.9039	0.9999	1.45E-05	0
Enth MJ/h	-1.10E+05	-51837	-83998	-83989
Tc C	-72.8589	-147.9985	406.0021	406.0021
Pc bar	76.0388	57.7091	167.726	167.726
Std. sp gr. wtr = 1	0.516	0.394	1.011	1.011
Std. sp gr. air = 1	0.643	0.478	5.638	5.638
Degree API	142.8779	228.0054	8.4857	8.4857
Average mol wt	18.6323	13.8529	163.291	163.291
Actual dens kg/m3	32.6188	24.3846	1021.9521	1021.9531
Actual vol m3/h	395.2234	295.2311	63.1226	63.1226
Std liq m3/h	24.9979	18.2906	63.8181	63.8181
Std vap 0 C m3/h	15508.0234	11647.9717	8854.541	8854.541
- - Vapor only - -				
Molar flow kmol/h	625.4269	519.6509	0.0057	
Mass flow kg/h	11694.1768	7198.542	0.104	
Average mol wt	18.6979	13.8527	18.213	
Actual dens kg/m3	29.6793	24.3828	31.1344	
Actual vol m3/h	394.0184	295.2306	0.0033	
Std liq m3/h	23.8004	18.29	0.0002	
Std vap 0 C m3/h	14018.0986	11647.2715	0.1279	
Cp kJ/kg-K	1.826	2.3164	1.8588	
Z factor	0.9837	0.9925	0.9778	
Visc N-s/m2	1.62E-05	1.43E-05	1.53E-05	
Th cond W/m-K	0.0798	0.091	0.0773	
- - Liquid only - -				
Molar flow kmol/h	66.474	0.0313	395.0129	395.0186
Mass flow kg/h	1197.5297	0.565	64507.7109	64507.8086
Average mol wt	18.015	18.0453	163.3053	163.3032
Actual dens kg/m3	993.7549	999.4991	1022.0001	1021.9485
Actual vol m3/h	1.2051	0.0006	63.1191	63.1224
Std liq m3/h	1.1975	0.0006	63.8176	63.8178
Std vap 0 C m3/h	1489.9255	0.7017	8853.6807	8853.8086
Cp kJ/kg-K	4.187	4.1816	1.7439	1.7438
Z factor	0.0374	0.0409	0.2905	0.2977
Visc N-s/m2	0.0007528	0.001623	0.001911	0.001911
Th cond W/m-K	0.6195	0.569	0.1646	0.1645
Surf. tens. N/m	0.0704	0.0757	0.0289	0.0289
CHEMCAD 6.5.2			Page	10

Simulation: Results Final Date: 01/25/2015
STREAM PROPERTIES

Stream No.	37	38	39	40

Name		To Claus		
- - Overall - -				
Molar flow kmol/h	395.0513	172.3185	395.0513	222.7328
Mass flow kg/h	64508.3125	5719.0107	64508.3125	58789.3008
Temp C	92	100	125	102.677
Pres bar	6.9	1.0132	6.9	1.0132
Vapor mole fraction	0.2643	1	0.3753	0
Enth MJ/h	-73398	-55503	-67564	-14169
Tc C	406.0021	133.6676	406.0021	431.6341
Pc bar	167.726	72.9796	167.726	21.3556
Std. sp gr. wtr = 1	1.011	0.849	1.011	1.03
Std. sp gr. air = 1	5.638	1.146	5.638	9.113
Degree API	8.4857	35.0867	8.4857	5.898
Average mol wt	163.291	33.1886	163.291	263.9454
Actual dens kg/m3	125.5294	1.0887	84.7937	944.5303
Actual vol m3/h	513.8899	5253.2651	760.768	62.2418
Std liq m3/h	63.8181	6.7329	63.8181	57.0851
Std vap 0 C m3/h	8854.54	3862.2852	8854.54	4992.2554
- - Vapor only - -				
Molar flow kmol/h	104.385	172.3185	148.2471	
Mass flow kg/h	4163.5659	5719.0112	5111.8467	
Average mol wt	39.8866	33.1886	34.4819	
Actual dens kg/m3	9.2469	1.0887	7.3472	
Actual vol m3/h	450.2651	5253.2651	695.7542	
Std liq m3/h	5.0677	6.7329	6.0654	
Std vap 0 C m3/h	2339.6484	3862.2852	3322.7583	
Cp kJ/kg-K	1.0134	1.161	1.1991	
Z factor	0.9805	0.9958	0.9784	
Visc N-s/m2	1.76E-05	1.66E-05	1.81E-05	
Th cond W/m-K	0.0247	0.0246	0.0274	
- - Liquid only - -				
Molar flow kmol/h	290.6337		246.7716	222.7002
Mass flow kg/h	60344.25		59396	58788.8008
Average mol wt	207.6299		240.6921	263.9818
Actual dens kg/m3	948.4427		913.5931	944.5255
Actual vol m3/h	63.6246		65.0136	62.2416
Std liq m3/h	58.7502		57.7524	57.0849
Std vap 0 C m3/h	6514.1611		5531.0508	4991.5234
Cp kJ/kg-K	2.0208		2.1027	2.0206
Z factor	0.0525		0.0562	0.0094
Visc N-s/m2	0.001031		0.000852	0.001376
Th cond W/m-K	0.156		0.1481	0.1527
Surf. tens. N/m	0.0248		0.0222	0.0252
CHEMCAD 6.5.2			Page	11

Simulation: Results Final Date: 01/25/2015
STREAM PROPERTIES

Stream No.	41	42	43	44
Name		Inert slag		
- - Overall - -				
Molar flow kmol/h	222.7328	78.2064	222.7328	222.7328
Mass flow kg/h	58789.3008	2545.71	58789.3008	58789.3008
Temp C	103.4435	80	90.4328	-6
Pres bar	40	1	40	40
Vapor mole fraction	0	1	0	0
Enth MJ/h	-13883	-10099	-15411	-25626
Tc C	431.6341	-142.7556	431.6341	431.6341
Pc bar	21.3556	52.9111	21.3556	21.3556
Std. sp gr. wtr = 1	1.03	2.55	1.03	1.03
Std. sp gr. air = 1	9.113	1.124	9.113	9.113
Degree API	5.898	-76.0064	5.898	5.898
Average mol wt	263.9454	32.5512	263.9454	263.9454
Actual dens kg/m3	943.6232	1011.1479	958.9461	1068.5309
Actual vol m3/h	62.3017	2.5176	61.3062	55.0188
Std liq m3/h	57.0851	0.9984	57.0851	57.0851
Std vap 0 C m3/h	4992.2554	1752.8895	4992.2554	4992.2554
- - Vapor only - -				
Molar flow kmol/h		0.0517		
Mass flow kg/h		0.9167		
Average mol wt		17.716		
Actual dens kg/m3		0.6034		
Actual vol m3/h		1.5193		
Std liq m3/h		0.0018		
Std vap 0 C m3/h		1.1597		
Cp kJ/kg-K		1.7521		
Z factor		1.0001		
Visc N-s/m2		1.85E-05		
Th cond W/m-K		0.0805		
- - Liquid only - -				
Molar flow kmol/h	222.7002		222.7002	222.7002
Mass flow kg/h	58788.8008		58788.8008	58788.8008
Average mol wt	263.9818		263.9818	263.9818
Actual dens kg/m3	943.6185		958.9413	1068.526
Actual vol m3/h	62.3015		61.3059	55.0186
Std liq m3/h	57.0849		57.0849	57.0849
Std vap 0 C m3/h	4991.5234		4991.5234	4991.5234
Cp kJ/kg-K	2.0181		1.9755	1.6097
Z factor	0.368		0.3784	0.4935
Visc N-s/m2	0.00142		0.001738	0.02144

Th cond W/m-K	0.1525		0.1552	0.175
Surf. tens. N/m	0.0251		0.0264	0.0368
CHEMCAD 6.5.2			Page	12

Simulation: Results Final Date: 01/25/2015
STREAM PROPERTIES

Stream No.	45	46	47	48
Name		To FC		
- - Overall - -				
Molar flow kmol/h	519.6821	519.6821	519.6821	519.6821
Mass flow kg/h	7199.1069	7199.1069	7199.1069	7199.1069
Temp C	-4.2053	90	490	490
Pres bar	1.0132	1.0132	1.0132	1.0132
Vapor mole fraction	1	1	1	1
Enth MJ/h	-51836	-50307	-43607	-43607
Tc C	-147.9985	-147.9985	-147.9985	-147.9985
Pc bar	57.7092	57.7092	57.7092	57.7092
Std. sp gr. wtr = 1	0.394	0.394	0.394	0.394
Std. sp gr. air = 1	0.478	0.478	0.478	0.478
Degree API	228.0054	228.0054	228.0054	228.0054
Average mol wt	13.8529	13.8529	13.8529	13.8529
Actual dens kg/m3	0.628	0.4649	0.2256	0.1829
Actual vol m3/h	11463.3604	15486.252	31908.8984	39371.3047
Std liq m3/h	18.2906	18.2906	18.2906	18.2906
Std vap 0 C m3/h	11647.9717	11647.9717	11647.9717	11647.9717
- - Vapor only - -				
Molar flow kmol/h	519.6821	519.6821	519.6821	519.6821
Mass flow kg/h	7199.1069	7199.1069	7199.1069	7199.1069
Average mol wt	13.8529	13.8529	13.8529	13.8529
Actual dens kg/m3	0.628	0.4649	0.2256	0.2256
Actual vol m3/h	11463.3604	15486.252	31908.8984	31908.8984
Std liq m3/h	18.2906	18.2906	18.2906	18.2906
Std vap 0 C m3/h	11647.9717	11647.9717	11647.9717	11647.9717
Cp kJ/kg-K	2.1967	2.3038	2.5079	2.5079
Z factor	0.9997	1.0002	1.0003	1.0003
Visc N-s/m2	1.36E-05	1.76E-05	3.07E-05	3.07E-05
Th cond W/m-K	0.0871	0.1118	0.1977	0.1977
- - Liquid only - -				
Molar flow kmol/h				
Mass flow kg/h				
Average mol wt				
Actual dens kg/m3				
Actual vol m3/h				
Std liq m3/h				

Std vap 0 C m3/h
Cp kJ/kg-K
Z factor
Visc N-s/m2
Th cond W/m-K
Surf. tens. N/m
CHEMCAD 6.5.2 Page 13

Simulation: Results Final Date: 01/25/2015
STREAM PROPERTIES

Stream No.	49	50	51	52
Name	Air to FC		Air to FC	
- - Overall - -				
Molar flow kmol/h	728.6795	728.6795	728.6795	577.8518
Mass flow kg/h	21096	21096	21096	10410
Temp C	25	482.8367	482.8367	99.9983
Pres bar	1.0132	1.0132	1.0132	1.0132
Vapor mole fraction	1	1	1	0
Enth MJ/h	-5.1297	9992.3	9992.3	-1.62E+05
Tc C	-140.7	-140.7	-140.7	374.2
Pc bar	37.74	37.74	37.74	221.1823
Std. sp gr. wtr = 1	0.862	0.862	0.862	1
Std. sp gr. air = 1	1	1	1	0.622
Degree API	32.6531	32.6531	32.6531	10
Average mol wt	28.951	28.951	28.951	18.015
Actual dens kg/m3	1.1839	0.4666	0.4666	957.8149
Actual vol m3/h	17819.5938	45212.9492	45212.9492	10.8685
Std liq m3/h	24.4734	24.4734	24.4734	10.41
Std vap 0 C m3/h	16332.3643	16332.3643	16332.3643	12951.7666
- - Vapor only - -				
Molar flow kmol/h	728.6795	728.6795	728.6795	
Mass flow kg/h	21096	21096	21096	
Average mol wt	28.951	28.951	28.951	
Actual dens kg/m3	1.1839	0.4666	0.4666	
Actual vol m3/h	17819.5938	45212.9492	45212.9492	
Std liq m3/h	24.4734	24.4734	24.4734	
Std vap 0 C m3/h	16332.3643	16332.3643	16332.3643	
Cp kJ/kg-K	1.0033	1.0842	1.0842	
Z factor	0.9997	1.0004	1.0004	
Visc N-s/m2	1.85E-05	3.52E-05	3.52E-05	
Th cond W/m-K	0.026	0.0546	0.0546	
- - Liquid only - -				
Molar flow kmol/h				577.8518
Mass flow kg/h				10410

Average mol wt				18.015
Actual dens kg/m3				957.8149
Actual vol m3/h				10.8685
Std liq m3/h				10.41
Std vap 0 C m3/h				12951.7666
Cp kJ/kg-K				4.2251
Z factor				0.0008
Visc N-s/m2				0.0002806
Th cond W/m-K				0.676
Surf. tens. N/m				0.0586
CHEMCAD 6.5.2			Page	14

Simulation: Results Final Date: 01/25/2015
STREAM PROPERTIES

Stream No.	53	54	55	56
Name			Hot water	
- - Overall - -				
Molar flow kmol/h	577.8518	433.3889	486.65	486.65
Mass flow kg/h	10410	7807.5005	8767	8767
Temp C	99.9983	99.9983	10	111.5619
Pres bar	1.0132	1.0132	1.0132	1.0132
Vapor mole fraction	0	0	0	1
Enth MJ/h	-1.62E+05	-1.22E+05	-1.40E+05	-1.16E+05
Tc C	374.2	374.2	374.2	374.2
Pc bar	221.1823	221.1823	221.1823	221.1823
Std. sp gr. wtr = 1	1	1	1	1
Std. sp gr. air = 1	0.622	0.622	0.622	0.622
Degree API	10	10	10	10
Average mol wt	18.015	18.015	18.015	18.015
Actual dens kg/m3	957.8149	957.8149	999.3663	0.5752
Actual vol m3/h	10.8685	8.1514	8.7726	15240.9785
Std liq m3/h	10.41	7.8075	8.767	8.767
Std vap 0 C m3/h	12951.7666	9713.8242	10907.6016	10907.6016
- - Vapor only - -				
Molar flow kmol/h				486.65
Mass flow kg/h				8767
Average mol wt				18.015
Actual dens kg/m3				0.5752
Actual vol m3/h				15240.9785
Std liq m3/h				8.767
Std vap 0 C m3/h				10907.6016
Cp kJ/kg-K				2.0408
Z factor				0.9922
Visc N-s/m2				1.26E-05

Th cond W/m-K				0.0257
- - Liquid only - -				
Molar flow kmol/h	577.8518	433.3889	486.65	
Mass flow kg/h	10410	7807.5005	8767	
Average mol wt	18.015	18.015	18.015	
Actual dens kg/m3	957.8149	957.8149	999.3663	
Actual vol m3/h	10.8685	8.1514	8.7726	
Std liq m3/h	10.41	7.8075	8.767	
Std vap 0 C m3/h	12951.7666	9713.8242	10907.6016	
Cp kJ/kg-K	4.2251	4.2251	4.187	
Z factor	0.0008	0.0008	0.001	
Visc N-s/m2	0.0002806	0.0002806	0.001318	
Th cond W/m-K	0.676	0.676	0.5837	
Surf. tens. N/m	0.0586	0.0586	0.0747	
CHEMCAD 6.5.2			Page	15

Simulation: Results Final Date: 01/25/2015
STREAM PROPERTIES

Stream No.	59	60	63	64
Name			Hot Water	
- - Overall - -				
Molar flow kmol/h	486.65	222.7328	920.0388	144.463
Mass flow kg/h	8767	58789.3008	16574.5	2602.5
Temp C	168.627	150	99.9983	99.9983
Pres bar	1.0132	1.0132	1.0132	1.0132
Vapor mole fraction	1	0	0	0
Enth MJ/h	-1.15E+05	-8333.9	-2.58E+05	-40500
Tc C	374.2	431.6341	374.2	374.2
Pc bar	221.1823	21.3556	221.1823	221.1823
Std. sp gr. wtr = 1	1	1.03	1	1
Std. sp gr. air = 1	0.622	9.113	0.622	0.622
Degree API	10	5.898	10	10
Average mol wt	18.015	263.9454	18.015	18.015
Actual dens kg/m3	0.4996	887.256	957.8148	957.8149
Actual vol m3/h	17546.4258	66.2597	17.3045	2.7171
Std liq m3/h	8.767	57.0851	16.5745	2.6025
Std vap 0 C m3/h	10907.6016	4992.2554	20621.4258	3237.9417
- - Vapor only - -				
Molar flow kmol/h	486.65			
Mass flow kg/h	8767			
Average mol wt	18.015			
Actual dens kg/m3	0.4996			
Actual vol m3/h	17546.4258			
Std liq m3/h	8.767			

Std vap 0 C m3/h	10907.6016			
Cp kJ/kg-K	1.9718			
Z factor	0.9948			
Visc N-s/m2	1.50E-05			
Th cond W/m-K	0.0306			
- - Liquid only - -				
Molar flow kmol/h		222.7002	920.0388	144.463
Mass flow kg/h		58788.8008	16574.5	2602.5
Average mol wt		263.9818	18.015	18.015
Actual dens kg/m3		887.2512	957.8149	957.8149
Actual vol m3/h		66.2595	17.3045	2.7171
Std liq m3/h		57.0849	16.5745	2.6025
Std vap 0 C m3/h		4991.5234	20621.4258	3237.9417
Cp kJ/kg-K		2.1706	4.2251	4.2251
Z factor		0.0086	0.0008	0.0008
Visc N-s/m2		0.000776	0.0002806	0.0002806
Th cond W/m-K		0.143	0.676	0.676
Surf. tens. N/m		0.0205	0.0586	0.0586
CHEMCAD 6.5.2			Page	16

Simulation: Results Final Date: 01/25/2015
STREAM PROPERTIES

Stream No.	65	66	67	68
Name				
- - Overall - -				
Molar flow kmol/h	546.666	0.0006	0.0001	546.666
Mass flow kg/h	10269.3154	0.0474	0.0045	10269.3154
Temp C	923.2656	25	25	923.2656
Pres bar	1.0132	1.0132	1.0132	1.0132
Vapor mole fraction	1	0	1	1
Enth MJ/h	-47839	-0.53622	-1.17E-06	-47839
Tc C	-68.044	0	-118.57	-68.044
Pc bar	47.7551	0	50.7638	47.7551
Std. sp gr. wtr = 1	0.604	2.217	1.128	0.604
Std. sp gr. air = 1	0.649	2.901	1.105	0.649
Degree API	102.5986	-67.6758	-6.0011	102.5986
Average mol wt	18.7854	84.007	31.999	18.7854
Actual dens kg/m3	0.1913	2217.0259	1.3089	0.1913
Actual vol m3/h	53673.332	0	0.0034	53673.332
Std liq m3/h	16.9897	0	0	16.9897
Std vap 0 C m3/h	12252.7783	0.0126	0.0032	12252.7783
- - Vapor only - -				
Molar flow kmol/h	546.666		0.0001	546.666
Mass flow kg/h	10269.3154		0.0045	10269.3154

Average mol wt	18.7854	31.999	18.7854
Actual dens kg/m3	0.1913	1.3089	0.1913
Actual vol m3/h	53673.332	0.0034	53673.332
Std liq m3/h	16.9897	0	16.9897
Std vap 0 C m3/h	12252.7783	0.0032	12252.7783
Cp kJ/kg-K	1.9573	0.9189	1.9573
Z factor	1.0002	0.9994	1.0002
Visc N-s/m2	4.49E-05	2.04E-05	4.49E-05
Th cond W/m-K	0.1683	0.0262	0.1683
- - Liquid only - -			
Molar flow kmol/h			
Mass flow kg/h			
Average mol wt			
Actual dens kg/m3			
Actual vol m3/h			
Std liq m3/h			
Std vap 0 C m3/h			
Cp kJ/kg-K			
Z factor			
Visc N-s/m2			
Th cond W/m-K			
Surf. tens. N/m			